



Tiplady, Eleanor Margaret (2018) *Expression and modulation of atypical chemokine receptors on epithelial cells*. PhD thesis.

<https://theses.gla.ac.uk/30618/>

Copyright and moral rights for this work are retained by the author

A copy can be downloaded for personal non-commercial research or study, without prior permission or charge

This work cannot be reproduced or quoted extensively from without first obtaining permission in writing from the author

The content must not be changed in any way or sold commercially in any format or medium without the formal permission of the author

When referring to this work, full bibliographic details including the author, title, awarding institution and date of the thesis must be given

Enlighten: Theses

<https://theses.gla.ac.uk/>
research-enlighten@glasgow.ac.uk

Expression and Modulation of Atypical Chemokine Receptors by Epithelial Cells

Eleanor Margaret Tiplady BSc. MRes.



A thesis submitted to the College of Medicine, Veterinary and Life Sciences, University of Glasgow in fulfilment of the requirements for the degree of Doctor of Philosophy

June 2018

Institute of Infection, Immunity and Inflammation
University of Glasgow
120 University Place
G12 8TA

Table of Contents

Declaration	6
Acknowledgements.....	7
Abstract	8
List of Figures.....	10
List of Tables	15
Abbreviations	16
1 Introduction	21
1.1 General Introduction	21
1.1.1 Innate Immunity.....	23
1.1.2 Adaptive Immunity	24
1.2 Lymph Nodes	25
1.2.1 Structure and Function	25
1.2.2 Overview of the Immune Response.....	27
1.2.3 Lymph Node Development	32
1.3 Spleen	34
1.3.1 Structure and Function	34
1.3.2 Splenic Dendritic Cells	37
1.4 Skin.....	39
1.4.1 Anatomy and Function of the Skin	39
1.4.2 Langerhans Cells.....	42
1.4.3 $\gamma\delta$ T Cells.....	43
1.4.4 Dendritic Cell Migration from Skin to Draining Lymph Nodes.....	43
1.5 Chemokines	45
1.5.1 Post-translational Regulation of Chemokine Function	45
1.5.2 Inflammatory vs Homeostatic Chemokines	46
1.6 Chemokine Receptors	48
1.6.1 CCR7.....	49
1.6.2 CXCR4.....	50
1.7 Atypical Chemokine Receptors.....	52
1.7.1 ACKR3.....	53
1.7.2 ACKR4.....	54
1.8 Aims.....	56

1.9	Hypotheses.....	58
2	Materials and Methods.....	60
2.1	Cell Culture.....	60
2.1.1	Treatment of Human Cells with Immune Stimuli.....	60
2.1.2	RNA Extraction from Cultured Cells.....	61
2.1.3	Chemokine Scavenging Assay.....	61
2.1.4	Immunofluorescent staining of cultured cells.....	62
2.2	Animals.....	62
2.2.1	Sample Handling and Preparation.....	63
2.2.2	Genotyping of Genetically-modified Mice.....	66
2.2.3	<i>In vivo</i> Methods.....	68
2.3	General Techniques.....	70
2.3.1	Protein Extraction from Tissue.....	70
2.3.2	Immunofluorescent Staining of Frozen Tissue Sections.....	70
2.3.3	Flow Cytometry.....	72
2.3.4	Fluorescent Chemokine Uptake.....	75
2.3.5	Bradford Assay.....	76
2.3.6	SDS-PAGE and Western blotting.....	76
2.3.7	RNA Extraction from Tissue.....	77
2.3.8	Quantitative Polymerase Chain Reaction.....	77
2.4	Analysis.....	79
2.4.1	Flow Cytometric Analysis.....	79
2.4.2	Statistical Analysis.....	79
3	Atypical Chemokine Receptor Expression and Function <i>in vitro</i>	81
3.1	Introduction.....	81
3.2	Aims.....	81
3.3	Expression and Modulation of ACKRs on Human Dermal LECs.....	82
3.3.1	Cultured Human Dermal LECs Express ACKR3, ACKR4 and CXCR4.....	82
3.3.2	ACKR3, ACKR4 and CXCR4 in Cultured HD-LECs Are Mostly Intracellular.....	84
3.3.3	ACKRs Expressed by HD-LECs Rarely Co-Localise.....	86
3.3.4	ACKR3 and ACKR4 Proteins Are Not Localised in Lysosomes.....	86
3.3.5	ACKR4 Protein is Localised in RAB5A+ Vesicles.....	87
3.3.6	mRNA Expression of ACKRs and Related Genes by HD-LECs May Be Regulated in Response to Inflammation.....	87
3.3.7	ACKR4-Mediated Chemokine Uptake Occurs at Low Levels on Cultured Cells.....	89
3.3.8	Chemokine Scavenging Assays on Human Dermal-LECs.....	91
3.3.9	Expression and Modulation of ACKRs on Cultured Human Keratinocytes.....	92

3.3.10	Cultured Human Keratinocytes Express ACKR4 Protein.....	93
3.3.11	mRNA of ACKRs and Ligands are Regulated in Response to Inflammation.....	94
3.3.12	ACKR4-Mediated Chemokine Scavenging is Not Detected on nHEKs.....	95
3.4	Key Findings.....	95
4	Exploring ACKR3 and ACKR4 Expression <i>in vivo</i>	119
4.1	Introduction	119
4.2	Aims.....	119
4.3	Characterisation of <i>Ackr3</i>^{+/<i>gfp</i>} Reporter Mice.....	119
4.3.1	<i>Ackr3</i> Expression in the Skin.....	120
4.3.2	<i>Ackr3</i> Expression in the Gut.....	125
4.3.3	<i>Ackr3</i> Expression in the Mesenteric Lymph Node	126
4.3.4	<i>Ackr3</i> Expression in the Spleen	127
4.4	Exploring ACKR4 Expression <i>in vivo</i>	127
4.4.1	Investigating a Role for ACKR4 in Splenic Dendritic Cell Positioning	127
4.5	Key Findings.....	130
5	ACKR4 Involvement in Chronic Skin Inflammation.....	155
5.1	Introduction	155
5.2	Aims.....	156
5.3	Optimising Aldara Treatments.....	156
5.3.1	Feasibility of Aldara Model in Male Mice	156
5.3.2	Single Aldara Treatments Do Not Modulate <i>Ackr4</i> mRNA Expression.....	157
5.4	Potential Role for ACKR4 in Response to Multiple Aldara Treatments.....	157
5.4.1	Multiple Aldara Treatments Modulate mRNA Expression of ACKRs and Ligands in the Skin	157
5.4.2	Reporter Mice Show Reduced eGFP Expression in Response to Aldara.....	158
5.4.3	<i>Ackr4</i> Deficiency Has No Detectable Effect on Keratinocyte Proliferation	159
5.4.4	Aldara Treatment Leads to Follicle Formation in the Ear-Draining Lymph Nodes ..	159
5.4.5	Differential Phenotype in <i>Ackr4</i> ^{-/-} Mice is Resolved in <i>Ackr4</i> ^{-/-} , <i>Ccl19</i> ^{-/-} Mice ...	163
5.5	Key Findings.....	164
6	Discussion.....	186
6.1	Function of ACKR3 and ACKR4 on Cultured Human Cells.....	186
6.1.1	Cell Culture Issues.....	187
6.1.2	Lack of Chemokine Scavenging Activity <i>in vitro</i>	188
6.2	ACKR3/CXCR4 Expression <i>in vivo</i>.....	190

6.2.1	Modulation in the Infundibulum Subset.....	190
6.2.2	Challenges with <i>Ackr3</i> ^{+gfp} Mice	193
6.3	Increased Lymph Node Cellularity in Aldara-Treated <i>Ackr4</i>-Deficient Mice	193
6.3.1	Roles for ACKR4 in Chronic Inflammation.....	194
6.3.2	Limitations of the Aldara Model	196
6.3.3	Future Investigations.....	197
6.4	Conclusions.....	198
7	Additional Outputs	201
8	References	202

Declaration

“I declare that, except where explicit reference is made to the contribution of others, that this dissertation is the result of my own work and has not been submitted for any other degree at the University of Glasgow or any other institution.”

Printed Name: _____

Signature: _____

Acknowledgements

I'd like to thank my supervisors Rob and Gerry for allowing this project to take place at all. Rob in particular provided a lot of advice and pep talks, which I am very grateful for.

For experimental support, I'd especially like to thank Steven Bryce and Carolyn Thomson who contributed a lot of expertise, time and effort into helping me out.

Abstract

The immune system relies on the correct spatial and temporal positioning of cells in order to function; cells need to be able to move throughout the circulatory system to survey for pathogens, to migrate from their resident sites in tissues when they sense infection or injury to alert other cells, or to migrate to the site of damage or infection to help mobilise a response. These functions often involve chemokines, small cytokines that signal through chemokine receptors, which are G-protein coupled receptors expressed on the cell membrane. Different chemokines are regulated differentially and can be associated with certain tissues or developmental processes, meaning the suite of receptors expressed by each cell type determines which tissues it is capable of entering, and the precise location it takes up once inside the tissue.

Atypical chemokine receptors are a class of chemokine receptors that do not initiate the downstream signalling pathways typical of a G-protein coupled receptor, as they do not recruit intracellular G-proteins, and generally don't induce cell migration. Instead, these receptors are thought to function mainly as chemokine scavenging receptors, internalising and destroying their ligands before rapidly recycling to the cell surface. In this way, the levels of chemokines in the body are prevented from becoming oversaturated thus dampening the ability of cells to respond to signals.

ACKR3 and ACKR4 are two atypical chemokine receptors that are expressed on endothelial cells and keratinocytes in the skin. Here, I have studied their expression on cultured human lymphatic endothelial cells and keratinocytes, and modulation in response to immune stimuli on these cells using a combination of qPCR and immunofluorescent staining. These strategies revealed that ACKR3 and ACKR4 are expressed on cultured LECs and keratinocytes and may be differentially regulated by both cell types in response to inflammatory stimuli including bacterial (LPS) and viral (Unmethylated CpG DNA) signatures. Although chemokine scavenging activity could not be detected on these cells, these findings suggested a role for ACKRs 3 and 4 in the inflammatory response.

Further experiments in vivo explored the expression and modulation of ACKR3/CXCR4 and ACKR4 on epithelial cells including lymphatic endothelial cells, keratinocytes and vascular endothelial cells in the spleen. Flow cytometry was used to examine tissues both at rest and after inflammation (Aldara-mediated psoriasis model, or TPA-mediated contact hypersensitivity model) and investigate the regulation of ACKR3/CXCR4 or ACKR4 in

response to these stimuli. Key findings included the strong overlap and differential regulation of ACKR3 and CXCR4 in response to TPA in the infundibulum subset of keratinocytes.

Additionally, lymph nodes of *Ackr4^{-/-}* mice were significantly enlarged after repeated treatments with Aldara. This appeared to be due to CCL19 dysregulation, but adoptive transfer suggested that there was no defect in leukocyte homing in these mice. This suggested an as yet undetermined response to enhanced CCL19 bioavailability that did not prevent the correct migration of leukocytes to secondary lymphoid organs.

Overall, these experiments suggested that ACKR3 and ACKR4 are modulated in response to several inflammatory stimuli both in vivo and in vitro, and that the modulation of homeostatic chemokines can play a role in the response to inflammatory events. This was particularly important in the context of skin inflammation, where inflammatory chemokines, CXCR4 and ACKR2 have all been implicated in severity and duration of inflammatory events, but few studies have yet described the potential contributions of ACKR3 or ACKR4.

List of Figures

Figure 1-1: Structure of the lymph node.	26
Figure 1-2: Extravasation of a naïve T cell from a high endothelial venule to the lymph node cortex.	31
Figure 1-3: Structure of the spleen.	35
Figure 1-4: Structure of the skin.	40
Figure 2-1: Example genotyping result for <i>Ackr4-gfp</i> reporter mice.	68
Figure 2-2: Flow Cytometry Gating Strategy for Identifying Counting Beads.	73
Figure 3-1: ACKR4 and CCL21 proteins are expressed by cultured HD-LECs.	97
Figure 3-2: ACKR3 protein is expressed by cultured HD-LECs.	98
Figure 3-3: ACKR3 and CXCR4 proteins are expressed by cultured HD-LECs.	100
Figure 3-4: ACKR3, ACKR4 and CXCR4 are mainly expressed intracellularly by cultured HD-LECs.	101
Figure 3-5: ACKR3 and ACKR4 rarely co-localise in HD-LECs.	102
Figure 3-6: ACKR2 and ACKR4 do not co-localise in HD-LECs.	103
Figure 3-7: ACKR2 and ACKR3 rarely co-localise in HD-LECs.	104
Figure 3-8: ACKR3 protein localisation relative to lysosomes in cultured LECs.	105
Figure 3-9: ACKR4 protein localisation relative to lysosomes in cultured LECs.	106
Figure 3-10: ACKR4 co-localises with RAB5+ early endosomes in cultured HD-LECs.	107

Figure 3-11: Cultured human LECs may alter mRNA expression of <i>ACKR4</i> and <i>CCL21</i> in response to inflammatory stimuli.	108
Figure 3-12: Cultured human LECs may alter mRNA expression of <i>ACKR3</i> and <i>CXCL12</i> in response to inflammatory stimuli.	109
Figure 3-13: ACKR4-mediated uptake of CCL19 and CXCL12 by human dermal LECs cannot be detected via flow cytometry.	110
Figure 3-14: Cultured human LECs show no evidence of ACKR4-mediated CCL19 uptake via microscopy.	111
Figure 3-15: Cultured human dermal LECs show no evidence of ACKR4-mediated CCL19 uptake by <i>in vitro</i> scavenging assay.	112
Figure 3-16: Incubation with HiCa media induces morphology changes by cultured human keratinocytes.....	113
Figure 3-17 Basal and differentiated cultured human keratinocytes show differential expression of ACKR4 at the protein, but not the mRNA, level.....	114
Figure 3-18: Cultured human keratinocytes may alter mRNA expression of <i>ACKR4</i> , <i>ACKR3</i> and <i>CXCR4</i> in response to inflammatory stimuli.	116
Figure 3-19: Cultured human keratinocytes show no evidence of ACKR4-mediated CCL19 uptake by flow cytometry.	117
Figure 4-1: eGFP expression in the epidermis of <i>Ackr3^{+gfp}</i> mice is mainly restricted to CD45- cells.....	132
Figure 4-2: Flow cytometry gating strategy for identifying epidermal cell types.	133
Figure 4-3: eGFP is expressed by subsets of CD45- cells in the skin of <i>Ackr3^{+gfp}</i> mice.	134
Figure 4-4: CXCR4 is expressed by keratinocytes, Langerhans Cells and other leukocytes in the epidermis.	135

Figure 4-5: eGFP and CXCR4 are coexpressed by subsets of keratinocytes in <i>Ackr3^{+gfp}</i> mice.....	137
Figure 4-6: ACKR3 mRNA is downregulated and CXCR4 mRNA is upregulated in response to TPA in cultured human keratinocytes.....	139
Figure 4-7: A single topical TPA treatment leads to an increased proportion of leukocytes in both epidermis and dermis.....	140
Figure 4-8: CXCR4 expression in the skin increases 16 hours after a single TPA treatment due to increased proportions of CXCR4 ⁺ cells.....	141
Figure 4-9: Repeated TPA treatments lead to changes in the proportions of epidermal leukocytes and keratinocytes.....	142
Figure 4-10: CXCR4 expression by keratinocytes is increased after repeated TPA treatments.....	143
Figure 4-11: Repeated TPA treatments reduce eGFP expression in the infundibulum of <i>Ackr3^{+gfp}</i> mice.....	144
Figure 4-12: eGFP is widely expressed in the small intestine and colon of <i>Ackr3^{+gfp}</i> mice.....	145
Figure 4-13: eGFP is expressed by LECs and BECs in the mesenteric lymph nodes of <i>Ackr3^{+gfp}</i> mice.....	147
Figure 4-14: eGFP is expressed by stromal cells and MZ B cells in the spleen of <i>Ackr3^{+gfp}</i> mice.....	148
Figure 4-15: ACKR4 protein in the spleen is mainly located on CD31 ⁺ cells in the red pulp.....	149
Figure 4-16: ACKR4 is expressed on vascular endothelial cells in the spleen.....	150
Figure 4-17: Flow cytometry gating strategy to identify DC subsets in the spleen.....	151

Figure 4-18: CD8+ and CD11b+ DCs show similar expression levels of CCR7 and CXCR4.....	152
Figure 4-19: Anti- DCIR2 and CD205 antibodies identify distinct populations of cells in the spleen.....	153
Figure 5-1: Pilot of Aldara model on mouse back skin shows a limited inflammatory phenotype.....	165
Figure 5-2: Expression of <i>Ackr4</i> and related genes is largely stable up to 24 hours after a single Aldara treatment.....	166
Figure 5-3: Expression of <i>Ackr4</i> , <i>Ackr3</i> and related genes show variable responses to multiple Aldara treatments.....	167
Figure 5-4: Keratinocytes in the ear skin of Aldara-treated mice show no alteration in proliferation in the absence of <i>Ackr4</i>	169
Figure 5-5: Number, but not size, of B cell follicles is increased in the ear DLN following Aldara treatment.....	171
Figure 5-6: Flow cytometry gating strategy to identify lymphocyte subsets in the skin-draining lymph nodes.....	172
Figure 5-7: Overall cellularity and number of B, T and resident dendritic cells are increased in ear DLN of <i>Ackr4</i> -null mice, compared to WT, in response to Aldara treatment.....	174
Figure 5-8: Bioavailable CCL19 levels are increased in plasma and ear skin of <i>Ackr4</i> -null mice, compared to WT, after Aldara treatment.....	176
Figure 5-9: Migratory DCs are reduced in the ILN of <i>Ackr4</i> -null mice, compared to WT, after Aldara treatment.....	177
Figure 5-10: Mesenteric lymph node cellularity is not differentially affected in <i>Ackr4</i> -null mice, compared to WT, after Aldara treatment.....	178

Figure 5-11: Overall cellularity and B cell numbers are increased in <i>Ackr4</i> -null mice, compared to WT, after Aldara treatment.	179
Figure 5-12: Blood of <i>Ackr4</i> -null mice contains more circulating B cells than in WT mice following Aldara treatment.	180
Figure 5-13: Optimisation of Adoptive B Cell Transfer Protocol.	181
Figure 5-14: After adoptive transfer of CD45.1+ splenocytes, <i>Ackr4</i> -null mice have reduced numbers of donor cells in the blood, compared to WT, following Aldara treatment.....	182
Figure 5-15: Mice lacking both <i>Ackr4</i> and <i>Ccl19</i> transcripts show no difference in ear DLN cellularity, compared to WT, in response to Aldara treatment.	184
Figure 6-1: Proposed model for ACKR3/CXCR4-mediated TPA responses in keratinocytes.....	191
Figure 6-2: Summary of differential responses to five daily Aldara treatments between wild-type and <i>Ackr4</i> ^{-/-} mice.....	195

List of Tables

Table 2-1: Immune stimuli used for cultured human cells.....	61
Table 2-2: Details of Cutaneous Treatments	69
Table 2-3: List of Antibodies Used for Immunofluorescent Staining.....	71
Table 2-4: List of Antibodies Used for Flow Cytometry	73
Table 2-5: List of recombinant chemokines used	76
Table 2-6: List of TaqMan probes used	78

Abbreviations

A

ACKR - Atypical Chemokine Receptor

AF - Alexa Fluor

Ag - Antigen

APC - Allophycocyanin

APC - Antigen Presenting Cell

AU - Arbitrary Units

B

BB – Basal Bulge

BCR – B Cell Receptor

BEC - Blood Endothelial Cell

BM - Bone Marrow

BMDC - Bone Marrow-derived Dendritic Cell

BSA - Bovine Serum Albumin

BV - Brilliant Violet

C

CCL - CC Chemokine Ligand

CCR - CC Chemokine Receptor

CD - Cluster of Differentiation

cDC - Classical Dendritic Cell

cDNA - Complimentary
Deoxyribonucleic Acid

CXCL - CXC Chemokine Ligand

CXCR - CXC Chemokine Receptor

Cy – Cyanine

D

DC - Dendritic Cell

DKO - Double Knockout

DLN - Draining Lymph Node

DN - Double Negative

DTT – Dithiothreitol

E

ECL - Enhanced Chemoluminescence

ECM – Extracellular Matrix

EDTA - Ethylenediaminetetraacetic Acid

eGFP - Enhanced Green Fluorescent
Protein

ELISA - Enzyme-linked Immunosorbent Assay

F

FACS - Fluorescence Activated Cell Sorting

FBS/FCS - Foetal Bovine/Calf Serum

FDC – Follicular Dendritic Cell

FITC - Fluorescein Isothiocyanate

FRC - Fibroblastic Reticular Cell

FSC - Forward Scatter

G

GAPDH – Glyceraldehyde 3-Phosphate Dehydrogenase

GFP - Green Fluorescent Protein

GM-CSF - Granulocyte Macrophage Colony Stimulating Factor

GPCR - G-Protein Coupled Receptor

H

HBSS - Hanks Balanced Salt Solution

HD-LEC - Human Dermal Lymphatic Endothelial Cell

HF – Hair Follicle

HiCa - High Calcium

I

IE – Interfollicular Epidermis

IF – Immunofluorescence

IF – Infundibulum

IFN - Interferon

IHC - Immunohistochemistry

ILN - Inguinal Lymph Node

IM – Isthmus

IMQ - Imiquimod (1-(2-methylpropyl)-1*H*-imidazo[4,5-*c*]quinolin-4 amine)

K

KGF - Keratinocyte Growth Factor

KO – Knockout

L

LC - Langerhans Cell

LEC - Lymphatic Endothelial Cell

LN - Lymph Node

LoCa - Low Calcium

LPS – Lipopolysaccharide

M

mAb – Monoclonal Antibody

mDC - Migratory Dendritic Cell

MLN - Mesenteric Lymph Node

MMM – Marginal Metallophilic
Macrophage

mRNA - Messenger Ribonucleic Acid

MZ – Marginal Zone

MZM - Marginal Zone Macrophage

N

nHEK – Normal Human Epidermal
Keratinocyte

NK – Natural Killer

P

pAb – Polyclonal Antibody

PAGE - Polyacrylamide Gel
Electrophoresis

PALS – Periarteriolar Lymphoid Sheath

PAMP – Pathogen Associated Molecular
Pattern

PBMC – Peripheral Blood Mononuclear
Cell

PBS - Phosphate Buffered Saline

PBS/T - Phosphate Buffered Saline /
Tween-20

PCR – Polymerase Chain Reaction

PE - Phycoerythrin

PerCP - Peridinin Chlorophyll

pDC - Plasmacytoid Dendritic Cell

Q

qPCR - Quantitative Polymerase Chain
Reaction

R

RBC - Red Blood Cell

rDC - Resident Dendritic Cell

RP – Red Pulp

RT-PCR - Reverse Transcription
Polymerase Chain Reaction

RQ - Relative Quantification

S

SB – Suprabasal Bulge

SCS - Subcapsular Sinus

SD - Standard Deviation

SDS - Sodium Dioecyl Sulphate

SLO – Secondary Lymphoid Organ

SSC - Side Scatter

Sva - Streptavidin

T

TBP – TATA Box Binding Protein

TCR - T Cell Receptor

T_{FH} – Follicular Helper T Cell

TGF - Transforming Growth Factor

TLR - Toll-Like Receptor

TPA -12-O-Tetradecanoylphorbol-13-acetate

W

WP – White Pulp

WT - Wild-type

Chapter 1: Introduction

1 Introduction

1.1 General Introduction

The vertebrate immune system is composed of a complex interplay of highly specialised molecules, cells and organs. These interactions have been finely tuned over millions of years of evolution to form an essential part of the body's defence against external threats, such as pathogens and parasites. Cells of the immune system also maintain the body's integrity, destroying unfit or aberrant cells, helping to repair damaged tissues and preventing the formation of cancers. A fine balance is required for an effective immune system, as it must mount a robust response to any threat, without overreacting and attempting to destroy beneficial antigen. This extends to the body's own tissues (central tolerance), and to foreign antigen such as commensal bacteria or ingested food (peripheral tolerance). When tolerance breaks down, it can lead to severe autoimmune disorders; This highlights the incredibly sensitive nature of the immune system, where every aspect must be held in check.

The immune system of vertebrates is classified into two branches: the innate and the adaptive. The innate immune system is generally the first line of defence and is applicable to a broad range of threats. It relies on the recognition of specific molecules associated with foreign microorganisms and damaged tissues. These are known as pathogen-associated molecular patterns (PAMPs) and damage-associated molecular patterns, respectively, and are recognised by specific receptors known as pattern-recognition receptors (PRRs). These can be either membrane bound or cytoplasmic; membrane-bound PRRs include Toll-like Receptors (TLRs) and C-type Lectin Receptors. Upon ligand binding, PRRs initiate cellular defence mechanisms, which can include directly destroying damaged or infected cells via phagocytosis or induced apoptosis, or by secreting signals that attract other cells to the site to aid the immune response. The innate immune system can respond to threats extremely quickly; however, it is not always sufficient to clear infections and the adaptive immune system is required at this point.

The adaptive immune system is considerably slower to respond when a new threat is encountered, and generally has a lag phase of at least 2-3 days. Once immunity against an antigen is gained it is long-lasting, leading to a swift and specific response against any future infections by the same pathogen. Innate and adaptive immune systems can be linked by specialised cells, usually called innate-like cells, or by direct interactions between cells

of the innate and adaptive immune systems. Professional antigen-presenting cells (APCs) are a key class of cells that act as a link between innate and adaptive immune systems. APCs can be tissue-resident or migratory and possess PRRs on their surfaces, allowing them to recognise PAMPS and in turn activate molecular pathways that cause them to become 'mature' APCs capable of heightening the immune response. APCs continually sample antigen from their environment; these are processed into epitopes, short peptides that are displayed on the cell surface by Major Histocompatibility Locus Class II (MHC-II) molecules. Once this occurs, the APC is activated by upregulating specific proteins and receptors that allow it to migrate to a secondary lymphoid organ (SLO) and to interact directly with T cells to activate the adaptive immune response. This generates short-lived effector cells that can fight infection both directly and indirectly; for example, by releasing cytotoxins to destroy infected cells, or by secreting cytokines to activate other immune cells to clear a threat. Some effector cells give rise to memory cells that persist in the body for the remaining lifespan of the individual. These cells are capable of rapidly dividing to produce more effector and memory cells when they contact cognate antigen, meaning pathogens that have been encountered previously can be destroyed quickly.

Cell migration is a central requirement for immunity. Although the local microenvironment at the site of infection or tissue damage can often contribute to the resolution of trauma, or create preventative barriers against external threats, this is not sufficient to protect the organism from invasion by pathogens. Immunity requires a suite of specialised cells that can be rapidly deployed to a specific anatomical location when they are required. In addition, cell migration is essential for immunity even when the body is not undergoing a specific immune challenge: the development of the immune system requires precise spatial and temporal positioning of cells, and the selection processes that B and T leukocytes undergo during their maturation are also dependent on cell migration. Furthermore, cell migration is key to the processes of immune surveillance and tolerance.

Cell migration can be induced by the secretion of small cytokines called chemokines, which induce effects that can also include cell proliferation, survival and adhesion. Chemokines induce migration in responding cells via their chemokine receptors. Chemokine availability can be modulated by a class of proteins called Atypical Chemokine Receptors (ACKRs). The four confirmed members of this family are known as 'scavenging' receptors due to their ability to clear specific chemokines from the local environment or transport them across endothelial barriers. This provides a further layer of regulation to the immune system, where cell migration can be fine-tuned by cells at the site

of inflammation. Chemokines, chemokine receptors and atypical chemokine receptors will be discussed in depth later (See sections 1.5, 1.6, and 1.7).

1.1.1 Innate Immunity

The first wave of the inflammatory response is initiated by the innate immune system. This can be in response to a detected pathogen or to tissue damage and contributes to the typical redness and swelling seen at sites of infection or wounding. Tissue-resident macrophages and stromal cells of the affected tissue can both secrete cytokines including chemokines, and other inflammatory stimuli, to promote leukocyte recruitment to the site of infection or wounding. The first cells to arrive are typically neutrophils. These are highly mobile cells that are mainly found in the bloodstream. They are phagocytes, so are capable of directly engulfing infected or damaged cells and bacteria, and can also secrete granules and chromatin which coalesce to form neutrophil extracellular traps, structures that can engulf and destroy bacteria ¹. as well as secreting a host of cytokines including chemokines to attract further cells to the site ². Monocytes from bone marrow are also early recruits to the site of infection or inflammation and can differentiate into macrophages and classical dendritic cells (cDCs) once in the tissue. Macrophages, as their name suggests, are large phagocytic cells, but can also aid the immune response by secreting inflammatory stimuli. Although they are professional phagocytes, macrophages are also capable of presenting antigen to T cells via MHC-II molecules ³, providing a bridge between innate and adaptive immunity.

This gap is also crossed by innate-like cells, which possess features of both innate and adaptive arms of the immune system. These include $\gamma\delta$ T cells, natural killer (NK) T cells, marginal zone (MZ) B cells, and B1 B cells ⁴. Although these cells possess B or T cell receptors (BCR and TCR, respectively), they do not undergo the same processes of recombination that lead to the diverse suite of antigen B and T cells are typically capable of recognising. Instead, they recognise specific antigen defined by the B or T cell receptor variant(s) they express ⁴. Upon antigen recognition, these cells can often carry out similar functions to B or T cells, including secreting antibodies and cytokines, but do not require activation by other cells, so can mount a response much more quickly ⁴.

1.1.2 Adaptive Immunity

There are two types of lymphocyte central to the adaptive arm of the immune system, both of which are derived from haematopoietic stem cells in the bone marrow: B cells, which remain in the bone marrow to complete their maturation, and T cells, which migrate to the thymus to finish their development. On maturation, both B and T cells migrate to populate SLOs. At this stage, they are known as naïve cells, as they have not yet contacted their cognate antigen. Once this occurs, they are activated and will upregulate specific proteins and receptors as well as proliferating to increase the population of cells that can recognise the specific antigen and differentiating into effector cells that carry out specific functions; this varies depending on the type of cell and the subset it belongs to. B and T cells can generally be found circulating through secondary lymphoid organs (SLOs) seeking their cognate antigen, and the main routes to their activation in the SLOs will be discussed below (See section 1.2.2).

1.2 Lymph Nodes

1.2.1 Structure and Function

The lymph nodes are key SLOs that play a vital role in immune surveillance and response. Lymph nodes are small nodular organs that form as outgrowths of the lymphatic network and are located at multiple sites throughout the body. The main benefit of the lymph nodes is in providing a site where rare lymphocyte populations can meet, and where resident cells can sample blood and lymph circulation for antigen. The structure of the lymph node reflects this purpose, as it funnels the flow of lymph through the node via a complex labyrinth of channels interspersed with lymphocyte-rich regions, maximising contact between tissue-resident cells and the lymph.

Structurally, the lymph node consists mainly of an outer capsule, a vascular medullary region and an inner cortex, which consists of a densely packed collection of lymphocytes (Figure 1-1). Interspersed with the cortex is a network of sinuses lined with lymphatic endothelium, which allows lymph to flow through the node past the cortex, converging at the medulla before leaving the lymph node via efferent lymphatics ⁵.

The sinus immediately beneath the capsule is called the subcapsular sinus (SCS), and this is the first space cells and antigen will reach on entering the lymph node via the afferent lymph. Proximal to the capsule, the cortex contains B cell follicles with germinal centres where clonal proliferation can occur. The SCS is lined with lymphatic endothelial cells (LECs) and SCS macrophages. The latter are characterised by CD169 expression and play an important role as a biological barrier against pathogens arriving at the lymph node via the afferent lymph ⁶.

The SCS drains into the intermediary sinuses allowing lymph to flow past the B cell follicles through the lymphatic labyrinths, loosely-packed networks of lymphatic endothelium and reticulum supporting a network of fibroblastic reticular cells (FRCs) and lymphocytes, largely T cells and macrophages ⁵. The FRCs form a system called the lymphatic conduits, which lymph and small molecules (<4 nm) can flow through ⁷. The conduits originate at the SCS and are interspersed throughout the cortex. They are formed largely from bundles of collagen fibres secreted by FRCs; the FRCs wrap around these to form a matrix of interconnected tubules. Lymph node resident DCs can sample lymph through small gaps between neighbouring FRCs ⁸.

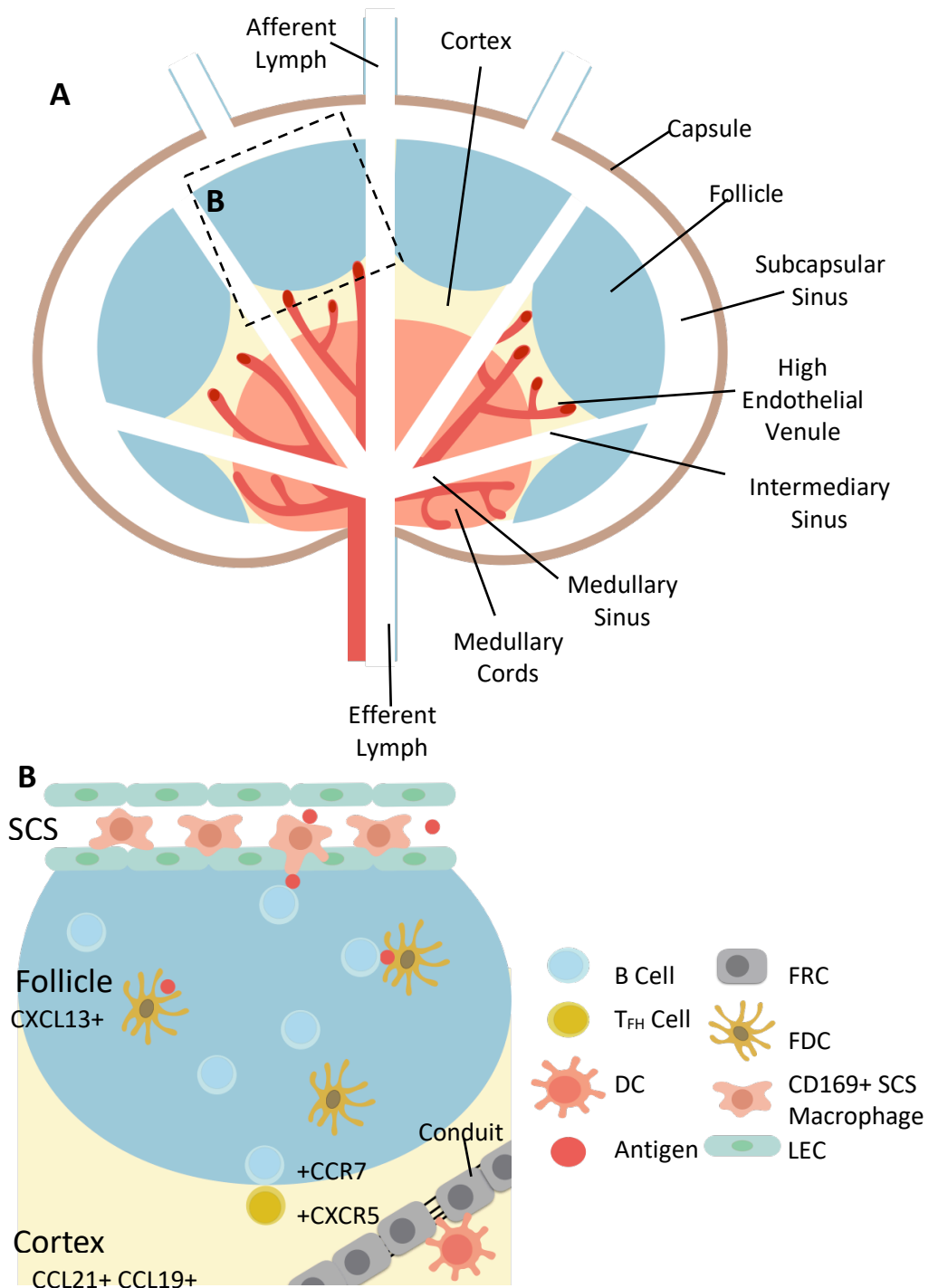


Figure 1-1: Structure of the lymph node.

A) Diagram representing the main anatomical features of the lymph node **B)** Detailed view of the highlighted region in A. CD169⁺ SCS macrophages within the afferent lymph capture antigen complexes, which are transported to FDCs by B cells. Upon antigen recognition, B cells upregulate CCR7 to approach the CCL21⁺ CCL19⁺ cortex. Meanwhile, the activated TFH cell has upregulated CXCR5 to approach the CXCL13⁺ follicle. Also shown is a conduit, formed from FRCs wrapped around extracellular matrix fibres to form spaces where lymph carrying small molecules can flow. A tissue resident DC samples the lymph in a space between two FRCs

Finally, the lymphatic flow will reach the medulla, a region rich in blood vessels and containing mainly lymphocytes in the process of leaving the lymph node. There are also

cortical regions interspersed between the medullary sinuses known as the medullary cords. These contain mainly macrophages, plasma cells and small populations of DCs. The medullary sinuses are lined with a single layer of lymphatic endothelium, allowing cells to migrate between the sinuses and the cortex⁵. Also found within the medullary region are SIGIRR1+ medullary macrophages, which continually sample the lymph and phagocytose pathogens that have been able to pass through the lymph node. They also clear dead or apoptotic lymphocytes from the medullary region, particularly following an immune response⁹ or to maintain tolerance¹⁰.

1.2.2 Overview of the Immune Response

1.2.2.1 T Cell Activation

All T cells express a TCR on their surface. The TCR is part of the immunoglobulin superfamily, and each is able to recognise a MHC class I or II molecule bearing a specific peptide. TCRs exist as heterodimers; most T cells bear TCRs composed of α and β chains, but a small subset of T cells have γ and δ chains and are known as $\gamma\delta$ T cells. They are functionally unique among T cells and will be discussed separately (See section 1.4.3). In addition to TCRs, mature T cells express either CD4 or CD8 molecules on their surface. These are both transmembrane glycoproteins that act as co-receptors for the TCR, recognising domains of the MHC-II and MHC-I molecules, respectively.

Mature naïve T cells mainly circulate through the lymphatic system, residing in each lymph node for 12-24 hours, then continuing their migration if they do not contact cognate antigen. Once in the cortex, T cells are constantly in motion seeking a DC bearing their cognate antigen. Although this migration can appear to be random, intravital imaging experiments have shown that T cells are in direct contact with FRCs over 90% of the time¹¹. FRCs are known to secrete the chemokines CCL19 and CCL21¹² which control the migration of naïve T cells and activated DCs, attracting them to the cortex¹³; these cells also secrete IL-7 to promote the survival of T cells and activated DCs¹². This suggests that the FRC conduit system plays a key role not only in transporting molecules to the cortex, but in supporting the function and survival of naïve T cells and activated DCs.

T cells can only recognise antigen when it is bound to an MHC molecule. In the case of a CD4+ naïve T cell, this will be a MHC-II molecule on the surface of a professional APC such as a DC. Because the TCR has a low affinity for its target, activated DCs express the

co-stimulatory molecules CD80 and CD86 which interact with CD28 on the T cell's surface to promote activation and survival. DCs also express the adhesion molecule ICAM-1 which binds to the integrin LFA-1 on the T cell's surface to allow for close cell-cell contact, enhancing T cell activation and survival ^{14,15}.

Once activated by this method, the naïve CD4+ T cell becomes a mature follicular helper T (T_{FH}) cell, which will upregulate CXCR5 ¹⁶ and downregulate CCR7 ¹⁷ in order to migrate towards the B cell follicle. Chemokine receptor expression alone is not sufficient to induce T cell migration into follicles, suggesting a role for further factors such as adhesion molecules ¹⁸.

DCs can also present exogenous antigen to naïve CD8+ T cells on MHC-I molecules. This is known as cross-priming, and has been shown to be restricted to a CD8+ subset of DCs ¹⁹. Cross-priming allows the adaptive immune system to detect antigen that cannot be displayed on MHC-II molecules, for example pathogens that hide within infected cells. It also means that infected DCs could still present the antigen to a naïve CD8+ T cell.

DC-T cell interactions do not always lead to an active immune response; they are also involved in generating and maintaining peripheral tolerance to self and harmless antigen. As DCs are constantly sampling antigen from their environment via endocytosis, this will regularly include harmless or self-antigen. In the absence of inflammatory signals such as pro-inflammatory cytokines and TLR ligands that indicate infection or tissue damage, a DC will process and present epitopes without becoming activated ²⁰. When an immature DC presents antigen to a T cell, depending on its lineage the T cell may be targeted for apoptosis or anergy, or develop into a mature regulatory T cell (Treg) ²¹. Although Tregs are largely generated in the thymus during the development of central tolerance ²², their induction by immature DCs ensures that there is a mechanism for the removal of self-reactive cells that escaped from the thymus, and for preventing overreaction to benign antigen that is encountered later in life.

1.2.2.2 B Cell Activation

Naïve B cells are most commonly found in lymph node follicles, although similarly to T cells they continually circulate between SLOs via blood and lymph. Upon maturation, B cells upregulate CXCR5, the receptor for the chemokine CXCL13. Also known as B-Lymphocyte Chemoattractant, CXCL13 is strongly expressed by FDCs in the lymphoid

follicles which leads to naïve B cells homing from the bone marrow to the lymph nodes¹⁸. FDCs also secrete B cell activating factor (BAFF) to promote B cell survival⁹, and are required for B cell survival and retention in follicles and germinal centre formation²³. In turn, B cells express lymphotoxin $\alpha_1\beta_2$, which promotes the survival and CXCL13 expression of FDCs²⁴.

Opsonised antigen (that bound to factors which enhance phagocytosis, e.g. antibodies or C3b complement) is normally presented to follicular B cells by FDCs which capture opsonised antigen complexes on extracellular receptors. There is evidence that SCS macrophages play a role in transporting these antigen complexes from the afferent lymph to follicles by capturing antigen and extending processes into the follicle to present it to B cells, which in turn transport the antigen to FDCs^{25,26}. In the case of non-opsonised antigen, SCS macrophages can also present directly to the cognate B cell⁹.

B cell migration within the follicle is dependent on each cell's ability to respond to chemokines and other migratory signals in the lymph node microenvironment. While naïve B cells are highly CXCR5+, responding to CXCL13 signals to remain in the follicle as described above, they also express Epstein-Barr Virus induced molecule-2 (EBI2), a G-protein coupled receptor (GPCR) that binds to 7α , 25-dihydroxycholesterol (7α , 25-OHC). EBI2 signalling is thought to attract B cells to the extrafollicular regions²⁷. Naïve B cells also express low levels of CCR7, allowing them to respond weakly to CCL19 and CCL21 and migrate towards the T cell zone. It is thought that balancing these migratory signals allows B cells to circulate throughout the follicle, seeking cognate antigen on FDCs or SCS macrophages²⁸.

Upon encountering its cognate antigen, a B cell requires an interaction with an activated T_{FH} cell to become activated itself. This means B cell responses rely on the ability of the antigen-bearing B cell and activated T_{FH} cell to find one another within the vast cellular milieu of the lymph node. Cell migration plays a key role in this interaction. After binding its cognate antigen, the B cell processes it to generate a peptide, which it presents on its surface via MHC-II. The cell also alters its chemokine receptor expression profile, upregulating CCR7 to respond more strongly to CCL19 and CCL21 in the cortex^{17,29}. Concurrently, the corresponding activated T_{FH} cell will alter its own expression profile as described above, upregulating CXCR5 and downregulating CCR7¹⁶ to allow both cell types to migrate to the boundary between the follicle and cortex where they can interact³⁰.

On formation of the MHC-II-antigen-TCR complex between the cells, the T_{FH} cell can perform a wide range of functions to support B cell activation, survival and development of effector cells³¹. One example is the protein CD40L, expressed on the surface of the T_{FH} cell, which binds to CD40 on the surface of the B cell and acts as a co-stimulatory molecule promoting B cell proliferation³¹. T_{FH} cells can also secrete cytokines or chemokines to aid the activated B cell³¹.

Upon activation, B cells upregulate CXCR4 and then can undergo one of two main fates: they can upregulate EBI2, allowing them to migrate to the edge of the follicle where they differentiate into short-lived plasmablasts, which then leave the follicle by migrating towards S1P in the circulation (See section 1.2.2.3) and CXCL12 (the ligand for CXCR4) in the bone marrow or splenic red pulp; or they can downregulate EBI2³² and migrate to the centre of the follicle, which is CXCL12+, to form the germinal centre dark zone³³ and give rise to long-lasting immunity via plasma cells and memory B cells²⁷.

During germinal centre formation, the antigen-binding site of the BCR undergoes somatic hypermutation to rapidly diverge; this will lead to some B cell clones with higher affinity for the target antigen which are promoted in a process of affinity maturation. Activated B cells are short-lived but differentiate to both expand their own population and to produce plasma cells and memory B cells. Plasma cells have extensive labyrinths of endoplasmic reticulum, allowing them to secrete antibodies on a vast scale. While most plasma cells are the short-lived plasmablasts, memory B cells can often survive for the lifespan of the organism, conferring long-lasting immunity by rapidly proliferating and differentiating to produce more plasmablasts if reinfection occurs.

1.2.2.3 Ingress and Egress of Lymphocytes

High endothelial venules (HEVs) are specialised blood vessels that allow the ingress of lymphocytes to the cortex of the LN (Figure 1-2). In skin-draining LN, lymphocytes expressing L-selectin on their surfaces bind to these endothelial cells, which express Peripheral Lymph Node Addressin (PNAd). This leads to a weak adhesion of the lymphocyte to the vessel wall, initiating a phase known as rolling where the cell continues to move with the blood flow, but is slowed and closely associated with the vascular endothelial cells. At this stage, chemokines bound to glycosaminoglycan (GAG) molecules on the surface of the endothelial cells bind to chemokine receptors on the lymphocyte

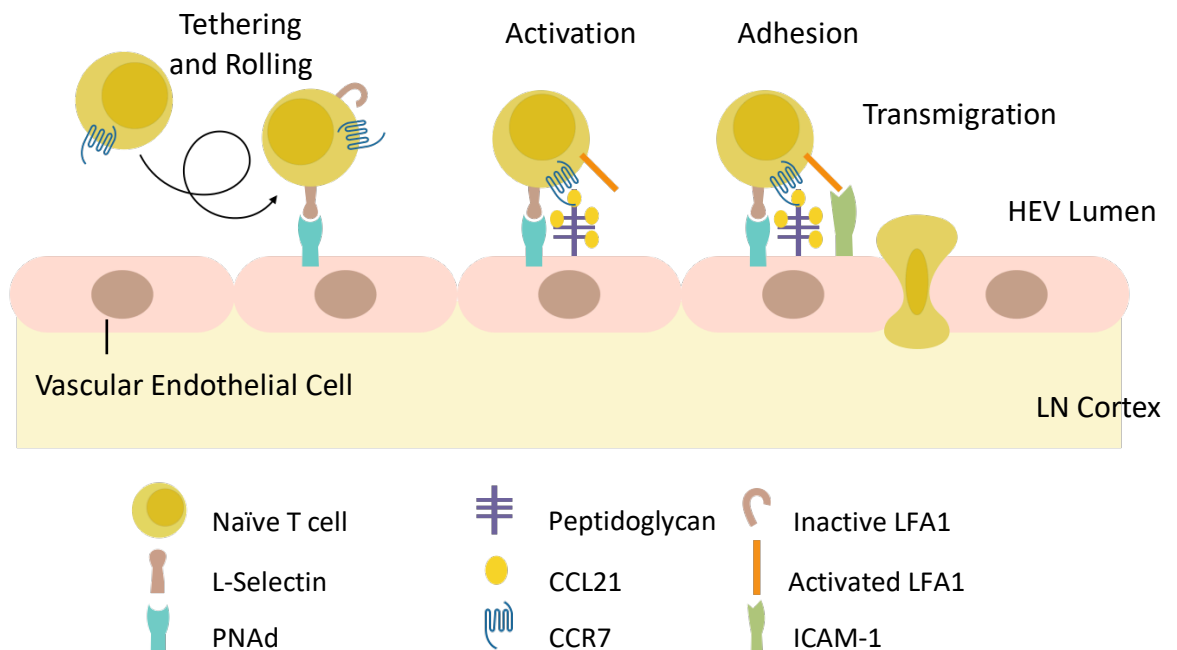


Figure 1-2: Extravasation of a naïve T cell from a high endothelial venule to the lymph node cortex.

The T cell becomes **tethered** to the endothelium via L-selectin and PNAd binding, begins the **rolling** process and is able to recognise CCL21 immobilised on a GAG side-chain of a peptidoglycan molecule expressed on the surface of the endothelial cells. CCL21 signalling via CCR7 on the T cell **activates** the integrin LFA1 on the surface of the T cell, allowing it to bind with ICAM-1 on the endothelial cell, leading to **adhesion** followed by **transmigration** into the lymph node cortex.

surface leading to the activation of integrins expressed on the lymphocyte's surface including leukocyte function-associated antigen 1 (LFA1). This binds to intercellular adhesion molecule-1 (ICAM-1) on the surface of the endothelium, leading to the firm adhesion of the lymphocyte to the endothelial wall. The cell can now extravasate by either migrating between or across the cells of the endothelium³⁴. Although this is the mechanism by which cells migrate to the skin draining lymph nodes, the specific cell adhesion molecules, selectins, integrins and addressins vary in lymph nodes of the mucosa; additionally, different chemokines are required to attract different lymphocyte populations.

Sphingosine-1-Phosphate (S1P) is a sphingolipid signalling molecule that plays a crucial role in lymphocyte egress from the lymph nodes. Lymphocytes express receptors for S1P, most commonly S1P₁, which is essential for lymphocyte egress from lymph nodes mature T cell egress from the thymus³⁵. High levels of S1P are present in the blood, while lymph nodes and other SLOs are low in S1P due to the activity of the enzyme S1P lyase, which degrades S1P³⁶. The accepted model for S1P₁/S1P activity holds that lymphocytes migrate towards S1P chemotactically, but exposure to high levels of S1P in the blood or lymph

leads to receptor desensitisation, meaning the cells are temporarily unresponsive to S1P allowing them to enter areas of low S1P abundance such as the lymph nodes. Once receptor turnover is complete, cells become responsive to S1P again and egress from the lymph node³⁷, as signals from S1P override other chemotactic signals from chemokines within the lymph node³⁸. Under inflammatory conditions, particularly IFN signalling, S1P₁ expression is negatively regulated by the CD69 receptor on lymphocytes, meaning they are retained in the lymph nodes³⁹.

1.2.3 Lymph Node Development

Lymph node development occurs during embryogenesis and involves signalling between stromal organiser cells at the site of the future lymph node, which eventually give rise to the stromal cell populations of the tissue, and cells derived from haematopoietic precursors called lymphoid tissue inducer (LTi) cells. The initial LTi progenitors are recruited from the foetal liver to the site of future lymph nodes by the chemokines CXCL13 and CCL21 expressed by the stromal organiser cells⁴⁰. Upon arrival at the future lymph nodes, LTi cells promote lymph node development by signalling to the stromal organiser cells via lymphotoxin- $\alpha_1\beta_2$ (LT $\alpha_1\beta_2$), a member of the tumour necrosis factor (TNF) superfamily. Stromal organiser cells express the receptor for LT $\alpha_1\beta_2$, Lymphotoxin- β Receptor (L β R), and ligand binding leads to differentiation, enhanced expression of cellular adhesion molecules and the chemokines CCL19, CCL21 and CXCL13 by the stromal cells⁴¹. These chemokines are crucial for correct lymph node development, as mice which lack all three chemokines had severe disruptions in lymph node formation, although MLN appeared to be unaffected⁴².

Stromal cells are also induced to express Receptor activator of nuclear factor kappa-B ligand (RANKL) and interleukin-7 (IL-7), both of which induce further LT $\alpha_1\beta_2$ expression by LTi cells⁴³. The receptors for these factors on LTi cells, Receptor activator of nuclear factor kappa-B (RANK) and interleukin-7 receptor (IL-7R), respectively, are essential for LN development^{44,45}.

Retinoic acid signalling has also been shown to play a role in lymph node formation; LTi cells express the retinoic acid receptor, ROR γ t, and require it for their identity as LTi cells⁴⁶. RA is also essential for stromal organiser cells to express CXCL13 to attract LTi cells; nerve fibres near the stromal organiser cells are positive for RALDH2, the enzyme

required to synthesise RA, suggesting the nerve fibres are the source of RA signalling that initiates LTi cell recruitment ⁴⁰.

1.3 Spleen

1.3.1 Structure and Function

The spleen is the largest of the SLOs, and is the key site of immune surveillance of the blood for pathogens, particularly by macrophages, which are continually replenished by a large reservoir of monocytes constituting more than half of the monocytes in the body⁴⁷. The spleen is also host to significant populations of T cells, B cells and dendritic cells. Unlike other SLOs, the spleen is not part of the lymphatic network, and cells must migrate to and from the spleen from the blood circulation via splenic arterioles and venules.

Histologically, the spleen is composed from two main tissue types: the red pulp and the white pulp. Red pulp regions are rich in microvasculature; white pulp regions, which form around the termini of the larger splenic arterioles, are where the majority of lymphocytes are located.

1.3.1.1 *White Pulp*

The architecture of the splenic white pulp is broadly comparable with that of the lymph node (Figure 1-3). Adjacent to the arteriole is the periarteriolar lymphoid sheath (PALS), composed mainly of T cells, similar to the lymph node cortex. Towards the periphery of the white pulp are the B cell follicles, which contain the majority of FO B cells in the spleen. The whole white pulp region is bordered by the marginal zone, which has some similarities to the subcapsular sinus in the lymph node as it is lined with CD169+ macrophages, known as marginal metallophilic macrophages (MMM). There is also an outer ring of SIGNR1+ marginal zone macrophages (MZM) in the marginal zone. In between lies the marginal sinus. In rodents, this area is connected to the circulation, allowing blood-borne cells and antigen to directly enter the white pulp. The ring of MMMs also contains gaps, known as bridging channels, that allow leukocytes to enter and exit the PALS via the marginal sinus⁴⁸.

There is much similarity between the structure of the T cell zones and B cell follicles of the white pulp compared to those of the lymph node. T cell zones are home to mainly naïve T cells and DCs, interspersed with a network of conduits formed by FRCs that transport small molecules from the marginal zone to the PALS. B cell follicles are interspersed with

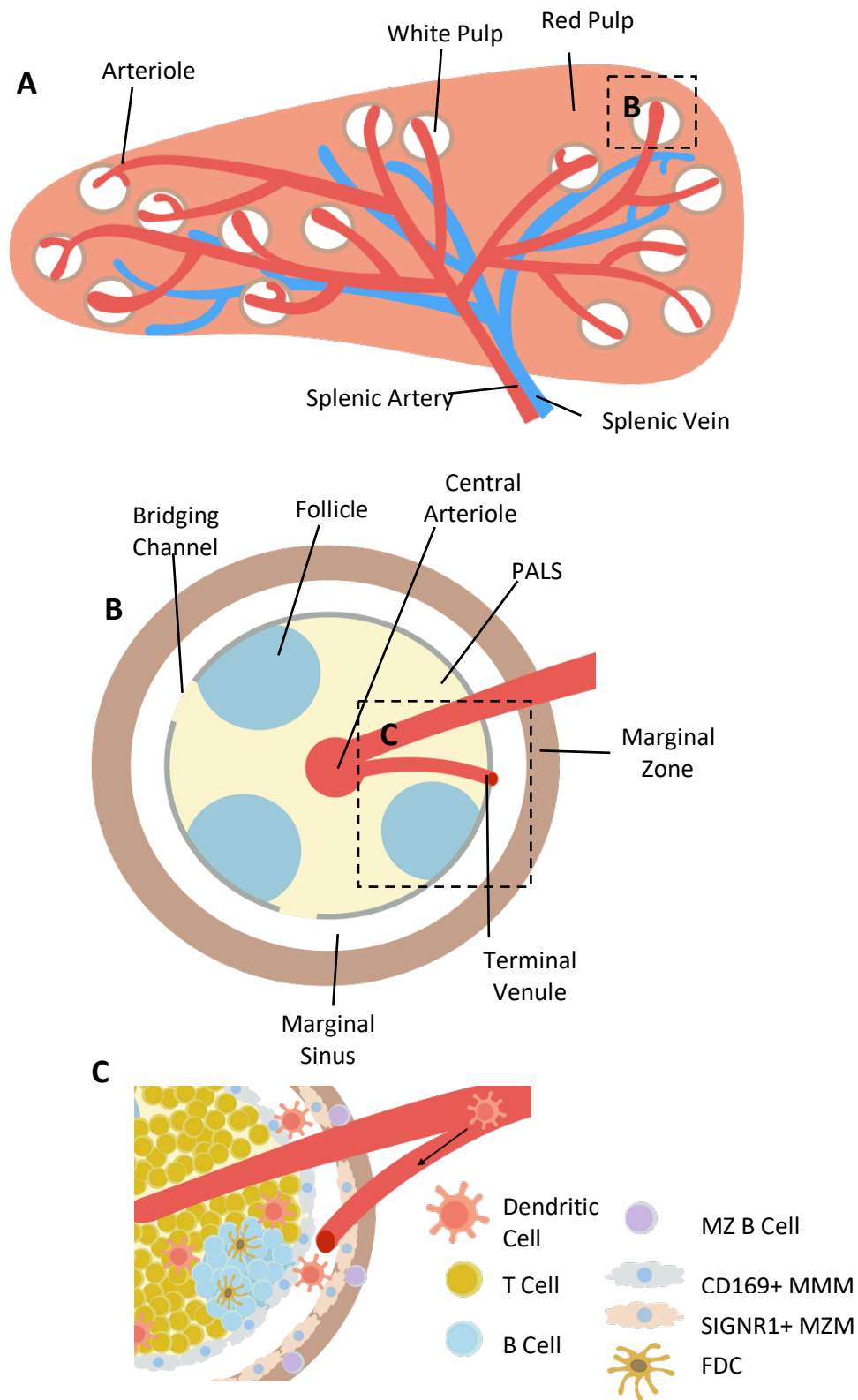


Figure 1-3: Structure of the spleen.

A) Overview of the main anatomical features of the spleen. **B)** detailed view of the highlighted region in **A**, showing the arrangement of the splenic white pulp and marginal zone. **C)** detailed view of the highlighted region in **B**, showing the B cell follicles with FDCs, T cell areas with associated DCs, and DCs entering the marginal sinus via a terminal venule. The marginal sinus is bordered by MMMs towards the white pulp, and MZMs towards the red pulp. In the marginal zone reside the MZ B cells.

FDCs that present antigen to B cells and secrete CXCL13 that maintains their localisation in the follicle. CCL19 and CCL21 expressed by endothelial cells lining the splenic venules are required for T cell and DC localisation in the PALS^{17,49}.

1.3.1.2 *Marginal Zone*

The marginal zone can be considered an intermediate tissue type in between red and white pulp. It is a specialised network of macrophages, B cells, FRCs and endothelial cells that are involved in the surveillance of blood arriving via terminal venules⁴⁸. The key populations of cells unique to the marginal zone are MMMs, MZMs and MZB cells.

MMMs are located closest to the white pulp. Similar to CD169+ macrophages in the SCS of the lymph node, they interact closely with B cells in the follicles. CD169 (SIGLEC-1) binds to sialic acid, potentially using this as a mechanism for capturing pathogens expressing these residues on their surfaces⁴⁸. They produce high levels of IFN- α and β in response to viral challenge⁵⁰.

MZMs are highly phagocytic and are characterised by their expression of scavenging receptors including MARCO and SIGNR1. One key role for these cells is in detecting and phagocytosing apoptotic cells that enter the spleen from the blood. They also play a role in clearing viruses and polysaccharide antigen, as well as clearing important bacterial pathogens including *Mycobacterium tuberculosis* and *Streptococcus pneumoniae*⁴⁸. MZMs also express high levels of IFN- α and β , though not as large a quantity as MMMs⁵⁰.

MZ B cells are the final key population of the marginal zone. They are innate-like B cells, meaning they express an invariant BCR rather than the extreme BCR heterogeneity shown by follicular (FO) B cells. MZ B cells also distinguish themselves from FO B cells by responding directly to cognate antigen detected in the blood without the requirement for activation by a helper T cell. MZ B cells play a key role in inducing T-cell independent immune responses⁵¹. Interestingly, MZ B cells are also capable of priming CD4+ T cells in the white pulp⁵². MZ B cell localisation appears to rely on a combination of CXCL13 and S1P signalling, as FTY720 leads to MZ B cell migration into the white pulp, while this response is not present in CXCL13-null mice⁵³. Moreover, during challenge with LPS, MZ B cells downregulate S1P and move into the follicles⁵³, suggesting these chemotactic signals are balanced during steady-state and inflammatory conditions. When mice are

treated with pertussis toxin, which ablates G α i signalling, MZ B cells are absent from the marginal zone, while the B and T cell architecture of the white pulp is unaffected, suggesting that additional chemokine receptors are involved in MZ B cell positioning ⁵⁴.

MZ B cells are derived from immature B cells in the spleen that exit the bone marrow before completing maturation, but only a subset will become MZ B cells, while the rest develop into FO B cells as normal ⁵⁵. Notch-2 signalling is essential for the development of MZ B cells while all other B cell subsets develop normally ⁵⁶. Recombining binding protein suppressor of hairless (RBP-J), a DNA-binding protein that can be activated by binding to the intracellular domain of the Notch receptor, has also been shown to be vital for MZ B cell development ⁵⁷, while the protein Msx2-interacting nuclear target protein (MINT), which competes with Notch for RBP-J binding, is highly prevalent in FO B cells of the spleen ⁵⁸, suggesting that cell fate decisions are influenced by intracellular levels of MINT in FO B cells. There is also evidence to suggest that the strength of BCR signalling is partially responsible for the FO vs MZ B cell fate decision, with cells that have weak BCR signalling becoming MZ B cells ⁵⁵.

1.3.1.3 Red Pulp

The red pulp region has a critical role in blood surveillance and filtration. Specialised vessels are lined with sinusoidal endothelial cells, which have holes in between the cell-cell junctions. When red blood cells attempt to pass through these fenestrae to enter the red pulp, they are forced to compress themselves putting strain on their cell membranes. Old or damaged red blood cells will break apart under this pressure, and resident macrophages scavenge the haemoglobin, as well as free haemoglobin in the blood ⁴⁸. The red pulp is also home to plasma cells, which secrete antibodies into the bloodstream ⁵⁹.

1.3.2 Splenic Dendritic Cells

The spleen is home to several subsets of tissue-resident DCs that are specialised to surveying the blood for antigen to present to naïve T cells. The main subsets of resident cDCs in SLOs including the spleen are characterised by their expression of various surface markers: CD11c⁺ MHC-II^{low} CD8 α ⁺ CD205⁺ CD11b⁻ DCIR2⁻ (referred to here as CD8⁺ DCs) or CD11c⁺ MHC-II^{low} CD8 α ⁻ CD205⁻ CD11b⁺ DCIR2⁺ (referred to here as CD11b⁺ DCs). The receptors CD205 on CD8⁺ DCs, and DCIR2 on CD11b⁺ DCs have been shown to function in antigen uptake and processing ^{60,61}. CD11b⁺ DCs can be further

subdivided into CD4⁺ or CD4⁻ ⁶². CD8⁺ DCs appear to be lymphoid in origin, while both subsets of CD11b⁺ DCs are derived from the myeloid lineage ⁶³.

In the spleen, CD8⁺ DCs appear to be mainly localised in the T cell areas ^{60,64}, while CD11b⁺ DCs are more concentrated in the marginal zone and the red pulp ⁶⁰. Although the distinctions between different DC subsets appear plastic to some extent ⁶⁵, some distinct functions have been identified for these subsets. CD8⁺ DCs appear to be specialised for cross-presentation to CD8⁺ T cells ⁶⁶, deletion of self-reactive CD8⁺ T cells ⁶⁷ and endocytosis of dead cells ⁶⁸. Conversely, CD11b⁺ DCs appear to be specialised towards priming CD4⁺ T cells ⁶⁹⁻⁷¹. This appears to be related to differential antigen processing by these cells: CD8⁺ DCs are capable of presenting antigen on both MHC class I and II molecules, while CD11b⁺ DCs are restricted to presentation via MHC-II, but process and display antigen in this way more efficiently than do CD8⁺ DCs ⁶⁰.

1.4 Skin

1.4.1 Anatomy and Function of the Skin

As a functional barrier between the organism and the outside world, the skin is the largest organ involved in immune surveillance. The skin is considered by some to be an SLO in its own right due to its importance in this regard ⁷². The skin consists of two main tissues: the epidermis and the dermis (Figure 1-4). The epidermis consists mainly of keratinocytes which form a tightly-connected sheet, interspersed with secreted keratins. The dermis consists mainly of a network of fibroblasts associated with an extracellular matrix (ECM) of collagen and elastin. Fibroblasts secrete these proteins to maintain ECM integrity. The dermis is rich in capillaries and in lymphatic vessels allowing cells to travel to and from the skin from distal sites. There are several anatomical differences between human and murine skin, and this section will focus on the latter.

Keratinocytes in the interfollicular epidermis form layers, with the epidermal stem cells in the stratum basale, closest to the basement membrane separating epidermis and dermis, followed by three layers of stratum granulosum which contain progressively more differentiated cells ⁷³. As they differentiate, cells are pushed upwards and eventually reach the stratum corneum, which is a thick outer layer of senescent and dead cells and keratin. The stratum corneum forms a physical barrier against the environment. This protective layer is continually shed and replenished as more keratinocytes from the epidermis eventually senesce. Keratinocyte differentiation is controlled by extracellular Ca^{2+} concentrations, and cells have been shown to regulate their proliferation and their expression of differentiation-related proteins, including involucrin, loricrin and keratins in response to Ca^{2+} ^{74,75}. Ca^{2+} levels broadly increase from the most basal to distal regions of the skin, then decrease again in the stratum corneum; this gradient appears to form passively, maintained by the permeability barrier of the skin ⁷⁵.

The skin is interspersed with hair follicles, which are lined with keratinocytes, and therefore could be seen as representing ingrowths of the epidermis. Keratinocytes in the epidermis are heterogeneous, falling into five main subsets: interfollicular epidermis (epidermis not associated with the hair follicles), infundibulum (the upper region of the hair follicle, reaching to the entrance of the sebaceous glands), isthmus (the region

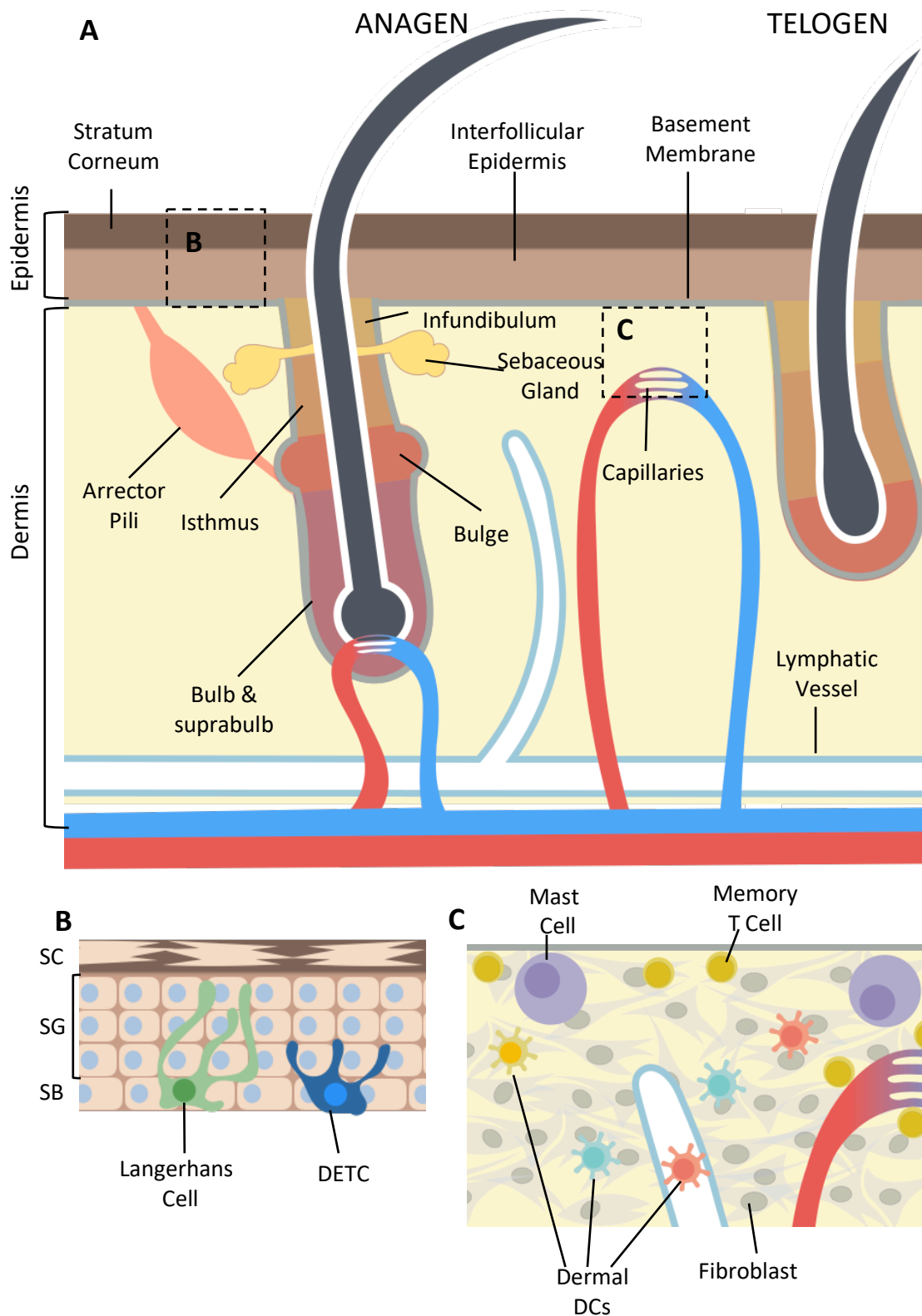


Figure 1-4: Structure of the skin.

A) Overview of the main anatomical features of the skin. Shown are two hair follicles, one in anagen and one in telogen. On the anagen follicle, the main anatomical features and keratinocyte subsets are outlined: infundibulum, isthmus, bulge, and bulb/suprabulb, and the connection of sebaceous glands and arrector pili muscle. Within the dermis are lymphatic vessels and capillaries allowing trafficking of leukocytes to and from the SLOs. **B)** magnified view of the area highlighted in A. This shows the layers of keratinocytes in the epidermis: SB = stratum basale, SG = stratum granulosum, SC = stratum corneum. In

the epidermis, Langerhans cells and DETCs extend processes between keratinocytes to contact antigen. **C**) magnified view of the region highlighted in A. This shows the major resident leukocyte populations of the dermis, including mast cells near the basement membrane, dermal DCs distributed throughout the tissue and memory T cells divided between the epidermis/dermis junction and capillaries.

extending from the sebaceous gland to the attachment of the arrector pili muscle), bulge (the region where the muscle attaches) and bulb (the cells that produce the growing hair bulb) ⁷⁶.

Hair follicles cycle through distinct growth phases, the most prominent being anagen (hair growth) and telogen (senescence and shedding). When hair follicles are in telogen, the follicle undergoes significant remodelling, particularly in the bulge and bulb regions, as hair production ceases and the bulb cells undergo apoptosis ⁷⁶. The stem cells of the hair follicle are located in the bulge region ^{77,78}, and all the cells of the hair follicle are derived from these cells. Bulge cells are capable of repopulating the epidermis upon injury ⁷⁸. Keratinocytes of the hair follicle have also been shown to play roles in immunity, by secreting chemokines during inflammatory conditions to attract immune cells, particularly Langerhans cells (LCs) ⁷⁹, which will be discussed further below.

While large numbers of leukocytes will be recruited to the skin during inflammation, there are several resident populations of leukocytes in non-inflamed skin. T cells are abundant in resting skin; the majority are CD4+ memory T cells ^{80,81}, but there are also populations of regulatory T cells ⁸⁰ and CD8+ memory T cells ⁸¹. Memory T cells are descended from T cells that migrated to the skin in response to a previous infection and formed a stable, long-lasting population to protect against future infections by the same pathogen.

Mast cells are mainly located in the upper dermis. They are known as the main cells involved in allergy; they irreversibly bind IgE antibodies produced by plasma cells to their cell-surface FcεRI receptors. When they encounter the antigen specific to the IgE molecules on their surface they respond by releasing histamine and cytokines to provoke an inflammatory response. Further roles for mast cells in immunity have been discovered, however, including secretion of cytokines, activating keratinocytes and remodelling ECM proteins to allow ingress of leukocytes ⁸².

There are also several resident populations of dendritic cells in the skin. In the dermis, there are three major subsets of DCs characterised by CD103 and Langerin expression: Langerin+ CD103+, Langerin+ CD103-, Langerin- CD103+ and Langerin- CD103-,

although the Langerin- cells can also be subdivided into CD11b⁺ and CD11b⁻ subsets⁸³. These cells are important for immune surveillance of the skin, and continually circulate between skin and skin-draining lymph nodes.

1.4.2 Langerhans Cells

Langerhans cells (LCs) are a unique class of myeloid-derived APCs. They are the only resident MHC-II⁺ cells in the epidermis. They express Langerin, a protein originally thought to be specific to LCs, but later discovered to be expressed by other DC subsets. In LCs, Langerin is found mainly in cytoplasmic organelles called Birbeck granules, which have an unknown function but are thought to be part of the endosomal recycling system and may be similar in role to clathrin-coated pits. Langerin has been shown to play a role in antigen processing⁸⁴

Immature LCs congregate in the epidermis, particularly in the hair follicles⁷⁹, and extend their dendrites to capture antigen entering the skin. Upon detecting antigen, LCs mature by upregulating MHC-II and co-stimulatory molecules such as CD80 and CD86, and downregulating E-cadherin to detach from the surrounding keratinocytes. They also increase expression of the chemokine receptors CXCR4 and CCR7; CXCR4 allows them to migrate out of the epidermis by sensing CXCL12 produced in the dermis. Once in the dermis, LCs further upregulate CCR7 and downregulate CXCR4, and migrate towards the dermal lymphatic vessels via CCL19/21. From here they migrate to a skin draining lymph node, again via CCR7, and enter the T cell follicle to prime naïve T cells.

Unlike other DC populations, Langerhans cells are initially derived from a precursor population that colonises the epidermis during development and is able to stably self-renew under steady-state conditions⁸⁵. During stress, LCs can also be replenished from Gr-1⁺ precursors recruited from the blood⁸⁶. LC development is driven by TGF- β 1, which is also essential for their survival^{87,88}. It is thought that paracrine TGF- β 1 from haematopoietic origin initiates LC development, then TGF- β 1 secreted by keratinocytes and LCs themselves maintains their survival once they reach the epidermis. LC precursors are attracted to the epidermis by chemokines produced by hair follicle keratinocytes in response to stress.

1.4.3 $\gamma\delta$ T Cells

The only skin-resident subset of T cells in the mouse are V γ 3/V δ 1 T cells, also known as dendritic epidermal T cells (DETCs). These are a form of innate-like leukocytes, meaning they possess invariant TCRs. DETCs are activated by self-antigen expressed by damaged keratinocytes⁸⁹. There is evidence that this self-antigen is recognised via the $\gamma\delta$ TCRs of DETCs⁹⁰. Upon activation, DETCs can enhance the immune response by secreting IFN- γ ^{91,92}, and a subset of DETCs can produce IL-17A⁹³. DETCs are also able to secrete the inflammatory chemokines CCL3, CCL4, CCL5 and XCL1, which could attract other immune cells to the epidermis⁹⁴. They appear to play a role in wound healing in the skin, by secreting keratinocyte growth factor (KGF), as TCR $\delta^{-/-}$ mice show impaired wound healing, and this could be restored in skin cultures by adding DETCs or KGF⁹⁵.

1.4.4 Dendritic Cell Migration from Skin to Draining Lymph Nodes

Skin-resident DCs are continually trafficking between skin and the T cell areas of skin-draining lymph nodes to present antigen to naïve T cells. This occurs both during inflammation when activated DCs induce an immune response, and during steady-state conditions when immature DCs help maintain peripheral tolerance. CCR7 signalling is crucial for the exit of DCs from the skin in both of these circumstances: while LCs are still able to migrate from the epidermis to dermis in CCR7 $^{-/-}$ mice, neither LCs or dermal DCs can enter lymphatic vessels or reach skin-draining lymph nodes. This is true both for inflamed and resting skin⁹⁶. CCR7 does not appear to be necessary, however, for the initial migration of LCs to the dermis; instead, the receptor CXCR4, which recognises CXCL12, is crucial during this process⁹⁷.

Of the two CCR7 ligands, CCL21 appears to be essential for DC egress from the skin, while CCL19 plays a redundant role^{12,98}. It has been shown that CCL21 is able to form stable concentration gradients in the skin, as it has a positively-charged C-terminal that strongly interacts with extracellular proteoglycans⁹⁹. As CCL19 and CCL21 are expressed by dermal lymphatic endothelial cells, CCR7 expression allows DCs to migrate towards these vessels and enter the lymph flow.

Once in the lymph node, CCR7 signalling is also required for DCs to reach the cortex and associate with naïve T cells. Upon reaching the lymph node in the afferent lymph, DCs migrate across the SCS floor and into T cell zones in a CCR7-dependent manner¹⁰⁰.

Again, functional gradients of CCL21 in this tissue appear to be required for DCs to cross the SCS ¹⁰¹.

1.5 Chemokines

Chemokines are small cytokines that are vital in controlling cell migration. This makes them key components of immunity, which requires the correct spatial targeting of cells from distant sites in the body. They are also important in processes related to immunity such as development of lymphoid organs, wound healing and angiogenesis. Aberrant chemokine expression and regulation is implicated in many diseases, including a variety of cancers and autoimmune disorders.

Chemokines are divided into four families: CXC, CC, XC and CX₃C, depending on a sequence of conserved cysteine residues near the N-terminal¹⁰². The N-terminal region is the main receptor-binding site¹⁰³, and appears to specify functions including receptor agonism/antagonism, desensitisation and signalling via mobilisation of Ca²⁺¹⁰⁴. Although the amino acid sequences of chemokines are highly variable, they show similar tertiary structures with conserved disulphide bonds between cysteine residues¹⁰².

1.5.1 Post-translational Regulation of Chemokine Function

Chemokines can be subject to several possible post-translational modifications to their N-terminal domains that affect their activity, including proteolysis by matrix metalloproteases¹⁰⁵ or CD26¹⁰⁶. These can alter their affinity for their receptors, and the response generated within the cell upon ligand binding, for example inactivating chemokines¹⁰⁵, or causing them to become receptor antagonists^{107,108}. These modifications can also affect the ability of chemokines to bind to other proteins¹⁰².

Chemokines often associate as dimers, tetramers or oligomers¹⁰² and although they are generally believed to function as monomers when inducing cell migration¹⁰², receptor agonism has been reported for dimerised chemokines including CXCL1¹⁰⁹, and CXCL8¹¹⁰. Some chemokines are also capable of heterodimerising¹¹¹⁻¹¹³, although there is no conclusive evidence that hetero-oligomers are capable of directly inducing any signalling via their respective receptors and may instead be involved in modulating chemokine availability¹⁰².

Cell responses to chemokines are also modified depending on the form the chemokine is encountered in; glycosaminoglycans (GAGs) are glycoproteins that can often be found bound to a protein backbone to form membrane-bound peptidoglycans on the surface of

cells. These proteins are negatively charged and can form stable electrostatic bonds with the positively-charged C-terminal domains of certain chemokines. This interaction leads to chemokine immobilisation on the surface of cells and is vital to the function of many chemokines ¹¹⁴.

When a responding cell recognises a chemokine bound in this way it initiates integrin-mediated cell-cell adhesion, and leads to either directed migration along a gradient (haptotaxis) or random movement (haptokinesis) ¹¹⁵. This is most common on endothelial surfaces, including lymphatic endothelium as described (See section 1.2.2.3).

Alternatively, cells can respond to soluble chemokines, either directed along a soluble gradient (chemotaxis) or randomly (chemokinesis) ^{116,117}. Different chemokines have varying affinities for GAGs ¹¹⁸, making them more or less likely to be found in soluble or immobilised forms. The importance of the C-terminal domain for chemokines is illustrated by the observation that DCs are capable of cleaving the highly positively-charged C-terminal domain of CCL21, generating a soluble form of CCL21 that behaves similarly to CCL19 ¹¹⁹. Endothelial cells also express different GAGs on their surfaces, which will bind to different chemokines, potentially allowing the tissue-specific trapping of different chemokines ¹²⁰.

Chemokines can also be modified by the addition of various chemical groups, including nitration (the addition of peroxynitrite, a reactive oxygen species), which can affect the affinity and signal transduction capacity of chemokines for their receptors, or the ability of chemokines to bind GAGs ¹¹⁸.

1.5.2 Inflammatory vs Homeostatic Chemokines

Chemokines are separated into two families: homeostatic and inflammatory. Homeostatic chemokines are expressed constitutively during steady-state conditions to mediate leukocyte migration to and from tissues, and often also have roles in cell positioning during development. Inflammatory chemokines are generally only upregulated in response to a challenge such as infection or wounding. These chemokines are released to attract specific subsets of cells to a site of inflammation to carry out their intended function. In reality, there are overlaps between the functions of these chemokines, but this definition is useful to segregate between events during immune homeostasis and challenge.

Two examples of homeostatic chemokines are CCL19 and CCL21, which mediate APC migration to the T-cell zones of the lymph node at rest ⁹⁶. These chemokines also play a role in T cell development in the thymus. *plt*^{-/-} mice, which do not express CCL19 or CCL21, show a lack of T cells and reduced lymph node size ¹²¹, showing the importance of these chemokines in T cell and lymph node development.

CXCL12 is another example of a homeostatic chemokine. It is constitutively expressed, and plays an important role in bone marrow homeostasis, maintaining the pool of haematopoietic stem cells within this tissue ¹²². It is also vital during development, as mice lacking CXCL12 or its receptors die during embryogenesis ¹²². In zebrafish, CXCL12 signalling has shown to be important in development of the posterior lateral line as the initial primordial cells, which seed precursors along the flank of the embryo that develop into sense organs, follow a trail of CXCL12 ¹²³.

One example of an inflammatory chemokine is CCL2, which binds to CCR2 on monocytes and memory T cells, recruiting them to the site of inflammation. Inflammatory chemokines generally attract multiple cell types spanning both innate and adaptive arms of the immune system, and these cells will often release chemokines themselves as part of their immune response, leading to multiple waves of different cell types that can arrive at the site of inflammation as the immune response progresses.

1.6 Chemokine Receptors

As discussed previously, chemokines play a pivotal role in cell migration. In order to induce this effect, chemokines must bind to a receptor on the surface of the responding cell. Every cell is limited in which chemokines it can respond to, based on the complement of chemokine receptors it possesses. There is a large degree of redundancy in these relationships, as many chemokines bind multiple receptors and vice versa, allowing each cell to respond to a range of overlapping stimuli with varying affinities ¹²⁴.

Chemokine receptors are a class of G-protein coupled receptors (GPCRs) which have seven membrane-spanning domains. A conserved DRYLAIV motif on the second intracellular loop is thought to be important for chemokine receptor function ¹²⁵.

Like other GPCRs, chemokine receptors initiate downstream signalling via heterotrimeric G-proteins. Each G-protein is formed from $G\alpha$, $G\beta$ and $G\gamma$ subunits. $G\alpha$ binds to guanosine diphosphate (GDP) and is the subunit that interacts directly with the C-terminal of the receptor. Upon ligand binding, the conformation of the receptor C terminal changes, activating $G\alpha$ and allowing it to replace GDP with guanosine triphosphate (GTP). $G\alpha$ then leaves the receptor, while $G\beta$ and γ remain dimerised, and both $G\alpha$ -GTP and $G\beta\gamma$ initiate their own downstream signalling cascades ¹⁰². Chemokine-mediated cell migration is thought to be strictly via the G_i sub-family of G-proteins as it is sensitive to pertussis toxin, which ablates G_i activity ¹²⁶.

Once $G\alpha$ and $G\beta\gamma$ proteins have carried out their downstream functions, they will be available for receptor binding once again. The C-terminal domain of the receptor, however, is phosphorylated by a G-protein coupled receptor kinase (GRK) upon ligand binding, making the previously activated receptor unavailable for G-protein binding ¹²⁷. Instead, the phosphorylated GPCR binds to a β -arrestin which mediates receptor silencing. This is either transient, leading to receptor dephosphorylation and recycling to the cell surface, or can lead to long-term receptor silencing or permanent degradation ¹²⁷. This means that cells will eventually become unresponsive to high levels of chemokines.

Below, the main roles for the key receptors relevant to this work have been summarised.

1.6.1 CCR7

CCR7 is the receptor for the chemokines CCL19 and CCL21, both of which are homeostatic chemokines with a role in leukocyte migration to SLOs. It is vital for the trafficking of APCs and T cells throughout the SLOs and tissues both during inflammation and homeostasis⁹⁶, which has been described in more detail above (See section 1.4.4), and it is also crucial for correct positioning of T_{FH} and FO B cells within the lymph node (See section 1.2.2). Here, I will detail the role of CCR7 and CCR9 in thymocyte development.

1.6.1.1 $\alpha\beta$ T Cell Development in the Thymus

T cell precursors, or thymocytes, migrate to the thymus from the bone marrow to undergo maturation into naïve T cells. T cell maturation involves a number of crucial interactions between thymocytes and the thymus stroma. For these interactions to occur, the spatial positioning of thymocytes at various stages of development is key. Chemokines and their receptors are a vital part of this process.

Thymocytes initially lack expression of CD4, CD8 and TCR proteins, and are known as double negative (DN) cells. As they mature, DN thymocytes pass through several developmental stages characterised by different surface receptors: DN1 cells are CD44+, CD25-; these cells upregulate CD25 to become DN2 CD44+ CD25+ cells. CD44 is then downregulated in DN3 cells, and DN4 cells then downregulate CD25 to become CD44- CD25-¹²⁸. While they progress through these developmental stages, thymocytes begin to express recombinase-activating genes (RAG-1 and RAG-2), and begin to undergo V(D)J recombination in their TCR loci¹²⁹. In this manner, a vast range of different TCR subunits can be produced from a single gene. This allows the body to produce T cells capable of recognising almost any conceivable protein, without the huge genetic burden it would require expressing each TCR variant as an individual gene.

Thymocytes enter the thymus at the cortico-medullary junction, and progression through these developmental stages occurs in the cortex of the thymus while the cells migrate through this tissue. Chemokine receptor expression has shown to be important for cells to progress through these checkpoints, while both CCR7 ligands appear to be constitutively expressed in the thymus¹³⁰. About half of DN1 and DN2 cells are CCR7+¹³⁰ but mainly CCR9-¹³¹, while DN3 and DN4 cells are largely CCR7- and CCR9+¹³¹. These receptors have both been shown to be essential for cells to progress correctly through development

and become T cells; deleting CCR7 or CCR9 leads to developmental delay at the DN2 or DN3 stages, respectively ^{130,131}.

DN4 cells migrate back towards the cortico-medullary junction, where they begin to progress into the double positive (DP) stage. These cells are characterised by expression of both CD4 and CD8 and a lack of CD69 expression. DP cells interact with cortical thymic endothelial cells that present MHC molecules ¹⁷, and the strength of the interaction between the TCR of each DP cell and MHC determines the cell's fate. Death by neglect occurs when cells react too weakly with self-antigen, and do not receive signals for survival and proliferation. Positive selection is the promoted survival of cells that weakly interact with self-peptides, and negative selection is the active destruction cells that strongly react ¹²⁹. This process is an important part of central tolerance, where strongly self-reactive cells are selected against to prevent autoimmunity.

DP cells that survive this selection continue to migrate from the cortico-medullary junction towards the medulla where they undergo further selection based on their reaction to self-peptides presented by DCs and medullary thymic endothelial cells, and mature into either CD4+ or CD8+ single positive (SP) T cells which are highly CCR7+ ¹³⁰. CCR7 may play a role in the migration of SP cells to the medulla, and their retention there while completing maturation; this appears to rely on CCL21 as thymus architecture appears normal in *Cell19*^{-/-} mice ¹². CCR9 expression on DP cells has also been noted to aid in migration of these cells to the medulla, potentially allowing them to outcompete CCR9- cells ¹³¹. Once in the medulla, most SP cells downregulate CCR9 ¹³¹, and CCR9 expression on mature T cells is variable; in mice, the receptor is restricted to a gut-homing population of CD4+ memory T cells, while in humans it is expressed on a subset of CD8+ T cells ^{131,132}.

1.6.2 CXCR4

CXCR4 is the receptor for the chemokine CXCL12. It has been implicated in many processes in immunity, development and disease, including HIV entry to T cells, cancer metastasis, haematopoiesis and cardiac development. As this work focused mainly on the skin, I will focus on the involvement by CXCR4 in cutaneous wound healing.

CXCL12/CXCR4 have been shown to play a role in skin wound healing and chronic inflammation. In one study, mice showed increased levels of CXCL12 mRNA and protein at the site of a wound which peaked at days 1 and 5 after wounding but returned to normal

in between, while anti-CXCL12 antibodies applied to the wound site decreased the rate of wound healing; CXCR4-dependent trafficking of bone marrow stem cells to the wound site was also observed¹³³. Direct application of CXCL12 to wounds has also been shown to increase the rate of wound healing, and increase recruitment of infiltrating cells to the wound site¹³⁴. Conversely, topical application of the CXCR4 antagonist AMD3100 improved wound healing in diabetic mice, leading to enhanced CXCL12 mRNA expression¹³⁵ and applying the CXCR4 antagonist 4F-benzoyl-TN14003 led to increase epithelialization in burn wounds¹³⁶.

There is also some conflicting evidence for CXCL12/CXCR4 involvement in psoriasis. In the K14-VEGF-A mouse model of psoriasis - where over proliferation of basal keratinocytes is induced by expressing VEGF-A from the keratin 14 promoter¹³⁷ - there was significant upregulation of CXCR4 and CXCL12 in inflamed skin. Inflammation and angiogenesis was reduced by treatment with AMD3100, including reducing the number of infiltrating macrophages and CD8+ T cells in the tissue. CXCL12 neutralizing antibodies reduced inflammation and number of infiltrating macrophages and T cells in these mice¹³⁸.

Despite this potential role for CXCL12/CXCR4 signaling in driving inflammation, another model of psoriasis has been generated by deleting CXCR4 from basal keratinocytes using a K14-Cre conditional knockout and injecting IL-23, a key cytokine involved in psoriasis, to locally induce inflammation. This suggested that CXCR4 expression on basal keratinocytes has a protective role against IL-23-mediated inflammation¹³⁹. IL-23 induces proliferation of keratinocytes via STAT3 signaling. SOCS3, an inhibitor of STAT3 phosphorylation¹⁴⁰, was found to be upregulated in response to CXCL12, suggesting that the CXCL12/CXCR4 axis negatively regulates IL-23 mediated cellular proliferation via SOCS3¹³⁹.

1.7 Atypical Chemokine Receptors

In this introduction, several key processes in immunity have been described which require precise and directed cell migration. Chemokine-mediated cell migration is required for many of these processes. In particular, the chemokines CCL19, CCL21, CCL25 and CXCL12 have been discussed for their roles in immune homeostasis and development. Leukocyte trafficking to, and migration within, the lymph nodes is critical for the initiation of an adaptive immune response. The fine balance between tolerance and immune response that must be maintained in epithelial surfaces contacting the external environment is typified by the microenvironment of the skin.

A further level of regulation is present in the chemokine system was added with the discovery of atypical chemokine receptors. Atypical chemokine receptors (ACKRs) are a class of chemokine receptors that do not induce cell migration upon ligand binding and are not reported to initiate G-protein mediated signalling. Instead, they induce alternative cellular functions which may include the internalisation and destruction of chemokines coupled with rapid receptor recycling (scavenging) or transporting chemokines across endothelial barriers ¹⁴¹. In at least one case, an atypical chemokine receptor can heterodimerise with a typical chemokine receptor to directly modify its function ¹⁴². The four members of the ACKR family are ACKR1 (Duffy Antigen/Chemokine Receptor, DARC), ACKR2 (D6), ACKR3 (CXCR7) and ACKR4 (CCX-CKR, CCR11, CCRL1) ¹²⁵. The general function of ACKRs in the immune system appears to be to modulate cell migration by maintaining the formation of stable gradients of chemokine, however, this is an oversimplification of the true complexity and diversity of ACKR function.

The structural reasons for atypical chemokine receptors' unique behaviour are unknown. Atypical chemokine receptors have been characterised by the modification of a conserved DRYLAIV motif typically found in the second intracellular loop of chemokine receptors. In ACKR1, this motif is absent, and in ACKR2, 3 and 4 there are substantial modifications to this amino acid sequence; however, the atypical chemokine receptors have many other differences to the typical receptors, and there is no clear evidence that altering the DRYLAIV motif affects chemokine receptor signalling ¹²⁵.

ACKR1 and ACKR2 are highly promiscuous ACKRs that each bind to a host of chemokines. ACKR1 is expressed on erythrocytes and vascular endothelial cells ¹⁴³, particularly HEVs ¹⁴⁴. Ligand binding in ACKR1 does not activate any detectable

downstream signalling, but instead the receptor associates with caveolae, vesicles which are involved in transcytosis (transport of molecules across cells), suggesting that ACKR1 on endothelial cells is able to transport chemokines across vessels ¹⁴³. ACKR1 on erythrocytes appears to modulate levels of chemokines in plasma by scavenging them, thus maintaining homeostatic chemokine levels ¹⁴³.

ACKR2 binds to most inflammatory CC chemokines, and is most abundantly expressed on LECs, although it can also be found on innate-like B cells ^{143,145}. D6 appears to function as a scavenging receptor, as the receptor is internalised via β -arrestin signalling then rapidly recycled to the cell surface while the ligand is degraded ^{146,147}. D6 often appears to play a protective role in inflammation, commensurate with its function as a scavenger for pro-inflammatory chemokines. For example, *Ackr2*^{-/-} mice show increased susceptibility to skin inflammation upon immune challenge ¹⁴⁸ and ACKR2 is raised in non-involved skin of psoriasis patients suggesting an anti-inflammatory role ¹⁴⁹.

In this work, I have focused on the two remaining members of the ACKR family: ACKR3 and ACKR4, which between them bind the homeostatic chemokines discussed in this work so far: CXCL12, and CCL19/21/25, respectively.

1.7.1 ACKR3

ACKR3 is expressed mainly on endothelial and epithelial cells in a wide range of tissues including heart, kidney, liver, spleen and lung ¹⁵⁰. ACKR3 expression has also been reported by some on MZ B cells, although this is controversial ¹⁵⁰⁻¹⁵³. ACKR3 binds two ligands: CXCL11, which also binds to CXCR3, and CXCL12, which binds CXCR4. ACKR3 has been shown to scavenge both of these chemokines ¹⁵⁴, and in fact binds CXCL12 with a greater affinity than CXCR4 does ¹⁵⁵. In this work, the CXCL12/CXCR4 axis has been the focus; partly due to the important roles for this chemokine/receptor pairing in diverse processes including skin inflammation, and due to the lack of functional CXCL11 in C57BL/6 mice ¹⁵³, which is the genetic background all transgenic mice used in these experiments were bred in.

ACKR3 has been shown to heterodimerise with CXCR4 where both receptors are coexpressed ¹⁵⁶, and modulate cell responses to CXCL12 ^{142,157}. It has been shown that ACKR3 biases CXCL12 signalling towards β -arrestin-mediated responses rather than the G_i -mediated responses that predominate when CXCR4 is expressed alone ¹⁵⁷. β -arrestin

signalling through CXCR4/CXCR7 activates cell proliferation and survival-related pathways including p38 MAPK, SAPK and ERK1/2 ¹⁵⁷. The disruption of G_i-mediated signalling does not ablate cell migration completely, but does potentially reduce chemotaxis towards low concentrations of CXCL12 *in vivo* ¹⁴².

ACKR3 has important roles in development: most *Ackr3*^{-/-} mice die as neonates due to cardiac defects ¹⁵³ similar, but not identical, to those seen in *Cxcr4*^{-/-} and *Cxcl12*^{-/-} mice ^{122,158}, suggesting roles for ACKR3 in this process beyond modulating CXCR4/CXCL12 activity. ACKR3 scavenging of CXCL12 by endothelial cells is also required for the correct development of the posterior lateral line in zebrafish ¹⁵⁹. Additionally, ACKR3 on the vasculature appears to scavenge CXCL12 from the blood and allow the directed migration of CXCR4+ leukocytes to tissues ¹⁵⁰.

In addition to its ability to act as a chemokine scavenging receptor, ACKR3 also appears to be capable of downstream signalling events in response to chemokine binding, including β-arrestin binding, cell growth, survival, and even cell migration ^{155,160-163}. In the liver, ACKR3 expressed on sinusoidal endothelial cells appears to promote regeneration and decrease fibrosis after liver injury ¹⁶⁴. The ability of ACKR3 to promote cell growth and survival is likely the reason why it has been implicated in progression of many types of cancer, including breast cancer ¹⁶⁵, melanoma ¹⁶⁶, liver cancer ¹⁶⁷ and kidney cancer ¹⁶⁸.

Here, I have studied ACKR3 mainly in the context of skin inflammation. Conflicting roles for CXCR4/CXCL12 involvement in this process have been reported, as described (See section 1.6.2), and the functional significance of ACKR3 expression in the skin has not yet been explored in depth.

1.7.2 ACKR4

ACKR4 is a scavenging receptor for the chemokines CCL19 and CCL21, which are the ligands for CCR7 ^{101,169-172}. It also binds the CCR9 ligand, CCL25 ¹⁷³. Both CCR7 and CCR9 play important roles in thymocyte development, as discussed previously (See section 1.6.1.1), and CCR7 is involved in homeostasis of APCs and T cells. CCR9 is also involved in homing of plasmacytoid DCs (pDCs) ¹⁷⁴ and specific subsets of T cells to the gut ¹⁷⁵, where subsets of fibroblasts have been reported to be ACKR4+ (C. Thomson, personal communication).

ACKR4 appears to play a role in the homing of DCs to the lymph node under both steady-state and inflammatory conditions ^{176,177}, most likely by scavenging CCL19 and/or CCL21: both chemokines are elevated in the lymph node, and CCL21 is elevated in the serum, of *Ackr4*^{-/-} mice ¹⁷⁸. LECs in the LN SCS express ACKR4, and in *Ackr4*^{-/-} mice DCs appear to congregate in the SCS, unable to enter the lymph node proper, while CCL21 accumulates near the SCS wall ¹⁰¹. ACKR4 also appears to be important for DC migration to the skin-draining lymph nodes during cutaneous inflammation. ACKR4 protein expression and function has been reported in keratinocytes in the epidermis, and lymphatic vessels in the dermis, using GFP reporter mice ¹⁷⁷, immunofluorescence ¹⁷⁹ and uptake of fluorescently-labelled chemokines ¹⁷⁹. In *Ackr4* knockout mice, Langerhans cell migration from the skin to the skin-draining lymph nodes during TPA-mediated inflammation is impaired, and this is likely due to the dysregulation of CCL19 in the skin leading to ineffective migration of these cells from the dermis to lymphatic vessels ¹⁷⁹. ACKR4 on LECs could also play a role in the transport of chemokines across endothelial cells, as ligand binding can lead to internalisation via caveolae ¹⁴³, which mediate transcytosis ¹⁸⁰.

1.8 Aims

Chemokine-mediated cell migration is vital to both development and to immunity. Evidence is emerging to suggest that atypical chemokine receptors can act as an important component of immune regulation by carrying out functions including the modulation of chemokine availability. The often protective role of ACKR2 scavenging inflammatory chemokines in disease models including psoriasis^{149,181}, cancer¹⁸², inflammation-induced miscarriage¹⁸³ and lung inflammation¹⁸⁴, have been explored to date, but the scavenging activity of ACKRs 3 and 4 are less well defined. Despite binding to homeostatic chemokines, rather than inflammatory, there is increasing evidence that ACKR3 and ACKR4 can also be involved in the innate immune response. In contrast to the inflammatory ACKRs, these receptors are fairly restricted in the ligands they can bind, making it more feasible to form a more comprehensive model of their interactions with chemokines and the cells expressing their receptors.

The skin is the largest epithelial surface in the body. Cells of the skin are in constant contact with foreign antigen and must present both a physical and immunological barrier to external pathogens as well as physical injury. In this work, the relationships between ACKRs 3 and 4, their ligands and related receptors were further characterised in a model system. Other epithelia, particularly in the lungs and the gut, play important roles in immune surveillance and tolerance, but the skin was chosen as the main tissue of use for this study due to its relative ease of manipulation and dissection, availability of cells derived from donor human tissue, the past work carried out by other group members on this tissue, and the expression of both ACKR3 and ACKR4 by several subsets of stromal cells, along with the widespread presence of both CXCL12 and CCL19/21 in this tissue.

The dynamics of CCL19/21-mediated leukocyte trafficking to and from skin-draining lymph nodes during steady state and inflammation have been well characterised, and previous investigations in this group have shown that ACKR4 deficiency can upset this balance, leading to impaired DC migration from the skin during inflammation. These investigations were continued by exploring the function of ACKR4 on skin cells *in vitro*, to obtain a more detailed picture of the mechanisms by which ACKR4 activity may be modified. These findings were followed up and expanded using a model of inflammation *in vivo* informed by these *in vitro* results.

ACKR3 has been less extensively studied in this group, and its main role in the literature is as a survival factor, particularly important as a negative prognostic factor in several types of cancer, and as a co-receptor with CXCR4 for HIV entry to CD4+ T cells; however, its role as a chemokine scavenging receptor has received somewhat less attention. Given the close similarity in its expression pattern to that of ACKR4, both of these being receptors largely restricted to endothelial and epithelial cells, a parallel study into ACKR3 responses to inflammation both *in vitro* and *in vivo* appeared to be a logical step.

1.9 Hypotheses

The aims of the study were formulated in order to test the following hypotheses:

1. ACKR3 and ACKR4 are expressed by keratinocytes and LECs in the skin and modify their activity in response to inflammatory stimuli *in vitro*.
2. ACKR3 and CXCR4 are coexpressed by keratinocytes and LECs in the skin, and expression levels of these receptors are modified in response to inflammatory stimuli *in vitro*.
3. ACKR4 deficiency leads to an enhanced inflammatory phenotype in a model of chronic skin inflammation.
4. ACKR3 and ACKR4 on endothelial cells scavenge homeostatic chemokines to modify dendritic cell positioning in the spleen.

Throughout the course of this project, these hypotheses were modified and refined. Some parts of the work had to be prioritised over others, or altered in scope, due to technical challenges. The results are presented as a whole in the Discussion section (Chapter 6).

Chapter 2: Materials and Methods

2 Materials and Methods

2.1 Cell Culture

Normal human epidermal keratinocytes (nHEK) and human dermal lymphatic endothelial cells (HD-LEC) were obtained from single juvenile donors of foreskin tissue, purchased from PromoCell. Cells were sub-cultured per the manufacturer's directions, using the recommended media and passaging reagents and splitting cells when 70-80% confluent. All cells were used between passages 7-9. For long-term storage, cells were immersed in liquid nitrogen in cryoSFM media (PromoCell). When thawing cells, tubes were quickly warmed to 37° C in a water bath and cells were transferred directly to a T25 (Corning) containing fresh pre-warmed media. Media was replaced the following day. nHEKs were routinely cultured using media with a low calcium concentration (0.06 mM Ca²⁺; LoCa) as directed by the manufacturer; if producing differentiated keratinocytes for experimental reasons, cells were switched to high calcium (0.18 mM Ca²⁺; HiCa) media five days before use.

2.1.1 Treatment of Human Cells with Immune Stimuli

Cells were seeded on 6-well plates and cultured until near-confluent. The following treatments (Table 2-1) were applied for durations specified in the individual experimental descriptions and cells were either used for further experiments or RNA was harvested.

Table 2-1: Immune stimuli used for cultured human cells

TREATMENT	CONCENTRATION	SUPPLIER
CpG	100 nM	unknown
IFN- α	100 ng/ml	R&D Systems
IFN- β	100 ng/ml	R&D Systems
IFN- γ	100 ng/ml	R&D Systems
KGF	20 ng/ml	R&D Systems
LPS	500 ng/ml	unknown
TPA	100 nM	Invitrogen

2.1.2 RNA Extraction from Cultured Cells

Cells were grown in 6-well plates using standard growth media until 70% confluent, and treatments (e.g. TLR ligands or cytokines) were added as appropriate. After the allotted time determined by the individual experiment, media was aspirated, cells were washed three times with ice-cold PBS and cells were lysed and RNA extracted using a PureLink RNEasy Mini Kit (Ambion) per the manufacturer's instructions. RNA concentration was measured using a NanoDrop spectrophotometer, and samples were stored at -80° C until required.

2.1.3 Chemokine Scavenging Assay

Cells were cultured for 3 days in 12-well plates; at the same time, media-only control wells were also set up. Media was aspirated from all wells, and 500 μ l phosphate buffered saline (PBS)/10% bovine serum albumin (BSA) (w/v) in culture media was added and allowed to coat the cells or empty wells for 5 minutes. Recombinant CXCL12 or CCL19 (Almac, Peprotech) were added to media and 500 μ l was added to each well still containing PBS/BSA to give a final chemokine concentration of either 1.56 ng/ml or 7.8 ng/ml. Plates were mixed gently, and 25 μ l of supernatant was taken from each well and stored at -20° C. Cells were cultured with chemokine for 24 hours total, with further aliquots of media taken

at fixed timepoints. Chemokine levels in each sample were determined using an ELISA kit (R&D Systems) per the manufacturer's directions.

2.1.4 Immunofluorescent staining of cultured cells

Cells were grown in 12-well plates on pre-sterilised glass coverslips until confluent. Media was aspirated and cells were fixed in warm 4% paraformaldehyde in PBS for 15 minutes. Cells were then washed three times for five minutes with ice-cold PBS. Cells were incubated for 1 hour at room temperature with blocking buffer [PBS, 10% v/v donkey serum]. The buffer was aspirated, and primary antibodies were diluted in blocking buffer per the manufacturer's directions and added to wells under a layer of Parafilm. Plates were incubated at 4° C overnight, then washed three times in PBS. Secondary antibodies were added at the manufacturer's recommended concentration in blocking buffer, and plates were incubated for 2 hours at room temperature in the dark. If a second primary antibody was used, the procedure was repeated as described using antibodies from different species. Cells were washed three times in PBS and coverslips were removed from wells and mounted on untreated glass slides using Vectashield mountant with 4',6-diamidino-2-phenylindole (DAPI; VectorLabs), and sealed with clear nail varnish. Slides were stored in the dark at 4° C until viewing with a Zeiss AxioImager M2 fluorescence microscope at 20X or 35X magnification.

2.2 Animals

All animals were bred and maintained under specific pathogen-free conditions (SPF) at the Central Research Facility (CRF) at the University of Glasgow unless otherwise indicated. All procedures were conducted in accordance with the UK Home Office regulations, were designed to comply with the necessary project and personal licenses and received ethical approval from the University of Glasgow ethics committee.

Male animals aged between 6-12 weeks were used for all experiments and age-matched as closely as possible within each individual experiment, unless otherwise stated. For crosses between wild-type and transgenic mice, wild-type females and transgenic males were normally used; for the *Ackr3^{gfp/+}* colony this was not always possible due to low numbers of transgenic mice retrieved from initial matings.

- Wild-type (WT) *C57BL/6J OlaHSD* mice were purchased from Envigo.

- *Ackr4*^{-/-} mice on a C57Bl-6 background were generated as described previously ¹⁷⁸. These mice have been reported to show reduced numbers of Langerhans cells in skin-draining lymph nodes at rest ¹⁷⁹ but no overall defects in lymphoid tissue development. *Ackr4*^{+/*gfp*} knock-in mice on a C57BL/6 background were a kind gift from Thomas Bohm and were generated as described ¹⁷⁷. Briefly, the N-terminus of the coding exon of *Ackr4* in these mice was replaced with an in-frame eGFP cassette, so that eGFP expression reflects *Ackr4* mRNA expression. No differential phenotype between *Ackr4*^{+/*gfp*} heterozygotes and wild-type mice has been reported. *Ackr4*^{*gfp/gfp*} homozygotes are functionally *Ackr4*-null. *C57BL/6-Ackr3*^{*tm1Litt/J*} (*Ackr3*^{+/*gfp*}) knock-in mice were generated by Dan Littman on a C57BL/6 background ¹⁸⁵. These mice were purchased from The Jackson Laboratory and imported by Charles River. As with the *Ackr4*^{+/*gfp*} knock-in mice, eGFP expression reflects *Ackr3* expression in this strain. The heterozygotes of this strain have no reported phenotype, but homozygotes die as neonates due to cardiac defects.
- *Ackr4*^{-/-} *Ccl19*^{-/-} Double Knockout (DKO) mice were generated by crossing *Ackr4*^{-/-} mice with *Ccl19*^{-/-} mice, which were obtained from Sanjiv Luther and generated as described ¹². The phenotype of these mice has not been characterised in detail but is presumed to be similar to the single knockouts. *Ccl19*^{-/-} mice were not reported to display any defects in lymphoid tissue development or leukocyte homing at rest ¹².
- OT1 x Ly5.1 mice on a C57BL/6J background were bred and maintained at the Beatson Institute under SPF. These mice express the CD45 isoform, CD45.1 on all leukocytes. They also express transgenic TCRs leading to MHC-I restricted T cells that react specifically to the protein ovalbumin. These mice are slightly immune compromised due to their limited T cell repertoire but possess no gross abnormalities.

2.2.1 Sample Handling and Preparation

All tissue was obtained from mice previously culled by asphyxiation in a rising concentration of CO₂.

2.2.1.1 in vitro Generation of Murine Langerhans Cells

Bone marrow was obtained from wild-type and *Ackr4^{+gfp}* knock-in mice by extracting bones from hind legs, cutting either end and flushing the bone marrow out using complete RPMI (Gibco) in a syringe. Tissue was passed through a 45 µm cell strainer and rinsed with complete RPMI. Cells were centrifuged at 300 x g for 5 minutes, resuspended in 10 ml of RPMI with 40 ng/ml GM-CSF, 2.5 ng/ml TGF-β1 and 5 ng/ml TNF-α. Cells were counted and added to 10 cm ultra-low adhesion plates at between 1 x 10⁶- 1 x 10⁸ cells per plate. Cytokine-supplemented media as described was added to give a total volume of 10 ml on each plate. 5ml fresh media was added every second day; cells were re-plated after 4 days by aspirating media to a centrifuge tube, rinsing plates with 5 ml PBS and centrifuging cells at 300 x g for 5 minutes. Cells were resuspended in 10 ml of fresh cytokine-supplemented media and seeded on to new 10 cm plates. After 8 days, cells were plated on tissue culture-treated plates overnight, and non-adherent cells removed and used for further analysis.

2.2.1.2 Collection and Processing of Mouse Blood

Prior to blood collection, 100 µl 0.5 M Ethylenediaminetetraacetic acid (EDTA) was added to one 1.5 ml Eppendorf per mouse and each aliquot was passed through a syringe to coat the interior. Blood was extracted using pre-coated syringes either via the aorta or the posterior vena cava between the kidneys. Blood was transferred to the Eppendorf containing EDTA, removing the needle from the syringe to avoid shearing cells. Samples were optionally centrifuged at 800 x g for 5 minutes and plasma aspirated if required for analysis. Samples were mixed thoroughly with 9 ml dH₂O and incubated for one minute to lyse red blood cells before 1 ml 10X PBS was added and samples were passed through a 100 µm cell strainer. Samples were centrifuged at 400 x g for 5 minutes; cell pellets were then resuspended in FACS buffer [PBS, 2 nM EDTA, 2% FCS, 0.1% NaNH₃] and used for flow cytometry analysis.

2.2.1.3 Preparation of Cell Suspensions from Mouse Ears

Ears were excised and kept on ice before being split with forceps into dorsal and ventral halves and floated dermis-side down on 0.25% Trypsin-EDTA (Sigma). Dorsal halves were incubated at 37° C for 22 minutes; the thicker ventral halves (including collagen and subcutaneous fat) were incubated at 37° C for 45 minutes. Trypsin was washed from ears

by briefly floating dermis side down in PBS. Epidermis was peeled off using forceps from the outer tip of the ear in one motion. Epidermis was transferred to a 2 ml Eppendorf tube containing 1 ml RPMI and stored on ice until incubation of both dorsal and ventral halves was complete. Dermis, if required in the experiment, was transferred to a 2 ml Eppendorf tube containing 1 ml RPMI. Tissue was minced with scissors and 1 ml 2X stromal digest cocktail [RPMI-1640, 1.6 mg/ml Dispase (Roche), 0.4 mg/ml Collagenase P (Roche), 0.2 mg/ml DNase I (Roche)] was added to each tube. Samples were incubated at 37° C for 10-12 minutes and passed through 100 µm cell strainers on ice, then flushed with media until the tube contained a total volume of 20 ml. Samples were centrifuged at 400 x g at 4° C for 5 minutes, supernatants discarded, and cells were resuspended in FACS buffer to use for flow cytometry analysis.

2.2.1.4 Preparation of Cell Suspensions from Mouse Heart

Hearts were excised and stored in RPMI on ice until needed. Each heart was transferred to a petri dish containing 5 ml Hank's Balanced Salt Solution (HBSS; Gibco), cut open to expose the inner surfaces of the ventricles and rinsed to remove any traces of blood. The heart was transferred to the lid of the dish and minced finely with scissors. The tissue from each heart was transferred to a 15 ml Falcon tube on ice containing 5 ml Collagenase I solution [HBSS, 1 mg/ml Collagenase I (Roche)]. The tubes were gently mixed and incubated at 37° C with shaking for 30 minutes. The tubes were manually agitated every 5-10 minutes to minimise formation of tissue aggregates. After digestion, tissue was disrupted with a 10 ml serological pipette. Samples were centrifuged at 400 x g for 5 minutes and supernatants were discarded and tissue resuspended in 5 ml ice cold Dispase solution [HBSS, 0.25 mg/ml Dispase]. Tubes were incubated for a further 20 minutes at 37° C with shaking, and the digestion was terminated by adding 5 ml ice-cold HBSS and placing on ice. Samples were agitated with a 10 ml serological pipette and passed through a 50 µm cell strainer. Cells were centrifuged at 400 x g for 5 minutes and resuspended in FACS buffer, then used for flow cytometry analysis.

2.2.1.5 Preparation of Cell Suspensions from Mouse Lymph Nodes

Lymph nodes were excised (unless otherwise stated, inguinal lymph nodes were used), pierced with fine forceps and stored on ice in RPMI (Gibco) until needed. Media was replaced with 3 ml of 1X stromal digest cocktail [RPMI-1640, 0.8 mg/ml Dispase, 0.2 mg/ml Collagenase P, 0.1 mg/ml DNase I (Roche)] and tissue was incubated at 37° C for

20 minutes with shaking. Lymph nodes were gently agitated with a P1000 pipette to release leukocytes, tissue was allowed to settle to the bottom of the vial, and the supernatant was transferred to a 15 ml Falcon tube on ice containing 5 ml FACS buffer with care not to transfer any particulate matter. 2 ml of fresh stromal digest cocktail was added to each vial and incubated at 37° C for a further 5 minutes with shaking. Meanwhile, the collected supernatant was centrifuged at 400 x g for 5 minutes, and the cells were resuspended in 5 ml fresh FACS buffer and stored on ice. The procedure of agitating tissue, removing and washing the supernatant and digesting any remaining particulate matter was repeated until either the nodes were completely digested or 1 hour elapsed from the first addition of stromal digest cocktail. The collected cells and any remaining tissue were passed through an 80 µm cell strainer, then used for flow cytometry analysis.

2.2.1.6 Preparation of Cell Suspensions from Mouse Spleen

Spleens were excised and kept on ice in RPMI until needed. In a Petri dish, as much fat and connective tissue was removed as possible and the spleens were minced using scissors. 1 ml of HBSS with 1 mg/ml Collagenase D (Roche) was used to flush the tissue into a 1.5 ml Eppendorf tube. A further 500 µl was used to rinse the Petri dish and ensure all tissue was recovered. Tissue was incubated at 37° C for 40 minutes, triturated using a 5 ml serological pipette and passed through a 70 µm cell strainer, rinsing with FACS buffer. Cells were centrifuged at 400 x g for 5 minutes at 4° C and the pellet was gently resuspended in residual buffer to prevent forming of aggregates. Cells were resuspended in 1 ml RBC lysis buffer (Sigma). After one minute, the samples were flooded with 25 ml of FACS buffer. Samples were centrifuged as before and resuspended in 10 ml of FACS buffer, then used for flow cytometry analysis.

2.2.2 Genotyping of Genetically-modified Mice

Tail tips or ear punches were obtained by animal facility staff and stored in 1.5 ml Eppendorfs at -20° C. Samples were incubated at 55° C in 100 µl tail-tip lysis buffer [5 mM EDTA, 0.1 mg/ml Proteinase K, 0.2% w/v SDS, 100 mM Tris.HCl, 200 mM NaCl] for 5 hours or overnight. Samples were heated to 95° C for 5 minutes and 500 µl dH₂O was added. Samples were then centrifuged for 5 minutes at 13000 rpm in a microcentrifuge to remove cellular debris.

The supernatant was used in a PCR reaction to determine the genotype of each mouse: A stock working primer mix was made by combining equal volumes of all primers required for the reaction and diluting this 1:10 in PBS. Each reaction contained 12.5 µl GOTaq G2 Hot Start Green Master Mix (Promega), 10 µl nuclease-free water, 1.5 µl primer mix and 1 µl supernatant from lysed tissue. Tubes were mixed gently with a pipette, pulsed in a micro centrifuge and the following PCR program was used:

94°C 5 min
94°C 15 sec
60°C 30 sec
72°C 45 sec
72°C 10 min
4°C ∞

} x35

Samples were electrophoresed for 45 minutes at 100 V on a 2% agarose gel containing 0.5 µg/ml Ethidium Bromide (EtBR). DNA was visualised using a UV transilluminator.

PCR Primers used and expected band sizes were as follows:

Ackr4-gfp

Forward 1: TGAACTTGTGGCCGTTTACGT

Reverse 1: CACACACAGCAACAGATGATCC

Reverse 2: TAGGATTTAGTGACTAAGAGC

WT band: 300bp

GFP band: 600bp

Ackr3-gfp

Forward 1: GATGTAGCAGTGCGTGTCGT

Reverse 1: GAACTTCAGGGTCAGCTTGC

Reverse 2: GTCACTTGGTCGCTCTCCTC

WT band: 275bp

GFP band: 175bp

Ccl19^{-/-}

Forward 1: GCCTCAGATTATCTGCCAT

Reverse 1: CATTAAGAAGGTAGCGGAAGG

Reverse 2: ACCTTGTATTCCTTTGTCGAGAGG

WT band: 1270 bp

KO band: 1169 bp

Ackr4^{-/-}

Forward 1: TGA ACT TGT GGC CGT TTA CGT C

Reverse 1: CAC ACA CAG CAA CAG ATG ATC C

Reverse 2: TAG GAT TTA GTG ACT AAG AGC

WT band: 700 bp

KO band: 320 bp

Note: *Ackr4*^{-/-} *Ccl19*^{-/-} mice were genotyped by Carolyn Thomson. Positive and negative controls were not used for genotyping.

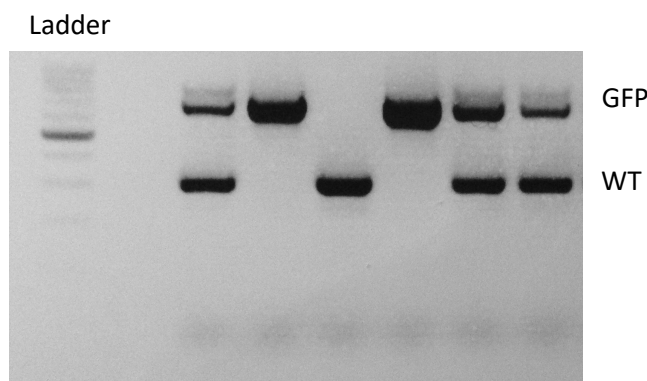


Figure 2-1: Example genotyping result for *Ackr4-gfp* reporter mice.

2.2.3 *In vivo* Methods

2.2.3.1 Chemokine Receptor Blockade

To block CXCR4 function, AMD3100 (Sigma) reconstituted in PBS was injected subcutaneously 24 hours before application of topical irritants at a concentration of 5 mg/kg (estimated from standard growth curve for C57BL/6J mice provided by Harlan) and repeated every 12 hours thereafter over the course of the experiment.

2.2.3.2 Induction of Cutaneous Inflammation

Mice were treated on both surfaces of each ear with topical irritants; alternatively, the lower back was shaved and Nair depilatory cream added for 30 seconds before thoroughly washing with PBS one day prior to treating the back with topical irritants.

Table 2-2: Details of Cutaneous Treatments

IRRITANT	PROCEDURE (EAR)	PROCEDURE (BACK)
TPA (12-O-tetradecanoylphorbol-13-acetate – Invitrogen)	50 µl TPA [50 µM, acetone] per ear. Control: 50 µl acetone per ear Single application or three daily applications.	100 µl TPA [50 µM, acetone] Control: 100 µl acetone Single application or three daily applications.
IMQ (Aldara cream, 5% imiquimod -3M)	42 mg 5% IMQ (1/6 sachet) per ear Control: Vaseline Five daily applications	62.5 mg 5% IMQ (1/4 sachet) per mouse Control: Vaseline Single application or three daily applications.

2.2.3.3 Adoptive Transfer of Murine Splenocytes

All steps were carried out in a sterile hood and all reagents were filter sterilised before use. Spleens were harvested from male OT1 x Ly5.1 mice aged between 6-8 weeks. Typically, 1 or 2 pooled spleens were used. Tissue was passed through a 70 µm cell strainer in separation buffer [PBS, 2% Foetal Calf Serum, 1 mM EDTA]. Cells were counted and either resuspended at 1×10^7 cells/ml in PBS to adoptively transfer all splenocytes, or to transfer B cells only splenocytes were resuspended in separation buffer to use with a B Cell separation kit (Stem Cell Technologies) per the manufacturer's directions. Cells were then resuspended at a volume of 1×10^7 cells/ml in PBS. Whether splenocytes or B cells were used, 100 µl of single cell suspension was injected into each host mouse via the tail vein. After 16 hours recipient mice were culled using a Schedule 1 method and lymph

nodes, blood and/or spleens were harvested and used for flow cytometry analysis. Adoptively transferred splenocytes were identified using anti-CD45.1 antibody.

2.3 General Techniques

2.3.1 Protein Extraction from Tissue

Tissues were excised and kept on ice in RPMI until needed. 2 ml Eppendorf tubes were placed on dry ice, and a 5 mm stainless steel bead (Qiagen) was placed into each tube. A maximum of 30 mg of tissue was added to each tube. Samples were transferred to ice, and 200 μ l of T-PER (Thermo Fisher) was added to each. Tissue was disrupted using a Qiagen TissueLyser at 40 Hz for 5 minutes. Homogenized samples were aspirated and centrifuged at 13000 rpm in a bench-top centrifuge for 5 minutes. Supernatants were removed and stored at -20° C until required.

2.3.2 Immunofluorescent Staining of Frozen Tissue Sections

Excised tissues were immersed in OCT (Tissue Tek) in plastic disposable cryomolds as quickly as possible after dissection; however, for GFP knock-in mice, tissues were fixed overnight in 4% formaldehyde prior to embedding and protected from light to preserve GFP signal. Tissues in OCT were frozen on dry ice then stored at -80° C before preparing sections using a cryotome (Thermo Scientific). Sections were cut between 7-15 μ m depending on the tissue (7 μ m: spleen, 15 μ m: skin) and transferred to Polysine slides (Thermo Scientific). Slides were air dried for 30 minutes or overnight then stored at -80° C until required. When using, slides were air-dried for 30 minutes, fixed for 15 minutes in cold acetone (this step was not carried out for formaldehyde-fixed sections) then removed and the perimeter of each tissue section was marked with a wax pen, forming a hydrophobic barrier to keep reagents on the slide and prevent mixing. Slides were blocked with blocking buffer [10% donkey serum in PBS] for 30 minutes at room temperature. Blocking buffer was removed gently, and primary antibodies were added in PBS at the manufacturer's recommended dilution for 2 hours at room temperature or overnight at 4° C. Slides were washed three times for 5 minutes with shaking in PBS. Secondary antibodies were added in PBS at the manufacturer's recommended dilution for 30 minutes at room temperature. Slides were washed as before and mounted using Vectashield mountant (with or without DAPI as appropriate; Vector Labs) and sealed under a coverslip with clear nail varnish.

Table 2-3: List of Antibodies Used for Immunofluorescent Staining

Note: all antibodies are anti-mouse and used at 1:200 unless otherwise stated.

ANTIGEN	CLONE	SUPPLIER	CONCENTRATION
ACKR3 CXCR7 (α -human)	11G8 (mouse)	R&D Systems	1:100
ACKR3 (α -human)	Polyclonal (rabbit)	Abcam	1:100
ACKR4 CCRL1	Polyclonal (goat)	Santa Cruz Biotech	1:50
ACKR4 CCRL1 (α -human)	13E11	BioLegend	1:50
B220	RA3-6B2	eBioscience	
CCL21	Polyclonal (goat)	R&D Systems	
CD169	3D6.112	eBioscience	
CD205	DEC-205	BioLegend	1:100
CD31	390	BioLegend	
CXCR4 (α -human)	12G5	R&D Systems	1:100
CXCR4 (α -human/ mouse)	Polyclonal (rabbit)	Abcam	1:100
DCIR2	33D1	BioLegend	1:100

LYVE-1	223322	R&D Systems	
MHC-II	M5/114.15.2	BioLegend	

2.3.3 Flow Cytometry

Cells were counted using a haemocytometer or Luna FL (Labtech) with Trypan Blue exclusion. Up to 5×10^6 cells were used per tube for flow cytometry. Half of one sample was removed and heat-killed by incubating at 65°C for 5 minutes, then mixed with the live half to serve as a live-dead only control. Cells were centrifuged at $400 \times g$ for 5 minutes and resuspended in 0.1% v/v APC-e780 fixable viability dye (eBioscience) in PBS, then incubated on ice for 20 minutes. Cells were centrifuged as before and resuspended in FACS buffer containing Fc blocker (BD Biosciences or BioLegend) at a concentration of 1:100. Samples were incubated on ice for 20 minutes then centrifuged as before. Samples were resuspended in FACS buffer containing panels of antibodies for extracellular staining, normally at a concentration of 1:200; Fluorescence-minus-one (FMO) controls were set up to aid gating, by staining cells with all but one antibody from the panel. In practice, this was only done for markers that were difficult to discriminate, to conserve antibodies and samples when using large panels of antibodies. Samples were incubated on ice for 15 minutes then centrifuged as before. For immediate FACS analysis, cells were resuspended in FACS buffer. For future analysis or intracellular staining, cells were resuspended in CytoFix/CytoPerm (BD Biosciences) on ice for 20 minutes. If staining for intracellular markers, cells were resuspended in antibody diluted in 1 X PermWash (BD Biosciences) for 20 minutes on ice. Cells were resuspended in FACS buffer and analysed within 3 days.

When blood was analysed via flow cytometry, the original volume of every sample was noted before processing and $10\mu\text{l}$ fluorescent counting beads (BD Biosciences) was added to each tube immediately prior to sample acquisition. The total cell count was obtained by the following calculation:

$$\frac{\text{number of live cells recorded}}{\text{number of beads recorded}} \times \frac{\text{number of beads added}}{\text{volume of blood}}$$

where the number of beads added was the manufacturer’s stated number of beads per μl multiplied by the volume added to each tube. Beads were identified by their high fluorescence in the FITC/PerCP channels and FSC/SSC properties.

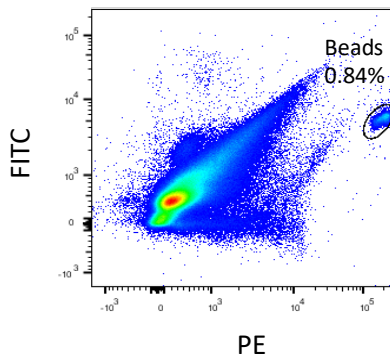


Figure 2-2: Flow Cytometry Gating Strategy for Identifying Counting Beads.

Single-stained compensation controls were set up for each antibody using UltraComp eBeads (eBioscience) according to the manufacturer’s directions. For viability dyes, a small sample of heat-killed cells (incubated for 10 minutes at 64°C) mixed equally with viable cells was stained with viability dye as described.

Table 2-4: List of Antibodies Used for Flow Cytometry

Note: all antibodies are anti-mouse and used at 1:200 unless otherwise stated.

ANTIGEN	CLONE	SUPPLIER	CONCENTRATION
ACKR3 (α -human/ mouse)	11G8 (mouse)	R&D Systems	1:100
ACKR4	Polyclonal (goat)	Santa Cruz	1:50
B220	RA3-6B2	eBioscience	
CCR2	475301	R&D systems	1:20
CD101	Moushi101	eBioscience	
CD103	2E7	BioLegend	
CD11b	M1/70	BioLegend	

CD11c	N418	eBioscience	
CD205	DEC-205	BioLegend	1:100
CD207 Langerin	EbioL31	eBioscience	1:50
CD31	390		
CD31	390	BioLegend	1:200
CD326 EpCAM	G8.8	eBioscience	
CD34	MEC14.7	BioLegend	
CD3ε	145-2C11	BioLegend	
CD4	RM4-5	eBioscience	
CD45	30-F11	BioLegend	
CD45.1	A20	BioLegend	
CD49f α ₆ integrin (α-human/ mouse)	GoH3	BioLegend	
CD8α	53-6.7	BioLegend	
CXCR4 (α-human/ mouse)	Polyclonal (rabbit)	Abcam	1:100
CXCR4 (α-mouse)	2B11	eBioscience	1:50
DCIR2	33D1	BioLegend	1:100
gp38	8.1.1	BioLegend	

Ly6C	HK1.4	BioLegend	
LYVE-1	223322	R&D Systems	
MadCAM1	MECA-367	BD Biosciences	
MCAM-1 CD146	ME-9F1	BioLegend	
MHC-II	M5/114.15.2	eBioscience	
NK1.1	PK136	BioLegend	
Sca-1 Ly6A/E	D7	eBioscience	
SiglecH	440c	BD Biosciences	
TCR β	H57-597	BioLegend	
VCAM-1 CD106	429(MVCAM.A)	BD Biosciences	
VE-Cadherin CD144	BV13	eBioscience	
$\gamma\delta$ TCR	GL3	BioLegend	

2.3.4 Fluorescent Chemokine Uptake

Up to 2×10^6 cells per well were added to ultra-low binding round-bottom 96-well plates (Sigma). Cells were centrifuged at 400 x g for 5 minutes and resuspended in PBS to wash three times. Cells were then resuspended thoroughly in 50 μ l of serum-free RPMI with 2.5 nM chemokine fluorescently labelled with Alexa Fluor 647 (Almac), either with or without 25 nM unlabelled chemokine (Almac). The wells with unlabelled chemokine were used as controls to detect non-specific uptake of the labelled chemokine, as the excess concentration of unlabelled chemokine will out-compete labelled chemokines for receptor-

mediated uptake, whereas non-specific uptake (e.g. pinocytosis) is not saturated by the quantity of ligand. Cells were incubated for 1 hour at 37° C, then washed 3 times in PBS as previously described. At this stage cells were resuspended in FACS buffer and used for flow cytometry analysis.

Table 2-5: List of recombinant chemokines used

CHEMOKINE	FORMATS	SUPPLIER
CCL19	Biotinylated, AF647-conjugated, native	Almac
CXCL12	AF647-conjugated, native	Almac (both), Peprtech (native)
CXCL11	Native	Almac

2.3.5 Bradford Assay

Protein concentrations were determined using Bio-Rad Bradford reagent. The reagent was diluted 1:5 in distilled water and passed through Whatman no. 1 filter paper. Six standards were prepared by diluting appropriate volumes of a 1.5 mg/ml stock solution of BSA in 1 ml of Bradford reagent to obtain concentrations of 9 µg/ml, 7.5 µg/ml, 6 µg/ml, 4.5 µg/ml, 3 µg/ml and 1.5 µg/ml. 1 µl of each sample was added to 1 ml of Bradford reagent and 200 µl per well of each standard or sample was added in duplicate to a 96-well plate, and the absorbance was measured at 595 nm using a Teacan Sunrise plate reader.

2.3.6 SDS-PAGE and Western blotting

Samples were diluted in 4X LDS sample buffer (Invitrogen) with 50 mM DTT and heated to 65° C for 5 minutes. Proteins were run on 4-12% Bis-Tris gels (Invitrogen) at 200 V for 50 minutes in MOPS running buffer (Invitrogen). Gels were transferred to PVDF membranes using the Novex iBlot system per the manufacturer's directions. Membranes were then rinsed with PBS, blocked with 1% milk-PBS (dried milk powder: Marvel) for 30 minutes and incubated with primary antibodies in 5% BSA-PBS either for 3 hours at room temperature or overnight at 4° C. Membranes were washed 5 times for 5 minutes with

PBS/T [PBS, 0.1% v/v Tween-20], blocked for 30 minutes in 5% milk-PBS/T and incubated with HRP-conjugated secondary antibody in 1% milk-PBS/T for 2 hours at room temperature. Membranes were washed twice in PBS/T, twice in high salt PBS/T [1X PBS/T, 400 mM NaCl] and once in PBS/T. 1 ml ECL solution (Pierce) was added to each membrane for 1 minute, then images were developed by placing X-ray film (Kodak) over the blot in a developing cassette and using a film developer to obtain images. Successive films were typically exposed for 10 seconds, 30 seconds, 1 minute and 10 minutes.

2.3.7 RNA Extraction from Tissue

Tissue was harvested and placed immediately on ice. To process later, tissue was stored in RNAlater (Ambion) at -20° C until required. Up to 10 mg of tissue was placed in a 2 ml RNase free Eppendorf tube on dry ice containing one 5 mm stainless steel bead (Qiagen) along with 1 ml TriZol reagent (Ambion). Tubes were added to the pre-cooled insert of a Qiagen TissueLyser and processed for 5 minutes at 50 Hz. Samples were then placed on ice until chilled again. These steps were repeated until tissue was lysed. Samples were then centrifuged at 12000 rpm for 2 minutes in a micro centrifuge to pellet any debris, and supernatants transferred to fresh tubes. Samples were passed ten times through a 21 Ga syringe to homogenise. RNA was then extracted using a PureLink RNeasy mini kit (Ambion) per the manufacturer's directions.

2.3.8 Quantitative Polymerase Chain Reaction

Reverse transcription polymerase chain reaction (RT-PCR) was carried out on RNA samples using a QuantiTect Reverse Transcription Kit (Qiagen) per the manufacturer's directions to obtain cDNA. Samples were stored at -20° C until required. Samples were analysed in triplicate on 384-well plates using TaqMan probes (Applied Biosystems) and TaqMan 2X Master Mix without UNG (Applied Biosystems) according to the manufacturer's directions. All samples were run in triplicate, and each experimental group contained at least three biological replicates for mouse studies. For cultured human cells, using separate donors was not feasible but at least three separate wells of cells were used for each experiment as a technical replicate. In addition, every experiment included a - RT sample for each treatment group (no reverse transcriptase enzyme added during reverse transcription, to ensure no DNA contamination was present in the RNA samples) and a no-template control (to ensure no RNA contamination was present in the qPCR reagents). Additionally, all probes used spanned exons to prevent amplification of any DNA

contamination if present. Plates were analysed on an Applied Biosystems 7500 Fast or Applied Biosystems Quantstudio 6 Flex using the standard qPCR program. All samples were normalised to TBP or GAPDH expression by subtracting the CT value of the reference gene from the CT value of the target gene to obtain the Δ CT and calculating relative gene expression using the $2^{-\Delta$ CT method (Arbitrary Units; AU – used where no single ‘control’ sample exists) or the $2^{-\Delta\Delta$ CT method (Relative Quantification; RQ – where there is a single ‘control’ sample to express all other samples relative to). CV values of technical replicates were checked and any outliers excluded; sample groups showing multiple outliers were discarded or re-analysed.

Table 2-6: List of TaqMan probes used

TARGET	SPECIES	ASSAY ID
ACKR3	Human	Hs00664172_s1
ACKR4	Human	Hs00664347_s1
CCL19	Human	Hs00171149_m1
CCL21	Human	Hs00171076_m1
CXCL11	Human	Hs00171138_m1
CXCL12	Human	Hs03676656_mH
CXCR4	Human	Hs00607978_s1
Ackr3	Mouse	Mm04931206_s1
Ackr4	Mouse	Mm02620636_s1
Ccl19	Mouse	Mm00839967_g1
Ccl21	Mouse	Mm03646971_gH
Cxcl12	Mouse	Mm00445553_m1
Cxcr4	Mouse	Mm01996749_s1

2.4 Analysis

2.4.1 Flow Cytometric Analysis

All data obtained from flow cytometry was analysed using FlowJo software (Treestar). Samples were always gated initially on forward and side-scatter parameters to exclude debris, forward scatter average against height to exclude doublets and cells negative for viability dye to exclude dead cells which could be stained non-specifically. Individual stains were gated based on FMO, if available. For individual tissues and cell types, standard gating strategies were applied as detailed in the results section.

2.4.2 Statistical Analysis

For statistical analysis, Prism (GraphPad) was used. Unless otherwise stated, all analyses used the following methods: Where there were two groups, t-tests were used: these were unpaired two-tailed t-tests and the Holm-Sidak correction was applied where multiple comparisons were carried out. For three or more groups, one-way analysis of variance (ANOVA) was used with Tukey's correction for multiple comparisons. To compare two or more parameters simultaneously, two-way ANOVA was used with Tukey's correction for multiple comparisons. Statistical significance was denoted as follows: * $P \leq 0.05$, ** $P \leq 0.01$, *** $P \leq 0.001$, **** $P \leq 0.0001$, ns = $P > 0.05$. All error bars represented the standard deviation of the mean.

Chapter 3: Atypical Chemokine
Receptor Expression and Function *in*
vitro

3 Atypical Chemokine Receptor Expression and Function *in vitro*

3.1 Introduction

ACKR3 and ACKR4 both have potential roles to play during skin inflammation but have not yet been extensively studied in this context. As outlined in the introduction (See section 1.7.2), ACKR4 protein is known to be functional on keratinocytes and lymphatic endothelial cells (LECs) in the skin, and likely modulates Langerhans cell (LC) and dermal DC trafficking to the skin-draining lymph nodes both during homeostasis and immune challenge by scavenging CCR7 ligands^{177,179}.

CXCR4/CXCL12 are also expressed in the skin and appear to be implicated in inflammation and wound healing, but there is conflicting evidence over their precise roles. It is possible that this is at least partly due to the activity of ACKR3¹⁸⁶, which is expressed on many of the same cell types that express CXCR4 including keratinocytes and fibroblasts in the skin. Notably, several studies use AMD3100 as a CXCR4 antagonist, but as this molecule has also been shown to act as an ACKR3 agonist¹⁸⁷, it is conceivable that unintended effects occur in cells that express both receptors. Notably, ACKR3 has been shown to dimerise with CXCR4 on cells that express both receptors, and to modulate its function^{142,153}, supporting a role for ACKR3 in the CXCR4/CXCL12 axis.

3.2 Aims

- To determine expression levels of ACKR4, ACKR3, CXCR4 and their ligands in cultured human skin cells (keratinocytes and LECs) at both the mRNA and protein level.
- To evaluate whether ACKR3 and CXCR4 co-localise in these cells.
- To investigate whether the expression of atypical chemokine receptors and related transcripts are affected by inflammatory stimuli.
- To investigate whether chemokine scavenging by ACKR3 or ACKR4 is detectable on these cells, and whether it is affected by inflammatory stimuli or by coexpression of CXCR4 (in ACKR3+ cells).

3.3 Expression and Modulation of ACKRs on Human Dermal LECs

As discussed, ACKR4 has potential chemokine scavenging roles on LECs, and ACKR3 has also been reported on lymphatic vessels¹⁸⁸. LECs are a rare population of cells, however, and studying their function in further detail *in vivo* would be challenging. I was also interested in investigating a functional role for ACKR4 in human cells. As a consequence, I began by studying cultured human dermal LECs (HD-LECs) to determine whether ACKRs 3 and 4 are expressed in these cells, and whether these cells possess chemokine scavenging capabilities *in vitro*.

3.3.1 Cultured Human Dermal LECs Express ACKR3, ACKR4 and CXCR4

Antibody staining against chemokine receptors is often challenging, and atypical chemokine receptors are no exception. The 13E11 mouse monoclonal antibody (mAb) was one of the original antibodies raised against ACKR4¹⁸⁹. This antibody was used in immunofluorescent staining to determine whether cultured HD-LECs expressed detectable ACKR4 protein. Anti-ACKR4 staining intensity in these cells appears to be variable, though a clear majority are ACKR4⁺ (Figure 3-1A). The protein appears to be largely cytoplasmic, and the punctate staining pattern suggests it is localised in vesicles (Figure 3-1B). This is reminiscent of previous results for ACKR2, which shows a similar staining pattern on cultured HD-LECs¹⁹⁰. ACKR2 is recycled between the cell surface and endosomal vesicles, allowing it to rapidly internalise chemokines without being desensitised. Consequently, the large majority of ACKR2 protein produced by a cell is cytoplasmic and associated with intracellular vesicles¹⁴⁶.

HD-LECs also express CCL21 protein, which can be detected via immunofluorescence both extracellularly because its C-terminal interactions with GAGs tether it to the surface of cells, and intracellularly, because any protein that has not been secreted by the cell is also detectable via antibody staining. Anti-CCL21 staining on HD-LECs showed a variable pattern (Figure 3-1C), with some cells more positive than others. It appeared that the majority of the CCL21 detected was intracellular, as extracellular protein would tend to localise mostly to the edges of the cell; instead anti-CCL21 staining appeared similar in character to the punctate anti-ACKR4 staining, and occasionally overlapped with it.

Next, I examined whether HD-LECs expressed ACKR3 and the other receptor for CXCL12, CXCR4. Antibody staining for ACKR3 has also been challenging. Originally, a

polyclonal antibody (pAb) was used for immunofluorescence (Figure 3-2A). A mAb, 11G8, was recommended as the most specific antibody available ¹⁹¹ and showed similar staining patterns to the pAb previously used (Figure 3-2B); both antibodies appeared to be at least specifically detecting a target as determined by the isotype controls (Figure 3-2C). As both the polyclonal and monoclonal antibodies were raised in different species (rabbit and mouse, respectively), the specific antibody used from this point onwards was determined by the constraints dictated by the species of other antibodies used in each experiment.

Results for anti-ACKR3 staining showed a similar expression pattern to ACKR4, as expected for an atypical chemokine receptor: the majority appeared to be intracellular and localised in vesicles. Surprisingly, in some cells, there appeared to be nuclear staining for ACKR3 (Figure 3-2D). This was quantified by counting ACKR3 positive nuclei in at least 6 randomly-selected fields of view across three separate experiments. Although the average number of cells showing nuclear staining was about 12%, there was high variability between each field examined: many showed no nuclear staining in any of the LECs present, while the highest proportion of nuclear staining detected in one field of view was 75%.

Although CXCL12 and CXCR4 localisation to the nucleus have been reported ^{192,193}, there is no known precedent for ACKR3 protein expression at this site. Bioinformatics tools suggested a low possibility that ACKR3 could spend some time in the nucleus: the PredictProtein tool ¹⁹⁴ suggested the protein would only be localised in the cell membrane but with a very low confidence value (14 on a scale of 0-100), and the NucPred tool ¹⁹⁵ gave a score of 0.12, where values over 0.1 suggest a protein spends at least some time in the nucleus, but with a very low specificity (45%). These analyses did not rule out the possibility that ACKR3 can be localised in the nucleus but did not provide compelling evidence in favour of this observation, either.

To further examine this result, nuclear and cytoplasmic protein fractions were isolated from LECs and western blotting was used to attempt to locate ACKR3. Despite multiple efforts, and although the antibody used was validated for western blotting by the supplier (Abcam), ACKR3 could not be detected using this method. Lower temperatures were used for the protein denaturing stage of the protocol as previous experiments have shown the atypical chemokine receptor ACKR2 forms aggregates when higher temperatures are used ¹⁹⁶, more sensitive ECL reagents were tested, and human heart lysate (PromoKine) was

used as a positive control as this tissue is known to be ACKR3⁺ ¹⁵⁰, but no positive ACKR3 signal could be detected.

Anti-CXCR4 staining appeared to localise largely to the plasma membrane, as indicated by the intensity of signal near the edges of the cell (Figure 3-3A). The pattern of anti-CXCR4 staining appeared to be strand-like, as though associated with the cytoskeleton; however, anti-CXCR4 staining with a different antibody did not appear to replicate this pattern (data not shown).

The principal motivation for investigating CXCR4 staining on HD-LECs was to determine the degree of ACKR3 and CXCR4 co-staining in these cells, as it has been reported that ACKR3 and CXCR4 can heterodimerise in cells expressing both receptors ^{142,157}. These results were challenging to obtain, as the antibodies used most successfully for single staining of both these proteins were rabbit pAbs. Unfortunately, the mouse mAb 11G8 did not give satisfactory results when used in combination with anti-CXCR4 antibodies, showing weak and low-level antibody staining.

3.3.2 ACKR3, ACKR4 and CXCR4 in Cultured HD-LECs Are Mostly Intracellular

To verify the results obtained from immunofluorescence, and to obtain some quantification of the expression levels of ACKR4 on HD-LECs, the same anti-ACKR4 mAb (13E11) was used for flow cytometry analysis. Cells were either stained before fixing, or after fixing using buffer containing saponin to maintain the permeability of cell membranes. Results showed that only a small subset of non-permeabilised HD-LECs express detectable ACKR4 (Figure 3-4A, left panel). When permeabilised, the proportion of ACKR4⁺ cells detected rose substantially (Figure 3-4A, right panel). The overall fluorescence intensity also rose from non-permeabilised to permeabilised cells; this is likely due to the permeabilisation protocol leading to a higher level of background staining, as the isotype control also showed a similar increase in fluorescence intensity. As there was a larger differential between the anti-ACKR4 stained sample and the isotype control in the permeabilised samples, this suggested that there was a genuine increase in ACKR4 availability for antibody binding in the permeabilised cells. It also appears to agree with the immunofluorescence results obtained previously.

In this analysis, the peak of the isotype control was higher than the lowest-intensity signal for ACKR4 antibody staining both in the permeabilised and non-permeabilised samples.

This may have been because the specific kappa chain clone used as an isotype may have had a higher affinity for unblocked Fc receptors than the kappa chain on the anti-ACKR4 antibody¹⁹⁷. Alternatively, the number of fluorophore molecules per antibody (F:P ratio) may be different for the two reagents¹⁹⁷ (Both reagents were supplied by BioLegend, but it was not possible to obtain this information). From the appearance of the histograms, ACKR4 does appear to follow a bimodal distribution in cultured HD-LECs making an isotype control less necessary¹⁹⁸.

Anti-ACKR3 staining showed a similar pattern to ACKR4, with just under half of cells positive for ACKR3 surface staining (Figure 3-4B, left panel), while the majority appeared as ACKR3 positive when permeabilised (Figure 3-4B, right panel). A small population of cells showed surface staining for CXCR4 (Figure 3-4C, left panel), and just under half for intracellular staining (Figure 3-4C, right panel). This does not appear to reflect the results obtained using immunofluorescence, as most cells were CXCR4+ across many repeated experiments. The proportion of CXCR4+ cells obtained may have been underestimated as the staining appears to show a 'gradient' rather than a specific positive and negative population, which suggests some weakly-positive CXCR4+ cells may have been classed as negative; however, the gate was drawn based on the isotype, and this is the most reliable estimate for positive versus negative staining available in the experiment.

On cells that were analysed by flow cytometry, a substantial minority of the population showed surface staining for ACKR3, ACKR4 and CXCR4, while cells analysed by immunofluorescence showed very little extracellular staining. This may have been caused by using fixed cells for the immunostaining experiments, rather than the live cells used to detect surface staining in flow cytometry experiments. It is possible that paraformaldehyde fixation, which permeabilises cells, could lead to a lack of surface receptor detection. This could be tested by live-staining cells grown on coverslips prior to fixation.

Overall, however, the flow cytometry results obtained for ACKRs appear to concur with those obtained from immunofluorescence: ACKR3 and ACKR4 expression in cultured HD-LECs is heterogeneous, with a minority of cells expressing no detectable protein. A clear majority of these cells express ACKR3 and/or ACKR4 internally, although a significant fraction of these cells clearly carries detectable surface ACKR3 and/or ACKR4. Furthermore, the percentage of cells that expressed detectable intracellular ACKR3 was similar to the percentage of cells expressing detectable intracellular ACKR4.

3.3.3 ACKRs Expressed by HD-LECs Rarely Co-Localise

The results obtained from flow cytometry analysis suggested that ACKR3 and ACKR4 expression by HD-LECs is heterogeneous as both receptors only appeared to be present in a subset of cells. I was interested in determining to what degree expression of these receptors overlapped in HD-LECs, and whether cells expressing both receptors would indicate co-localisation. As heterodimerisation between chemokine receptors is well known¹⁹⁹, including ACKR3 with CXCR4^{142,156,157}, it is feasible that ACKRs expressed by the same cell could also perform a similar function. As cultured HD-LECs also express ACKR2¹⁹⁰, this protein was also included in the analysis. As all primary antibodies were raised in either rabbit or mouse, it was only possible to stain cells with two anti-ACKR antibodies simultaneously.

Staining cells with both anti-ACKR3 and anti-ACKR4 antibodies indicated that most HD-LECs expressed both ACKRs (Figure 3-5A). Close examination showed that some vesicles appeared to be positive for both ACKR3 and ACKR4 (Figure 3-5B), although the vast majority were positive for one receptor or the other. When both anti-ACKR2 and anti-ACKR4 antibodies were used, a similar pattern was seen (Figure 3-6A); however, anti-ACKR4 reactivity appeared to be weaker than often seen during single staining (e.g. figure 3-1A). Examining individual cells did not reveal any vesicles that appeared to be positive for both ACKRs (Figure 3-6B). Finally, when anti-ACKR2 and anti-ACKR3 co-staining was attempted, the vast majority of cells appeared to be positive for both receptors (Figure 3-7A), and occasionally vesicles appeared to be positive for both ACKR2 and ACKR3 immunoreactivity (Figure 3-7B), but this was rare.

Taken together, these results suggest that the majority of HD-LECs express ACKR2, ACKR3 and ACKR4 proteins, but there is little evidence that these receptors regularly co-localise, at least under steady-state conditions.

3.3.4 ACKR3 and ACKR4 Proteins Are Not Localised in Lysosomes

Because expression of ACKR2, ACKR3 and ACKR4 proteins do not appear to significantly overlap, I was interested in determining whether these proteins were localised in different subcellular compartments (ACKR2 has previously shown to be continually recycled between the cell surface and endosomal vesicles, and is associated with RAB5+ early endosomes¹⁴⁶). First, I investigated the lysosomes. This can be done using a pH-

responsive dye that is phagocytosed by cells. When exposed to the low-pH environment of the lysosomes, it becomes fluorescent and can be detected via fluorescence microscopy. This experiment showed that neither ACKR3 (Figure 3-8) nor ACKR4 (Figure 3-9) are localised in lysosomes.

3.3.5 ACKR4 Protein is Localised in RAB5A+ Vesicles

As ACKR3 and ACKR4 are not localised in the lysosomes, I hypothesised they would be constrained to the early recycling endosomes if they behave in a similar fashion to ACKR2. A transient transfection method was used to cause HD-LECs to express a Rab5a-GFP fusion protein from a virally-delivered plasmid. In these cells, anti-ACKR4 staining indicated that the protein was clearly co-localised with RAB5A+ vesicles (Figure 3-10), suggesting that it is functioning similarly to ACKR2. This result was interesting because ACKR2 and ACKR4 do not appear to co-localise, yet both are confined mainly to the early endosomes. Unfortunately, there was not time to finish these investigations by carrying out anti-ACKR3 staining in these cells.

3.3.6 mRNA Expression of ACKRs and Related Genes by HD-LECs May Be Regulated in Response to Inflammation

mRNA expression of *ACKR3* and *ACKR4* were also examined in HD-LECs, including their regulation in response to various inflammatory signals. It was not possible to include true biological replicates in these experiments, as the expense of obtaining cells from a sufficient number of donors would be prohibitive, but experiments were carried out on multiple technical replicates as a means to begin investigating expression of ACKRs and related transcripts in cultured human cells. Consequently, statistical analysis was not appropriate, and only large apparent differences in mRNA expression can be commented on.

I hypothesised that ACKRs would be upregulated in response to inflammation, increasing scavenging activity to balance out the available signal from chemokines which may be upregulated by other cell types (or LECs themselves) in response to inflammatory stimuli. *CXCL12* and *CCL21* were also included in this analysis as all of these chemokines are known to be expressed by LECs^{200,201} and I hoped to determine whether expression of these genes is regulated in tandem with their scavenging receptors. *CCL19* expression was not detected by HD-LECs. Although *CXCR4* was detected in HD-LECs, results were

extremely variable and there was no amplification in some samples, making the level of *CXCR4* expression uncertain. As detection of *CXCR4* protein in HD-LECs also appeared to be unreliable, given that flow cytometry and immunofluorescence results did not appear to agree, I decided to focus on investigating the receptors *ACKR3* and *ACKR4* only.

IFN- α , IFN- β and IFN- γ have previously been shown to induce *ACKR2* expression in cultured HD-LECs¹⁹⁰, and I hoped to determine whether other ACKRs would show similar expression patterns in these cells. Lipopolysaccharide (LPS) and unmethylated CpG DNA were also investigated as they are ligands for TLRs 4 and 9 respectively, both of which are expressed by LECs²⁰², and any modulation of ACKRs in response to these PAMPs would most likely represent a direct response to an inflammatory stimulus detected by LECs rather than to cytokines secreted by other cells. This may suggest specific response pathways ACKRs are involved in.

Results showed some interesting patterns of *ACKR4* mRNA expression. Both IFN- α (Figure 3-11A) and IFN- β (Figure 3-11B) appeared to cause a modest increase in *ACKR4* mRNA expression that had fallen by 48 hours post-treatment. IFN- γ led to greater than 100-fold increase in *ACKR4* mRNA (Figure 3-11C), but this response appeared to peak at 24 hours post-treatment and had returned to baseline levels by 48 hours post-treatment. CpG treatment also appeared to lead to an induction of *ACKR4* mRNA at 48 hours post treatment (Figure 3-11D). LPS did not appear to have any striking effect on *ACKR4* expression levels (Figure 3-11E).

CCL21 expression also appeared to be modulated in response to some of these stimuli, often appearing to peak later than *ACKR4*: an induction was seen at the 48-hour timepoint, but not before, in response to IFN- α (Figure 3-11A) and IFN- β (Figure 3-11B). No strong differences in *CCL21* expression were detected in response to IFN- γ (Figure 3-11C), CpG (Figure 3-11D) or LPS (Figure 3-11E).

ACKR3 and *CXCL12* expression showed some minor potential changes in response to inflammatory stimuli. Interestingly, *ACKR3* and *CXCL12* appeared to show either very similar, or opposing, changes in response to each treatment. All changes in expression, however, were too small to comment on further in the absence of any statistical analysis.

3.3.7 ACKR4-Mediated Chemokine Uptake Occurs at Low Levels on Cultured Cells

The results obtained so far suggested that expression of *ACKR3* and *ACKR4* by HD-LECs may be affected by immunomodulatory signals, particularly IFN- γ in the case of *ACKR4*. Given other studies showing ACKR4-dependent *in vivo* CCL19 scavenging capabilities of dermal LECs¹⁷⁹ and *in vitro* scavenging of CCL2 by cultured HD-LECs via ACKR2¹⁹⁰, I hoped to ascertain whether ACKR3 and ACKR4 expressed by HD-LECs may play a similar role *in vitro*. I further reasoned that treating HD-LECs with IFN- γ for 24 hours may lead to an increase in the reported chemokine scavenging function of ACKR4. To test this hypothesis, I used a chemokine uptake assay. This protocol was developed to overcome the issue of poor reagents for detecting chemokine receptors²⁰³, and is advantageous compared to antibody staining as it can measure receptor activity. The assay has been used in this manner previously, both *in vivo* and *in vitro*^{179,190,204,205}.

To perform an uptake assay, cells are incubated at a pre-determined optimal concentration of fluorescently-labelled recombinant chemokine. Some samples simultaneously receive an excess, normally ten times greater, of native chemokine. Cells possessing the correct chemokine receptor will bind and internalise the chemokine at a rate limited by the number and activity of receptor molecules present on their surface. In samples where cells also receive unlabelled chemokine, this will bind equally to the chemokine receptors and so outcompete the labelled chemokine for binding sites due to their vastly increased availability. Any non-specific uptake of labelled chemokine, for example through pinocytosis, is not limited by the availability of receptors so is not saturated by the quantity of chemokine present. Therefore, non-specific uptake of labelled chemokine will not be disrupted by adding unlabelled competition, but receptor-mediated uptake will. Similar results can be achieved by using biotinylated chemokine incubated with streptavidin-conjugated fluorophores, which form tetramers due to the four available biotin binding sites on each streptavidin molecule. Streptavidin-fluorophore alone is used as a control in this assay to detect non-specific uptake.

In these experiments, CCL19 was used as an ACKR4 ligand. CCL21 is less soluble due to its C terminal binding to GAGs on the surface of LECs, making it less suitable for *in-vitro* applications. The results showed no detectable CCL19 or CXCL12 uptake on HD-LECs. Although IFN- γ treatment induced *ACKR4* mRNA expression, there was no detectable effect on the receptor's scavenging activity *in vitro*. Murine splenocytes were used as a

positive control as there are large numbers of CCR7⁺ DCs and T cells and CXCR4⁺ cells including monocytes in the spleen. This validated the assay for CCL19 by showing a strong AF647 signal in CCL19-only samples that was abrogated by inclusion of unlabelled competitor (Figure 3-13A, left panel), while there was no difference in signal between HD-LECs cultured with CCL19-AF647 only or with competitor as well (Figure 3-13A, right panel). Interestingly, the peak of fluorescence for HD-LECs was far higher than that seen for splenocytes despite these cells being analysed sequentially using the same cytometer settings. If the positive gate was set based on the splenocyte control, nearly all HD-LECs were CCL19⁺ in the presence or absence of unlabelled CCL19. As there was no unstained HD-LEC control, however, higher levels of autofluorescence by these cells could not be ruled out.

As both CXCR4 and ACKR3 are capable of binding CXCL12, using the competitive binding assay with CXCL12 alone would not determine which receptor was responsible for the fluorescent signal. To investigate ACKR3-mediated scavenging, therefore, an uptake assay was carried out using three different conditions: labelled CXCL12 alone, labelled CXCL12 with excess unlabelled CXCL12 competitor and labelled CXCL12 with excess unlabelled CXCL11. As CXCL11 binds to ACKR3 and not CXCR4, I reasoned that both ACKR3 and CXCR4-mediated uptake would be inhibited by competition from CXCL12, while only ACKR3-mediated uptake would be inhibited by competition from CXCL11. As CXCL11 has a lower affinity for ACKR3 than CXCL12 does¹⁵⁵, unlabelled CXCL11 was added at five times the concentration of labelled CXCL12.

In this experiment, it was not possible to detect a very strong CXCL12 uptake signal from splenocytes (Figure 3-13C, left panel), although the vast majority of this did appear to be abrogated by competition from unlabelled CXCL12 and not CXCL11, suggesting the uptake detected was mainly due to CXCR4 activity. In HD-LECs, however, no CXCL12 uptake was detected (Figure 3-13C, right panel). This suggested issues with the assay itself, as there was a lack of uptake detected in the positive control, but it was not clear what differences in experimental technique could have led to this failure and repeated attempts to replicate the result obtained with CCL19 were unsuccessful.

Although chemokine scavenging activity has previously been reported on cultured HD-LECs via ACKR2¹⁹⁰, and on transfected cells via ACKR3 and ACKR4, these results could not be reliably reproduced. One potential explanation is that previous *in vitro* studies have often used transfected cells overexpressing *ACKR3* or *ACKR4*^{154,170}, while in the study

showing CCL2 uptake on LECs there was only significant signal detected when LECs were virally stimulated¹⁹⁰; it may be that neither of these scenarios represent a natural level of ACKR activity for HD-LECs.

Uptake assays were also attempted instead using microscopy, to determine whether the manual disruption caused by moving HD-LECs from their culture surface to a single-cell suspension had any effect on ACKR4 activity. Cells were cultured on coverslips then incubated with either biotinylated chemokines bound to streptavidin-conjugated fluorophores, or the streptavidin-fluorophore conjugate alone. The results of this assay showed that most of the fluorescent CCL19 signal was found outside cells (Figure 3-14A). Surprisingly, when streptavidin-fluorophore alone was used, more of the fluorescent signal was associated with LECs than when CCL19 tetramers were used (Figure 3-14B). Thus, there is no evidence for the specific uptake of CCL19 tetramers by cultured HD-LECs.

3.3.8 Chemokine Scavenging Assays on Human Dermal-LECs

In the uptake assays described here, cells may have degraded chemokines rapidly once they were internalised, leading to a lack of fluorescent signal. To address this potential issue, a chemokine scavenging assay was performed. In this assay, cells are incubated with media containing a known concentration of chemokine, and aliquots of the culture media are taken at fixed timepoints and analysed using ELISA to detect the chemokine concentration of the media. If cells are internalising and degrading the chemokine, the concentration would be expected to decrease. A well is also included containing no cells, as a control to detect chemokine removal from the media via protease activity, chemokine binding to GAGs on the surface of cells, or chemokine binding to the culture surface.

In this assay, both CCL19 (Figure 3-15A) and CXCL12 (Figure 3-15B) were rapidly removed from the media, whether cells were present or not; IFN- γ treatment was used on HD-LECs receiving CCL19, as I reasoned from the qPCR results shown previously that this may increase ACKR4 activity, but this did not lead to an increased rate of CCL19 removal (Figure 3-15A). Taken together, these findings suggested that chemokines were adhering to the surface of the culture vessel rather than being internalised by cells, or that they were being degraded by endogenous proteases in the endothelial cell growth medium. A variety of blocking strategies used prior to the addition of chemokines were tested, along with the addition of protease inhibitors to the media and altering the initial chemokine

concentrations, but it was not possible to prevent the rapid drop-off in chemokine concentration in the control wells.

It is possible that chemokines were also removed from the media by binding to GAGs or other proteins on the culture surface; although this occurred at the same rate in both wells containing cells and those that contained media only, so is unlikely to represent binding to factors specific to HD-LECs. An incubation with heparinase before removing aliquots for ELISA would release chemokines bound to GAGs. This would confirm whether chemokines were depleted from the media or sequestered on the cell surface.

Nevertheless, the observations made in the scavenging assays, along with the chemokine uptake experiments, provide no evidence that ACKR3 or ACKR4 expressed by cultured HD-LECs engage in chemokine scavenging *in vitro*.

3.3.9 Expression and Modulation of ACKRs on Cultured Human Keratinocytes

Due to the lack of detectable chemokine scavenging activity in cultured HD-LECs, another cell type was also studied. Cultured normal human keratinocytes (nHEKs) were chosen due to the expression and function of ACKRs reported on these cells. Results in the skin of *Ackr4^{gfp/+}* reporter mice have shown that keratinocytes are GFP⁺ and capable of internalising CCL19 *in situ* in an *Ackr4*-dependent manner ¹⁷⁹. ACKR4 has also been shown to be expressed by keratinocytes by immunofluorescent microscopy ¹⁷⁹ and *ACKR4* mRNA by qPCR (K. Shams, personal communication). Previous work in our group has suggested that GFP protein levels are highest in the basal layer of the interfollicular epidermis, decreasing in intensity in cells located closer towards the hair follicle bulge. As discussed in the introduction (See section 1.4.1), the cells in the bulge region of the hair follicle and the basal layer of the epidermis are the least differentiated and most proliferative cells, while those of the outer epidermis are the most differentiated and least proliferative cells. This suggests that murine *Ackr4* expression could be modulated during keratinocyte differentiation. ACKR3 expression by keratinocytes has not yet been studied in depth in these cells; therefore, the regulation and function of both these ACKRs in keratinocytes has not yet been determined.

To investigate this further, I examined whether there was any detectable *ACKR4* expression or function in nHEKs, and if so, if this was modified during keratinocyte differentiation. To maintain a basal, proliferative status, primary keratinocytes are typically

cultured in low calcium (LoCa) medium, with a calcium concentration of 0.06 mM. Increasing the calcium concentration in the growth medium induces terminal differentiation followed by senescence^{74,75}. When cultured at 0.18 mM Ca²⁺ (HiCa), nHEKs appear to alter their morphology and become less regular in shape and size, suggesting they may be at different stages of differentiation (Figure 3-16). Culturing cells in HiCa media for 5 days was sufficient to induce the described morphology, and these cells were used as a comparison with LoCa cells to determine whether any difference in *ACKR4* expression or function could be detected.

3.3.10 Cultured Human Keratinocytes Express ACKR4 Protein

The protein expression of ACKR4 appeared similar in most LoCa nHEKs to that of HD-LECs (Figure 3-17A). Expression appeared variable, with many cells showing low-level or absent anti-ACKR4 staining. Those that were ACKR4⁺ appeared to express the protein mainly within the cytoplasm, with a punctate staining pattern reminiscent of endosomal or lysosomal vesicles. Some cells showed a more limited, localised pattern of ACKR4 staining where the vesicles appeared to be restricted to one area of the cytoplasm. In HiCa nHEKs, almost all the cells that were ACKR4⁺ appeared to express the protein in this pattern, with only one or two concentrated foci of ACKR4 expression within the cell (Figure 3-17B). This suggests a potential for ACKR4 protein to be polarised to specific areas of the cytoplasm. When these cells were examined for *ACKR4* mRNA expression, however, there appeared to be no difference between LoCa and HiCa cells (Figure 3-17C). This suggests that any difference in ACKR4 expression between LoCa and HiCa nHEKs is at the protein level.

This result failed to support any evidence for the modulation of *ACKR4* mRNA levels in keratinocytes from different subsets, but this could indicate that HiCa keratinocytes represent a heterogeneous population at different stages of differentiation. Furthermore, anti-ACKR4 immunostaining suggested differential regulation of protein localisation in these cells, which could feasibly lead to notable differences in ACKR4 functionality in these cells. Therefore, although *ACKR4* mRNA levels do not appear to change in differentiated vs basal keratinocytes, this does not rule out any differences in *ACKR4* protein expression or function.

3.3.11 mRNA of ACKRs and Ligands are Regulated in Response to Inflammation

To further assess the expression and regulation of ACKRs and their pathways in nHEKs, the mRNA expression of *ACKR4*, *ACKR3* and *CXCR4* in LoCa cells was tested after 48 hours' incubation with various immunostimulatory treatments. As with the results obtained in HD-LECs, only one true biological replicate was possible, so statistical analysis was not carried out. The chosen treatments were IFN- α , IFN- β , IFN- γ , Keratinocyte Growth Factor (KGF) and LPS. Interferons were chosen due to their ability to elicit *ACKR3*, *ACKR4*, *CCL21* and *CXCL12* responses in cultured HD-LECs. KGF has previously been reported to induce *ACKR4* expression in keratinocytes (R. Nibbs, personal communication), and LPS was chosen as keratinocytes express TLR4²⁰⁶ and may modulate gene expression in response to its ligand.

Results showed that *ACKR4*, *ACKR3* and *CXCR4* mRNA were all expressed by keratinocytes, while *CXCL12*, *CCL19* and *CCL21* were all tested but could not be detected. *ACKR4* expression appeared to be induced by IFN- β and IFN- γ , but not IFN- α , KGF or LPS (Figure 3-18A). This data partially agrees with that obtained from HD-LECs, as IFN- β significantly raised *ACKR4* expression by 48 hours post-treatment in both cell types; however, *ACKR4* expression had returned to normal by 48 hours after IFN- γ treatment in HD-LECs, and was still raised by about 20-fold at this timepoint in nHEKs.

ACKR3 expression in nHEKs did not appear to show many similarities to that in HD-LECs (Figure 3-18B): in nHEKs, *ACKR3* appeared to be strongly induced by KGF and LPS, while it was downregulated by treatment with all three IFNs. In HD-LECs, *ACKR3* did not appear to be induced by LPS, and was not strongly affected by any of the IFNs used, while KGF was not tested on HD-LECs.

ACKR3 and *CXCR4* expression in nHEKs showed an interesting relationship: *ACKR3* was induced by KGF and LPS, but appeared to be downregulated in response to IFNs. Conversely, *CXCR4* appeared to be induced in response to IFNs and downregulated in response to KGF and LPS (Figure 3-18C). Taken together, these results suggested that *ACKR3*, *ACKR4* and *CXCR4* are expressed by nHEKs, and may be modulated in response to immunostimulatory treatments, but that the specific manner in which these genes were regulated often differed between nHEKs and HD-LECs.

3.3.12 ACKR4-Mediated Chemokine Scavenging is Not Detected on nHEKs

To determine whether ACKR4 scavenging function could be detected on nHEKs, and whether the modifications in mRNA expression of *ACKR4* had any effect on this, CCL19 uptake assays were performed on these cells. Inflammatory stimuli were used to treat the cells before performing the assay, and the mean fluorescence intensity compared between cells incubated with either CCL19-AF647 alone, or with an excess of unlabelled CCL19, as described for HD-LECs (Figure 3-19A). The results of this experiment showed no clear differences in CCL19-AF647 signal when competitor was present, although only two replicates were performed so it was not possible to perform statistical analysis. Nevertheless, the results of this experiment did not show any clear differences in chemokine uptake with or without unlabelled CCL19 or after stimulation with treatments shown to induce a large increase in *ACKR4* mRNA in these cells.

Uptake assays were repeated using a greater number of replicates but only IFN- γ treatment, as this cytokine had caused the strongest induction in *ACKR4* mRNA expression (Figure 3-19B). Again, no clear difference in uptake of fluorescently-labelled CCL19 was detected between samples with and without unlabelled competition, and IFN- γ treatment did not appear to affect this.

The assay was also attempted using biotinylated CCL19 incubated to form tetramers with sva-AF647, or sva-AF647 alone (Figure 3-19C). This variation of the assay showed a slight difference between samples with and without CCL19, but this only represented a small number of potentially CCL19+ cells when immunostaining results have suggested the majority of nHEKs express ACKR4 at the protein level. Although this experiment did not have a positive control, and therefore experimental error could not be ruled out, similar issues were encountered during experiments with HD-LECs and could not be accounted for. Due to the difficulty in performing chemokine uptake assays on both nHEKs and HD-LECs, these investigations were not pursued further.

3.4 Key Findings

- Cultured human dermal LECs express ACKR4, ACKR3 and CXCR4 at the protein level. ACKR3 and ACKR4 show staining patterns consistent with those observed for ACKR2, with the majority of the protein appearing to be associated with

intracellular vesicles that rarely overlapped in distribution between ACKRs 2, 3 and 4. For ACKR4, these were confirmed as RAB5A+ early endosomes.

- ACKR3 appeared to localise to the nucleus in a significant minority of cells by immunostaining, but this result could not be confirmed.
- CXCR4 expression by HD-LECs is uncertain, with cells showing positive staining by immunofluorescence, but unreliable mRNA expression. ACKR3/CXCR4 co-staining could not be determined.
- HD-LECs express CCL21 at the protein and mRNA level. CXCR4 was detected unreliably at the protein and mRNA level, and *CXCL12* was detected at the mRNA level.
- *ACKR4*, *CCL21*, *ACKR3* and *CXCL12* mRNA are potentially modulated by HD-LECs in response to immune stimuli. In particular, ACKR4 appeared to be upregulated in response to both IFNs and CpG. This suggests that expression of *ACKR4* on HD-LECs is modified both in response to pathogens detected directly by keratinocytes via TLR ligands, and to cytokines secreted by other cells.
- Cultured HD-LECs do not exhibit any detectable chemokine scavenging activity via ACKR3 or ACKR4.
- Cultured human epidermal keratinocytes express ACKR4 at the protein level, with basal proliferative cells showing staining patterns consistent with HD-LECs, while more differentiated cells appeared to localise most of their ACKR4 in discrete foci. This did not appear to represent any difference in *ACKR4* mRNA expression.
- nHEKs express *ACKR4*, *ACKR3* and *CXCR4* at the mRNA level. *ACKR4* appears to be induced in response to IFN- α , IFN- β and IFN- γ but not KGF or LPS. *ACKR3* and *CXCR4* expression profiles suggest reciprocal regulation, where *ACKR3* is induced in response to KGF and LPS but downregulated by IFNs, and *CXCR4* shows the opposite pattern. Overall, there appears to be little overlap between the regulation of *ACKR3* and *ACKR4* between nHEKs and HD-LECs in response to these inflammatory stimuli.

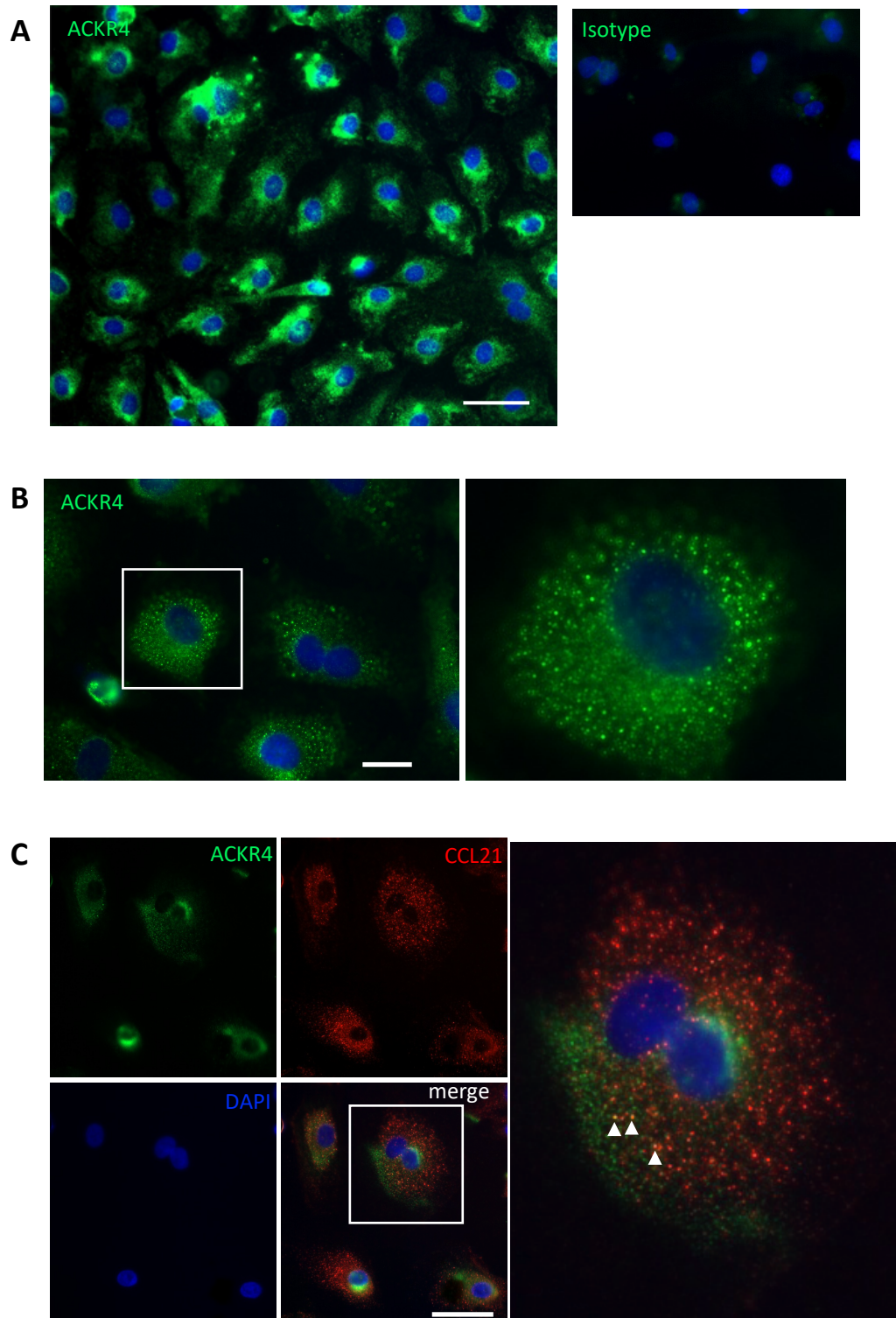


Figure 3-1: ACKR4 and CCL21 proteins are expressed by cultured HD-LECs.

Human dermal LECs were cultured on sterile coverslips until confluent, fixed in paraformaldehyde and incubated with anti-ACKR4 antibody. All images shown are representative of three replicates. **A)** Anti-ACKR4 staining (left panel) compared with mouse IgG2b, κ isotype (right panel); scale bar = 50 μm . **B)** Left panel: anti-ACKR4 staining on HD-LECs; right panel: magnified view of cell highlighted in left panel showing the punctate staining pattern of ACKR4 protein; scale bar = 20 μm **C)** Left panel: ACKR4 and CCL21 protein expression on cultured HD-LECs; right panel: magnified view of cell highlighted in left panel. Three potential areas of co-localisation are highlighted (arrows); scale bar = 50 μm .

experiment. The dotted line indicates the pooled mean value of 11%. Error bars represent SD of the mean.

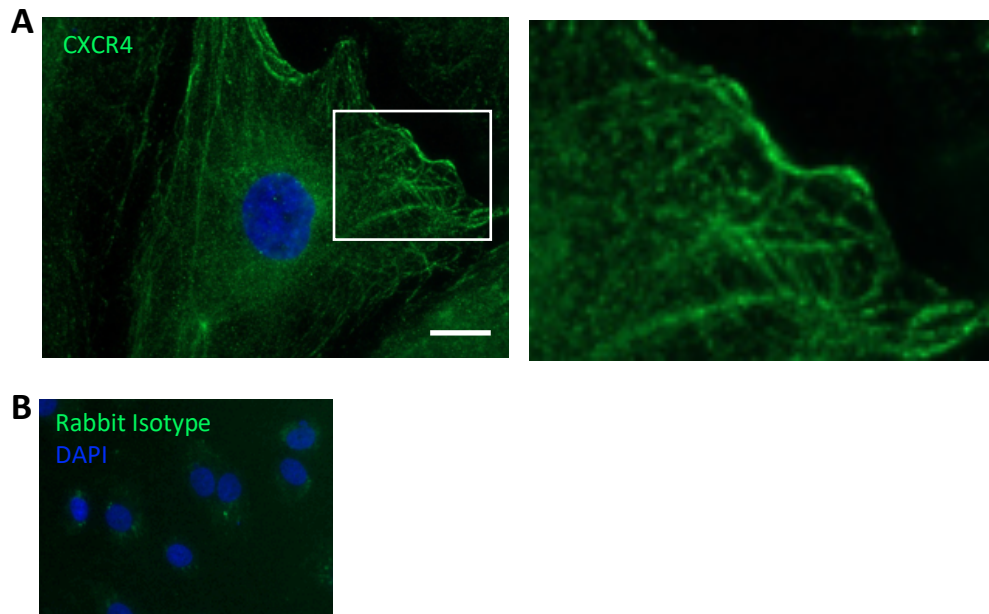


Figure 3-3: ACKR3 and CXCR4 proteins are expressed by cultured HD-LECs.

Human dermal LECs were cultured on sterile coverslips until confluent, fixed in paraformaldehyde and incubated with anti-CXCR4 antibody. All images shown are representative of three replicates. Scale bars: 20 μm . **A)** Left panel: anti-CXCR4 staining on cultured HD-LECs; right panel: magnified view of cell highlighted in left panel. **B)** Cultured HD-LECs stained with polyclonal rabbit IgG isotype control.

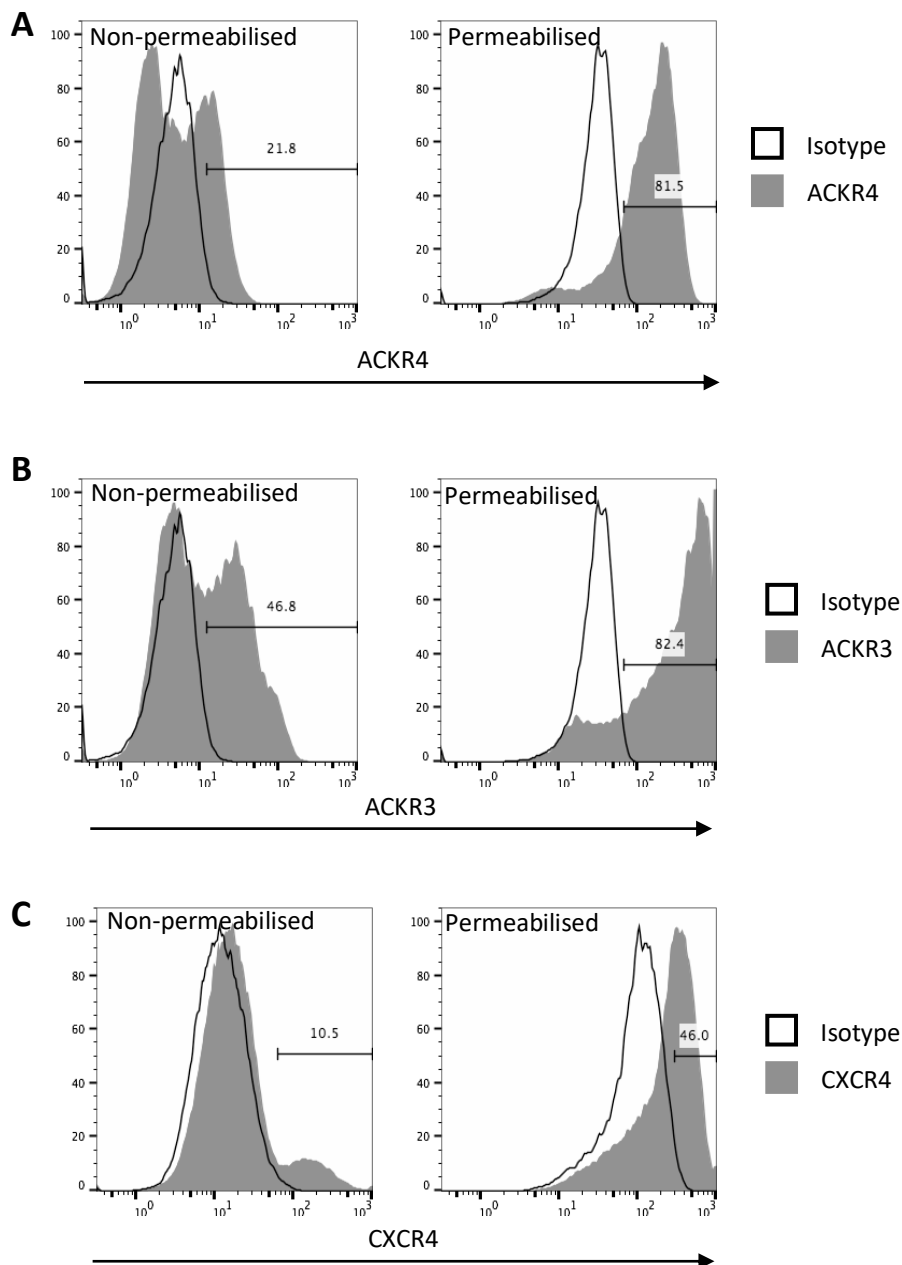


Figure 3-4: ACKR3, ACKR4 and CXCR4 are mainly expressed intracellularly by cultured HD-LECs.

Human dermal LECs were cultured until 70% confluent, removed from the culture vessel using trypsin and stained for flow cytometry. Cells were either fixed and permeabilised before antibody staining, or fixed after staining. Histograms are representative of three replicates for receptor staining (■); one sample was stained with each isotype (□). Gates and numbers represent the proportion of positive cells in the antibody-stained sample. **A**) Anti-ACKR4 surface staining (left panel) and intracellular staining (right panel) **B**) Anti-ACKR3 surface staining (left panel) and intracellular staining (right panel) **C**) Anti-CXCR4 surface staining (left panel) and intracellular staining (right panel)

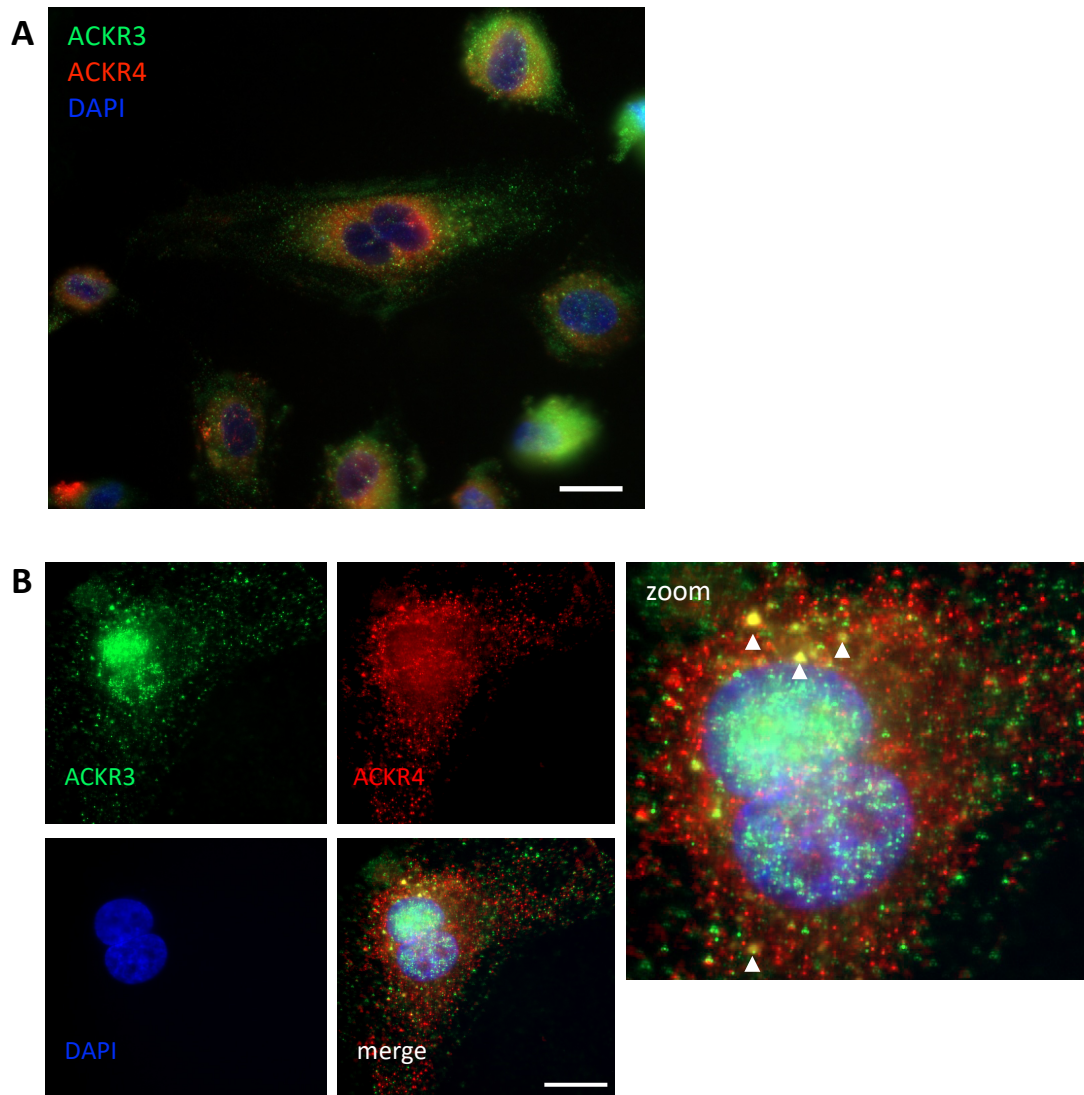


Figure 3-5: ACKR3 and ACKR4 rarely co-localise in HD-LECs

Human dermal LECs were cultured on coverslips until confluent, fixed and stained with anti-ACKR3 and anti-ACKR4 antibodies and DAPI counterstain. **A)** Overview of anti-ACKR3 and anti-ACKR4 staining. Image is representative of three replicates (scale bar = 50 μm). **B)** View of an individual cell stained with anti-ACKR3 and anti-ACKR4 antibodies. Left panels: individual stain images and merged views of anti-ACKR3 and anti-ACKR4 staining and DAPI counterstaining. Right panel: magnified view. Arrows show possible overlap between anti-ACKR3 and anti-ACKR4 staining. Scale bar = 20 μm .

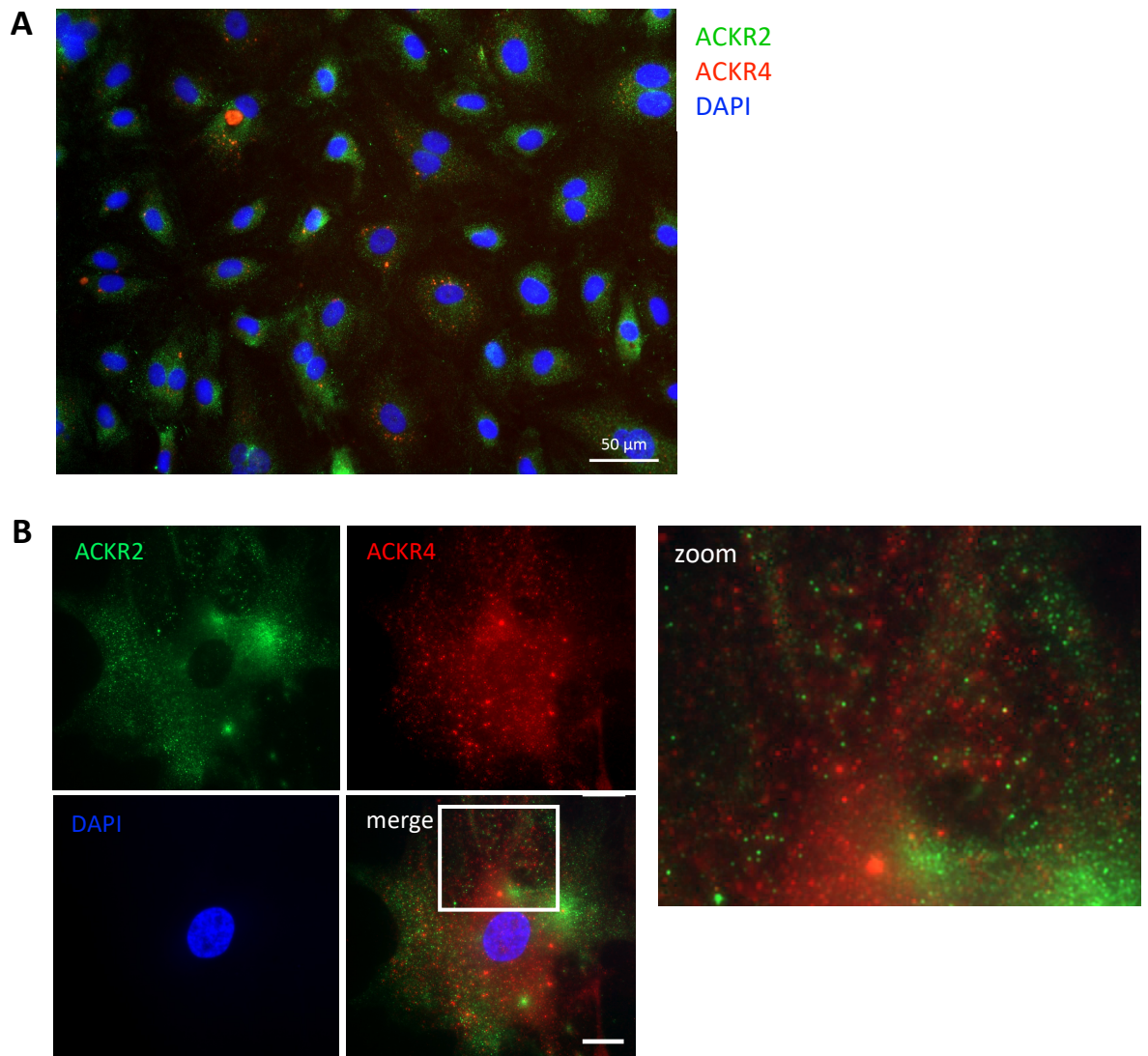


Figure 3-6: ACKR2 and ACKR4 do not co-localise in HD-LECs

Human dermal LECs were cultured on coverslips until confluent, fixed and stained with anti-ACKR2 and anti-ACKR4 antibodies and DAPI counterstain. **A**) Overview of anti-ACKR2 and anti-ACKR4 staining. Image is representative of three replicates (scale bar = 50 µm). **B**) View of an individual cell stained with anti-ACKR2 and anti-ACKR4 antibodies. Left panels: individual stain images and merged views of anti-ACKR2 and anti-ACKR4 staining and DAPI counterstaining. Right panel: magnified view. There was no detectable overlap between ACKR2+ and ACKR4+ vesicles.

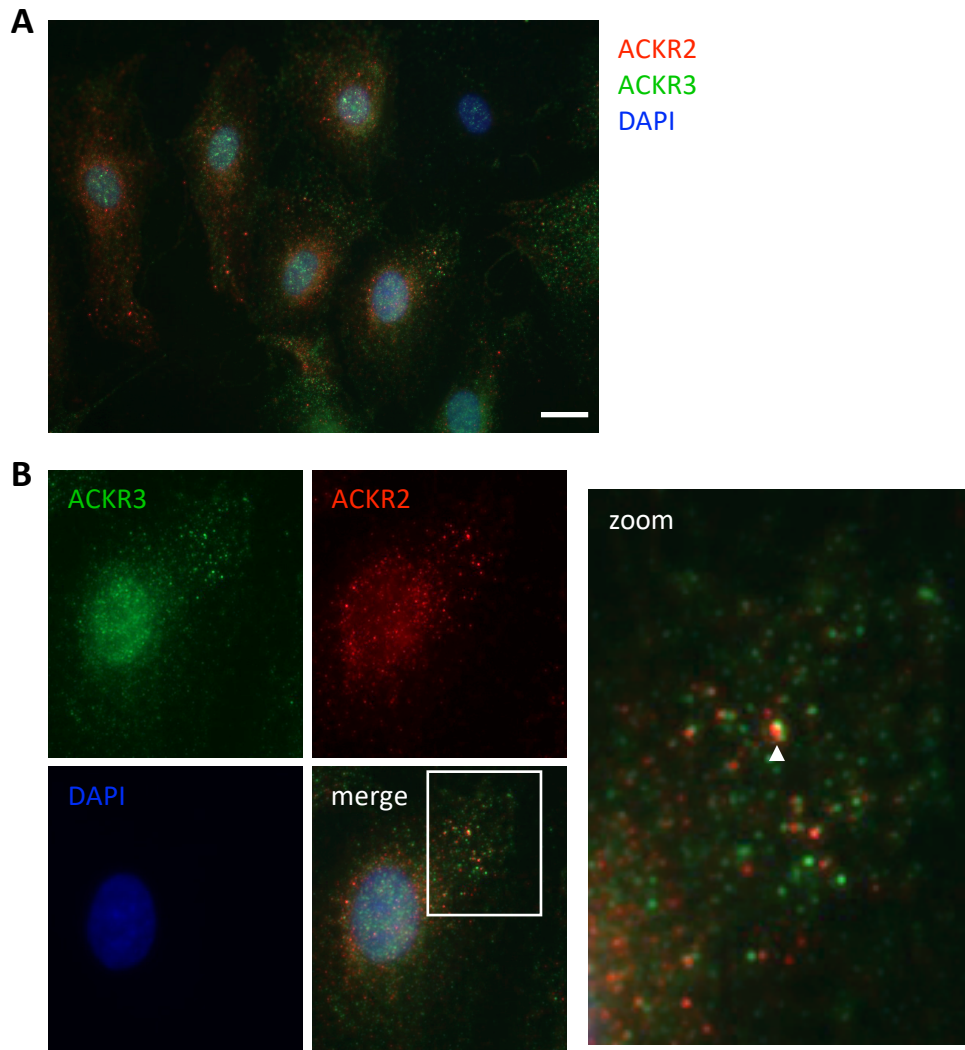


Figure 3-7: ACKR2 and ACKR3 rarely co-localise in HD-LECs

Human dermal LECs were cultured on coverslips until confluent, fixed and stained with anti-ACKR2 and anti-ACKR3 antibodies and DAPI counterstain. **A**) Overview of anti-ACKR2 and anti-ACKR3 staining. Image is representative of three replicates (scale bar = 50 μ m). **B**) View of an individual cell stained with anti-ACKR2 and anti-ACKR3 antibodies. Left panels: individual stain images and merged views of anti-ACKR2 and anti-ACKR3 staining and DAPI counterstaining. Right panel: magnified view. Arrow shows possible overlap between anti-ACKR3 and anti-ACKR4 staining.

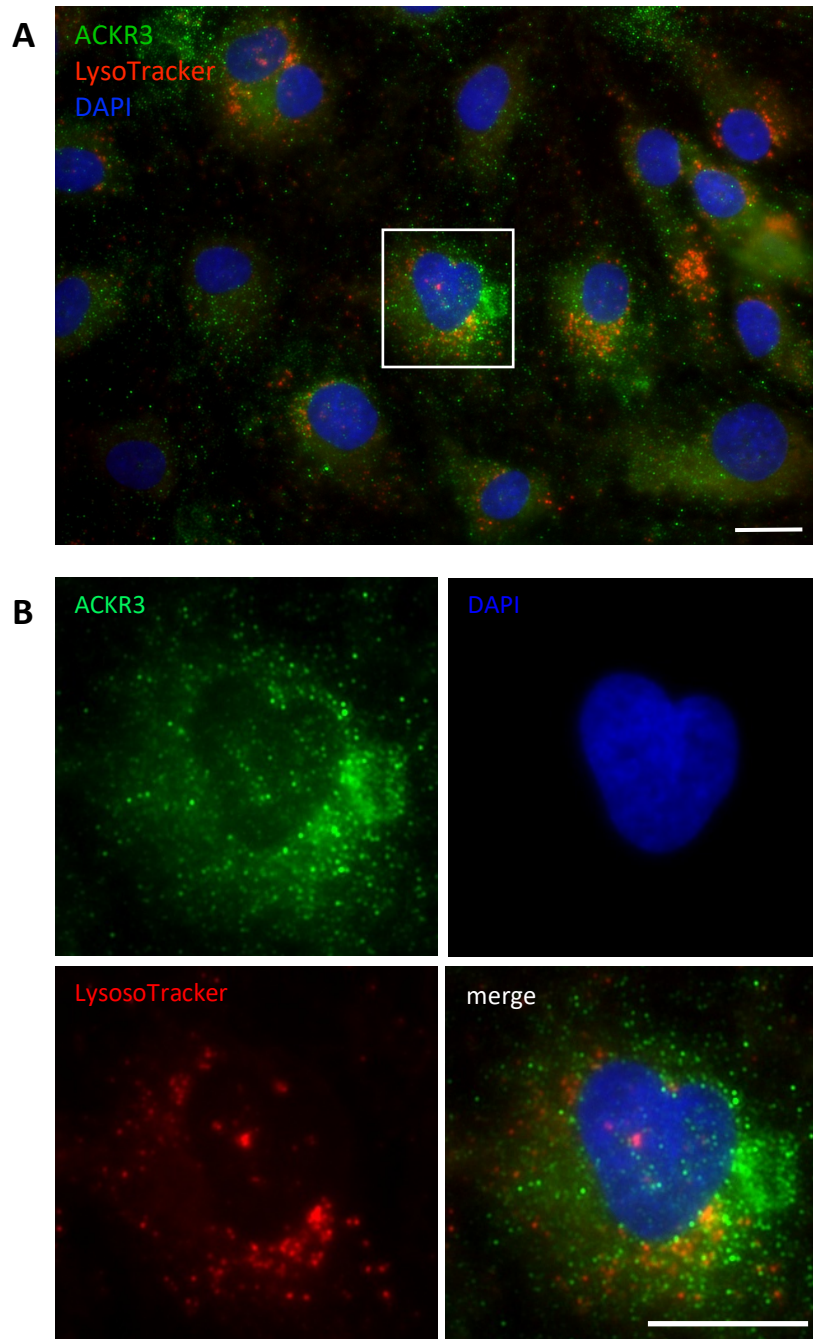


Figure 3-8: ACKR3 protein localisation relative to lysosomes in cultured LECs.

Human dermal LECs were grown until confluent on coverslips and incubated with LysoTracker (Molecular Probes) according to the manufacturer's directions before being fixed and stained with anti-ACKR3 antibody and counterstained with DAPI. Images are representative of three replicates. (scale bars = 20 μ m) **A)** Representative image of anti-ACKR3 staining overlaid with LysoTracker and DAPI counterstains. **B)** Magnified individual channel views of the cell highlighted in **A**.

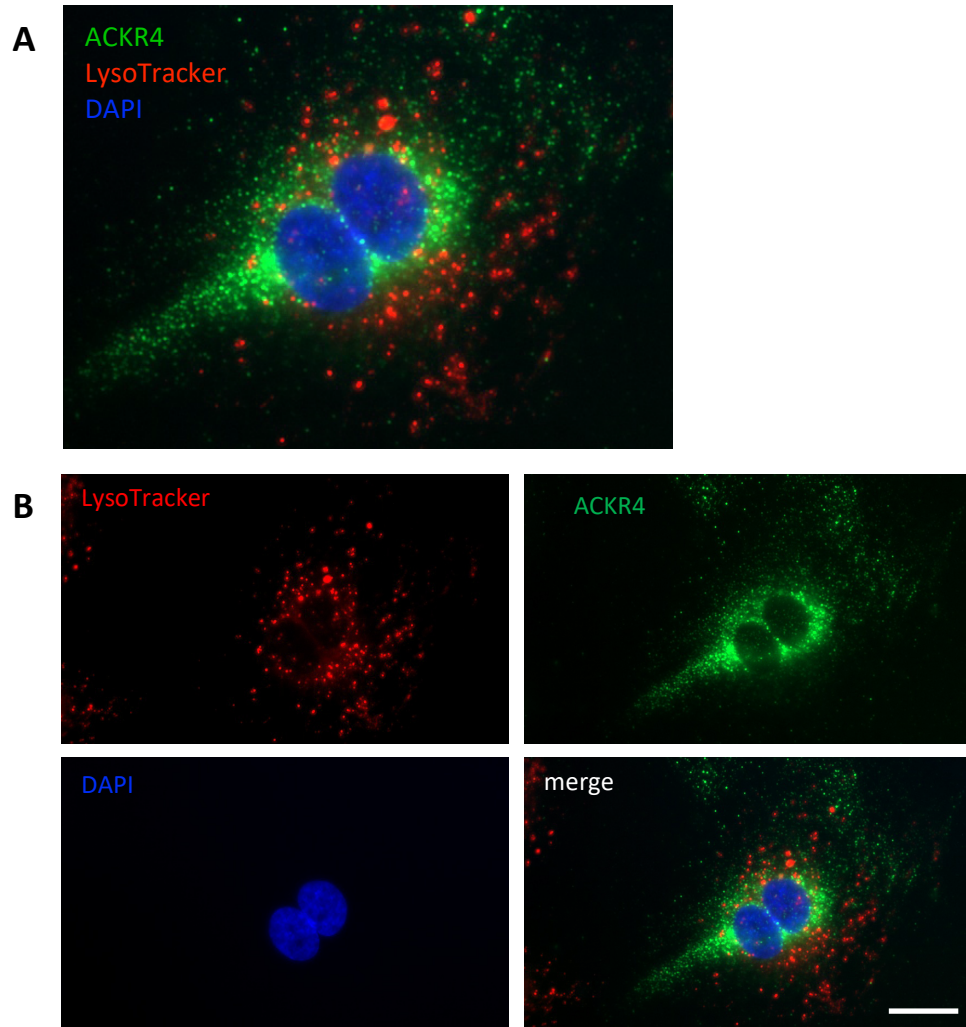


Figure 3-9: ACKR4 protein localisation relative to lysosomes in cultured LECs.

Human dermal LECs were grown until confluent on coverslips and incubated with LysoTracker (Molecular Probes) according to the manufacturer's directions before being fixed and stained with anti-ACKR4 antibody and counterstained with DAPI. Images are representative of three replicates. (scale bars = 20 μm) **A**) Representative image of anti-ACKR4 staining overlaid with LysoTracker and DAPI counterstains. **B**) Individual channel views of the cell shown in **A**.

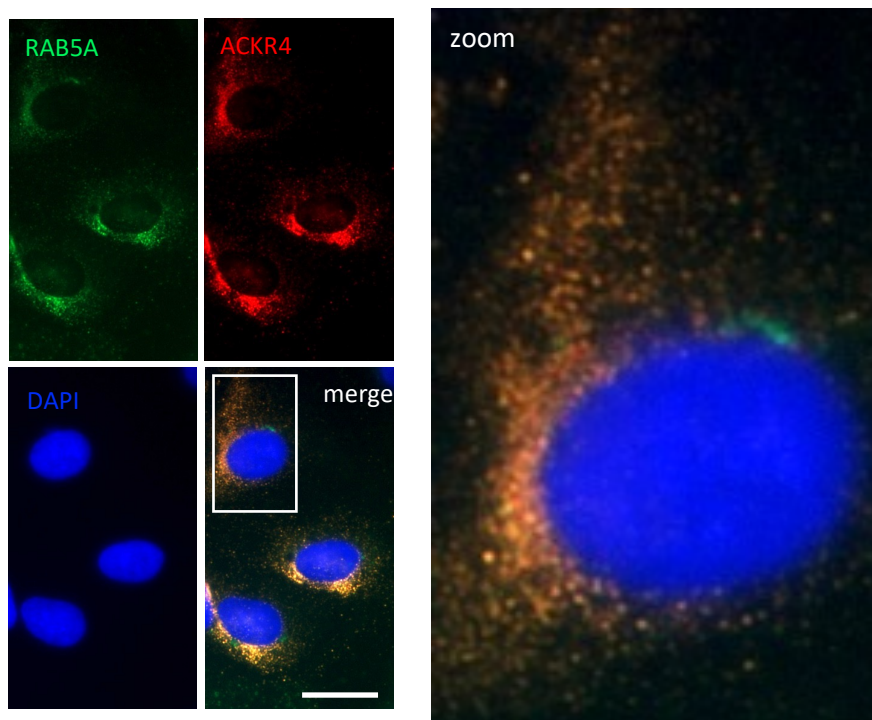


Figure 3-10: ACKR4 co-localises with RAB5+ early endosomes in cultured HD-LECs.

Human dermal LECs were grown until confluent on coverslips and incubated with CellLights Early Endosomes (Molecular Probes) according to the manufacturer's directions before being fixed and stained with anti-ACKR4 antibody and counterstained with DAPI. Images are representative of three replicates. (scale bars = 20 μm). Left panels: individual stain images and merged views of LysoTracker, anti-ACKR4 staining and DAPI counterstaining. Right panel: magnified view.

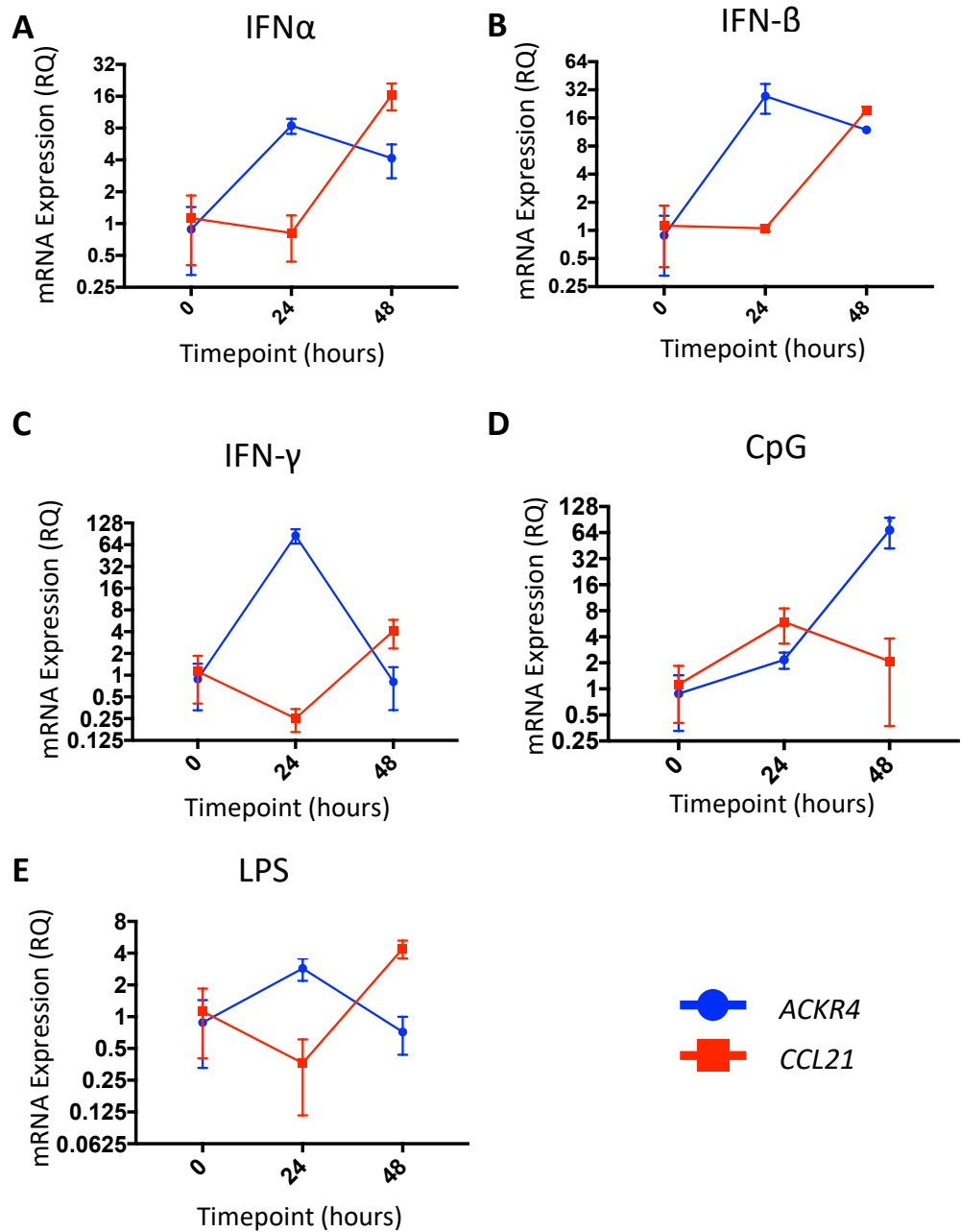


Figure 3-11: Cultured human LECs may alter mRNA expression of *ACKR4* and *CCL21* in response to inflammatory stimuli.

HD-LECs were cultured until 70-80% confluent and treated with cytokines and TLR ligands at the concentrations described in the materials and methods section. After either 24 or 48h, cells were harvested, and RNA was extracted to generate cDNA for qPCR analysis (n=1, 3 technical replicates per treatment group). Graphs show expression of *ACKR4* (■) and *CCL21* (■) as relative quantification (RQ) values calculated using the $2^{-\Delta\Delta CT}$ method. 0h timepoint was used as the calibrator and represents pooled measurements of PBS-treated cells taken at 24 and 48 hours. Error bars represent SD of the mean. mRNA expression is shown in cells treated with **A)** IFN- α , **B)** IFN- β , **C)** IFN- γ , **D)** Unmethylated CpG DNA or **E)** LPS.

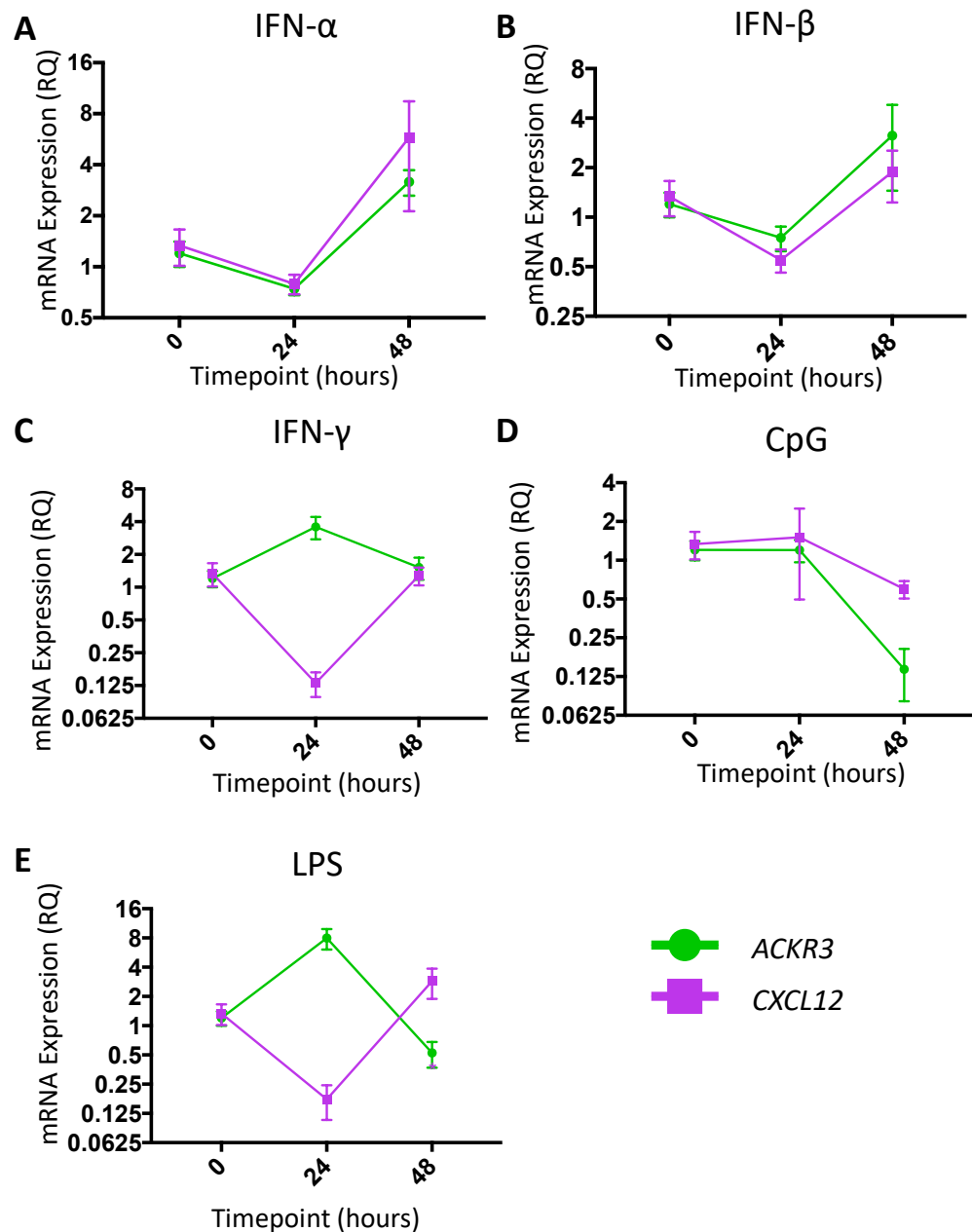


Figure 3-12: Cultured human LECs may alter mRNA expression of *ACKR3* and *CXCL12* in response to inflammatory stimuli.

HD-LECs were cultured until 70-80% confluent and treated with cytokines and TLR ligands at the concentrations described in the materials and methods section. After either 24 or 48h, cells were harvested, and RNA was extracted to generate cDNA for qPCR analysis (n=1, 3 technical replicates per treatment group). Graphs show expression of *ACKR3* (■) and *CXCL12* (■) as relative quantification (RQ) values calculated using the $2^{-\Delta\Delta CT}$ method. 0h timepoint was used as the calibrator and represents pooled measurements of PBS-treated cells taken at 24 and 48 hours. Error bars represent SD of the mean. mRNA expression is shown in cells treated with **A**) IFN- α , **B**) IFN- β , **C**) IFN- γ , **D**) Unmethylated CpG DNA or **E**) LPS.

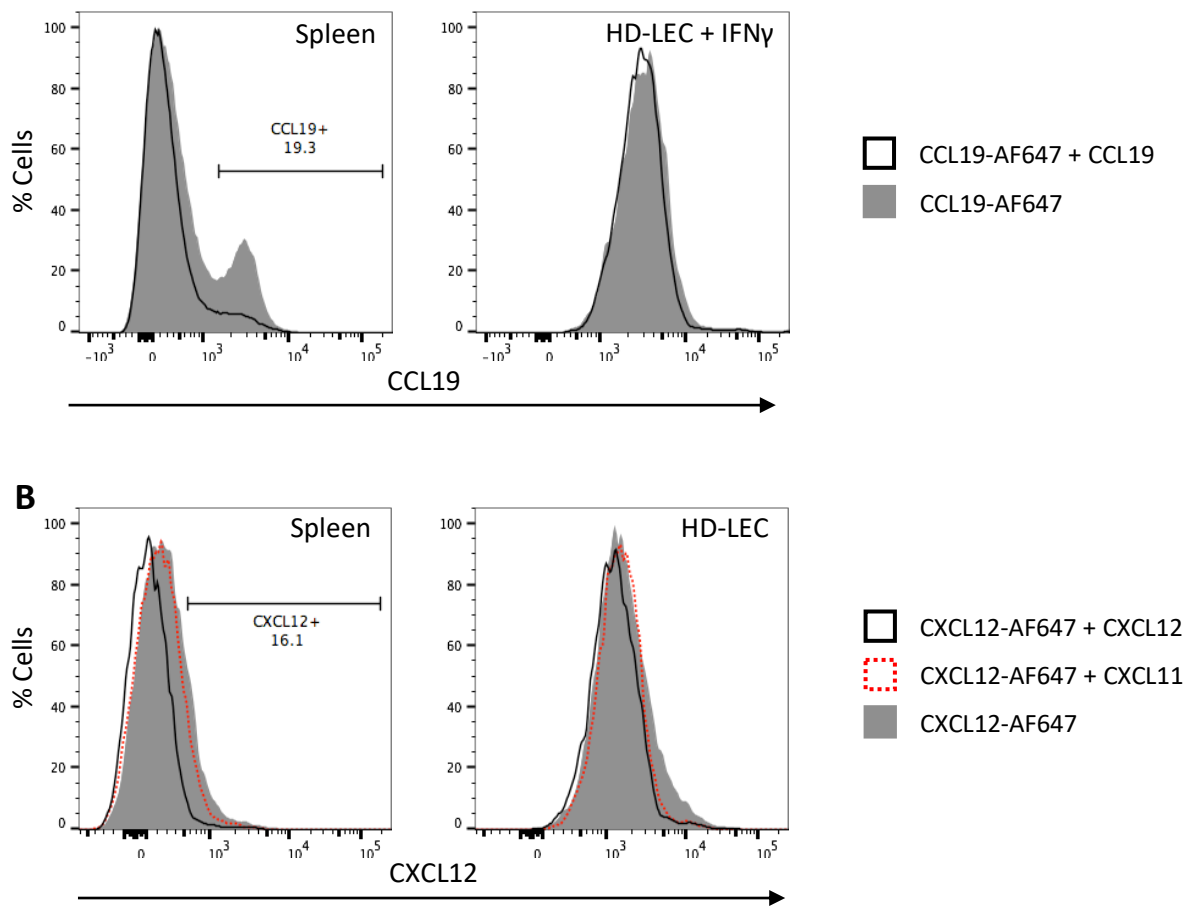


Figure 3-13: ACKR4-mediated uptake of CCL19 and CXCL12 by human dermal LECs cannot be detected via flow cytometry.

Cells were grown on 6-well plates until 70% confluent, and IFN- γ , if using, was added to media to a concentration of 100 ng/ml 24 hours prior to the uptake assay. Freshly harvested spleens were processed to obtain single-cell suspensions. Cells were then transferred to ultra-low binding plates and incubated with chemokines for 1 hour at 37 $^{\circ}$ C, before using for flow cytometry analysis. Histograms are representative of 3 replicates. **A**) Histograms showing fluorescent CCL19 uptake (■) and fluorescent CCL19 uptake with excess unlabelled CCL19 (□) in splenocytes (left panel) and cultured HD-LECs treated with IFN- γ (right panel). The gate on the left panel represents the percentage of CCL19+ cells in the CCL19-AF647 group. **B**) Histograms showing fluorescent CXCL12 uptake (■) and fluorescent CXCL12 uptake with excess unlabelled competition from CXCL11 (▨) or CXCL12 (□) in splenocytes (left panel) and cultured HD-LECs (right panel). The gate on the left panel represents the percentage of CXCL12+ cells in the CXCL12-AF647 group.

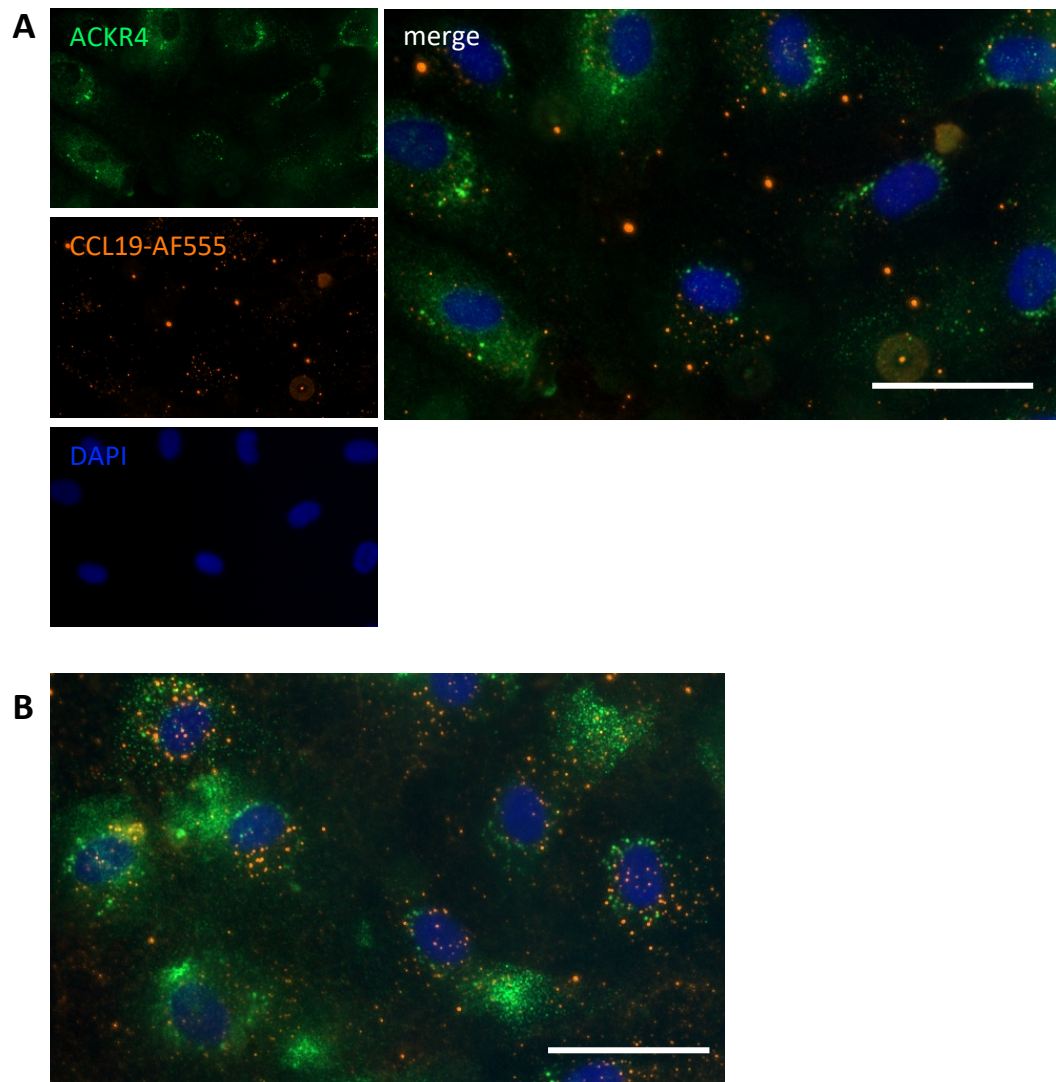


Figure 3-14: Cultured human LECs show no evidence of ACKR4-mediated CCL19 uptake via microscopy.

Human dermal LECs were grown on coverslips until 70-80% confluent and incubated with 25 ng/ml biotinylated CCL19 conjugated with 2.5 ng/ml sva-AF555, or 2.5 ng/ml sva-AF555 alone for one hour. Cells were stained with anti-ACKR4 antibody and counterstained with DAPI. Images are representative of three replicates. Scale bars = 50 μm **A)** HD-LECs incubated with biotinylated CCL19 conjugated with sva-AF555. **B)** HD-LECs incubated with sva-AF555 only.

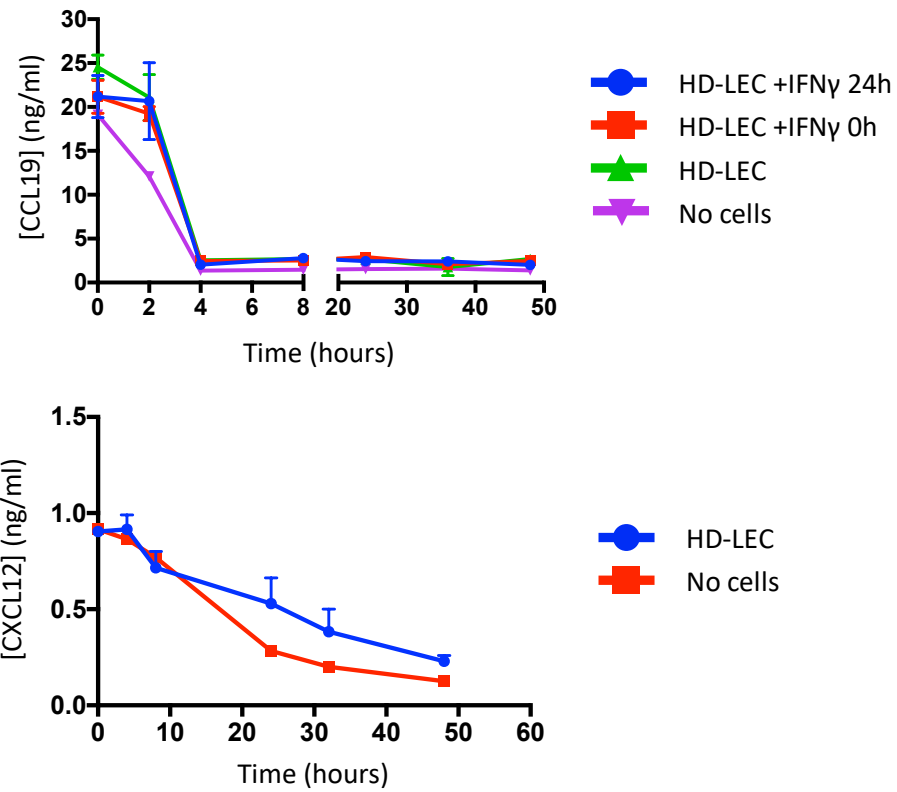


Figure 3-15: Cultured human dermal LECs show no evidence of ACKR4-mediated CCL19 uptake by *in vitro* scavenging assay.

Human dermal LECs were cultured in 12-well plates until confluent, and native recombinant CCL19 or CXCL12 were added to a final concentration of 75 ng/ml. No-cell control wells were included to detect non-specific binding of chemokines to culture surfaces. Aliquots of the media were taken 0h, 2h, 4h, 8h, 24h, 38h and 48h after addition of chemokine and ELISAs were used to determine chemokine concentration. (n=3 + 1 no-cell control well). Error bars represent SD of the mean. **A)** Concentration of CCL19 detected in the media over the time-course for wells containing HD-LECs pre-incubated with 100 ng/ml IFN- γ for 24 hours before addition of chemokine (■), HD-LECs with 100 ng/ml IFN- γ added concurrently with chemokine (■) and untreated HD-LECs (■) compared to the no-cell control well (■). **B)** Concentration of CXCL12 detected in the media over the time-course for wells containing untreated HD-LECs (■) compared to the no-cell control well (■).

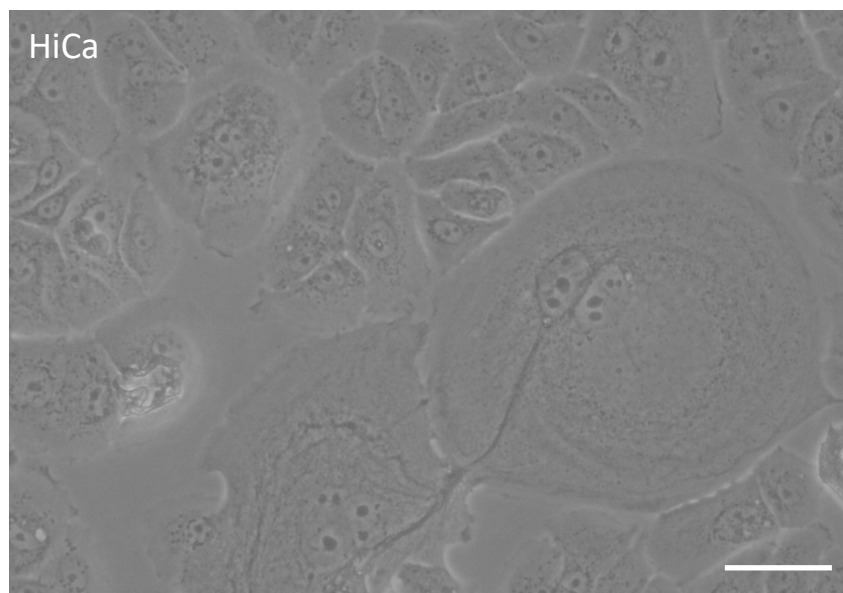
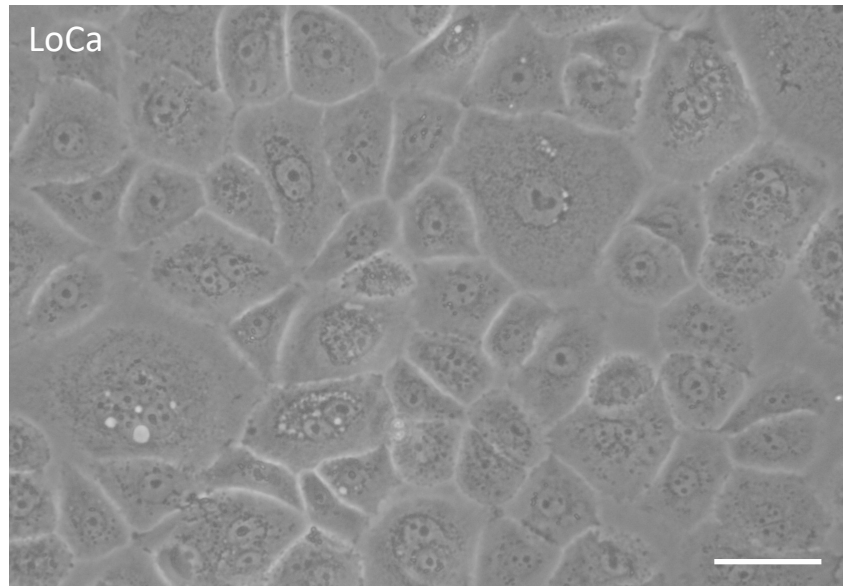


Figure 3-16: Incubation with HiCa media induces morphology changes by cultured human keratinocytes.

Cells were cultured for 5 days in either LoCa media to retain their basal proliferative state, or HiCa media to induce differentiation. Cells were viewed using phase contrast light microscopy at 20X magnification. Scale bars: 50 μ m. Upper panel: Basal keratinocytes, showing a typical 'cobblestone'-like morphology. Lower panel: differentiated keratinocytes, showing a more variable morphology.

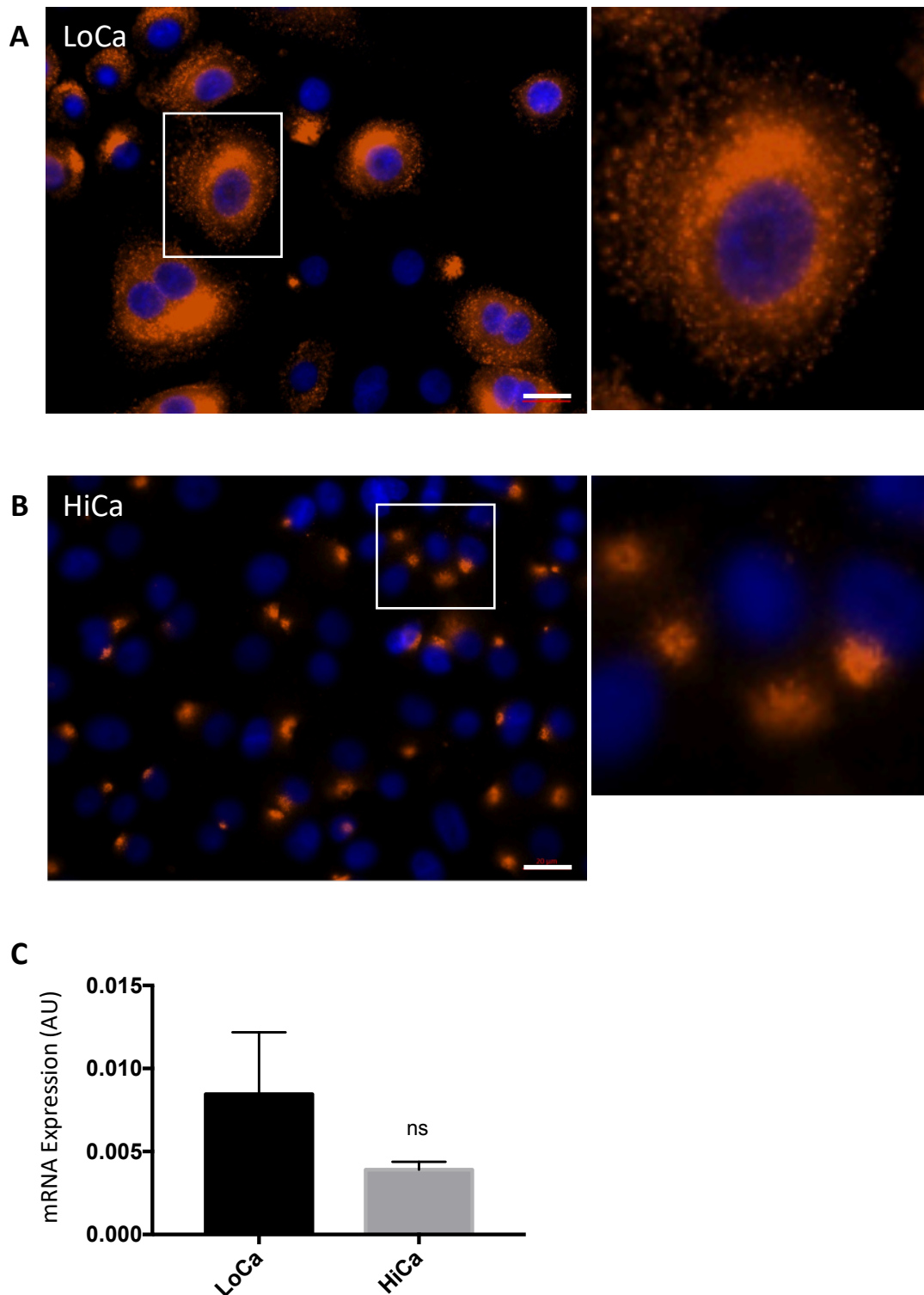


Figure 3-17 Basal and differentiated cultured human keratinocytes show differential expression of ACKR4 at the protein, but not the mRNA, level.

Normal human epidermal keratinocytes were cultured on coverslips in LoCa or HiCa media for 5 days, and either processed for immunofluorescence with anti-ACKR4 antibody and counterstained with DAPI, or RNA was extracted, and cDNA generated for qPCR analysis. Images are representative of three replicates. Scale bars = 20 μ m. **A**) Anti-ACKR4 staining on LoCa nHEKs. Left panel: overview of staining; right panel: magnified view of cell highlighted in left panel. **B**) Anti-ACKR4 staining on HiCa nHEKs. Left panel: overview of staining; right panel: magnified view of cell highlighted in left panel. **C**) mRNA expression of ACKR4 in LoCa (■) and HiCa (■) keratinocytes. Statistical

significance was determined using an unpaired t-test. Error bars represent SD of the mean.

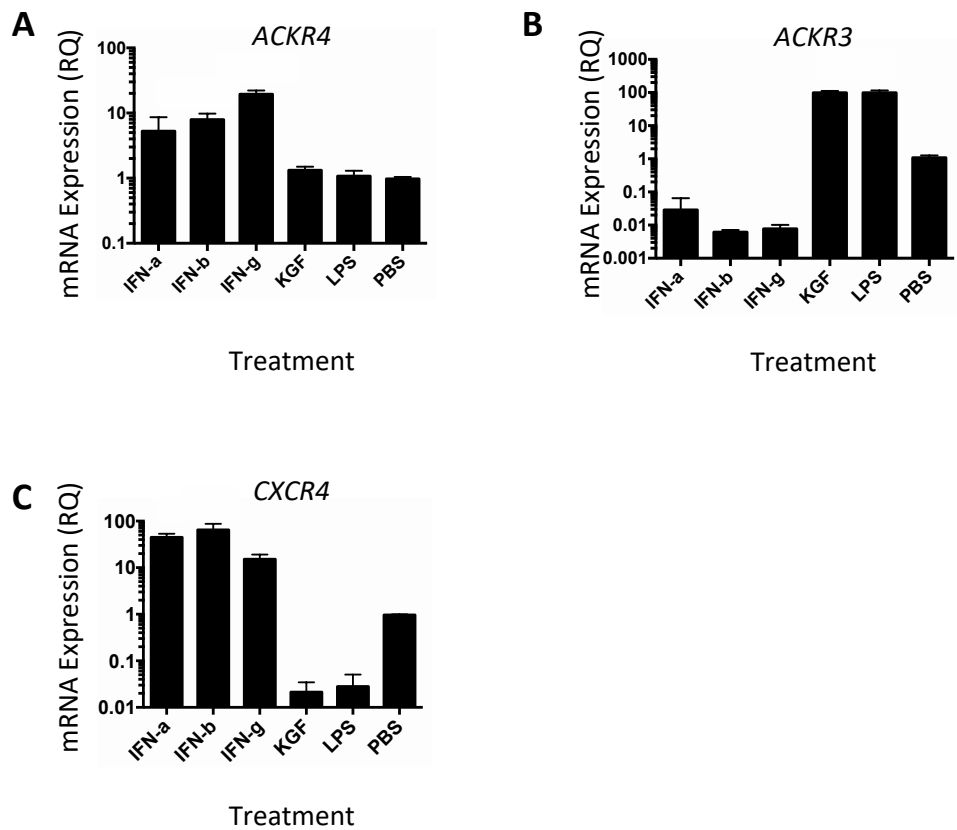


Figure 3-18: Cultured human keratinocytes may alter mRNA expression of *ACKR4*, *ACKR3* and *CXCR4* in response to inflammatory stimuli.

Normal human epidermal keratinocytes were cultured in LoCa media until 70-80% confluent and treated with cytokines or TLR ligands at the concentrations described in the materials and methods section. After 48h, cells were harvested, and RNA was extracted to generate cDNA for qPCR analysis. Three technical replicates were performed by carrying out each treatment on three separate wells, and each sample was run in triplicate. Graphs show expression of **A)** *ACKR4*, **B)** *ACKR3* and **C)** *CXCR4* as relative quantification (RQ) values calculated by the $2^{-\Delta\Delta C_T}$ method using cells treated with PBS as the reference sample; *CXCL12*, *CCL19*, *CCL21* and *CCL25* were also tested but were not detected. Error bars represent SD of the mean.

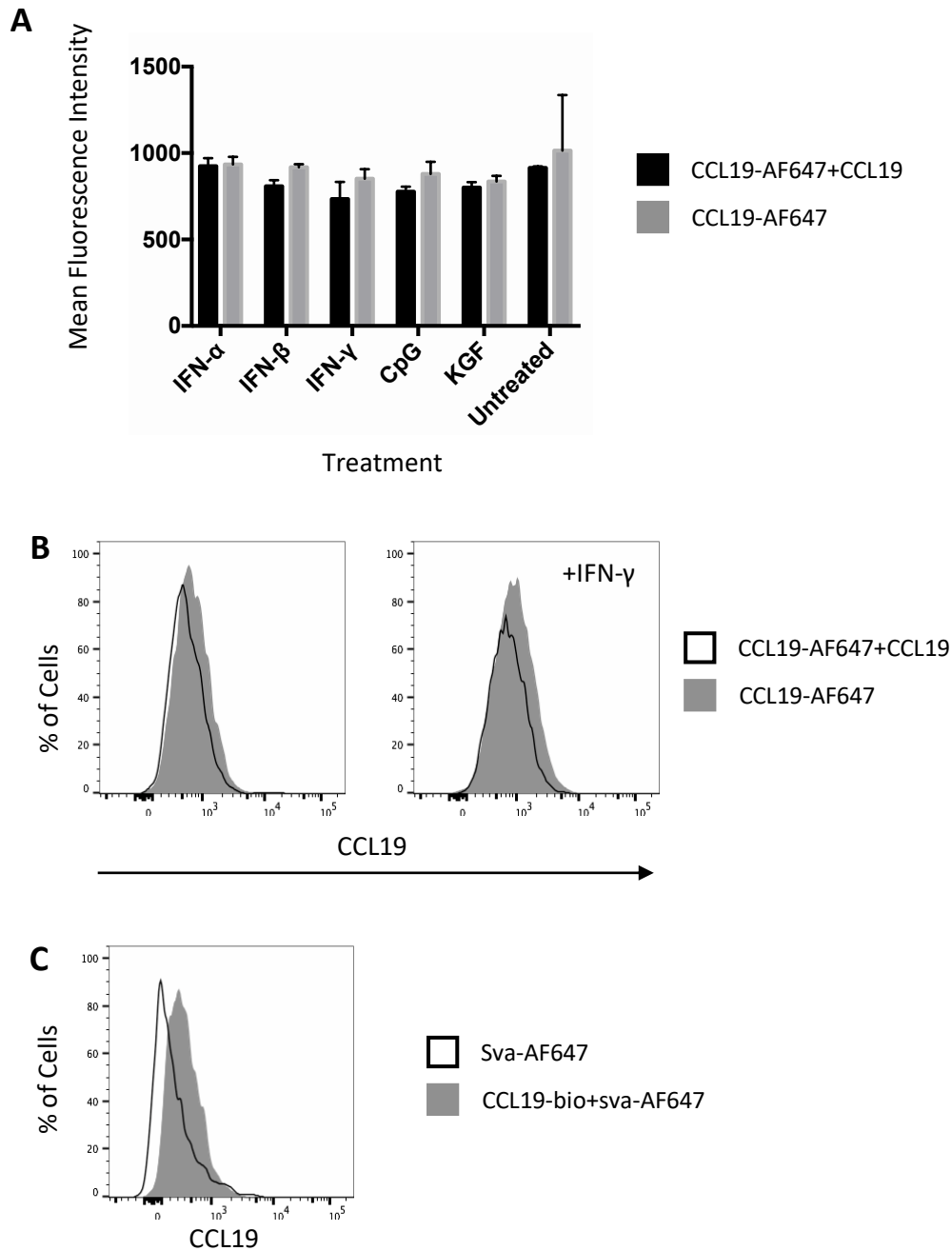


Figure 3-19: Cultured human keratinocytes show no evidence of ACKR4-mediated CCL19 uptake by flow cytometry.

Normal human epidermal keratinocytes were cultured in LoCa conditions until 70% confluent and immunostimulatory treatments, if using, were added for 24 hours (IFNs: 100 ng/ml, CpG: 100 nM, KGF: 20 ng/ml) before cells were transferred to 96-well ultra-low binding plates for chemokine uptake assays and analysed using flow cytometry. **A**) nHEKs were treated with IFN- α , IFN- β , IFN- γ , CpG, KGF or left untreated, and incubated either with CCL19-AF647 alone, or with CCL19-AF647 and a ten-fold higher concentration of unlabelled CCL19 as competition. Mean fluorescence intensity values were taken for each sample (n=2). Error bars represent SD of the mean. **B**) nHEKs were either left untreated or incubated with IFN- γ for 24 hours before performing uptake assays using CCL19-AF647 or CCL19-AF647 plus a ten-fold higher concentration of unlabelled CCL19. Representative histograms of each group are shown (n=3). **C**) nHEKs were incubated with either biotinylated CCL19 pre-incubated with sva-AF647, or sva-AF647 alone. Histogram is representative of two technical replicates.

Chapter 4: Exploring ACKR3 and ACKR4 Expression *in vivo*

4 Exploring ACKR3 and ACKR4 Expression *in vivo*

4.1 Introduction

Understanding the location where a gene or protein is expressed, and how it is regulated, are the first steps to understanding its function. The tissue and cell types that express the gene/protein have their own unique functions and capabilities and understanding these can give valuable insights into the potential role of the transcript. The types of conditions that modulate expression of the gene/protein can also provide clues as to the functions it is involved in. Additionally, determining the specific cells that express a transcript can allow more targeted functional analyses to be carried out; for example, isolating that particular niche for further study, as I did in the previous chapter by examining expression and modulation of *ACKR3*, *ACKR4* and related genes by cultured human cells.

In this chapter, I have investigated *ACKR3* and *ACKR4* gene and protein expression *in vivo* using GFP reporter mice and antibody staining, both at rest and under immune challenge, to further characterise the specific cell types that express these receptors and what their involvement in the immune response may be.

4.2 Aims

- To further characterise eGFP⁺ cells in *Ackr3^{+/gfp}* and *Ackr4^{+/gfp}* reporter mice.
- To determine whether enhanced CXCR4 signal in the skin following TPA treatment reflects only an influx of CXCR4⁺ cells or includes modulation of CXCR4 expression by keratinocytes.
- To identify whether any keratinocyte subsets show differential *ACKR3*/CXCR4 expression during inflammation.
- To explore a potential role for ACKRs in modulating the positioning of specific chemokine-receptor-expressing subsets of DCs in the spleen.

4.3 Characterisation of *Ackr3^{+/gfp}* Reporter Mice

ACKR3 protein expression has been previously reported on endothelial cells in a wide range of tissues by immunostaining¹⁵⁰, and I reasoned that it would be valuable to confirm these findings, potentially explore them in more detail, and relate this to expression data already obtained for *ACKR3* expression in cultured human cells.

To this end, I carried out experiments to characterise eGFP expression in several key tissues of *Ackr3^{+gfp}* reporter mice. To maximise the data obtained from a limited number of mice, I received support from Carolyn Thomson, who kindly carried out flow cytometry analysis on small intestine, colon and mesenteric lymph node (MLN) samples.

4.3.1 *Ackr3* Expression in the Skin

I was particularly interested to discover which cells in the skin expressed ACKR3 protein given the results from cultured human cells in the previous chapter showing ACKR3 to be found on keratinocytes and dermal LECs. ACKR3 has previously been reported on basal keratinocytes^{207,208} but I could find no detailed analysis of its precise localisation or function in healthy skin in the literature. I therefore chose to use flow cytometry to determine the specific subsets of cells that expressed eGFP in the skin of *Ackr3^{+gfp}* reporter mice at rest.

These experiments were carried out by separating epidermis and dermis and investigating the tissues individually. Generating single cell suspensions from the dermis for flow cytometry proved to be challenging, due to the complex extracellular matrix comprising this tissue, which led to poor cell yields and made it difficult to definitively identify subpopulations of cells. For this reason, no analysis beyond total CD45⁺ or CD45⁻ cells was carried out on the dermis. It was possible, however, to reliably isolate keratinocytes and leukocytes from the epidermis, although levels of extracellular debris were generally too high to allow for reliable absolute cell counts and yields often appeared low making it difficult to justify running FMO controls.

Initial examination of the epidermis showed that there was negligible eGFP signal on leukocytes (CD45⁺ cells), while the vast majority of stromal cells (CD45⁻ cells) were positive for eGFP (Figure 4-1). Cells were further analysed with surface markers to separate leukocytes and stromal cells into the major subsets present in the skin.

Keratinocytes were separated into four subsets relating to their position in the hair follicle (Figure 4-2A), ordered from superficial to basal using Sca-1 and EpCAM⁷⁹: EpCAM⁻Sca-1⁺ cells (interfollicular epidermis), EpCAM⁺Sca-1⁺ cells (Infundibulum), EpCAM⁺Sca-1⁻ cells (Isthmus) and EpCAM⁻Sca-1⁻ cells (hair follicle bulge) (Figure 4-2B,C). Due to the low yield of epidermal cells and the need to investigate leukocytes as well as stromal cells, the full panel of antibodies could not be used to definitively identify hair follicle bulge cells, which should express CD34 and can be further delineated into basal and supra-

basal bulge cells as α_6 integrin (CD49f) positive and negative cells, respectively. There was no clear information available on markers identifying hair follicle bulge cells, but it was assumed that all stromal cells in the epidermis were keratinocytes, and that EpCAM- Sca-1- cells therefore represented a combination of the hair follicle bulge and bulb subsets. Some degree of contamination of the epidermis with cells from the dermis, including fibroblasts, cannot be ruled out, making the EpCAM- Sca-1- population likely to be highly heterogeneous; nevertheless, this group of cells were referred to as 'bulge' for simplicity.

eGFP expression was clearly detected in some cell subsets identified in the epidermis of *Ackr3^{+gfp}* mice. Epidermal leukocytes were generally eGFP- (Figure 4-3A), but there were low levels of potential eGFP signal in dermal $\gamma\delta$ T cells and Langerhans cells (LCs); the signal from LCs appeared to be autofluorescence, as the eGFP signal in WT control mice was also raised. *Ackr3* expression has not previously been reported by any of these cells, and leukocytes are generally considered to be ACKR3 negative¹⁵¹; given that the eGFP signal was very weak, this was not considered to be a positive result.

Results from the epidermal stroma (Figure 4-3B) showed that eGFP expression is present on all keratinocyte subsets, but largely restricted to the cells nearest the outer surface of the skin; the cells of the interfollicular epidermis and infundibulum were both over 90% eGFP+, while isthmus and bulge cells were only 20-30% eGFP+ (Figure 4-3C).

4.3.1.1 *CXCR4 and Ackr3 Expression in the Skin*

Given this intriguing result suggesting differential expression of ACKR3 within the hair follicle, epidermal cell subsets were studied in more depth. CXCR4 expression has previously been reported on keratinocytes¹⁸⁶, and given the potential for ACKR3 to heterodimerise with CXCR4 and modulate its responsiveness to CXCL12^{142,156,157}, I hoped to determine whether CXCR4, too, was expressed differentially by keratinocyte subsets in the epidermis.

Anti-CXCR4 staining was used to explore CXCR4 expression in leukocytes and stromal cells at rest and determine whether this overlapped with eGFP expression. Due to low cell yields from the epidermis, and lack of available *Ackr3^{+gfp}* reporter mice to provide additional tissue for controls, a CXCR4 isotype or FMO control was not available for these studies. Instead, an internal control was used to set the gates for CXCR4 expression: Dendritic epidermal T cells (DETCs), the epidermis-resident subtype of $\gamma\delta$ T cells (See

section 1.4.3) are the only known subset of $\gamma\delta$ T cell that do not express CXCR4 according to the ImmGen database ²⁰⁹, and no reference to CXCR4 expression on these cells could be found in the literature. As expected, epidermal $\gamma\delta$ T cells in the epidermis appeared to be CXCR4 negative, and when overlaid as a histogram, their fluorescence peak coincided with the negative population in the bimodal CXCR4 expression of MHC-II- $\gamma\delta$ TCR-leukocytes in the skin (Figure 4-4A, left panel). Many of these CXCR4 positive cells are likely to be tissue-resident memory T cells and monocytes/macrophages. Interestingly, Langerhans cells in the epidermis appeared to be mainly CXCR4+ (Figure 4-4A, right panel), which would be expected of these cells upon activation, when they use CXCL12/CXCR4 signalling to migrate into the dermis ⁹⁷.

Results in the stroma showed that CXCR4 protein was present on keratinocytes, as expected, and that its expression varied between the subsets. The strongest CXCR4 expression was detected in the infundibulum (Figure 4-4B), while the cells in the bulge subset did not express CXCR4. CXCR4 expression in the four stromal cell subsets is summarised in Figure 4-4C.

Once the expression of both CXCR4 and ACKR3 had been detected on some subsets of keratinocytes, I investigated whether the expression of these receptors overlapped (Figure 4-5A). It did not appear that coexpression of these two receptors was common in keratinocytes, with the exception of the infundibulum subset, where the majority of CXCR4+ cells were eGFP+, and around half of eGFP+ cells were CXCR4+ (Figure 4-5B). Although the anti-CXCR4 antibody has been used successfully here, chemokine receptor staining is often difficult to interpret as cells can lie on a continuum from weakly to strongly positive. To corroborate these findings, the mean fluorescence intensity (MFI) of the CXCR4 channel was measured in eGFP+ and eGFP- cells from each keratinocyte subset. In IE and IF, eGFP+ cells showed a significantly higher MFI value than eGFP- cells, suggesting that eGFP+ cells are more likely to express CXCR4 than eGFP- cells in these subsets (Figure 4-5C). This can be confirmed visually by comparing populations 2 and 3 in the scatterplots shown in FIG 4-5A.

These experiments have shown that both eGFP and CXCR4 are differentially expressed in the four keratinocyte subsets examined in *Ackr3^{+/gfp}* mice, and that the degree of eGFP/CXCR4 coexpression also varies between subsets, with the infundibulum showing the highest proportion of CXCR4+ cells, the second-highest proportion of eGFP+ cells, and the highest proportion of eGFP+ CXCR4+ cells.

4.3.1.2 *CXCR4* and *Ackr3* in the TPA model

Previous results obtained in our group showed that after topical application of the phorbol ester 12-O-Tetradecanoylphorbol-13-acetate (TPA) to mouse ears, mRNA levels of both *Ackr3* and *Cxcr4* are raised in the epidermis (S. Bryce, personal communication). *Ackr3* expression peaks at 4 hours post treatment and *Cxcr4* expression peaks at 24 hours post treatment. As this experiment studied mRNA expression in the tissue as a whole, I aimed to determine whether TPA treatment had any direct effect on *ACKR3* or *CXCR4* expression by keratinocytes using cultured nHEKs.

Results showed that cultured human keratinocytes downregulated *ACKR3* and upregulated *CXCR4* four hours after treatment with TPA (Figure 4-6); this suggested that the upregulation of *Ackr3* seen in the mouse epidermis was not due to keratinocytes, but as cultured nHEKs in LoCa conditions are likely to represent only the most basal cells of the epidermis, I decided to investigate eGFP and *CXCR4* expression in *Ackr3^{+gfp}* reporter mice after TPA treatment to determine whether these transcripts were differentially regulated between keratinocyte subsets during inflammation.

4.3.1.3 *CXCR4⁺ Leukocytes Enter the Skin 16h Post TPA*

Initial experiments were carried out on WT mice only as *Ackr3^{+gfp}* mice were not yet available. These experiments were used to examine *CXCR4* expression and to determine whether a single TPA treatment or multiple treatments would be more suitable for future experiments. When the epidermis was examined 16 hours after a single treatment with TPA, flow cytometry analysis indicated leukocyte recruitment to the skin, as the proportion of live cells that were CD45⁺ significantly increased in both epidermis and dermis after TPA treatment (Figure 4-7A). There was very little change in the proportions of the leukocyte subsets examined after TPA treatment (Figure 4-7B). The 'other leukocytes' subset were stratified based on Ly6C expression in this experiment, which showed that Ly6C^{hi} cells, most likely monocytes or macrophages, made up a greater proportion of leukocytes in TPA-treated epidermis, while Ly6C⁻ cells were proportionally underrepresented. Amongst stromal cells, the infundibulum cells made up a higher proportion in TPA-treated epidermis, while none of the other subsets were significantly affected (Figure 4-7C).

Examining CXCR4 expression in these cells showed that the percentage of positive cells was unaffected in all of the leukocyte subsets identified (Figure 4-8A). There was also no detectable modulation of CXCR4 expression in any of the keratinocyte subsets, although there was a slight trend towards increased CXCR4 expression in all subsets except the bulge (Figure 4-8B). This appeared to combine to create a weakly significant increase in CXCR4 expression amongst stromal cells as a whole, in both epidermis and dermis (Figure 4-8C). CXCR4 expression in the dermal stroma is most likely on vascular endothelial cells

138

These results suggest that, while a single TPA treatment can induce detectable leukocyte infiltration to the skin, no detectable modulation of CXCR4 protein is detectable after 16 hours. It also indicated that the induction of Cxcr4 mRNA detected in mouse skin is most likely partially due to the infiltration of CXCR4⁺ leukocytes and partially due to the modest upregulation of CXCR4 by most keratinocyte subsets. Both treated and untreated skin showed a similar proportion of viable cells (data not shown), suggesting that these results were not due to excess cell death in the treated group.

4.3.1.4 Multiple TPA Treatments Enhance CXCR4 Expression in Keratinocytes

To determine whether CXCR4 might be modulated in response to a more severe inflammatory stimulus, flow cytometry analysis was carried out on skin that had been treated three times daily with TPA. When the cellularity of the epidermis was analysed, it showed significant infiltration of leukocytes. This was more pronounced than after a single TPA treatment (Figure 4-9A). As a proportion of leukocytes, $\gamma\delta$ T cells were significantly underrepresented after multiple TPA treatments but no other subset was affected (Figure 4-9B). Among the stroma, cells of the interfollicular epidermis were decreased as a proportion, while the infundibulum made up a larger proportion of keratinocytes after multiple TPA treatments; isthmus and bulge were unaffected.

Analysis of CXCR4 expression showed that leukocytes in the epidermis did not upregulate this receptor in response to multiple TPA treatments (Figure 4-10A). Among CD45⁻ cells in the epidermis, IE, IF and IM keratinocytes all significantly upregulated CXCR4 (Figure 4-10B). Among CD45⁻ cells as a whole, CXCR4 was significantly induced in both epidermis and dermis (Figure 4-10C). This suggested that multiple TPA treatments were required to induce upregulation of CXCR4 expression among keratinocytes in the skin.

4.3.1.5 *eGFP Expression Is Reduced in the Infundibulum After Multiple TPA Treatments*

Next, I hoped to determine whether the regulation of CXCR4 in response to multiple TPA treatments would reflect any modulation in *Ackr3* expression, particularly in the IF subset: previous analysis has shown that many of these cells coexpress eGFP and CXCR4 at rest in *Ackr3^{+gfp}* reporter mice. Differential *Ackr3* expression in keratinocyte subsets may correspond to differential regulation of ACKR3 in response to inflammatory stimuli.

Multiple TPA treatments on *Ackr3^{+gfp}* mice led to little modulation in the proportion of eGFP⁺ cells in most subsets, however, in the infundibulum there was a striking decrease in eGFP expression after TPA (Figure 4-11A, top right panel). Analysis showed that a significant reduction in the proportion of eGFP⁺ cells was apparent in the IF and bulge subsets (Figure 4-11B).

Although there were insufficient *Ackr3^{+gfp}* reporter mice available to complete these investigations, these initial results are intriguing and suggest differential regulation of *Ackr3* and CXCR4 in stromal cell subsets of the epidermis. This was most striking the infundibulum subset of keratinocytes, which appeared to significantly downregulate *Ackr3* and upregulate CXCR4 in response to multiple TPA treatments.

4.3.2 *Ackr3 Expression in the Gut*

Promising results were attained by exploring eGFP expression in the epidermis of *Ackr3^{+gfp}* reporter mice, particularly the EpCAM⁺ cells of the infundibulum. Because *Ackr3^{+gfp}* reporter mice have been poorly characterised to date, I further explored *Ackr3* expression on other epithelial surfaces, particularly those thought to be sites of *Ackr4* expression. For this reason, eGFP expression was examined in the small intestine and colon, and stromal cells were subdivided into epithelial (EpCAM⁺) cells, and non-epithelial LECs (CD31⁺ gp38⁺), blood endothelial cells (BECs; CD31⁺ gp38⁻), intestinal mesenchymal cells (iMCs; CD31⁻ gp38⁺) and double negative (DN; CD31⁻ gp38⁻) cells (Figure 4-12A).

In the small intestine, no GFP expression was detected on epithelial cells, while LECs and BECs included the highest proportions of eGFP⁺ cells (Figure 4-12B). This suggested that *Ackr3* expression is mainly restricted to the vasculature in the small intestine; however, a

significant proportion of iMCs were also eGFP⁺. In the colon, a small subset of epithelial cells was eGFP⁺, and while LECs and BECs were still highly eGFP⁺, a large proportion of iMCs and DN cells also expressed eGFP (Figure 4-12C). This suggests that *Ackr3* expression is more widespread in the colon than the small intestine, but in both tissues, this was restricted to stromal cells as eGFP signal was not detected on leukocytes (data not shown).

These results were of particular interest because eGFP expression has also been detected in the mesoepithelium and lumen of the gut in *Ackr4^{+gfp}* reporter mice ¹⁷⁷. Further analysis showed that the majority of eGFP⁺ cells in the intestine are specific subsets of fibroblasts in the lamina propria, which are part of the iMC gate (C. Thomson, personal communication). This suggests that *Ackr3* expression is much more widespread and less restricted to specific cell subsets in the intestine than *Ackr4*.

4.3.3 *Ackr3* Expression in the Mesenteric Lymph Node

Expression of both *ACKR4* and *ACKR3* were detected by human dermal LECs in the previous chapter, and *ACKR4* expression has also been shown by the lymph node stroma ¹⁰¹. CXCL12 also plays a role in FO B cell positioning in the lymph node ³³. *ACKR3* has been reported to be expressed on sinusoidal vessels in lymph node, but not on lymphatic endothelium in several tissues ¹⁵⁰; however, due to the results showing *Ackr3* expression on LECs in the gut, and expression of *ACKR3* by human dermal LECs, I examined eGFP expression in the MLN of *Ackr3^{+gfp}* reporter mice. Stromal cells in this tissue were divided into FRCs (CD31⁻, gp38⁺), LECs, BECs and DN cells (Figure 4-13A) LECs and BECs had the most convincing eGFP signals, while eGFP signals on FRCs and DN cells were negligible (Figure 4-13B). No eGFP expression was detected on leukocytes (data not shown).

This expression pattern is reminiscent of *Ackr4*, which labels a subset of LECs in eGFP reporter mice ¹⁰¹, and a small subset of BECs, but not FRCs or DN cells (S. Bryce, personal communication). *Ackr3* expression appeared to be less widespread in the lymph node compared to *Ackr4* expression, however, as the subset of LECs labelled by *Ackr3* is much smaller than the *Ackr4⁺* subset (S. Bryce, personal communication).

4.3.4 *Ackr3* Expression in the Spleen

ACKR3 protein expression has been previously reported on sinusoidal endothelial cells in the spleen by immunofluorescence¹⁵⁰. To confirm these findings, and to examine *Ackr3* expression in another SLO, I investigated whether these cells would show eGFP expression in *Ackr3^{+gfp}* mice. Flow cytometry analysis revealed a population of eGFP⁺ CD45⁻ cells (Figure 4-14A) but further investigation of these cells proved challenging, due to poor staining by endothelial markers; however, previous studies have shown that ACKR3 in the spleen is present on sinusoidal endothelial cells in the red pulp¹⁵⁰.

Investigating leukocytes in the spleen showed that most subsets were not eGFP⁺, but there was a small population of eGFP⁺ MZ B cells (Figure 4-14B), which concurs with some previous results showing antibody staining for ACKR3 in MZ B cells¹⁵². This result is interesting because MZ B cells have also been shown to express ACKR2¹⁴⁵; however, it is possible that *Ackr3* transcript in MZ B cells represents an upregulation due to the stress of experimental handling in these cells²¹⁰.

4.4 Exploring ACKR4 Expression *in vivo*

4.4.1 Investigating a Role for ACKR4 in Splenic Dendritic Cell Positioning

4.4.1.1 Characterisation of ACKR4⁺ Cells in the Spleen

I aimed to explore ACKR4 expression *in vivo* further and determine whether it is found in an SLO other than the lymph node. Because the white pulp of the spleen has a broadly analogous structure and function to the lymph node, and due to the expression of eGFP in splenic sinusoidal endothelial cells by *Ackr3^{+gfp}* mice, I investigated whether ACKR4 is also found there.

Immunostaining showed that ACKR4 is present in the spleen, and that it is restricted to CD31⁺ cells (Figure 4-15A). Anti-CD169 antibody was used as an anatomical marker to locate MMMs in the marginal zone. This made it possible to determine that the ACKR4⁺ CD31⁺ cells were located in the red pulp, which are likely to be blood vessels due to their morphological appearance. Although all ACKR4⁺ cells detected were CD31⁺, not all CD31⁺ cells were ACKR4⁺. This suggested only a subset of endothelial cells in the spleen express ACKR4, so I hoped to further characterise these cells. Spleen cells from

Ackr4^{gfp/gfp} mice were analysed using flow cytometry (Figure 4-16A). This revealed that the CD45- eGFP+ cells in the spleen are VE-Cadherin+, CD34+, CD31+, MCAM-1-, EpCAM+ (Figure 4-16B).

Unfortunately, it was not possible to determine whether splenic vascular cells coexpress ACKR3 and ACKR4. The most reliable antibody clone against ACKR3, 11G8¹⁹¹, is a mouse antibody and obtaining specific staining was too challenging. The antibody that gave reliable results for anti-ACKR4 staining in mouse tissues was a specific batch of a polyclonal antibody, and when the antibody was replaced to attempt staining on *Ackr3^{+gfp}* mice, specific anti-ACKR4 immunoreactivity was no longer attainable.

4.4.1.2 Investigating Chemokine Receptor Expression in Splenic DC Subsets

Previous work has indicated that different subsets of DCs in the spleen express the chemokine receptors CCR2, CXCR4 and CX3CR1 at varying levels (C. Cullen, personal communication). I intended to explore whether differential expression of chemokine receptors on these cells may allow them to fine-tune their positioning in the spleen to carry out specific functions; for example, priming specific T cell subsets or antigen capture. Furthermore, ACKRs may be involved in regulating the local concentrations of chemokines to aid in DC positioning. ACKR3 scavenges the CXCR4 ligand, CXCL12, and ACKR4 was investigated because it scavenges the CCR7 ligands CCL19 and CCL21, and mature DCs and T cells in SLOs are known to express CCR7¹⁰¹. *Ackr3* and ACKR4 have both been detected in the splenic vasculature in this chapter, and different subsets of DCs are known to occupy different locations in the spleen⁶⁰. I hypothesised that ACKR3 and ACKR4 could be involved in modulating the positions of DCs expressing varying levels of CXCR4 and/or CCR7 by modulating the availability of their ligands.

Splenic DCs are normally divided into CD8 α + CD11b- and CD8 α - CD11b+ subsets (these will be referred to as CD8+ and CD11b+, respectively) and their functions were discussed in the introduction (Section 1.3.2). Flow cytometry analysis has shown that among CD11b+ DCs, a further subdivision could be made based on CD4 and CD101 expression (C. Cullen, personal communication). Unfortunately, it was rarely possible to replicate CD4/CD101 staining on CD11b+ DCs, as the proportions falling into each subset varied from experiment to experiment, so only the total CD8+ and CD11b+ subsets were examined (Figure 4-18).

CXCR4 expression on DCs was measured using antibody staining, while CCR7 expression was investigated using uptake of fluorescently-labelled CCL19, with biotinylated CCL19/sva-AF488 tetramers and sva-AF488 only as a control. This was due to the lack of adequate antibodies available for this receptor. These experiments showed that CD11b⁺ and CD8⁺ DCs have comparable levels of functional CCR7 (Figure 4-19A) and anti-CXCR4 staining (Figure 4-19B), and that a significantly higher proportion of cells are CCR7⁺ in the CXCR4⁺ subset than the CXCR4⁻ subset for both CD8⁺ and CD11b⁺ DCs (Figure 4-19C). This suggests that, while chemokine receptor expression does not vary between the subsets, cells that express one chemokine receptor are more likely to express multiple receptors.

Although an analysis of splenic DC subsets in WT vs KO mice was attempted, there were no differences detected in the proportions of the different subsets identified via flow cytometry (data not shown).

4.4.1.3 Locating Splenic DC Subsets in the Spleen

To attempt to further examine splenic DC subsets, immunofluorescence was employed to reveal DC positioning within the spleen. Identifying CD8⁺ and CD11b⁺ DC subsets using traditional markers by immunostaining is challenging, as a large number of stains would be required to definitively identify these cells given that CD8 labels cytotoxic T cells and CD11b labels many leukocytes including NK cells and monocytes. It has been reported, however, that CD8⁺ and CD11b⁺ subsets can be recognised by their expression of the markers CD205 (CD8⁺) or DCIR2 (CD11b⁺)^{60,61}. Anti-CD205 and anti-DCIR2 staining was attempted to identify these DC subsets in the spleen.

Attaining anti-DCIR2 immunoreactivity was challenging. Initially, staining was attempted with a purified antibody (clone 33D1) followed by a labelled secondary antibody. According to the supplier (eBioscience), secondary antibodies raised in goat have a low affinity for this clone. The only other secondary antibody available was a mouse anti-rat antibody, and in mouse tissue this led to high levels of non-specific staining. The only directly-conjugated 33D1 antibody available was a PE conjugate, which is not suitable for microscopy because it is only weakly excited by the wavelengths used in most fluorescent microscope filter sets and becomes photobleached very quickly. The eventual solution to this problem was to use the PE-conjugated antibody followed by staining with biotinylated anti-PE antibody and finally sva-AF555.

These results showed anti-DCIR2 staining was confined mainly to the red pulp and to the bridging channels of the marginal zone, while CD205⁺ cells were mainly localised in the white pulp (Figure 4-20A). This was the pattern that would be expected if these markers successfully stained CD11b⁺ and CD8⁺ DCs respectively^{60,64}. Investigating further showed that DCIR2⁺ cells were very clearly localised in the bridging channels (Figure 4-20B), but CD205⁺ cells did not appear to be restricted to the T cell zones as expected; they appeared to be roughly evenly distributed between B cell follicles and the T cell zones (Figure 4-20C).

Due to this unexpected result, flow cytometry was used to attempt to validate CD205 and DCIR2 antibodies and determine whether CD11b⁺ and CD8⁺ subsets were correctly identified by these antibodies. Although CD205 expression was restricted to the CD8 α ⁺ subset as expected, both subsets were positive for DCIR2 (Data not shown).

There was a high level of variability in results from these investigations that made it impossible to continue, despite many efforts to fine-tune the concentrations of reagents and methods used. The lack of reproducibility encountered was most likely due to unreliability in the antibodies used, as immunostaining for chemokine receptors is often challenging; however, identifying the CD4 and CD101 subsets of CD11b⁺ cells also proved difficult on many occasions, with little positive staining obtained for either marker. The further inability to definitively identify the CD205⁺ and DCIR2⁺ subsets in immunostaining the spleen made these cells' spatial positioning uncertain. For these reasons, and despite some promising results, this line of investigation was not continued further due to limited time and resources.

4.5 Key Findings

- Keratinocyte subsets in the epidermis differentially express CXCR4 and *Ackr3* in *Ackr3*^{+/gfp} reporter mice. The highest degree of coexpression was seen in the infundibulum, while the lowest was in the heterogeneous bulge subset.
- Most subsets of keratinocytes significantly upregulate CXCR4 in response to multiple TPA treatments, while *Ackr3* is downregulated in the infundibulum and bulge.
- *Ackr3* is expressed on endothelial cells in gut, spleen, skin and mesenteric lymph nodes. The following cell types showed evidence of *Ackr3* expression:
 - A subset of LECs and BECs in the MLN

- All stromal cells in the colon
- LECs and BECs in the small intestine
- MZ B cells and endothelial cells in the spleen
- Keratinocytes in the skin
- ACKR4 is expressed on CD31+ VE-Cadherin+ EpCAM+ CD34+ MCAM-1- vessels in the splenic red pulp.
- Subsets of CD8+ and CD11b+ DCs in the spleen express CXCR4 and CCR7 receptors.

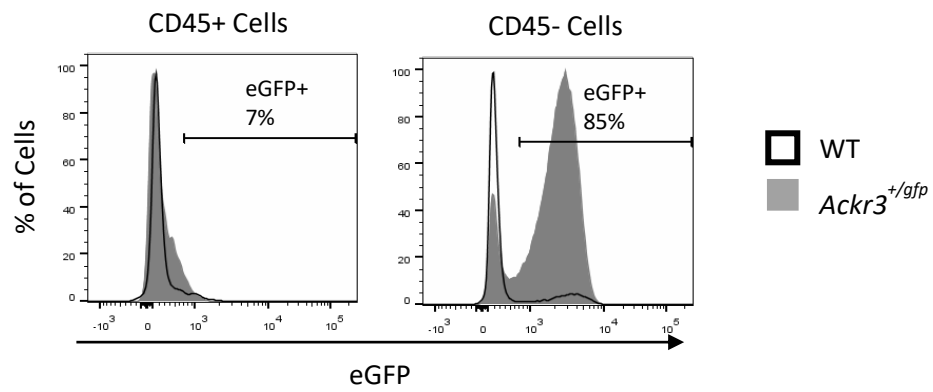


Figure 4-1: eGFP expression in the epidermis of *Ackr3*^{+/*gfp*} mice is mainly restricted to CD45- cells.

Ears from *Ackr3*^{gfp/+} reporter mice (■) or WT control (□) were excised and epidermal sheets were processed to obtain single cell suspensions for flow cytometry analysis (n=5, +1 WT control). Representative histograms show eGFP expression in CD45+ cells (left panel) and CD45- cells (right panel). Gates represent the proportion of eGFP+ cells in the *Ackr3*^{+/*gfp*} mouse.

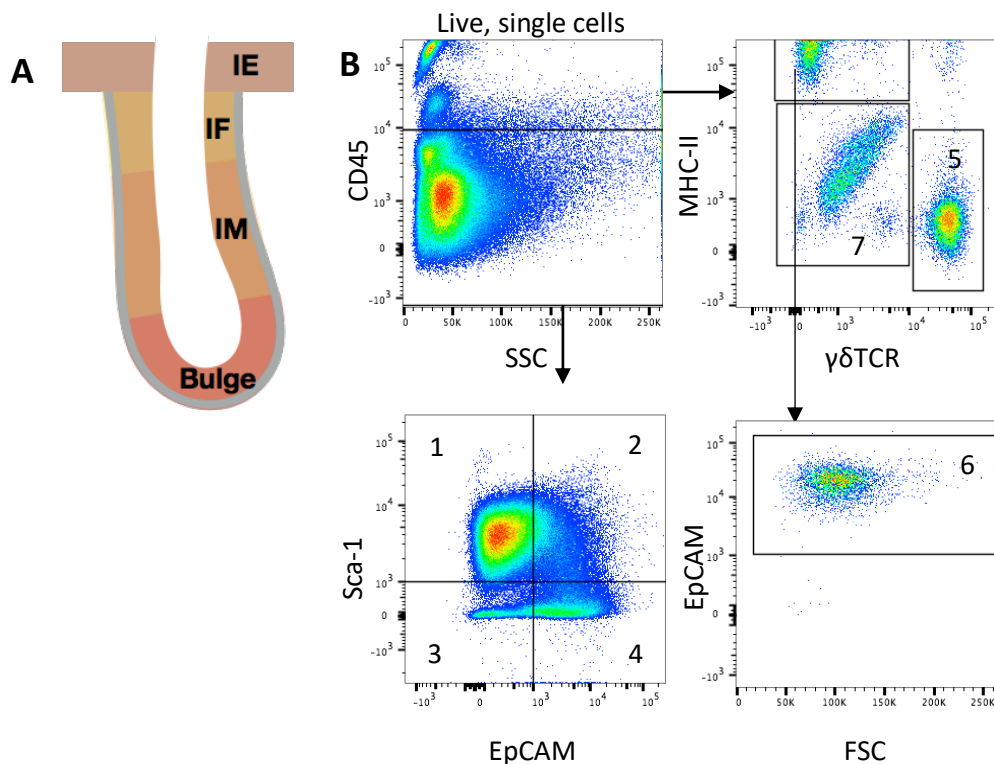


Figure 4-2: Flow cytometry gating strategy for identifying epidermal cell types.

Single cell suspensions were prepared from dermis and epidermal sheets and cells were analysed via flow cytometry. Samples were pre-gated to exclude debris, doublets and dead cells. **A)** Schematic diagram representing the locations of the four keratinocyte subsets in a telogen hair follicle. **B)** Representative scatter plots of inflamed epidermis (16h TPA) showing the gating strategies to identify epidermal cell types. (These cell types are all present in non-inflamed skin, but gating was easier in inflamed skin due to higher numbers of leukocytes). CD45⁻ cells were subdivided based on Sca-1 and EpCAM expression, while CD45⁺ cells were divided into $\gamma\delta$ TCR⁺ MHC-II⁻, $\gamma\delta$ TCR⁻ MHC-II⁺ and $\gamma\delta$ TCR⁻ MHC-II⁻ subsets. The $\gamma\delta$ TCR⁻ MHC-II⁺ subset was then gated for EpCAM⁺ cells. **C)** Table summarising the identified populations.

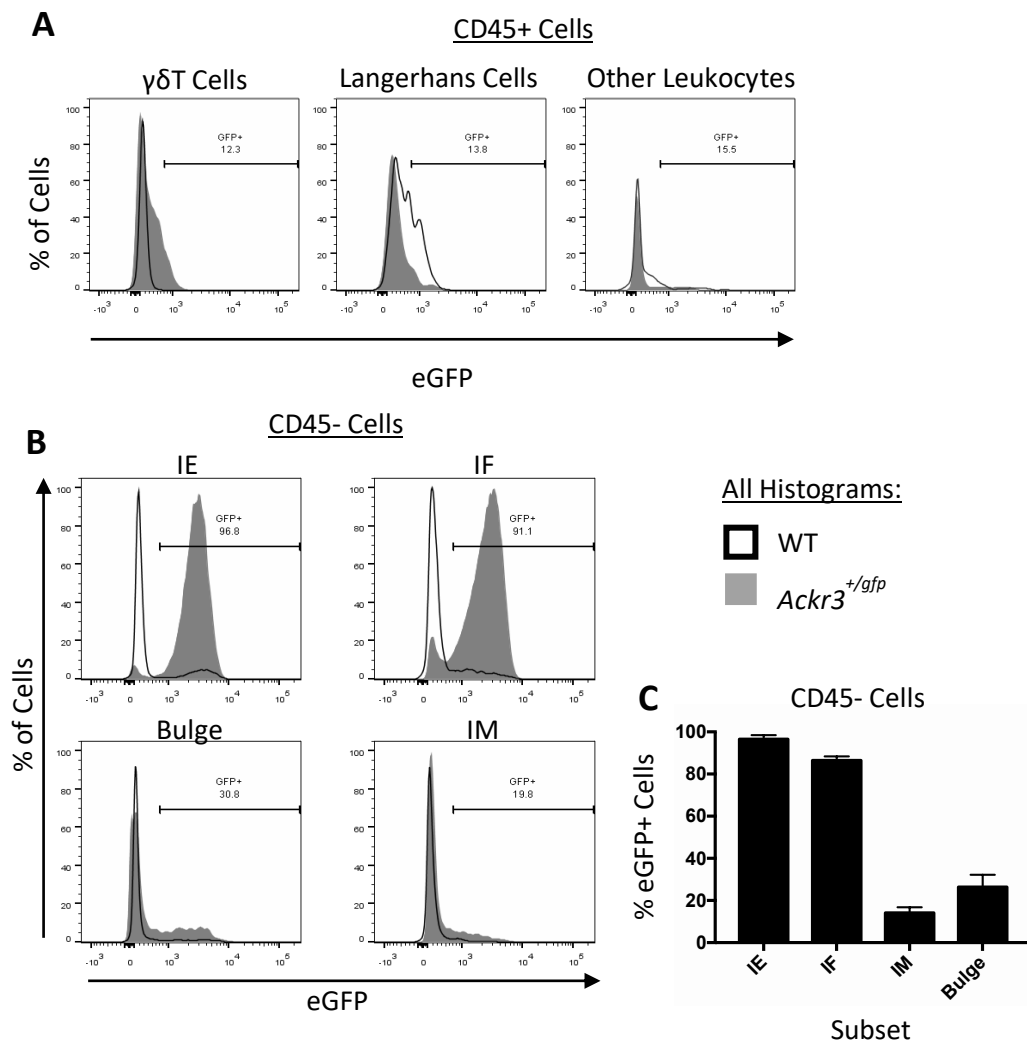


Figure 4-3: eGFP is expressed by subsets of CD45- cells in the skin of *Ackr3*^{+/*gfp*} mice.

Ears from *Ackr3*^{*gfp*/+} reporter mice (■) or WT control (□) were excised and epidermal sheets were processed to obtain single cell suspensions for flow cytometry analysis (n=5, +1 WT control). **A**) eGFP expression in epidermal CD45+ cell types: $\gamma\delta$ T Cells, Langerhans Cells and Other Leukocytes. Representative histograms show eGFP expression in WT vs *Ackr3*^{+/*gfp*} mice. **B**) eGFP expression in epidermal keratinocyte subsets identified in Figure 4-2. Representative histograms show eGFP expression in WT vs *Ackr3*^{+/*gfp*} mice. **C**) Graph summarising data obtained in B, showing comparative eGFP expression between keratinocyte subsets. Error bars represent SD of the mean.

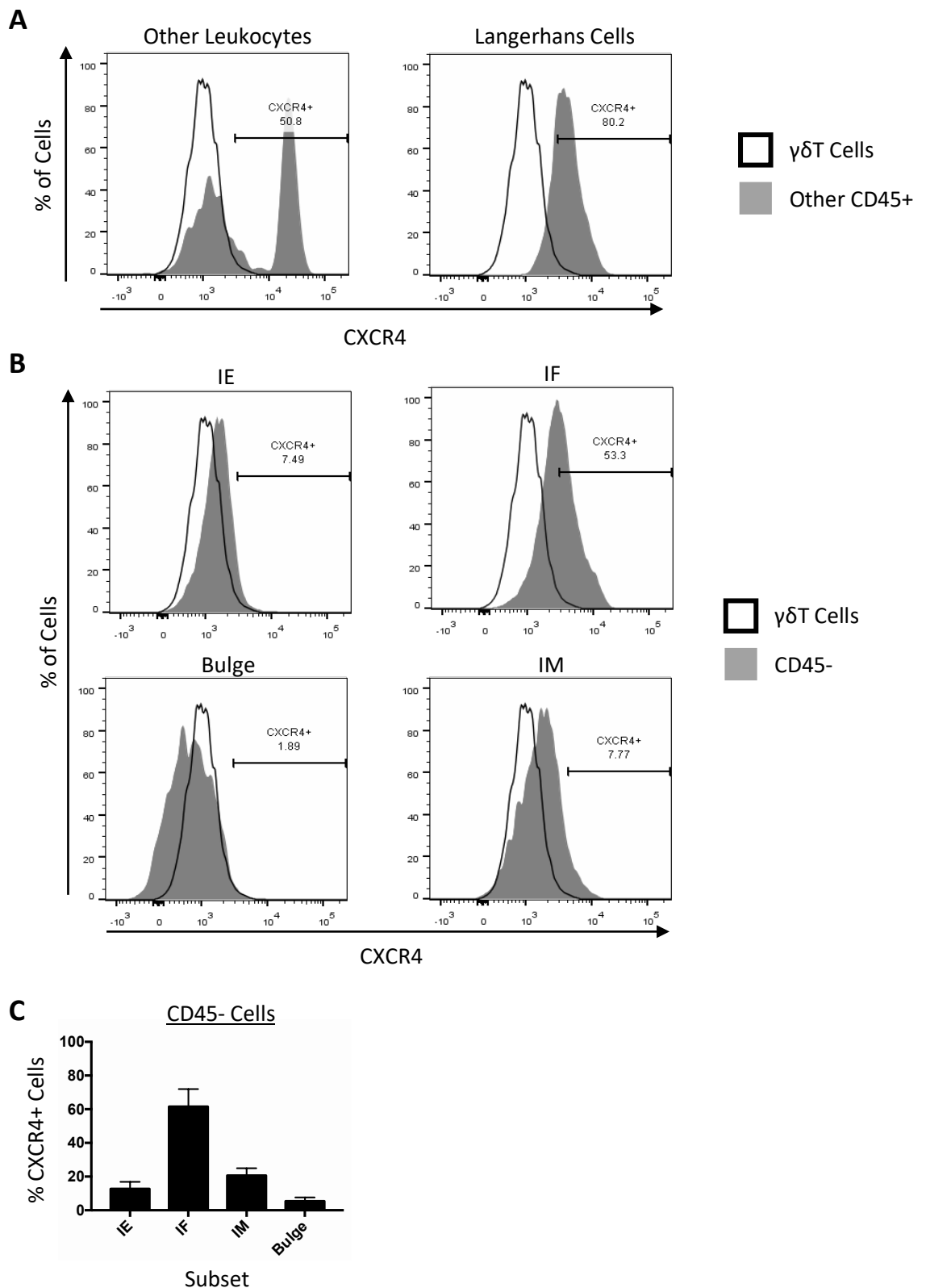


Figure 4-4: CXCR4 is expressed by keratinocytes, Langerhans Cells and other leukocytes in the epidermis.

Mouse ears were excised and epidermal sheets were processed to obtain single cell suspensions for flow cytometry analysis (n=5). $\gamma\delta$ T cells are used as a negative control for CXCR4 expression. **A**) Representative histograms show CXCR4 expression in CD45+ cell populations. **B**) Representative histograms show CXCR4 expression in the four keratinocyte subsets detected. **C**) Graph showing the percentage of CXCR4 positive cells

detected in the epidermal keratinocyte subsets identified in Figure 4-2. Error bars represent SD of the mean.

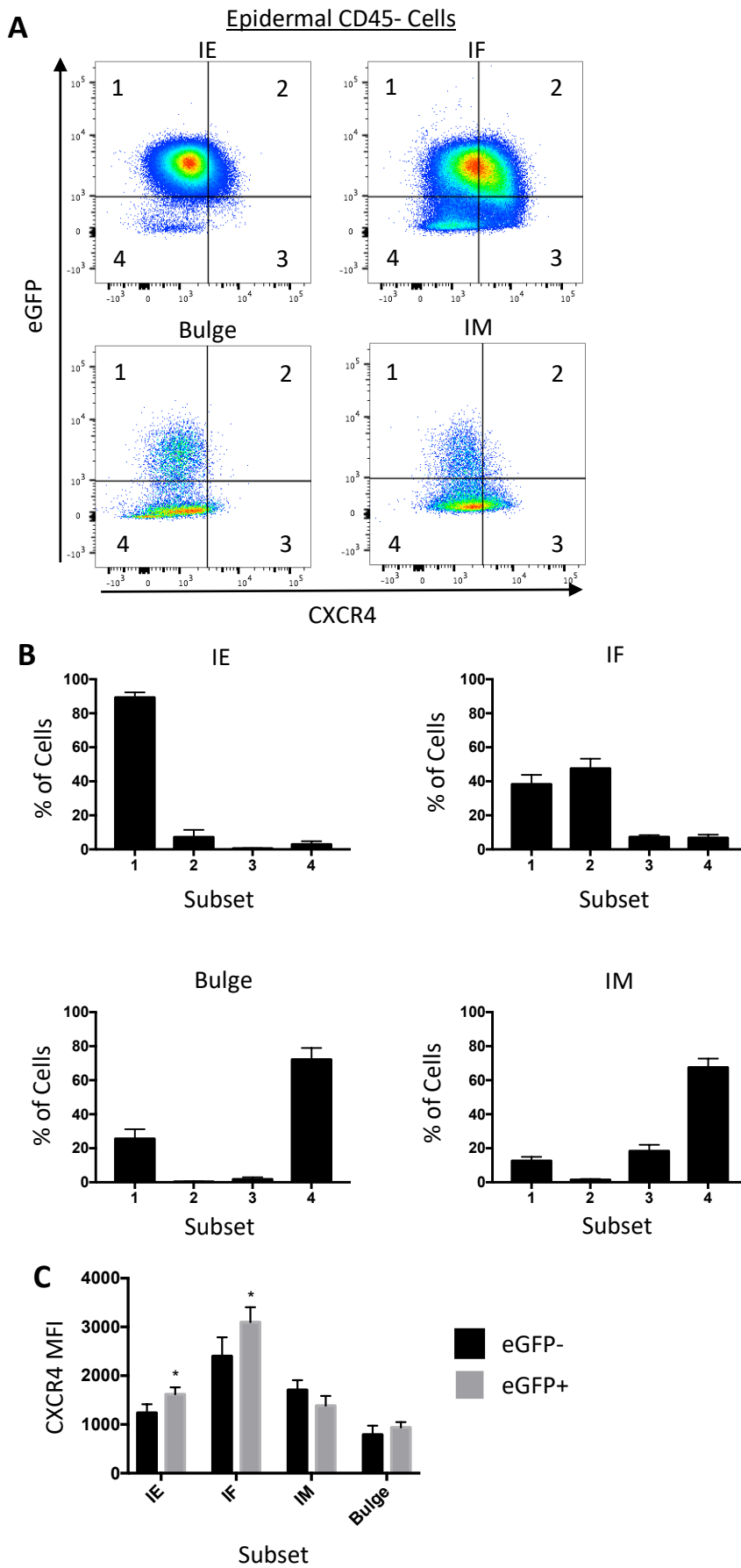


Figure 4-5: eGFP and CXCR4 are coexpressed by subsets of keratinocytes in *Ackr3*^{+gfp} mice.

Ears from $Ackr3^{gfp/+}$ reporter mice were excised and epidermal sheets were processed to obtain single cell suspensions for flow cytometry analysis (n=5). **A)** Representative scatter plots showing eGFP and CXCR4 expression in the four stromal subsets identified in Figure 4-2: Interfollicular Epidermis (IE), Infundibulum (IF), Isthmus (IM) and Hair follicle bulge (Bulge). Cells are separated into four subsets: 1) eGFP+ CXCR4-, 2) eGFP+ CXCR4+, 3) eGFP- CXCR4+, 4) eGFP- CXCR4-. Error bars represent SD of the mean. **B)** Expression of the four eGFP/CXCR4 subsets identified in A by the four stromal cell populations. Top left: Sca-1+ EpCAM- (interfollicular epidermis, IE), top right: Sca-1+ EpCAM+ (infundibulum, IF), bottom left: Sca-1- EpCAM- (hair follicle bulge), bottom right: Sca-1- EpCAM+ (isthmus, IM). **C)** Mean fluorescence intensity (MFI) of anti-CXCR4 staining on eGFP- (■) and eGFP+ (■) cells within the four identified keratinocyte subsets. Statistical significance between eGFP- and eGFP+ populations was calculated using t tests corrected for multiple comparisons using the Holm-Sidak method (* $P \leq 0.05$).

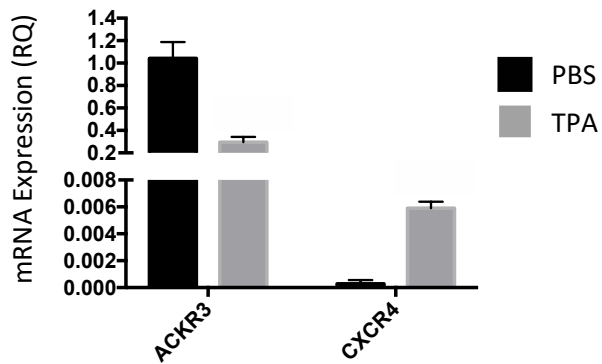


Figure 4-6: ACKR3 mRNA is downregulated and CXCR4 mRNA is upregulated in response to TPA in cultured human keratinocytes.

Normal human epidermal keratinocytes (nHEKs) were cultured in LoCa media until 70-80% confluent and treated with PBS (■) or 100 nM TPA (■). After 4h, cells were harvested and RNA was extracted to generate cDNA for qPCR analysis. Three technical replicates were performed by carrying out each treatment on three separate wells, and each sample was run in triplicate. Graphs show expression of ACKR3 and CXCR4 as arbitrary units (AU) calculated by the $\Delta\Delta CT$ method. Error bars represent SD of the mean.

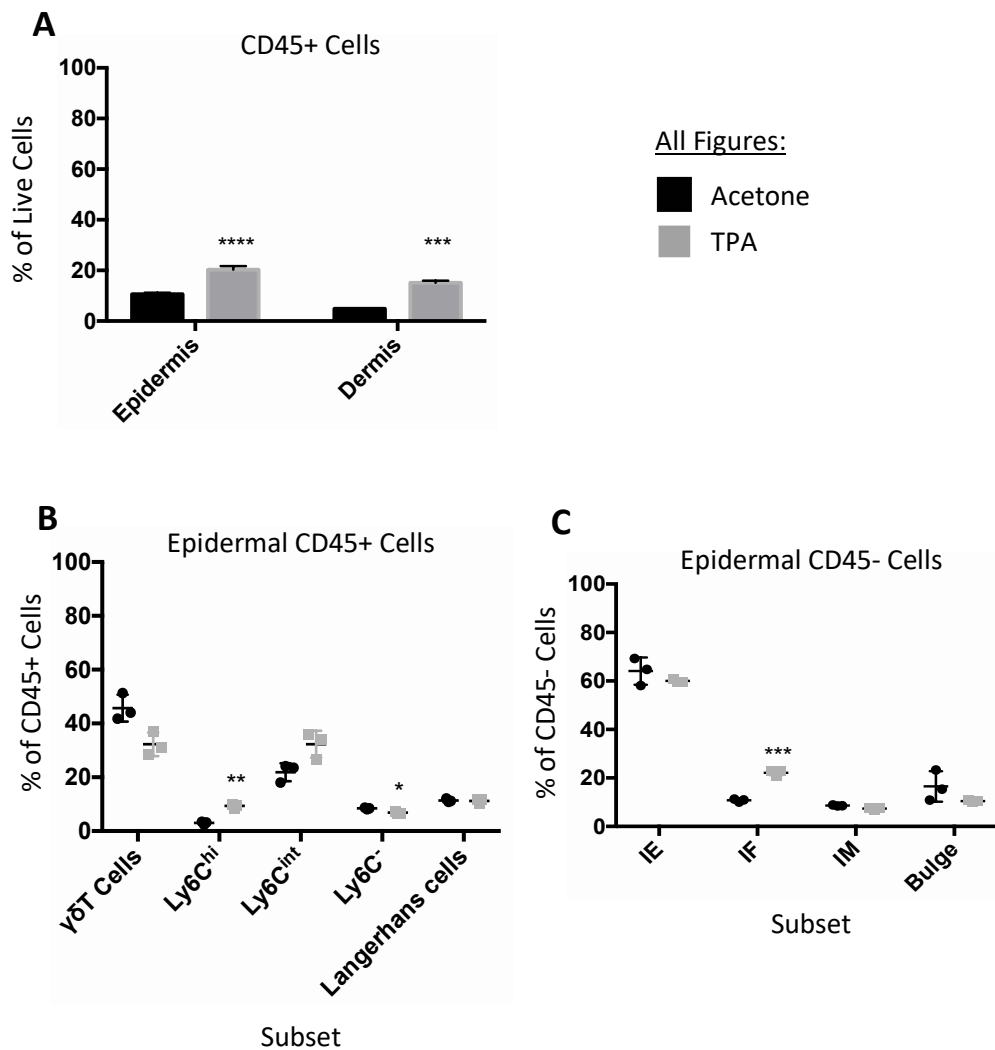


Figure 4-7: A single topical TPA treatment leads to an increased proportion of leukocytes in both epidermis and dermis.

WT mice were treated once on the ear skin with TPA (■) or acetone (■) and 16 hours after treatment, ears were separated into epidermis and dermis and processed to obtain single cell suspensions for flow cytometry analysis (n=3). Statistical significance was determined using t tests corrected for multiple comparisons using the Holm-Sidak method (* $P \leq 0.05$, ** $P \leq 0.01$, *** $P \leq 0.001$, **** $P \leq 0.0001$). Error bars represent SD of the mean. **A**) The percentage of live cells represented by leukocytes in the epidermis and dermis of acetone and TPA-treated mice. **B**) The percentage of CD45+ cells that fall into each leukocyte subset in the epidermis of acetone and TPA-treated mice. **C**) The percentage of CD45- cells represented by each subset of keratinocytes in the epidermis of acetone and TPA-treated mice.

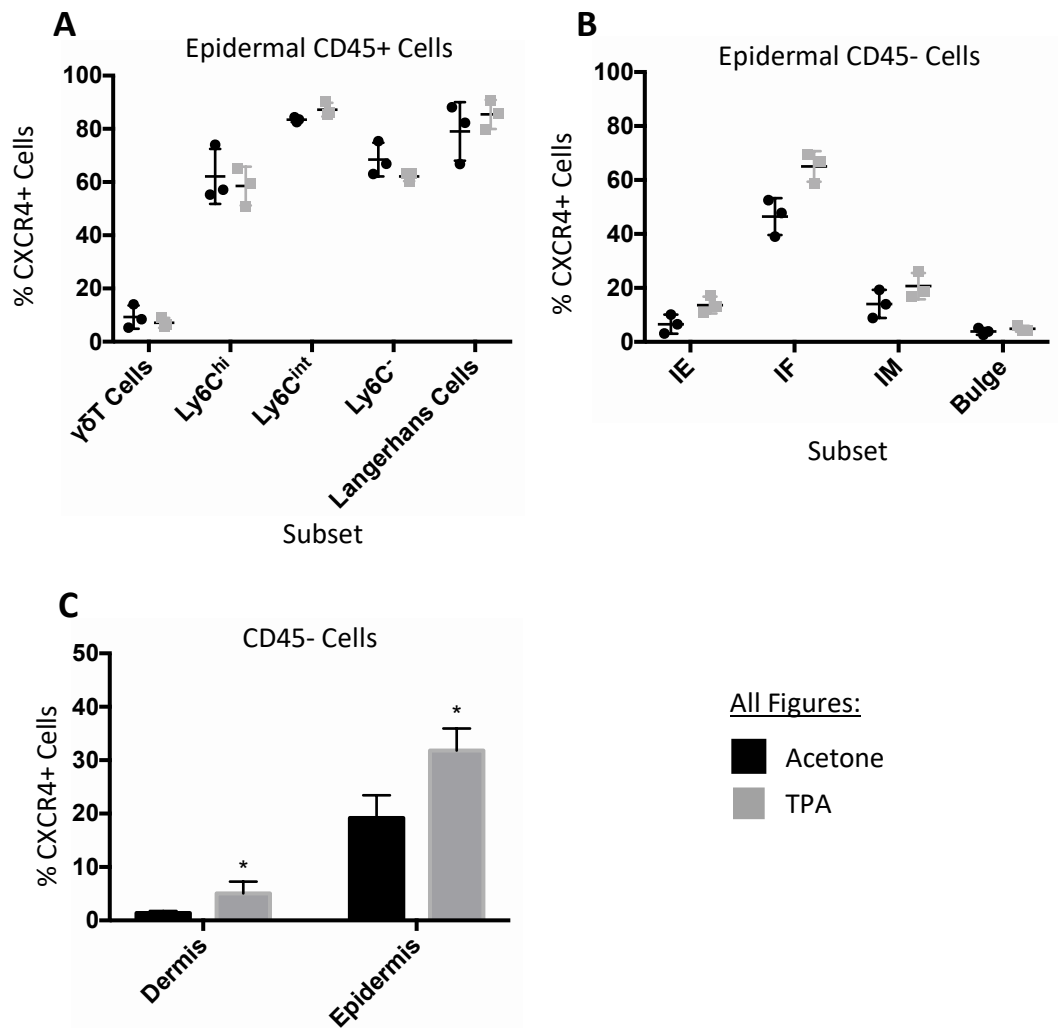


Figure 4-8: CXCR4 expression in the skin increases 16 hours after a single TPA treatment due to increased proportions of CXCR4+ cells.

WT mice were treated once on the ear skin with TPA (■) or acetone (■) and 16 hours after treatment, ears were separated into epidermis and dermis and processed to obtain single cell suspensions for flow cytometry analysis (n=3). Statistical significance was determined using t tests corrected for multiple comparisons using the Holm-Sidak method (*P≤0.05, **P≤0.01). Error bars represent SD of the mean. **A)** CXCR4 expression in epidermal leukocytes. **B)** Percentage of CXCR4+ cells in epidermal CD45- subsets. **C)** Percentage of all CD45- cells that are CXCR4+ in the dermis and epidermis.

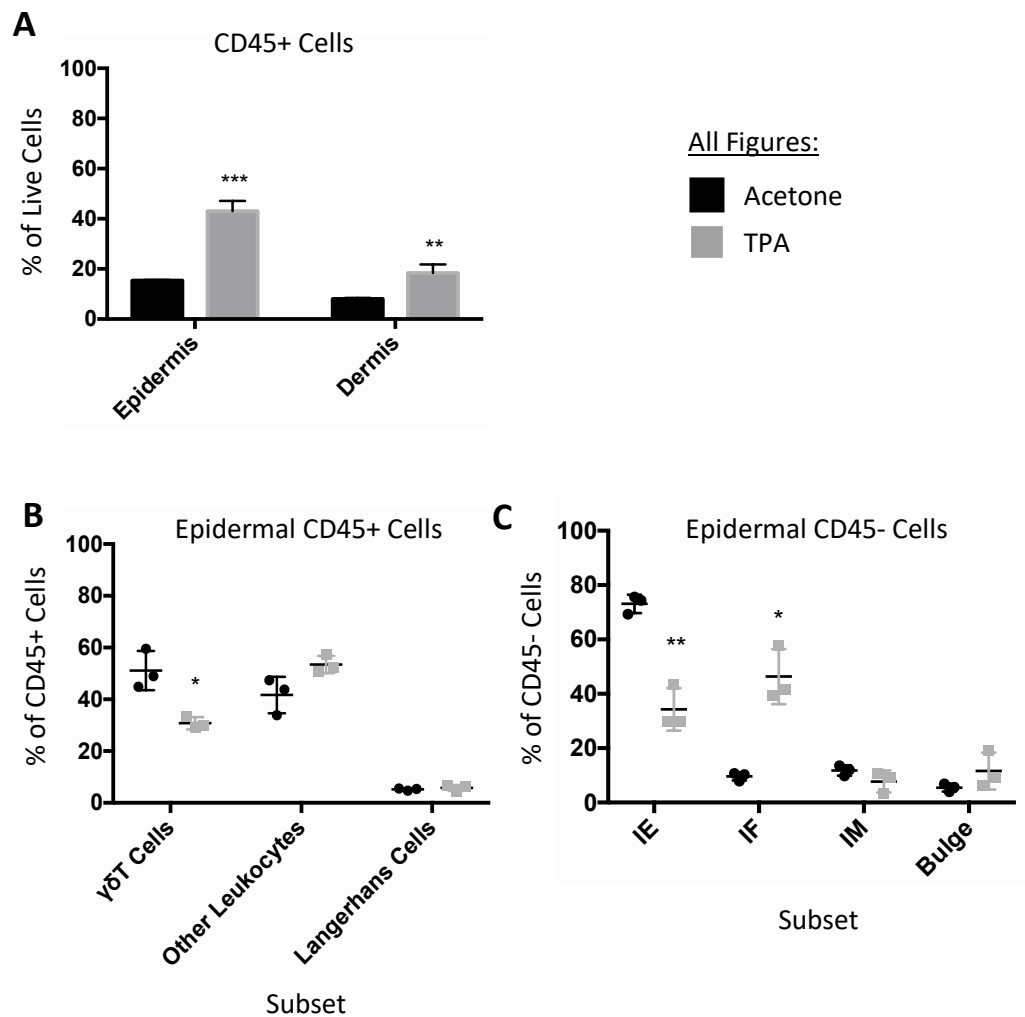


Figure 4-9: Repeated TPA treatments lead to changes in the proportions of epidermal leukocytes and keratinocytes.

WT mice were treated once daily for three days on the ear skin with TPA (■) or acetone (■) and 16 hours after the final treatment, ears were separated into epidermis and dermis and processed to obtain single cell suspensions for flow cytometry analysis (n=3). Statistical significance was determined using t tests corrected for multiple comparisons using the Holm-Sidak method (*P≤0.05, **P≤0.01, ***P≤0.001). Error bars represent SD of the mean. **A**) The percentage of live cells represented by leukocytes in the epidermis and dermis of acetone and TPA-treated mice. **B**) The percentage of CD45+ cells that fall into each leukocyte subset in the epidermis of acetone and TPA-treated mice. **C**) The percentage of CD45- cells represented by each subset of keratinocytes in the epidermis of acetone and TPA-treated mice.

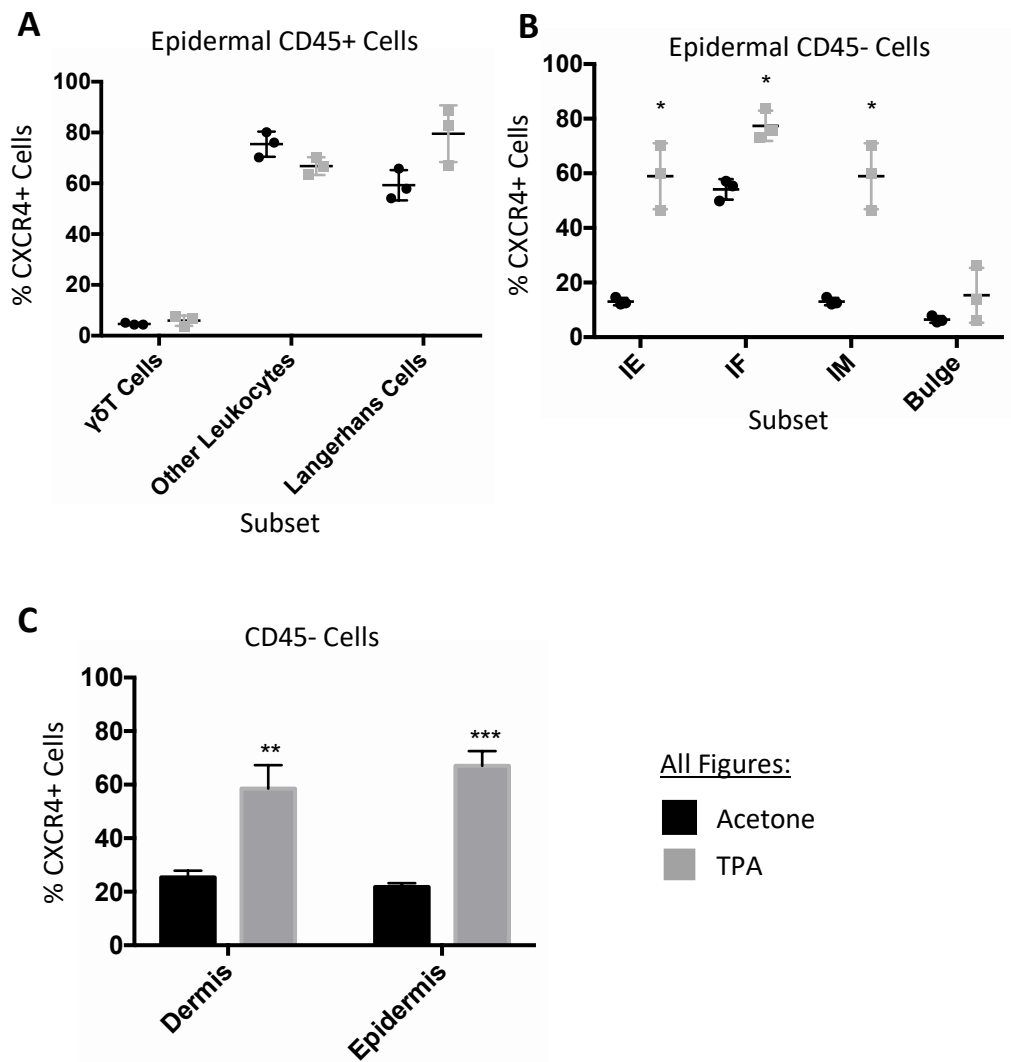


Figure 4-10: CXCR4 expression by keratinocytes is increased after repeated TPA treatments.

WT mice were treated once daily for three days on the ear skin with TPA (■) or acetone (■) and 16 hours after the final treatment, ears were separated into epidermis and dermis and processed to obtain single cell suspensions for flow cytometry analysis (n=3). Statistical significance was determined using t tests corrected for multiple comparisons using the Holm-Sidak method (*P≤0.05, **P≤0.01). Error bars represent SD of the mean. **A)** CXCR4 expression in epidermal leukocytes. **B)** Percentage of CXCR4+ cells in epidermal CD45- subsets. **C)** Percentage of all CD45- cells that are CXCR4+ in the dermis and epidermis.

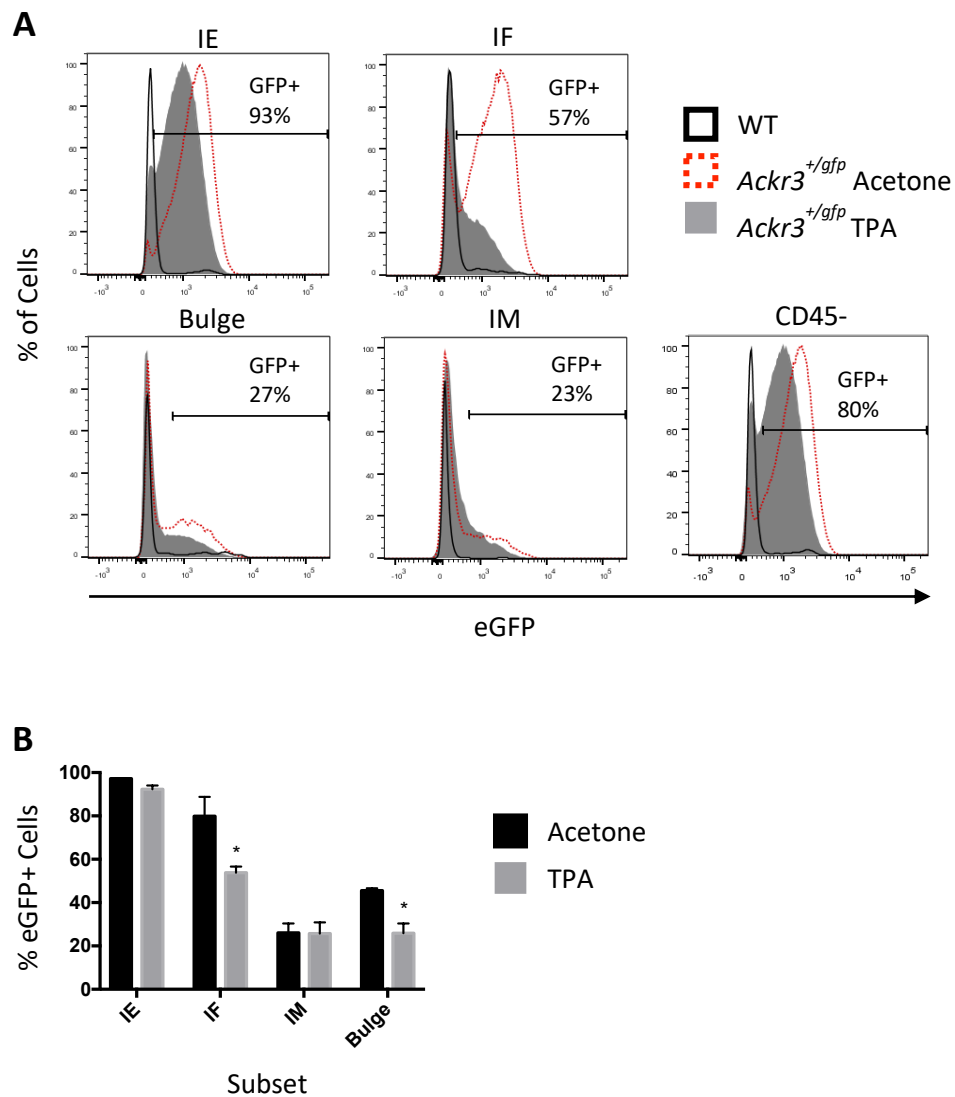


Figure 4-11: Repeated TPA treatments reduce eGFP expression in the infundibulum of *Akr3*^{+/*gfp*} mice.

Akr3^{+/*gfp*} mice were treated once daily for three days on the ear skin with TPA or acetone and 16 hours after the final treatment, ears were separated into epidermis and dermis and processed to obtain single cell suspensions for flow cytometry analysis (n=3 + 1 WT control). **A**) Representative histograms show eGFP expression in each keratinocyte subset of WT acetone-treated (□), *Akr3*^{+/*gfp*} acetone-treated (□) and *Akr3*^{+/*gfp*} TPA-treated (■) mice. Gates represent the proportion of eGFP+ cells in the *Akr3*^{+/*gfp*} TPA-treated sample. **B**) Graph showing the proportion of eGFP cells in each keratinocyte subset between mice treated with acetone (■) and TPA (■). Statistical significance was determined using t tests corrected for multiple comparisons using the Holm-Sidak method (*P≤0.05). Error bars represent SD of the mean.

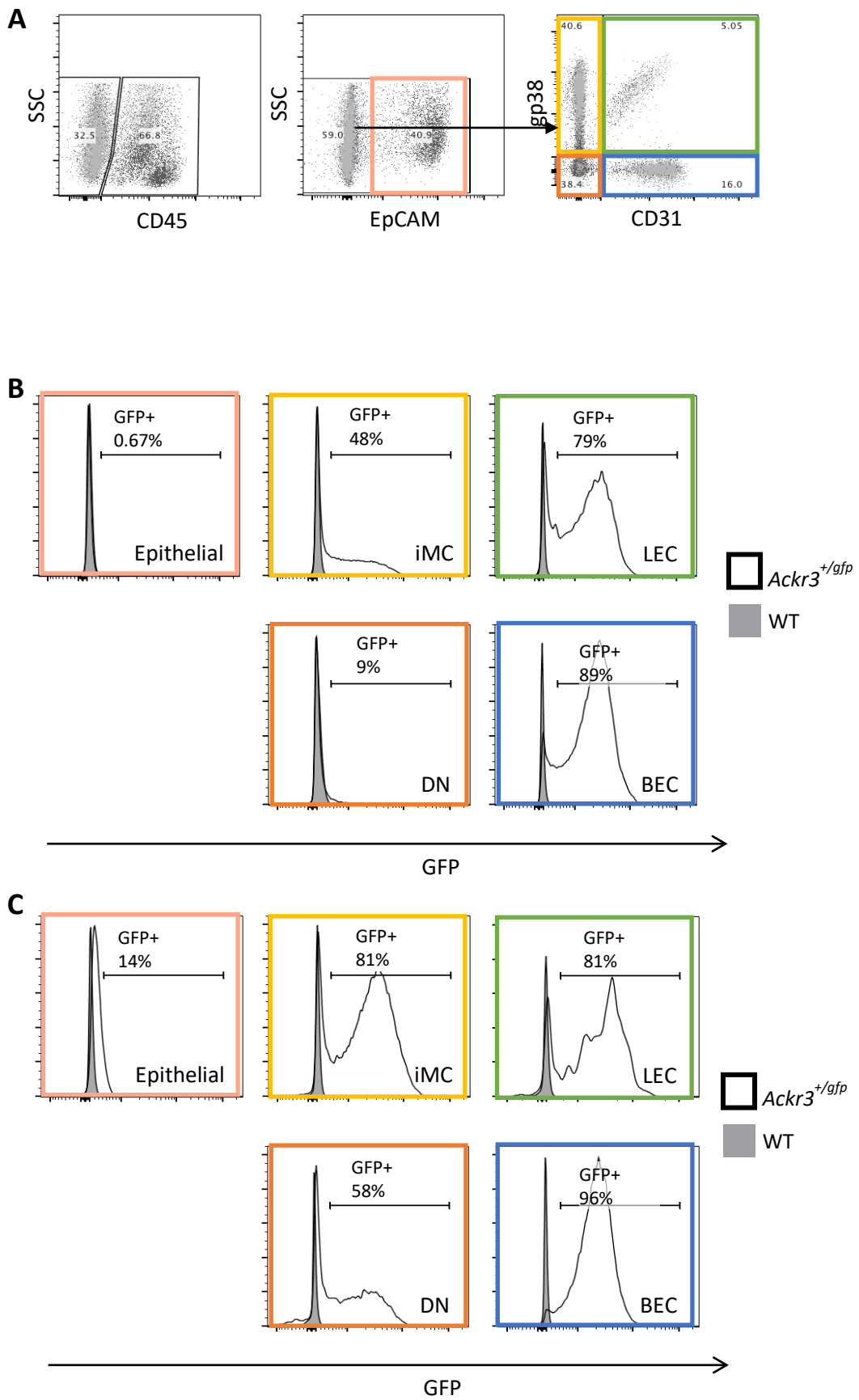


Figure 4-12: eGFP is widely expressed in the small intestine and colon of *Ackr3*^{+/*gfp*} mice.

Small intestine and colon were harvested from WT (■) and *Ackr3*^{+/*gfp*} (□) mice and processed to obtain single cell suspensions for flow cytometry analysis. (WT: n=1, *Ackr3*^{+/*gfp*}: n=3). Note that females 14 weeks of age were used for this analysis due to limited availability of mice. **A)** Gating strategy to identify the stromal cell subsets analysed. All samples were initially gated to exclude debris, doublets and dead cells. Cells were divided into CD45- EpCAM+ (Epithelial), CD45- EpCAM- gp38+ CD31- (iMC), CD45- EpCAM- gp38+ CD31+ (LEC), CD45- EpCAM- gp38- CD31+ (BEC), CD45- EpCAM- gp38- CD31- (DN). eGFP+ cells are overlaid over total cells in these plots to represent the distribution of eGFP expression. **B)** Expression of eGFP in the five identified stromal subsets of the small intestine in WT and *Ackr3*^{+/*gfp*} mice. **C)** Expression of eGFP in the five identified stromal subsets of the colon in WT and *Ackr3*^{+/*gfp*} mice.

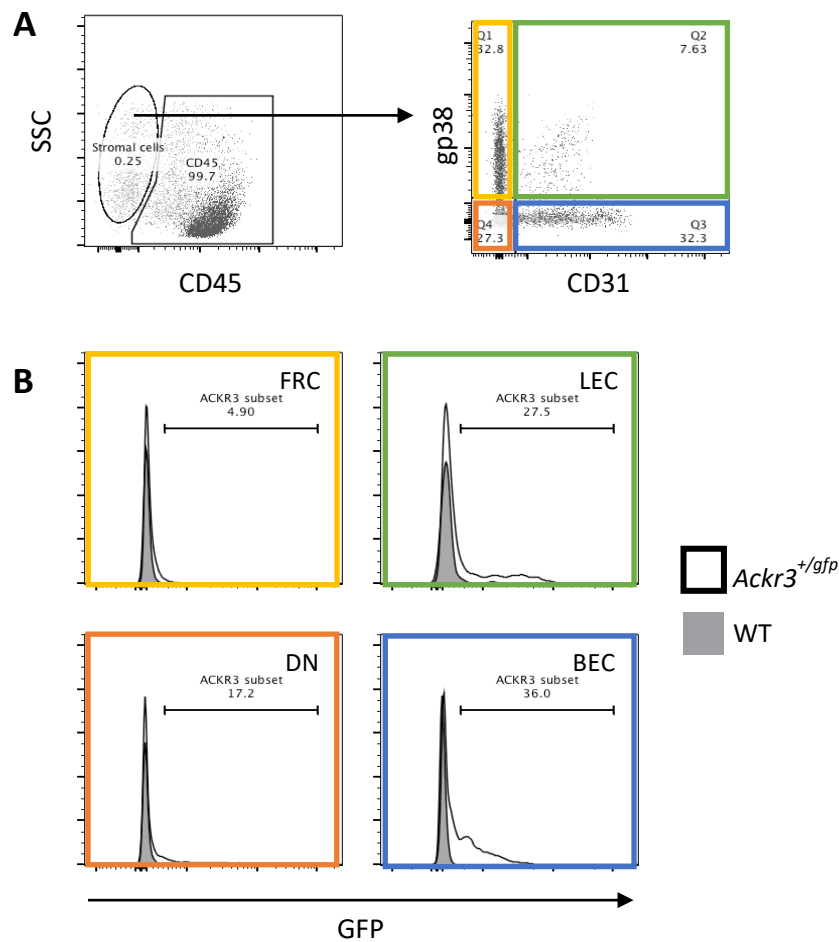


Figure 4-13: eGFP is expressed by LECs and BECs in the mesenteric lymph nodes of *Ackr3*^{+/*gfp*} mice.

Mesenteric lymph nodes were harvested from WT (■) and *Ackr3*^{+/*gfp*} (□) mice and processed to obtain single cell suspensions for flow cytometry analysis. (WT: n=1, *Ackr3*^{+/*gfp*}: n=3). Note that females 14 weeks of age were used for this analysis due to limited availability of mice. **A)** Gating strategy to identify the stromal cell subsets analysed. All samples were initially gated to exclude debris, doublets and dead cells. Cells were divided into CD45- gp38+ CD31- (FRC), CD45- gp38+ CD31+ (LEC), CD45- gp38- CD31+ (BEC) and CD45- gp38- CD31- (DN). eGFP⁺ cells are overlaid over total cells in these plots to represent the distribution of eGFP expression. **B)** Expression of eGFP in the four identified stromal subsets of the MLN.

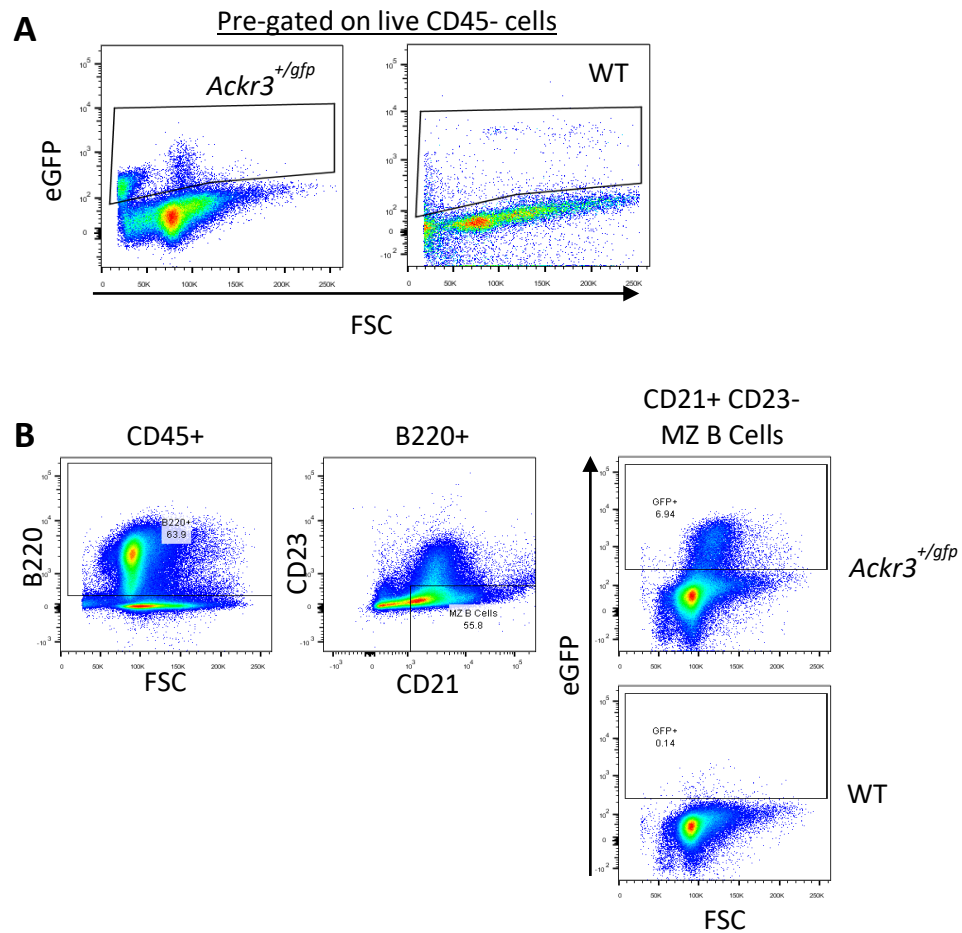


Figure 4-14: eGFP is expressed by stromal cells and MZ B cells in the spleen of *Ackr3*^{+/*gfp*} mice

Spleens were harvested from WT and *Ackr3*^{+/*gfp*} mice and processed to obtain single cell suspensions for flow cytometry analysis. (WT: n=1, *Ackr3*^{+/*gfp*}: n=3). Note that females 14 weeks of age were used for this analysis due to limited availability of mice. **A)** Representative scatter plots showing the identification of eGFP⁺ stromal cells. **B)** eGFP expression in splenic leukocytes: left panel shows the gating strategy to identify B220⁺ leukocytes, the middle panel shows MZ B cells within this gate (CD21⁺ CD23⁻ cells) and the right panels show eGFP expression by MZ B cells in *Ackr3*^{+/*gfp*} (top) and WT (bottom) mice.

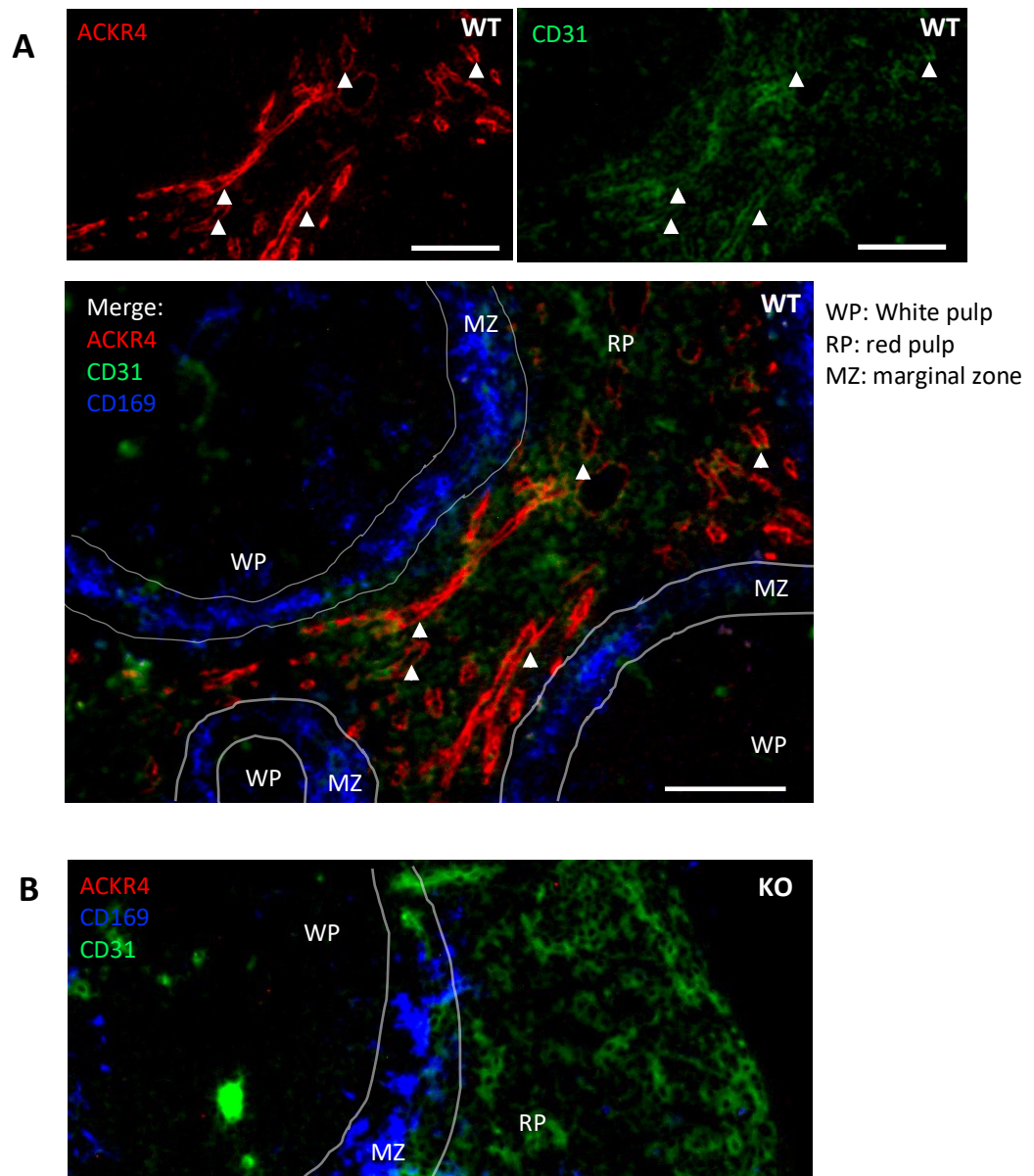


Figure 4-15: ACKR4 protein in the spleen is mainly located on CD31+ cells in the red pulp.

Spleens from resting WT and *Ackr4*^{-/-} (KO) mice were harvested and cryosections were prepared. Sections were incubated with anti-ACKR4, CD31 and CD169 antibodies and viewed using fluorescent microscopy. Images are representative of three replicates. Scale bars = 100 μ m. **A**) In a WT background, individual channel images show ACKR4 staining (top left panel) and CD31 staining (top right panel), and all channels are shown superimposed (lower panel) with anatomical details highlighted: WP = white pulp, RP = red pulp, MZ = marginal zone. All arrows in the three images highlight the same positions, showing vessels that appear to co-stain with ACKR4 and CD31 antibodies. **B**) The KO mouse shows no ACKR4 staining, indicating the antibody used has good specificity.

Pre-gated on CD45- cells

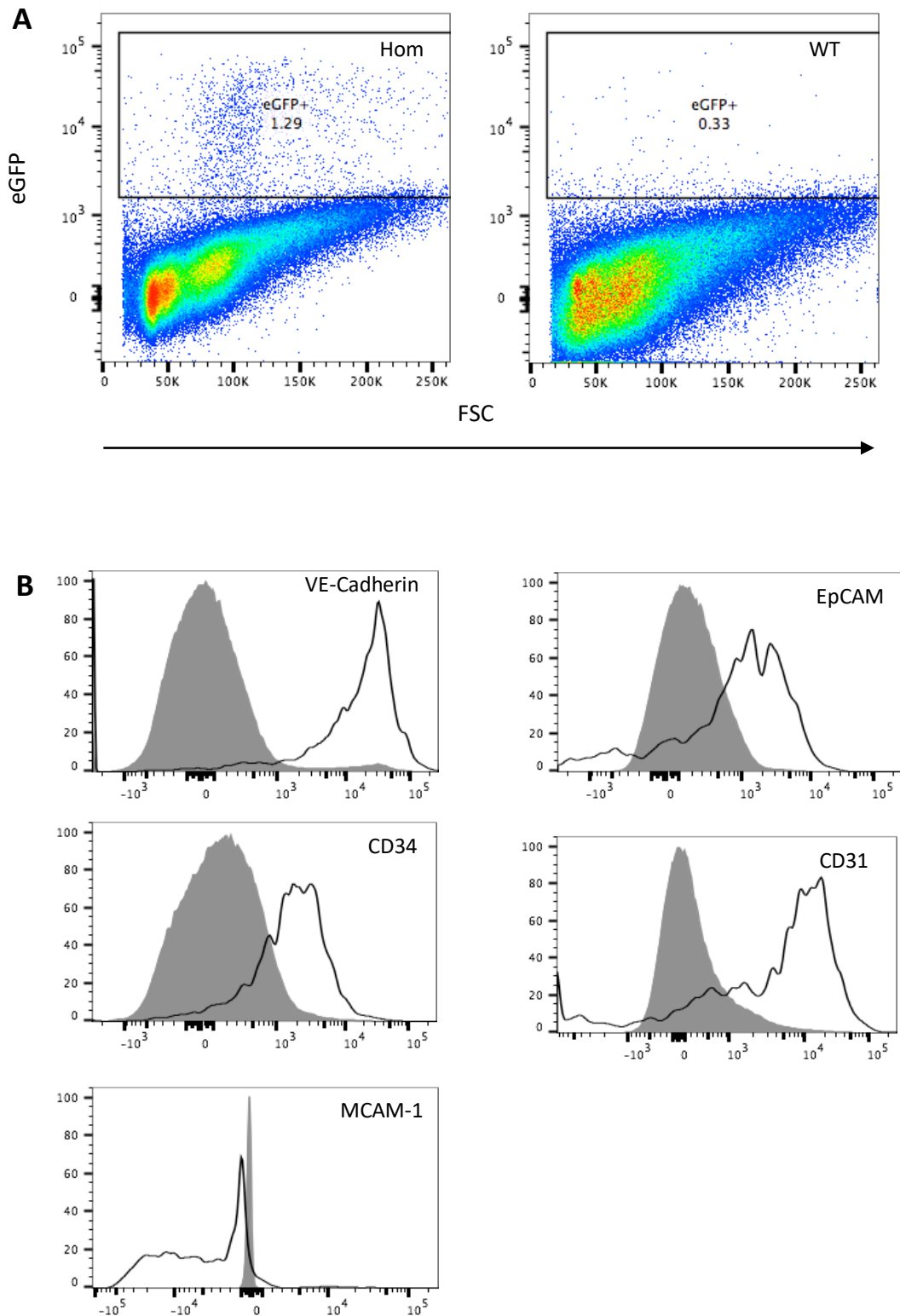


Figure 4-16: ACKR4 is expressed on vascular endothelial cells in the spleen.

Spleens from resting WT and *Ackr4^{gfp/gfp}* (Hom) mice were excised and processed to obtain single cell suspensions for flow cytometry analysis (n=2). **A**) Representative scatter plots showing the identification of eGFP⁺ stromal cells. **B**) Representative histograms showing expression of endothelial cell surface markers on eGFP⁺ cells (□) and eGFP⁻ cells (■).

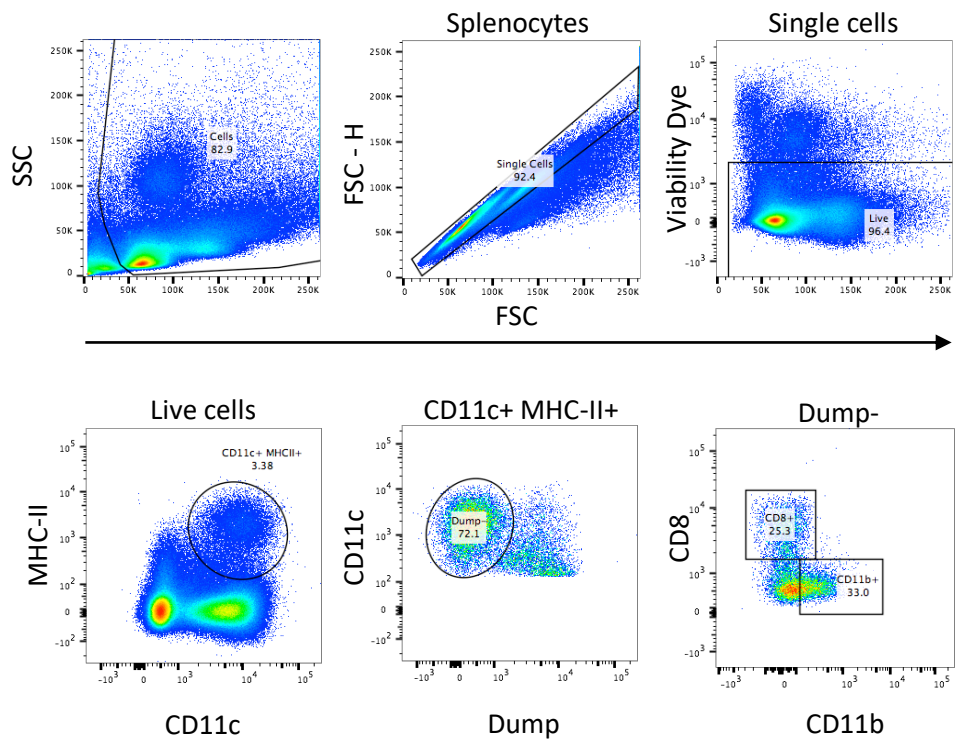


Figure 4-17: Flow cytometry gating strategy to identify DC subsets in the spleen.

Spleens from resting WT mice were processed to obtain single cell suspensions for flow cytometry analysis. Representative histograms show the gating strategy used to identify DC subsets in the spleen. First, debris, doublets and dead cells were excluded. DCs were defined as CD11b⁺ MHC-II⁺ CD3 ϵ ⁻ NK1.1⁻ B220⁻ cells (anti-CD3 ϵ , anti-NK1.1 and anti-B220 antibodies were all combined into a single dump channel). DCs were then subdivided into CD8 α ⁺ and CD11b⁺ subsets.

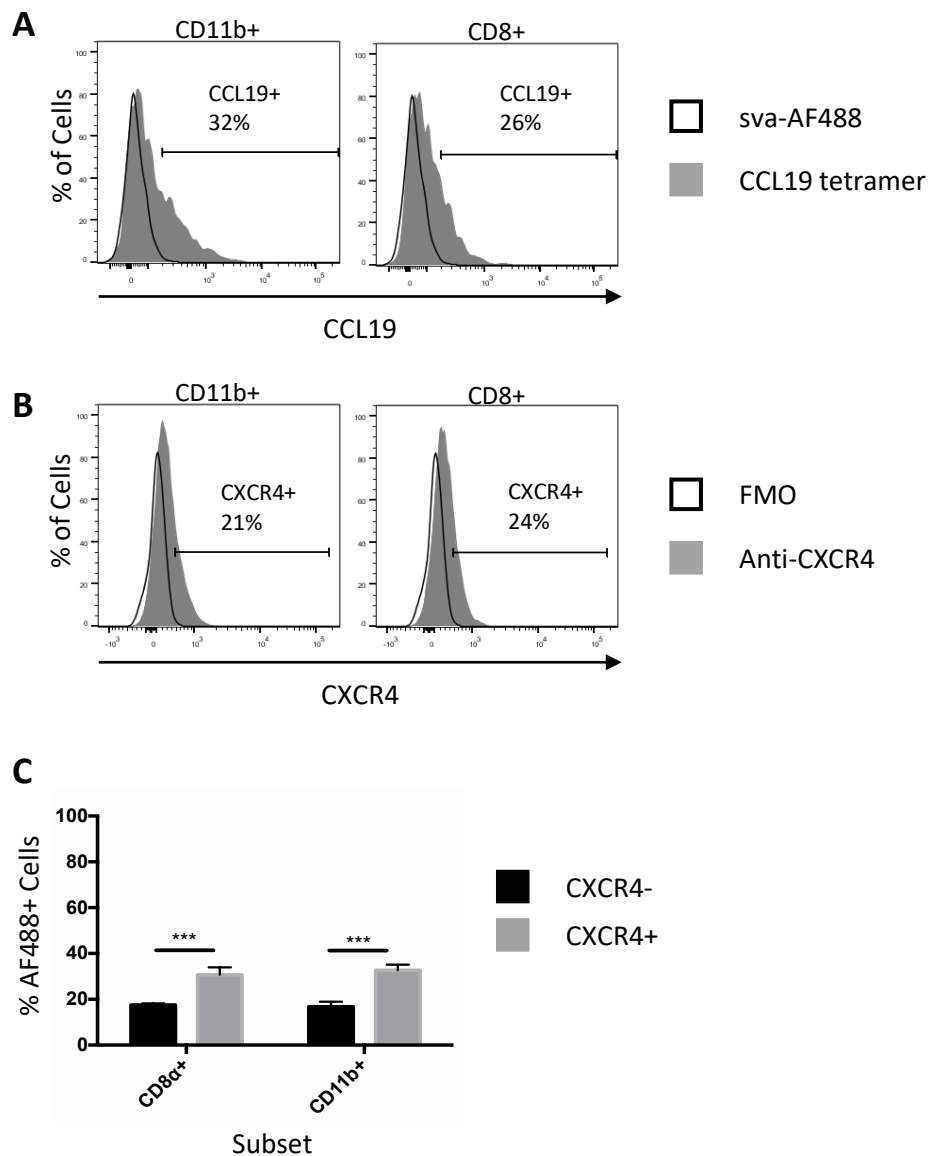


Figure 4-18: CD8+ and CD11b+ DCs show similar expression levels of CCR7 and CXCR4.

Spleens from resting WT mice were processed to obtain single cell suspensions for flow cytometry analysis and fluorescent chemokine uptake assays were carried out using tetramers of biotinylated CCL19 and sva-AF488, with sva-AF488 only as a control. Populations were defined as detailed in Figure 4-17. (n=3 + 1 sva-AF488 only control). Statistical significance was determined using two-way ANOVA (*=P≤0.05, **=P≤0.01, ***=P≤0.001). **A**) Representative histograms showing AF488 signal in cells receiving CCL19 tetramers (■) and sva-AF488 only (□). Left panel: CD11b+ DCs; Right panel: CD8+ DCs. **B**) Representative histograms showing anti-CXCR4 staining (■) compared to FMO control (□) on DCs. Left panel: CD11b+ DCs; Right panel: CD8+ DCs. **C**) Graph showing the percentage of AF488+ cells in CXCR4+ (■) and CXCR4- (■) CD8+ and CD11b+ DCs. Error bars represent SD of the mean.

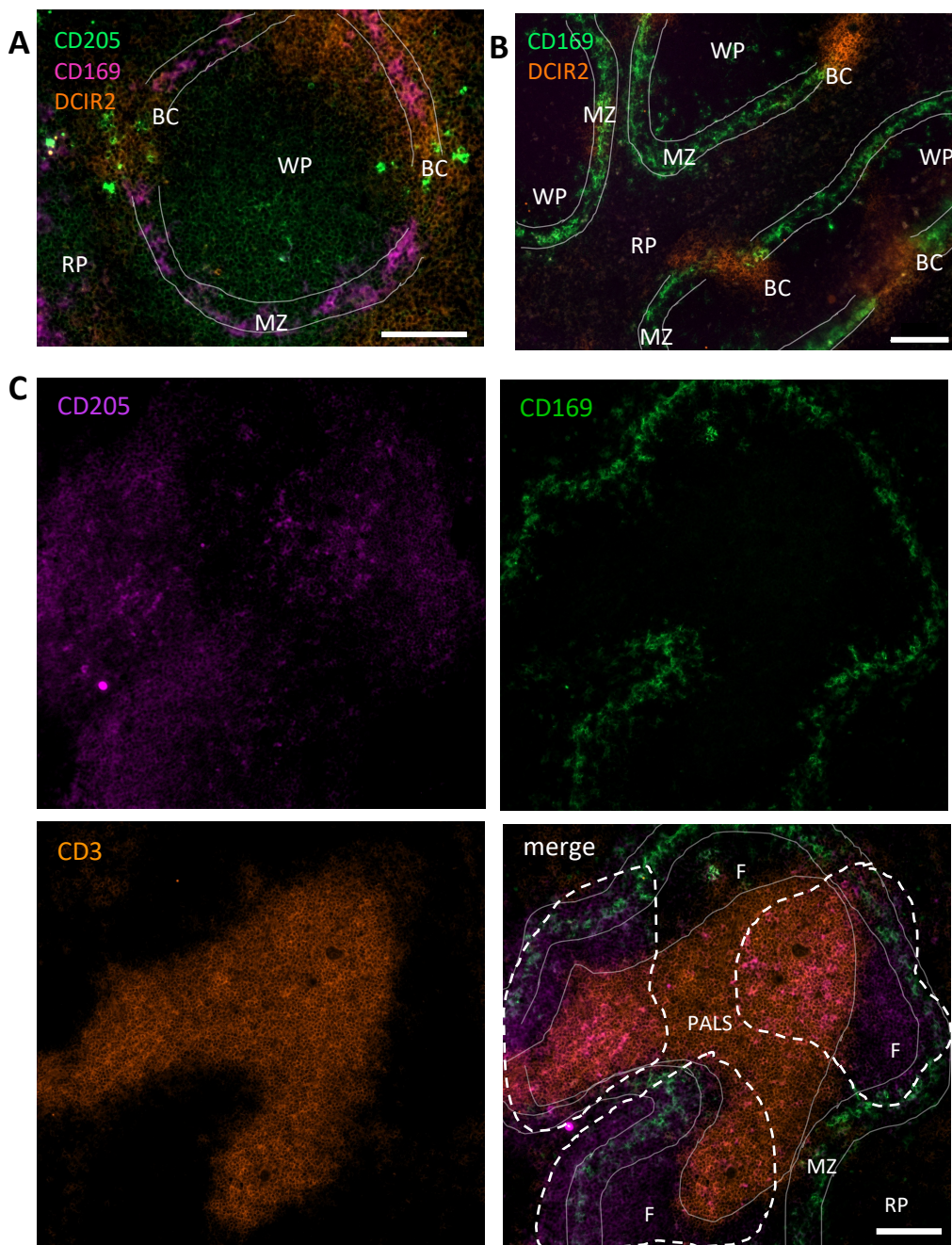


Figure 4-19: Anti-DCIR2 and CD205 antibodies identify distinct populations of cells in the spleen.

The spleen from a resting WT mice was harvested and processed to obtain cryosections. Sections were stained using anti-DCIR2, anti-CD205, anti-CD169 and anti-CD3 ϵ antibodies. Images are representative of at least three technical replicates from one individual. WP= White pulp, RP= Red pulp, MZ= Marginal zone, BC= Bridging channel, F= Follicle, PALS= Periarteriolar lymphoid sheath. Scale bars = 100 μ m. **A)** Anti-CD205 (green), anti-CD169 (purple) and anti-DCIR2 (orange) staining. CD169⁺ cells indicate the marginal zone. DCIR2⁺ cells appear to be mostly located in and near to the bridging channels, while CD205⁺ cells are mainly within the white pulp. **B)** Anti-CD169 (green) and anti-DCIR2 (orange) staining. DCIR2⁺ cells are clearly located in the bridging channels of the marginal zone. **C)** Individual channel images of anti-CD205 (top left), anti-CD169 (top right) and anti-CD3 (bottom left) staining. Merged image (bottom right) shows all stains plus key anatomical features. Dotted lines indicate the areas that are positive for anti-CD205 staining.

Chapter 5: ACKR4 Involvement in Chronic Skin Inflammation

5 ACKR4 Involvement in Chronic Skin Inflammation

5.1 Introduction

Having determined that *ACKR4* expression is modulated in response to inflammatory stimuli in cultured human keratinocytes and dermal LECs, I was interested in examining the functional implications of this regulation during inflammation. I therefore chose to use an *in vivo* model of inflammation to further examine the function and regulation of ACKR4. In addition, *Ackr4*^{-/-} (KO) mice were available for this study, making studying the specific contribution of ACKR4 more feasible.

The Aldara model was selected to investigate a potential role for ACKR4 in chronic cutaneous inflammation. Aldara is a cream currently used in the treatment of superficial basal cell carcinoma, actinic keratosis and genital warts. The main active ingredient in Aldara cream is imiquimod (IMQ), an immune modulator that activates the innate immune system via TLR7/8 signalling. Aldara is often used to generate a mouse model for psoriasis due to the heavy involvement of the IL-23/IL-17 axis, and resultant involvement of T_H17 and $\gamma\delta$ T T cells, which are hallmarks of human psoriasis^{211,212}.

In chapter 3, *ACKR4* expression and regulation was studied in human keratinocytes and dermal LECs. Although neither of these cell types express TLR7, IMQ activates plasmacytoid DCs (pDCs) which are known as the main producers of IFN- α and IFN- β ²¹³. *ACKR4* was shown to be upregulated in response to type I interferons in cultured human cells, suggesting *Ackr4* may be upregulated in the context of Aldara-mediated skin inflammation in mice. Previous studies involving acute TPA-mediated inflammation in mice have suggested that ACKR4 plays an important role in Langerhans cell (LC) migration from the skin upon activation, as these cells are present in the skin-draining LNs in lower numbers in KO mice¹⁷⁹. I reasoned that an exaggerated phenotype may be observed in chronic compared to acute inflammation, as loss of ACKR4 could lead to chemokine dysregulation causing accumulation of CCL19 and/or CCL21. I also reasoned that correct ACKR4 function may be particularly crucial to the immune response in a setting where it is upregulated, rather than downregulated as it is in response to TPA (S. Bryce, personal communication). Furthermore, *ACKR2* has previously shown to be upregulated in lesional and perilesional skin in psoriasis patients¹⁴⁹, so a role for another ACKR in chronic skin inflammation would be interesting.

5.2 Aims

- To determine whether mice lacking *Ackr4* show a differential response to Aldara-mediated inflammation.
- To investigate the potential contribution of CCL19 dysregulation to the inflammatory phenotype in *Ackr4*^{-/-} mice.
- To study cell migration in the context of Aldara-mediated inflammation in *Ackr4*^{-/-} mice and investigate whether there is a defect in cell migration in these mice similar to that reported in the skin during TPA-mediated inflammation.

5.3 Optimising Aldara Treatments

5.3.1 Feasibility of Aldara Model in Male Mice

The Aldara model was piloted by treating male mice with Aldara cream on the shaved lower back once daily for five days. Back skin was initially selected for analysis due to issues in obtaining sufficient tissue from the ears for flow cytometry analysis in previous experiments using TPA. Analysis of skin-draining lymph nodes showed some evidence of enlargement (Figure 5-1A), suggesting that an inflammatory response had occurred. Spleen enlargement was also observed in treated mice (data not shown) suggesting some systemic effects of Aldara treatment were occurring; however, superficial examination of the skin revealed only mild redness and no evidence of psoriasis-like lesions (Figure 5-1B). The lymph node and spleen enlargement observed were potentially due to ingestion of the cream, as the expected chronic skin inflammation phenotype previously reported²¹¹ did not appear to be present.

The dose of cream used was 8.33 mg per mouse, which appears to be sufficient from the literature²¹¹. The lack of inflammation could be due to the thickness of skin in male mice compared to females (A. McColl, personal communication), which may have prevented the IMQ from being absorbed sufficiently. Due to the restricted availability of genetically modified mice, it was not possible to use females for this study; the model was instead used on ear skin which is thinner. Ears are an advantageous treatment site as they are of comparable size between mice, making the affected area uniform between individuals. The hair on the ears is also extremely fine and does not require removal, so the risk of infection or inflammation caused by shaving the mouse and treating with depilatory skin is avoided.

5.3.2 Single Aldara Treatments Do Not Modulate *Ackr4* mRNA Expression

The effect of a single Aldara treatment on mRNA expression in the skin was analysed after 4, 16 or 24 hours. These time points were chosen to mirror previous experiments carried out in this lab using TPA in order to determine whether there was a similar role for ACKR4 in the early stages of the inflammatory response to IMQ. Genes tested were *Ackr4*, *Ccr7*, *Ccl19* and *Ccl21*. These transcripts were chosen in order to study the effects of Aldara treatment on all members of the ACKR4 pathway.

Results showed a weakly significant decrease in *Ackr4* expression in both epidermis and dermis by the 24 hour timepoint (Figure 5-2A), while *Ccr7* expression was modestly increased in the dermis, but not the epidermis, 16 and 24 hours after treatment suggesting either upregulation of this receptor or increased numbers of CCR7+ cells entering the dermis (Figure 5-2B). *Ccl19* expression was increased in the dermis 24 hours after treatment (Figure 5-2C), while *Ccl21* expression was unaffected (Figure 5-2D). In the epidermis, only *Ackr4* was affected at the 24 hour timepoint. As these results only extended 24 hours after a single treatment, it was determined that a more pronounced phenotype would be likely after multiple Aldara treatments.

5.4 Potential Role for ACKR4 in Response to Multiple Aldara Treatments

5.4.1 Multiple Aldara Treatments Modulate mRNA Expression of ACKRs and Ligands in the Skin

After finding a subtle response to a single Aldara treatment, a 5-day treatment model was used to investigate expression of *Ackr4*, *Ccr7* and their ligands once a more severe inflammatory response was observable. By the 5-day time point, considerable inflammation of the skin was apparent, including redness and scaling of the epidermis and increased ear thickness (data not shown). I hypothesised that *Ackr4* would be upregulated in response to Aldara treatment, due to the influx of pDCs producing type I interferon in the skin²¹³: in chapter 3, *ACKR4* was shown to be upregulated by type I interferon in HD-LECS and nHEKs. As expression of *ACKR3*, *CXCR4* and their shared ligand *CXCL12* have also been detected by HD-LECs and/or nHEKs, and *CXCR4/Ackr3* regulation has been detected by murine keratinocytes in response to acute inflammation, these transcripts were also included in the analysis to determine whether the ACKR3 pathway might also play a role in chronic inflammation.

Surprisingly, the results showed that *Ackr4* was in fact down-regulated between 20 and 30-fold in treated skin compared to control skin, while *Ccl19*, *Ccl21* and *Ccr7* expression were not affected in either tissue. *Ackr3* expression was also reduced in the epidermis following Aldara treatment, *Cxcr4* expression was unaffected and *Cxcl12* expression significantly decreased in the epidermis (Figure 5-3).

The interpretation of these results is not straightforward; as the ear skin was visibly inflamed after Aldara treatment, it likely contained a significant number of infiltrating leukocytes, so a greater proportion of RNA will originate from leukocytes in inflamed skin. Consequently, if stromal cells were to maintain the exact same gene expression profile between resting and inflamed skin, this could potentially appear as a downregulation of stroma-associated mRNAs due to the increased prevalence of the leukocyte expression signature; likewise, a modest mRNA upregulation in stromal cells could be neutralised. In particular, *Ackr4*, *Ackr3* and their ligands are not expected to be expressed by leukocytes in the skin^{151,173} while *Cxcr4* is widely expressed on both keratinocytes and infiltrating leukocytes, as demonstrated in Chapter 4, and expected to be expressed by dermal LECs from data generated in human cells in Chapter 3.

Nevertheless, the downregulation of *Ackr4* was the most striking result obtained, and it appears unlikely that such a large decrease in mRNA expression could be explained by infiltrating *Ackr4*- cells alone.

5.4.2 Reporter Mice Show Reduced eGFP Expression in Response to Aldara

To examine *Ackr4* expression further, Aldara-treated ear skin from *Ackr4^{+/-sgfp}* reporter mice was analysed via flow cytometry. This showed a striking reduction in eGFP expression in CD45⁻ cells of Aldara-treated mice (Figure 5-4A, B). CD45⁻ cells could not be analysed further to identify specific keratinocyte subsets as too few viable cells were retrieved from Aldara-treated skin to allow reliable estimation of eGFP expression, or confirmation that cells correctly fell into the gates set using untreated mice. This problem persisted both when using whole skin and epidermis only for flow cytometry analysis: the epidermis in Aldara-treated mice was observed to be extremely fragile and to slough off easily before enzymatic digestion. Nevertheless, these results confirm the finding that *Ackr4* expression in the skin is extensively downregulated at the mRNA level in response to repeated Aldara treatments.

Although downregulation of *Ackr4* was not the expected result, it is clearly strongly modulated during Aldara-mediated inflammation. TPA treatment also leads to downregulation of *Ackr4*, yet KO mice have impaired LC migration to the skin-draining lymph nodes, so this result does not necessarily exclude a role for ACKR4 during chronic skin inflammation.

5.4.3 *Ackr4* Deficiency Has No Detectable Effect on Keratinocyte Proliferation

As direct investigation of Aldara-treated skin by flow cytometry proved too challenging due to low cell viability, sections of ear skin from Aldara-treated WT and KO mice were analysed via immunofluorescent microscopy. Keratinocyte proliferation did not appear to be altered in KO mice, as antibody staining for ki67, a proliferation marker²¹⁴, showed a comparable distribution between WT and KO mice, with positive cells located in the basal layer of the epidermis and hair follicle bulge (Figure 5-4B). This analysis also showed that both WT and KO ear skin contained the same proportion of ki67+ cells after Aldara treatment (Figure 5-4C). In resting interfollicular epidermis, keratinocyte nuclei are flattened and only 1-2 layers of cells can normally be detected (Figure 5-4B, right panel), showing that the architecture of both WT and KO epidermis was significantly altered after Aldara treatment.

5.4.4 Aldara Treatment Leads to Follicle Formation in the Ear-Draining Lymph Nodes

To further investigate the effects of Aldara treatment, particularly with respect to *Ackr4* expression, the ear draining lymph nodes (DLN) were analysed by immunofluorescent microscopy in *Ackr4*^{+/*gfp*} mice (Figure 5-5). These mice contain one eGFP knock-in allele of *Ackr4*, and one WT allele. One copy of the *Ackr4* gene appears to be sufficient to confer a WT phenotype. Analysis of the images revealed that after five daily Aldara treatments, ear DLN contain more B cell follicles, but these are the same average size as those from untreated mice (data not shown). *Ackr4* also appears to be downregulated in the Aldara treated mice from visual inspection of these images, which would be commensurate with the results obtained for the skin; however, this experiment would need to be repeated using more animals and quantified to give confidence in this observation. Flow cytometry would be a useful tool for this analysis, as it could allow surface marker expression of multiple proteins to identify any cells that modify *Ackr4* expression and simplify quantification of

these results. Unfortunately, technical issues prevented the analysis of lymph nodes from *Ackr4^{gfp/gfp}* homozygous mice, which are analogous to *Ackr4^{-/-}* mice.

5.4.4.1 *Ackr4* Regulates the Size and Cellularity of Ear-Draining Lymph Nodes Draining Aldara-Inflamed Skin

As *Ackr4* deficiency appeared to have no detectable effect on keratinocyte proliferation in the skin, I sought to determine whether ACKR4 scavenging of CCL19 and/or CCL21 may play a role in the migration of DCs, particularly LCs, from the skin to the draining lymph nodes (DLN) during Aldara-mediated inflammation. As CCR7 ligands are also important for T cell and pDC migration to SLOs and the positioning of T cells, resident DCs and B cells within the nodes.

To investigate this, WT and KO mice were treated topically with Aldara on both ears daily for five days, and ear draining lymph nodes (DLN) were harvested and analysed using flow cytometry to identify the main lymphocyte populations: B cells, T cells, pDCs, migratory (MHC-II^{hi}) DCs, resident (MHC-II^{int}) DCs and pDCs (Figure 5-6A-C).

Results showed that the overall cellularity of ear DLN was increased in KO mice compared to WT, and that the numbers of B cells, T cells and rDCs were significantly higher in these mice (Figure 5-7A). Migratory DCs were subdivided based on CD207 and CD103 expression, which showed all four subsets of migratory DCs at the same proportions in WT and KO mice; The CD103⁺ and CD103⁻ subsets also represented the same proportions of resident DCs in WT and KO mice (Figure 5-7B).

As there is no difference in lymphocyte numbers or cellularity between resting WT and KO DLN (S. Bryce, personal communication), these data suggested that cells in the lymph node of Aldara-treated KO mice are either overproliferating, are showing an increased level of recruitment to the lymph node or are being retained in lymph nodes. Dysregulation of CCL19 and/or CCL21 due to the absence of ACKR4 could potentially play a role in aberrant cell migration; CCR7 is expressed by T cells, DCs and B cells. CCL19 and CCL21 can also direct the migration of B cells to the boundary of the T cell zone. The finding that migratory DCs are unaffected neither supports nor refutes the hypothesis that DC migration is impaired after Aldara treatment in KO mice: it is possible that the arrival of migratory DCs to the DLN from the skin is delayed in these mice, and that this defect is no longer detectable by five days after the first treatment. If an earlier timepoint was

studied, there may be a difference; however, as the aim was to study chronic inflammation, the initial wave of DC migration to the DLN is less relevant.

*5.4.4.2 Aldara Raises CCL19 Concentration in Plasma and Skin of *Ackr4*^{-/-} Mice*

In order to determine whether chemokine dysregulation was a feature of Aldara-treated KO mice, CCL19 levels in these animals were assayed. Plasma was used to estimate systemic CCL19 levels, while punch biopsies from treated ears were incubated in PBS to allow CCL19 to leach out. This method ensures that only bioavailable, post-transcriptionally modified CCL19 is measured, rather than including partially processed CCL19 present inside cells, which would be included in the analysis if whole protein lysate was used.

Resting mice were not tested in these experiments. Previous work has shown that resting WT and KO mice have serum CCL19 levels below the detection limit of standard ELISAs¹⁷⁸. A small subset of KO individuals has CCL19 levels just over the detection limit; this does not confer statistical significance but suggests that resting CCL19 levels may be elevated but still very low in KO mice (D. Asquith, personal communication).

After five daily Aldara treatments, plasma CCL19 levels in WT mice were below the detection level of the ELISA kit, but KO mice had a plasma CCL19 concentration of ~70 pg/ml (Figure 5-9). Plasma CCL19 was still raised 3 days post-treatment in KO mice, but had fallen from its level immediately following the final treatment. Analysis of bioavailable CCL19 also showed raised levels in KO mice compared to WT, and that two out of three WT individuals analysed had bioavailable CCL19 levels just above the detection limit of the assay suggesting some CCL19 is present in the ears of WT mice after Aldara treatment.

5.4.4.3 Increased Leukocyte Numbers Largely Restricted to Ear-Draining Lymph Nodes

The Aldara phenotype was further investigated by comparing the cellularity of ILN, mesenteric lymph node (MLN), spleen and blood between Aldara-treated WT and KO mice. In ILN, there were no significant differences in overall cellularity, and the only difference in any of the individual cell types was a decrease in the number of migratory DCs recovered from KO ILN (Figure 5-9). In MLN, there were no significant differences

in cellularity observed (Figure 5-10). In the spleens of KO mice, there were significantly more cells overall, with the B cells the only leukocyte population analysed that was increased in numbers (Figure 5-11). Analysis of the blood showed that there were significantly more circulating B cells in KO mice compared to WT (Figure 5-12).

Together, these results suggest that the differential phenotype seen in KO mice after Aldara treatment is largely restricted to the site-draining lymph nodes, although the increased numbers of circulating and splenic B cells suggests some systemic dysregulation is occurring during Aldara-mediated inflammation in KO mice. These results may indicate increased proliferation, but do not appear to suggest deficient migration of leukocytes to SLOs. The finding of fewer migratory DCs in ILN, however, could suggest this.

5.4.4.4 Adoptive Cell Transfer in Aldara-Treated Mice

After showing that lymphocyte numbers in the DLN and B cell numbers in the blood increase in KO mice more markedly than WT after Aldara treatment, I hoped to establish whether this was due to retention or proliferation of cells in the lymph node, or increased recruitment of cells to the lymph node. Adoptive cell transfer of splenocytes from resting WT mice was used 16 hours before culling mice treated with Aldara to help determine this; an increase in the number of donor cells retrieved from the tissues of KO recipient mice compared to WT would suggest increased recruitment, while any defect in donor leukocyte homing would suggest retention of cells that are unable to correctly migrate out of lymph nodes.

There was some difficulty in optimising the adoptive cell transfer protocol; initially, cells were stained with the fluorescent marker CMTPIX before transfer, but no cells were retrieved from recipient mice (Figure 5-13). After experimenting with different fluorescent labels, using *Ly5.1* donor mice and anti-CD45.1 antibody appeared to be the most effective method for retrieving adoptively-transferred cells. This variant of the CD45 molecule distinguishes donor mice from WT recipient mice. Although B cells were initially used for these experiments due to the accumulation of B cells in the blood of KO animals, whole splenocytes appeared to be more reliable to ensure a high yield of viable cells. This also made it possible to analyse the homing capabilities of specific splenocyte subsets; for example, the dysregulation of CCR7 ligands may disproportionately affect DCs and T cells as they rely more heavily on this receptor to migrate to SLOs, while B cells can use CXCR4 and CXCR5²¹⁵, and pDCs can use CXCR3, CXCR4 and CCR5²¹⁶.

Results showed that CD45.1+ cells could be clearly identified in spleen, blood, ILN, MLN and ear DLN (Figure 5-14). The spleen contained the largest number of adoptively-transferred cells. Although MLN appeared to contain more adoptively-transferred cells than ILN or ear DLN in terms of absolute numbers, these were pooled samples and there are more MLN than ILN or ear DLN. There were no apparent differences in the numbers of CD45.1+ cells retrieved from any tissue between WT and KO mice, although there were significantly fewer CD45.1+ cells in the blood of KO mice than WT. There were also no differences between the numbers of each subset of CD45.1+ cells retrieved from WT and KO mice (data not shown). The numbers of donor cells retrieved was low; 2×10^6 cells were transferred to each mouse, and only about a quarter of these were detected in each mouse. Although some SLOs were not analysed, given the numbers retrieved from ILN, MLN ear DLN and blood it is unlikely that the remaining 1.5 million cells were spread between these sites. This suggests a high level of cell death may have occurred.

Overall, these results did not suggest any defect in migration of cells to SLOs, indicating that the differential phenotype seen in KO mice may be due to increased retention and/or proliferation of lymphocytes.

5.4.5 Differential Phenotype in *Ackr4*^{-/-} Mice is Resolved in *Ackr4*^{-/-}, *Ccl19*^{-/-} Mice

To determine whether the increased lymph node cellularity observed following Aldara treatment in KO mice was due to CCL19 dysregulation, *Ackr4*^{-/-}, *Ccl19*^{-/-} (DKO) mice were used. I reasoned that if DKO mice showed a similar phenotype to WT mice after Aldara treatment, this would suggest that CCL19 dysregulation contributes to the increased number of lymphocytes retrieved from ear DLN. Conversely, if DKO mice showed increased lymphocyte numbers compared to WT, this would suggest that CCL19 dysregulation did not play a role.

Analysis showed no detectable difference in numbers of any leukocyte subset analysed. Along with data showing raised CCL19 levels in the plasma and treated ear skin, this suggests that the increased leukocyte numbers in the lymph nodes of KO mice compared to WT was due to CCL19 dysregulation in *Ackr4*-deficient mice. Although there was no gross defect in DC homing to the ear DLN at the time point studied, it is possible that this occurs earlier in the model, or that DC migration to the node is unaffected but egress is impaired.

5.5 Key Findings

- *Ackr4*, *Ccr7* and *Ccl19* expression are modulated in the skin, particularly the dermis, after a single Aldara treatment; however, after repeated Aldara treatments, only *Ackr4* is still modulated with a clear downregulation of transcript in both epidermis and dermis, while *Ackr3* and *Cxcl12* are also downregulated in the epidermis. The result for *Ackr4* was confirmed using eGFP expression on *Ackr4^{+/-gfp}* mice.
- Aldara treatment does not affect keratinocyte proliferation in KO mice compared to WT by ki67 staining, but epidermis appears to be increased in cellularity in both WT and KO mice compared to WT untreated, as expected for a psoriasis-like phenotype.
- Ear-DLN from KO mice are significantly enlarged compared to WT after five daily Aldara treatments. B cells, T cells and resident DCs were more numerous in KO nodes compared to WT, but migratory DCs and pDCs were unaffected. The proportions of migratory and resident DCs falling into each of the subsets examined were also unaffected in KO mice compared to WT.
- After five daily Aldara treatments, overall cellularity was unchanged in ILN and MLN of KO mice compared to WT, although there were fewer migratory DCs in the ILN of KO mice. Spleens were significantly enlarged in KO mice, and contained more B cells; there were also more B cells circulating in the blood of KO mice.
- CCL19 levels were significantly raised in plasma and ear skin of KO mice compared to WT, and plasma CCL19 levels remained raised three days after the final Aldara treatment.
- Adoptive transfer of WT splenocytes showed that there were no gross defects in leukocyte homing, as there were no differences in the number of donor cells isolated from any of the SLOs examined. There were significantly fewer donor cells isolated from the blood.
- The WT phenotype was restored in *Ackr4^{-/-} Ccl19^{-/-}* mice, suggesting that CCL19 dysregulation plays a role in the increased ear DLN size of *Ackr4*-deficient mice after repeated Aldara treatments.

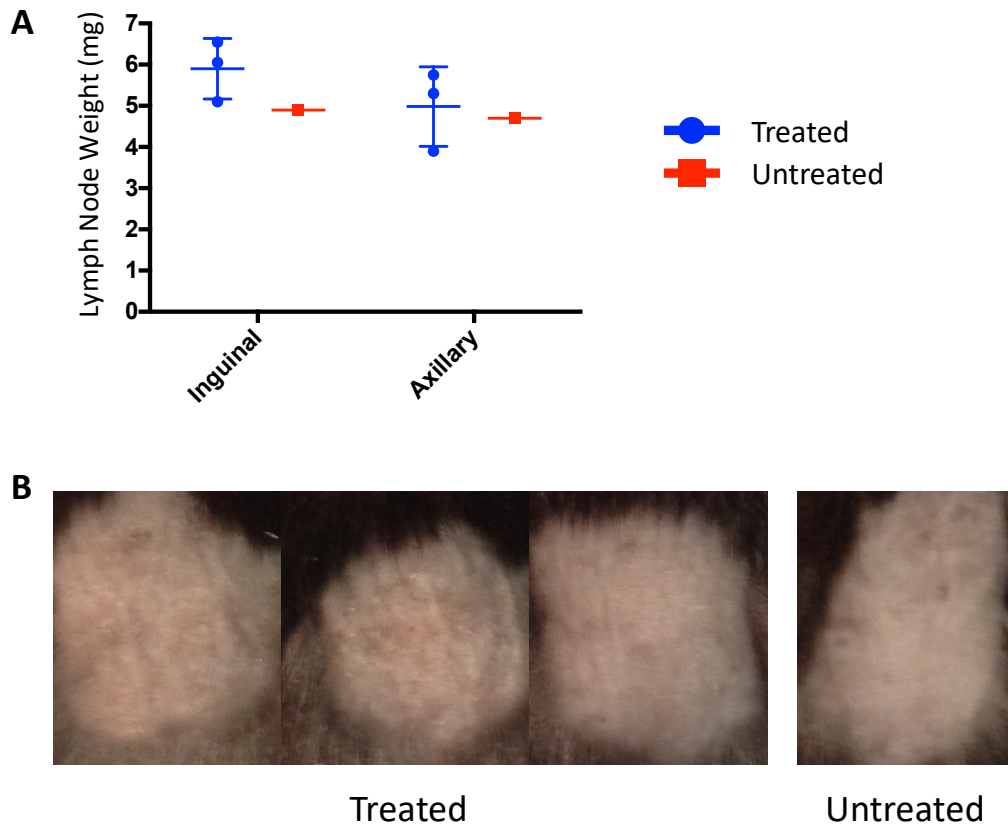


Figure 5-1: Pilot of Aldara model on mouse back skin shows a limited inflammatory phenotype.

Mice were treated with Aldara or Vaseline once per day for five days on the shaved lower back skin. Mice were culled, skin was photographed and inguinal and axillary lymph nodes harvested and weighed. (n=3 Aldara-treated plus one Vaseline-treated) **A**) graph showing weights of inguinal and axillary lymph nodes. Error bars represent SD of the mean. **B**) images of treated area of skin showing lack of visible inflammatory phenotype.

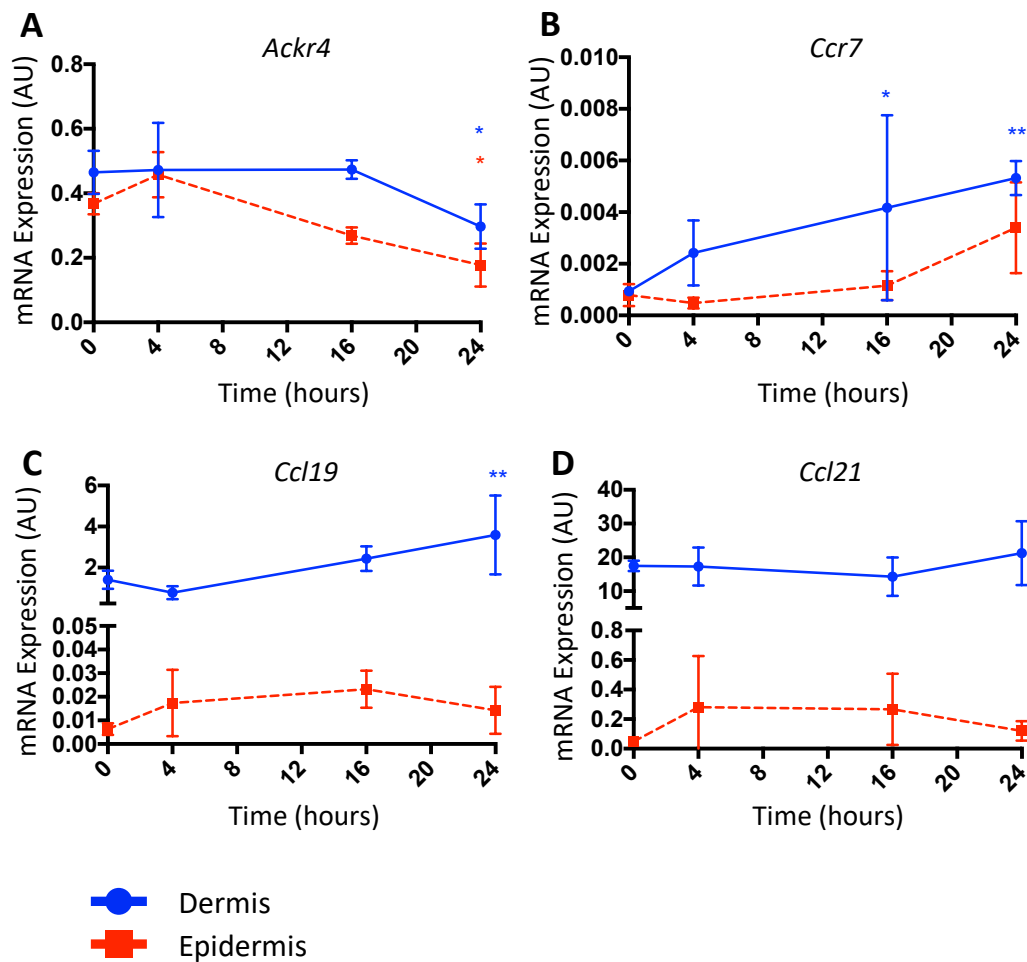


Figure 5-2: Expression of *Ackr4* and related genes is largely stable up to 24 hours after a single Aldara treatment.

Mice were treated once with Aldara on both ears and culled after 4, 16 or 24 hours; control mice received Vaseline and were culled after 24 hours. Ears were excised, epidermis (■) and dermis (●) were separated and RNA prepared (n=3). Results were normalised to TBP expression using the $2^{-\Delta CT}$ method. Statistical significance was determined using two-way ANOVA with Dunnett's correction to compare each timepoint to the control (0h) value (*P ≤ 0.05, **P ≤ 0.01). Error bars represent SD of the mean.

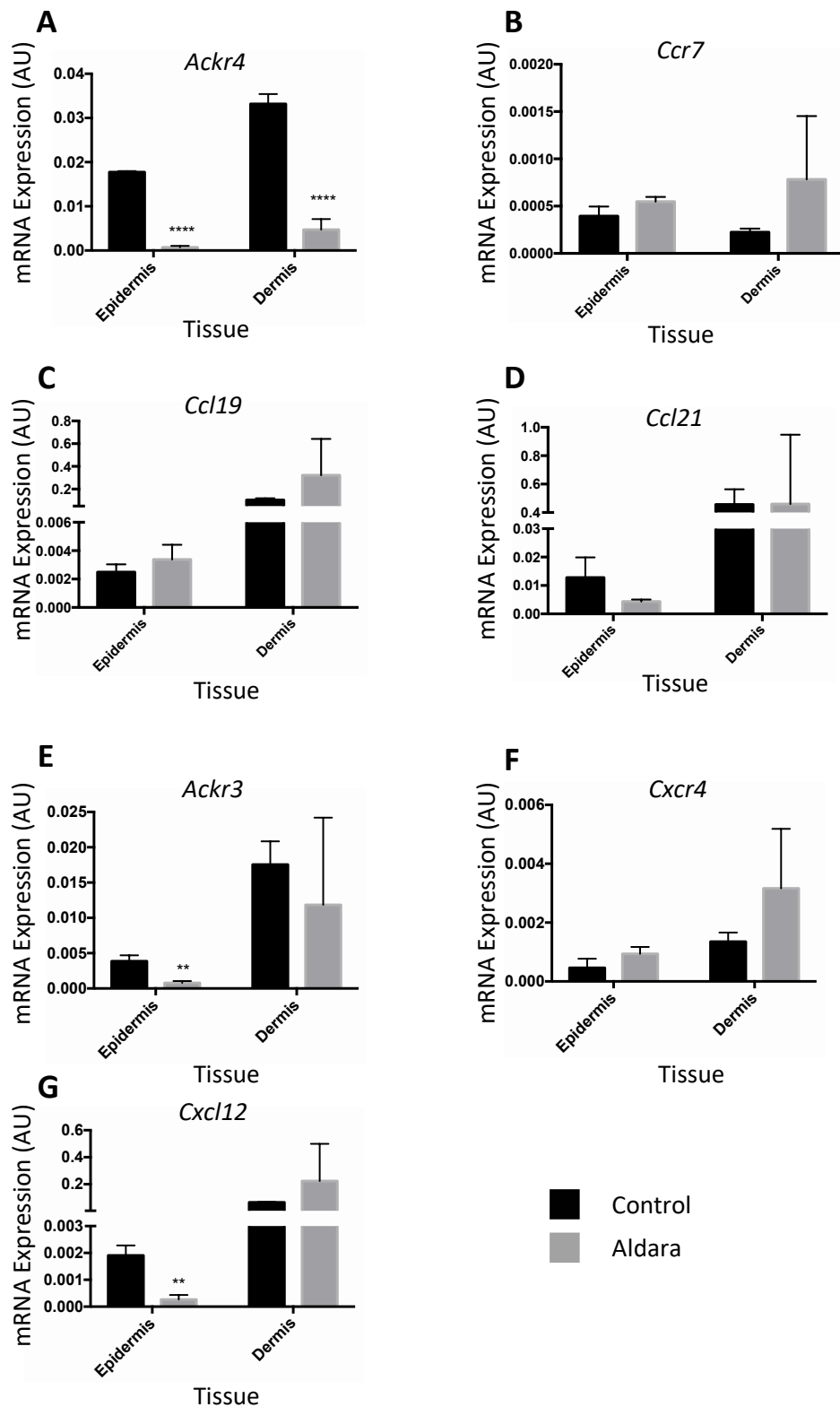


Figure 5-3: Expression of *Ackr4*, *Ackr3* and related genes show variable responses to multiple Aldara treatments.

Mice were treated once per day for five days with Aldara (■) or Vaseline (■) on both ears, ears were excised, epidermis and dermis were separated, and RNA prepared for qPCR analysis (n=3). mRNA expression of **A**) *Ackr4*, **B**) *Ccr7*, **C**) *Ccl9*, **D**) *Ccl21*, **E**) *Ackr3*, **F**) *Cxcr4* and **G**) *Cxcl12* were measured in each tissue and relative expression was represented using arbitrary units (AU) calculated using the $2^{-\Delta CT}$ method. Statistical

significance was determined using t-tests with Holm-Sidak correction (* $P \leq 0.05$, ** $P \leq 0.01$, *** $P \leq 0.001$, **** $P \leq 0.0001$). Error bars represent SD of the mean.

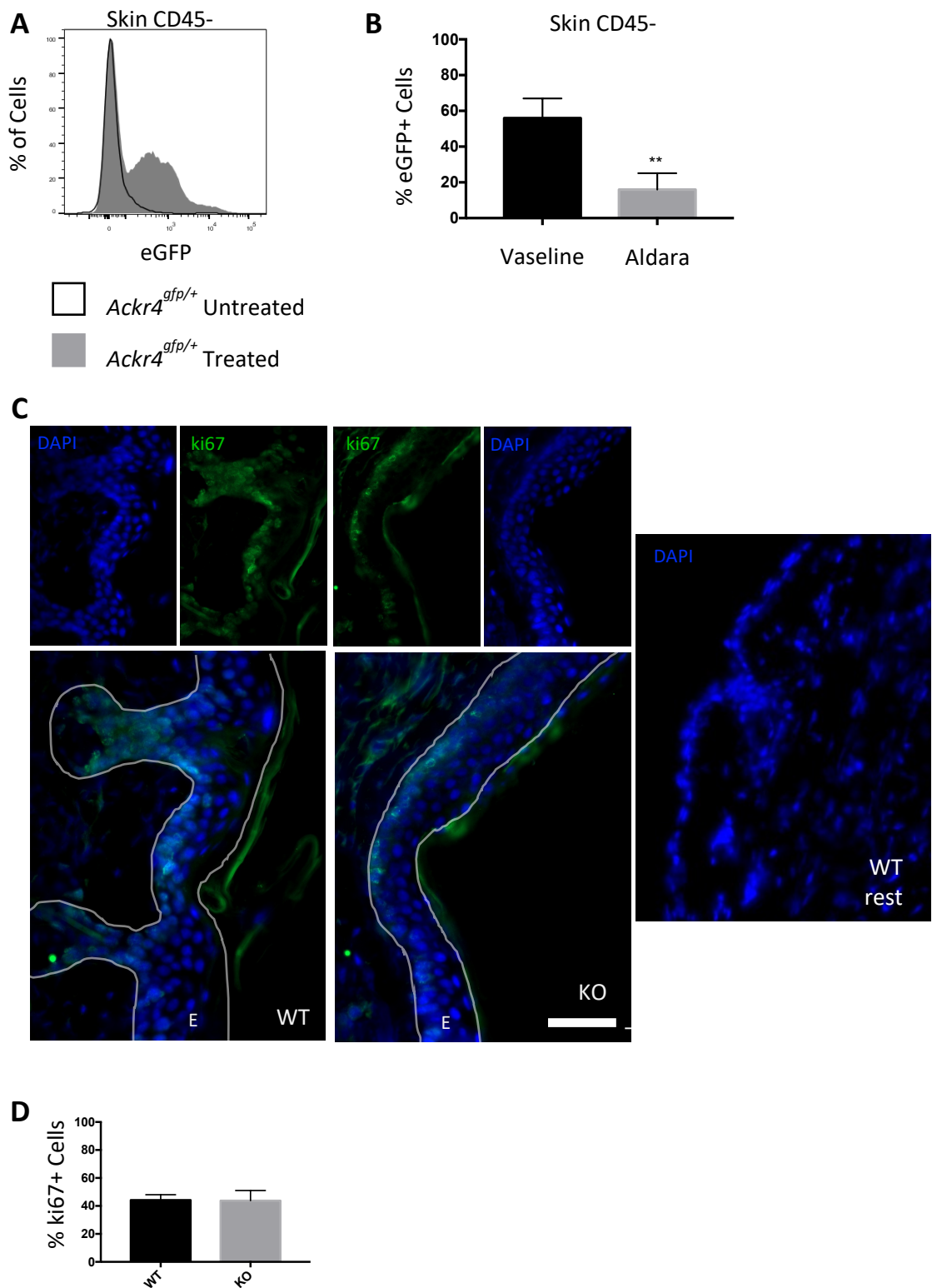


Figure 5-4: Keratinocytes in the ear skin of Aldara-treated mice show no alteration in proliferation in the absence of *Ackr4*.

Mice were treated once per day for five days with Aldara or Vaseline on both ears as previously described, ears were excised and processed for further analysis. **A-B**) Ears from Aldara or Vaseline-treated *Ackr4*^{+/gfp} mice were used to obtain whole-skin single cell suspensions for flow cytometry analysis. (n=4). Representative histogram in **A** shows eGFP expression in untreated, treated and WT keratinocytes. Graph in **B** shows overall percentage of eGFP+ cells among CD45- cells in Vaseline and Aldara groups. Error bars represent SD of the mean. **C-D**) Ears from Aldara-treated WT and KO mice were

processed to obtain cryosections and stained with anti-ki67 antibody along with DAPI counterstain. Images in **C** show representative ki67 and DAPI staining with markers to delineate the epidermis from dermis. E = epidermis. An image of DAPI stain in resting ear skin is shown for comparison. (scale bar = 50 μ m). Graph in **D** shows the percentage of ki67+ cells detected in the epidermis of WT and KO mice. 10 random objectives were taken per mouse, and ImageJ software was used to count nuclei and ki67+ nuclei. An unpaired t-test was used to determine statistical significance (n=3). Error bars represent SD of the mean.

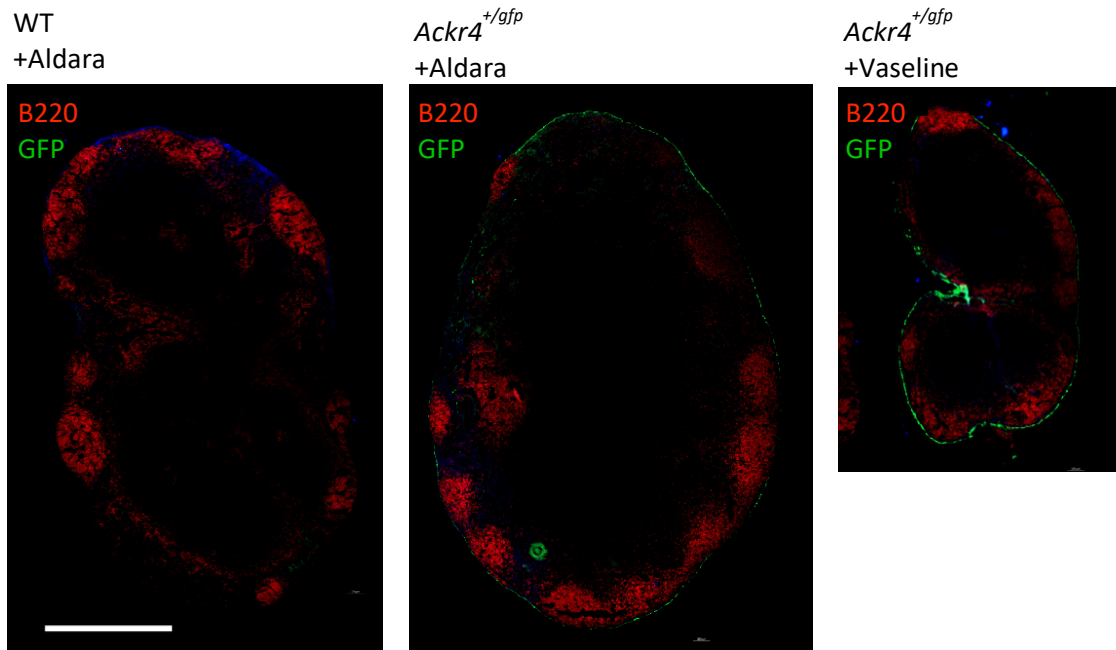


Figure 5-5: Number, but not size, of B cell follicles is increased in the ear DLN following Aldara treatment.

Ackr4^{+/*gfp*} heterozygous mice were treated once per day for five days with Aldara on both ears. One hour after the final treatment, ears were excised, snap frozen in OCT on dry ice and processed to obtain cryosections. Lymph node sections were stained with anti-B220 antibodies, and ImageJ software was used to stitch individual objectives into images of the whole node.. Images representative of both lymph nodes from two mice in each treatment group, and one WT control mouse used as a control for autofluorescence. (scale bar = 500 μ m).

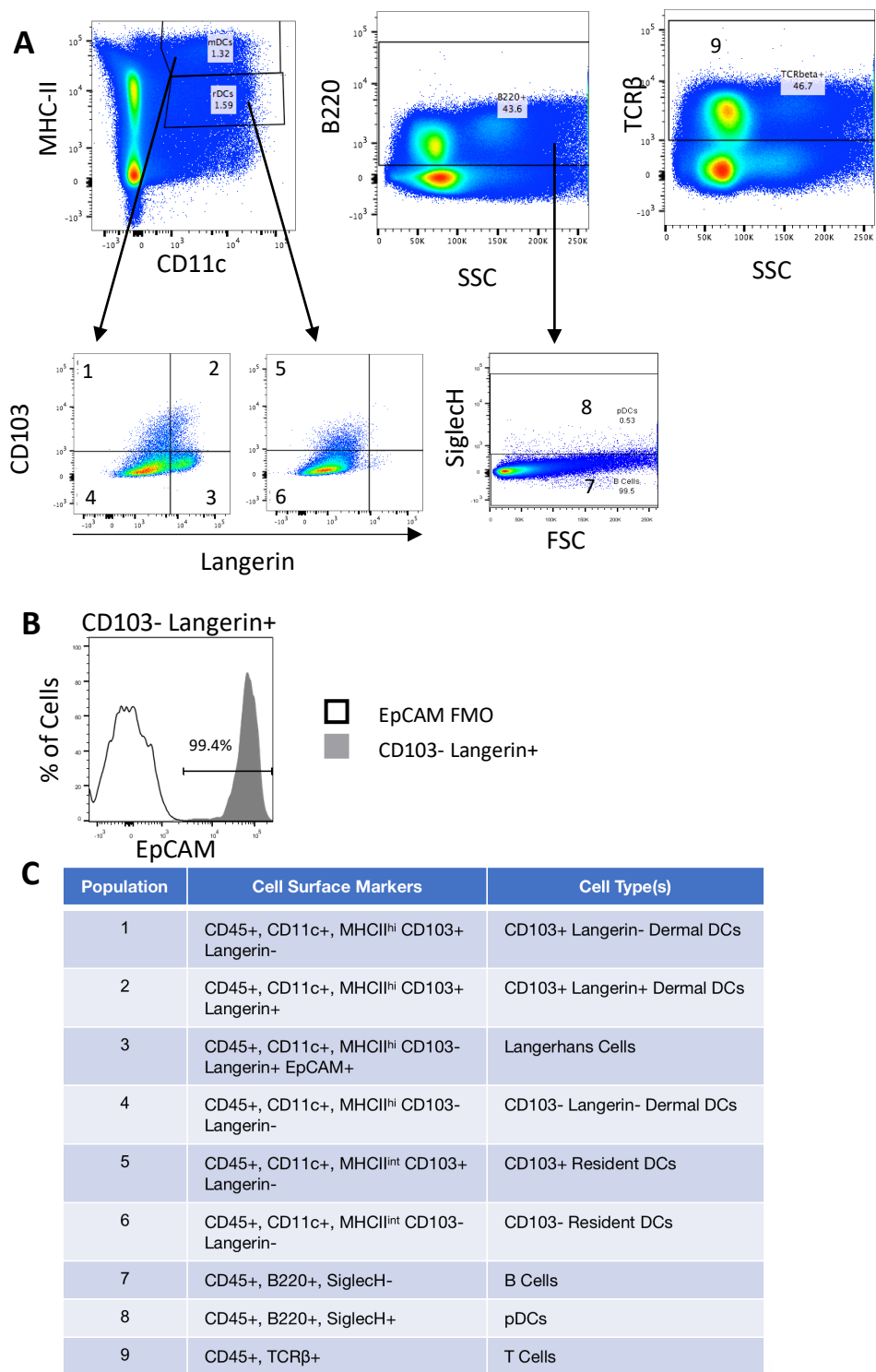


Figure 5-6: Flow cytometry gating strategy to identify lymphocyte subsets in the skin-draining lymph nodes.

DLN from Aldara-treated mice were excised and processed to obtain single cell suspensions for flow cytometry as described (materials and methods). **A**) Representative scatter plots showing the gating strategy used to identify cell subsets within the DLN. First, debris, doublets and dead cells were excluded, and cells were gated to show CD45⁺ cells only. Within this group, CD11c⁺ MHC-II^{hi} and MCH-II^{int} cells were taken as migratory and resident DCs respectively and were further subdivided based on CD103 and Langerin expression; B220⁺ cells were separated into SiglecH⁻ B cells and SiglecH⁺ pDCs; and TCRβ⁺ cells were defined as T cells. **B**) Representative histogram showing EpCAM expression in CD103⁻ Langerin⁺ cells (■) compared to FMO (□). **C**) Table summarising

the surface marker expression of cell populations outlined in **A**; the numbers on the plots in **A** correspond with the numbers in the 'Population' column.

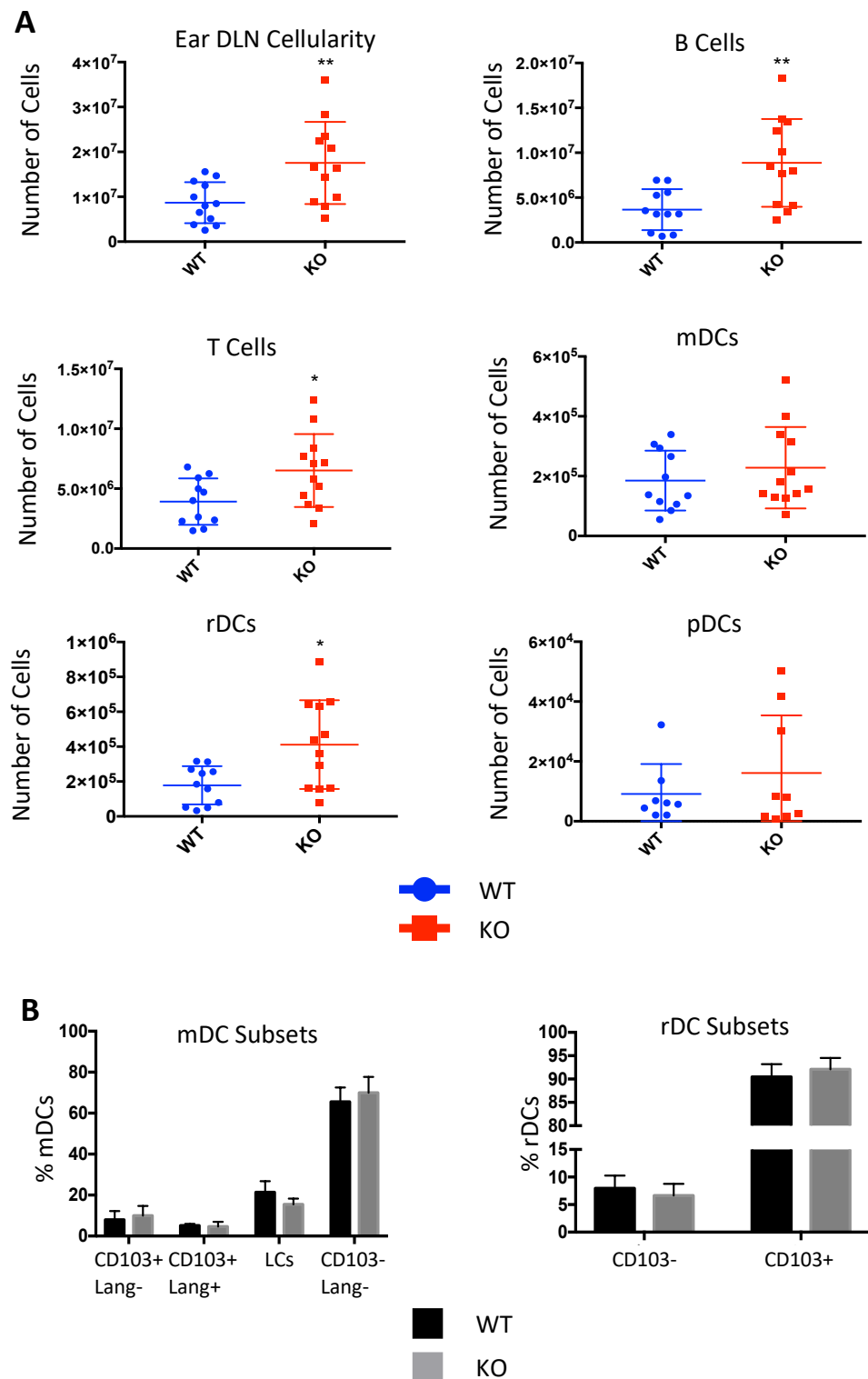


Figure 5-7: Overall cellularity and number of B, T and resident dendritic cells are increased in ear DLN of *Ackr4*-null mice, compared to WT, in response to Aldara treatment.

Wild-type (WT, ■) and *Ackr4*^{-/-} (KO, ■) mice were treated once per day for five days with Aldara on both ears as previously described. Ear draining lymph nodes were excised and processed to obtain single cell suspensions for flow cytometry. Measurements were pooled between multiple experiments; within each experiment n=3-5. Statistical significance was determined using unpaired t-tests (*P≤0.05, **P≤0.01, ***P≤0.001). Error bars represent SD of the mean. **A**) Total cellularity, and number of cells in each leukocyte

subset analysed between WT (■) and KO (■) mice. **B**) Percentage of cells in each mDC (left panel) and rDC (right panel) subset identified in Figure 5-6. (Lang = Langerin; LCs = Langerhans Cells).

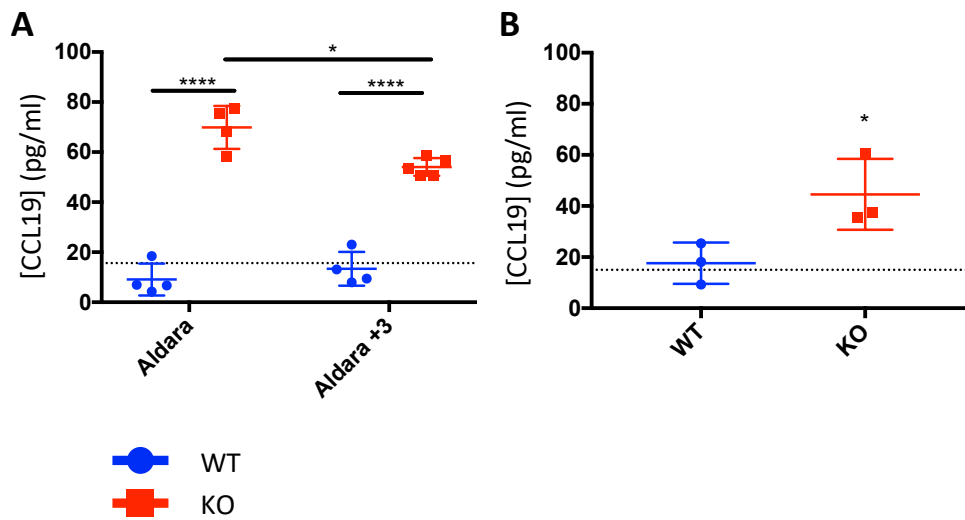


Figure 5-8: Bioavailable CCL19 levels are increased in plasma and ear skin of *Ackr4*-null mice, compared to WT, after Aldara treatment.

WT (■) and KO (●) mice were treated once per day for five days with Aldara on both ears. In one group (Aldara +3), mice were culled 3 days after the final treatment; in the other group (Aldara), mice were culled 1 hour after the final treatment. Ears and blood were harvested for analysis: plasma and total soluble protein from punch biopsies were used for ELISAs to determine CCL19 levels. (n=3-5). Statistical significance was determined using unpaired t-tests (* $P \leq 0.05$, ** $P \leq 0.01$, *** $P \leq 0.001$, **** $P \leq 0.0001$). Dotted lines on charts indicate the assay manufacturer's stated detection limit. Error bars represent SD of the mean. **A**) Plasma CCL19 levels in mice culled 1 hour after the final treatment (Aldara) and three days post-treatment (Aldara +3) in both WT and KO backgrounds. **B**) Bioavailable CCL19 levels in the ears of Aldara-treated WT and KO mice.

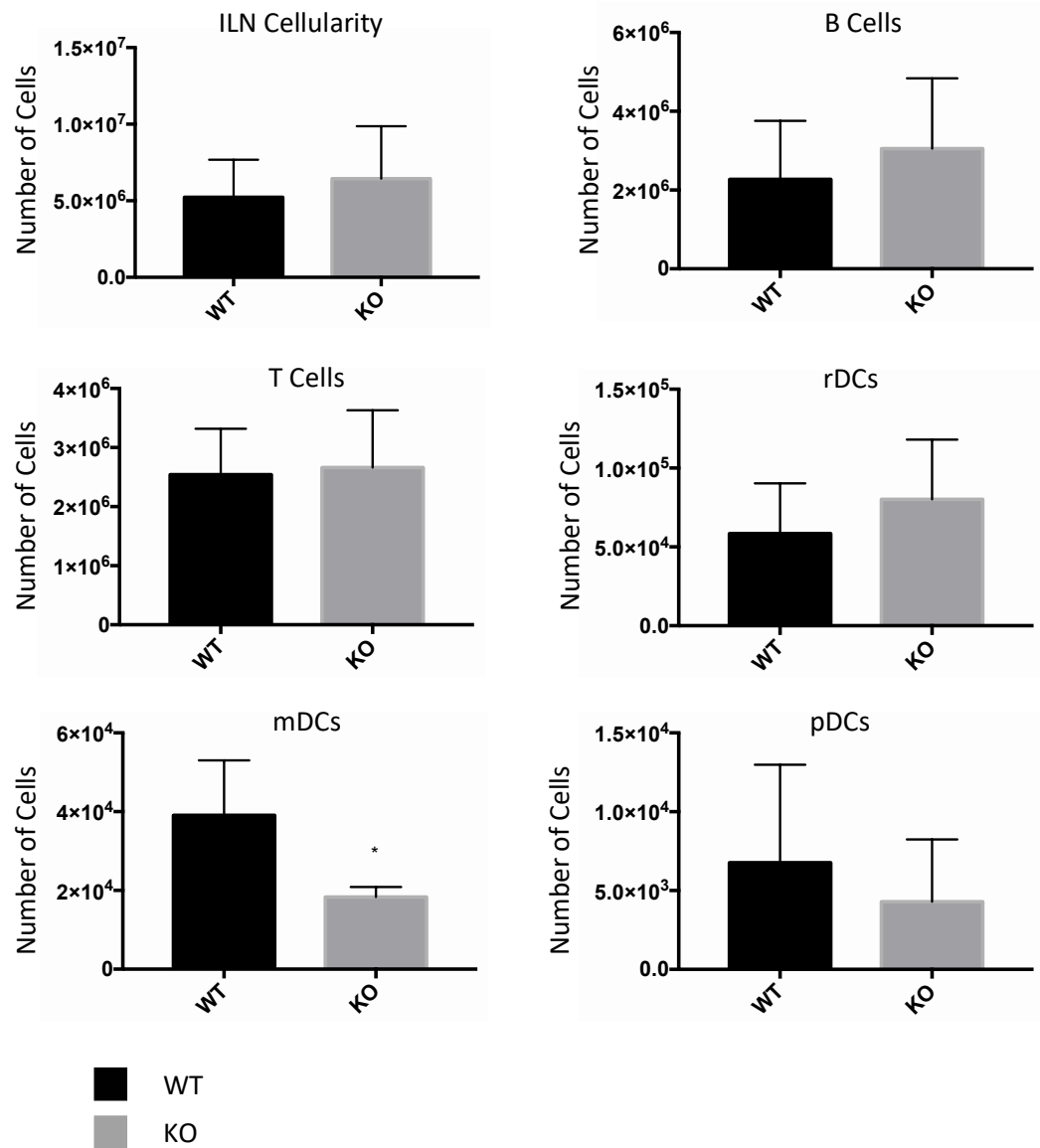


Figure 5-9: Migratory DCs are reduced in the ILN of *Ackr4*-null mice, compared to WT, after Aldara treatment.

WT (■) and KO (■) mice were treated once per day for five days with Aldara on both ears as previously described. Inguinal lymph nodes were excised and processed to obtain single cell suspensions for flow cytometry. Both lymph nodes were pooled within each animal and cell counts were used to obtain the absolute numbers of each cell population outlined in Figure 5-6. (n=4). Statistical significance was determined using unpaired t-tests (*P≤0.05). Error bars represent SD of the mean.

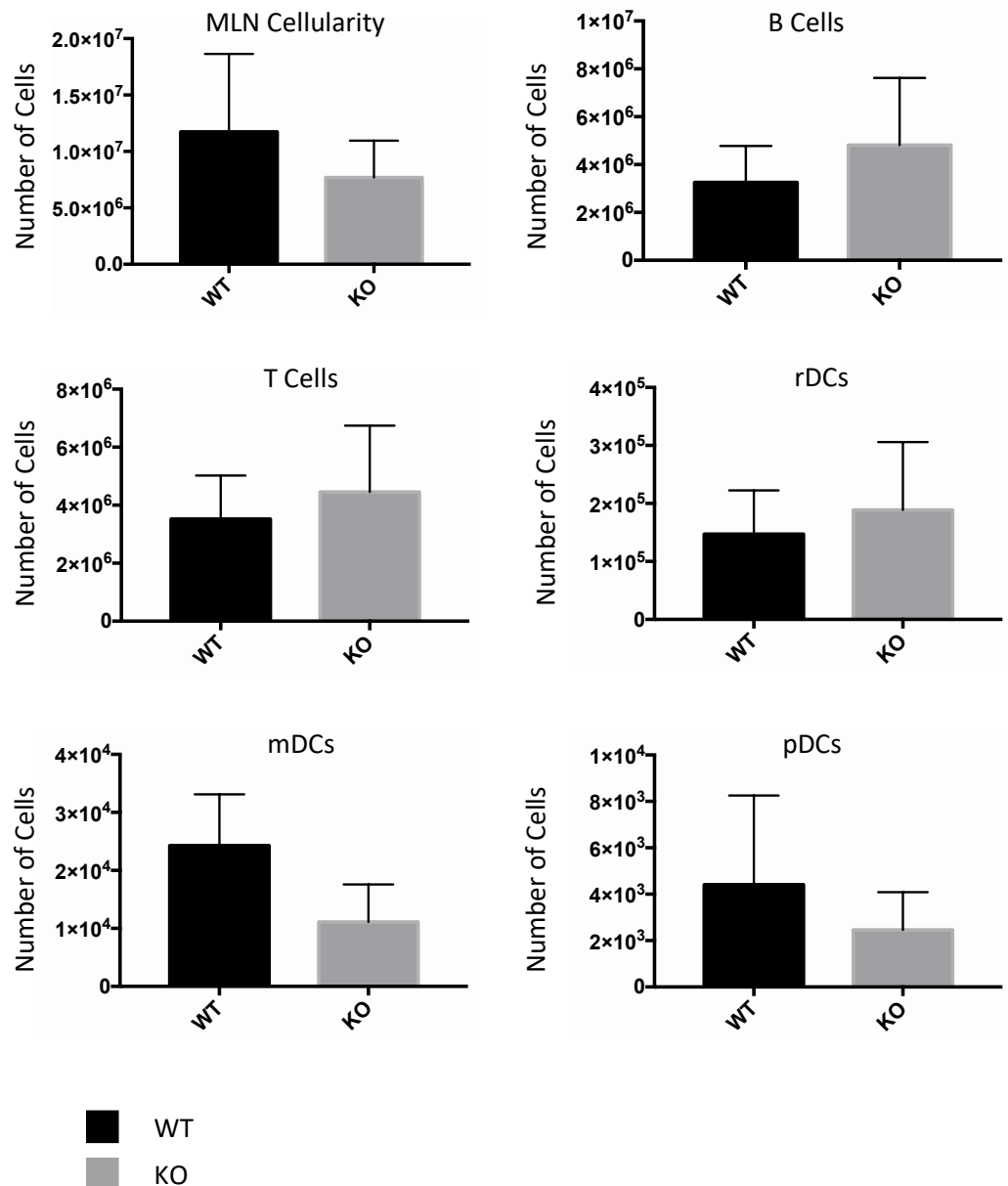


Figure 5-10: Mesenteric lymph node cellularity is not differentially affected in *Ackr4*-null mice, compared to WT, after Aldara treatment.

WT (■) and KO (■) mice were treated once per day for five days with Aldara on both ears as previously described. Mesenteric lymph nodes were excised and processed to obtain single cell suspensions for flow cytometry. All lymph nodes were pooled within each animal and cell counts were used to obtain the absolute numbers of each cell population outlined in Figure 5-6. (n=4). Statistical significance was determined using unpaired t-tests. Error bars represent SD of the mean.

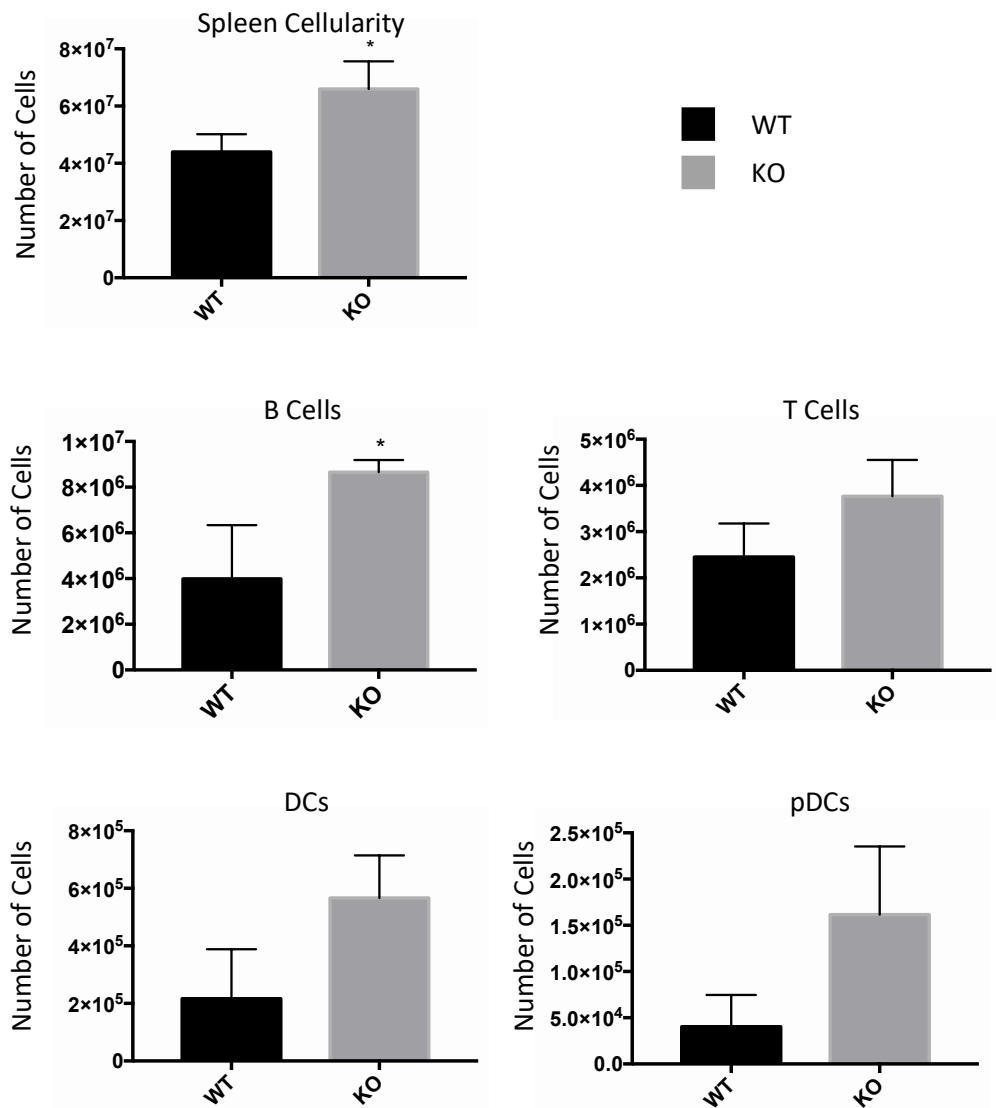


Figure 5-11: Overall cellularity and B cell numbers are increased in *Ackr4*-null mice, compared to WT, after Aldara treatment.

WT (■) and KO (■) mice were treated once per day for five days with Aldara on both ears as previously described. Spleens were excised and processed to obtain single cell suspensions for flow cytometry. Cell counts were used to obtain the absolute numbers of each cell population outlined in Figure 5-6. (n=4). Statistical significance was determined using unpaired t-tests (*P≤0.05). Error bars represent SD of the mean.

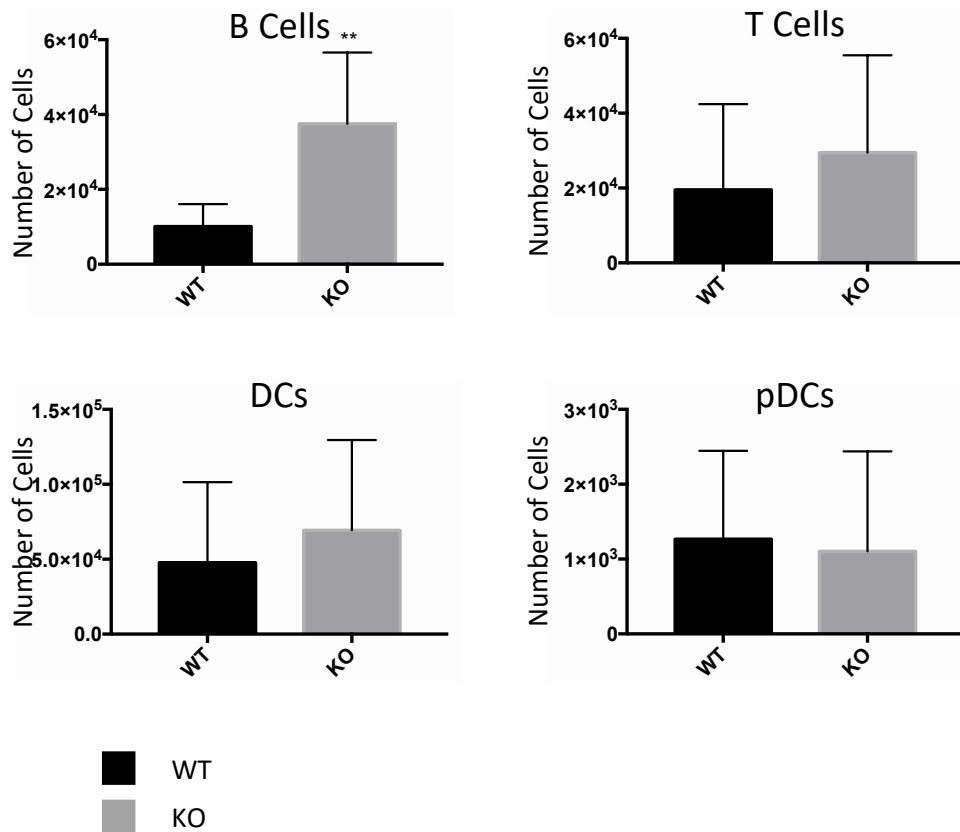


Figure 5-12: Blood of *Ackr4*-null mice contains more circulating B cells than in WT mice following Aldara treatment.

WT (■) and KO (■) mice were treated once per day for five days with Aldara on both ears as previously described. Blood was taken from the posterior vena cava and processed to obtain single cell suspensions for flow cytometry. Fluorescent counting beads, along with the original sample volume obtained from each mouse were used to calculate cell numbers of each cell population outlined in Figure 5-6, normalised to volume of blood (n=6). Statistical significance was determined using unpaired t-tests (* $P \leq 0.05$, ** $P \leq 0.01$). Error bars represent SD of the mean.

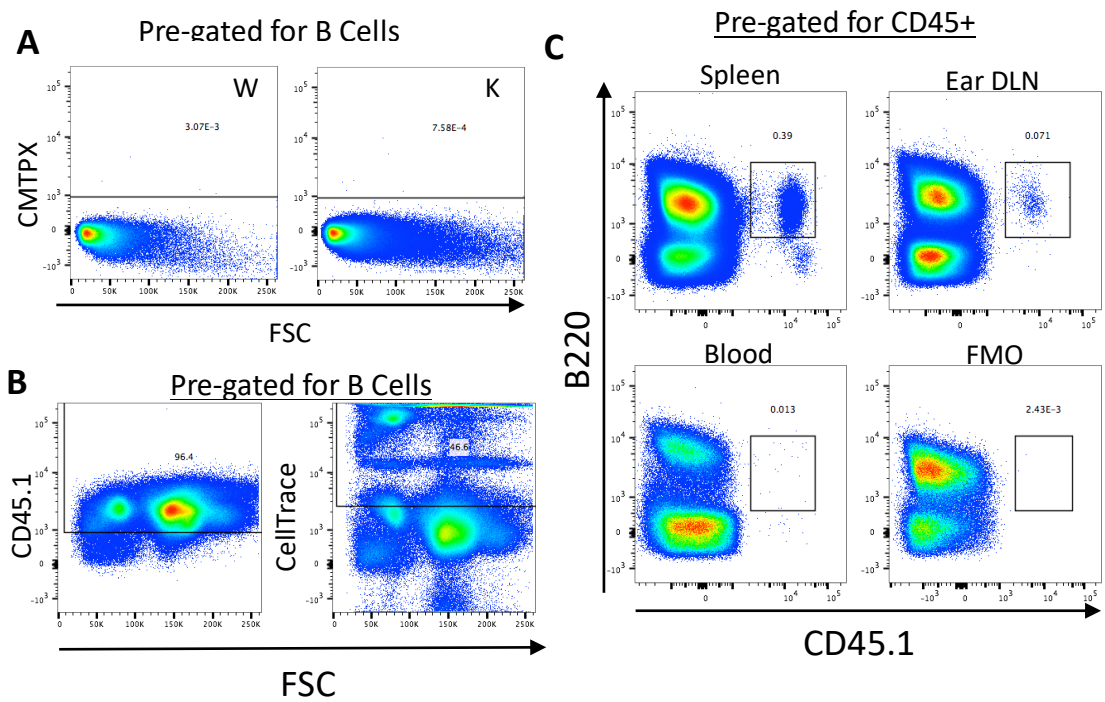


Figure 5-13: Optimisation of Adoptive B Cell Transfer Protocol.

Spleens were harvested from WT or Ly5.1+ mice and single cell suspensions were obtained before enriching for B cells and optionally labelling with CMTPX or CellTrace Violet. 2×10^6 cells were injected into the tail vein of each recipient mouse and tissues were harvested 16 hours later for flow cytometry analysis. **A)** Representative scatter plots show CMTPX-labelled B cells from WT donor mice retrieved from the ear DLN of WT or KO Aldara-treated mice. (n=3). **B)** Representative scatter plots show Ly5.1+ splenocytes, either labelled with CellTrace Violet or unlabelled, and mixed with unlabelled WT splenocytes (no adoptive transfer). Left panel: unlabelled splenocytes were detected using CD45.1 antibody; right panel: CellTrace-labelled splenocytes were detected using the V450 channel. **C)** Scatter plots show Ly5.1+ splenic B cells retrieved from spleen, ear DLN and blood of a WT recipient mouse (n=1).

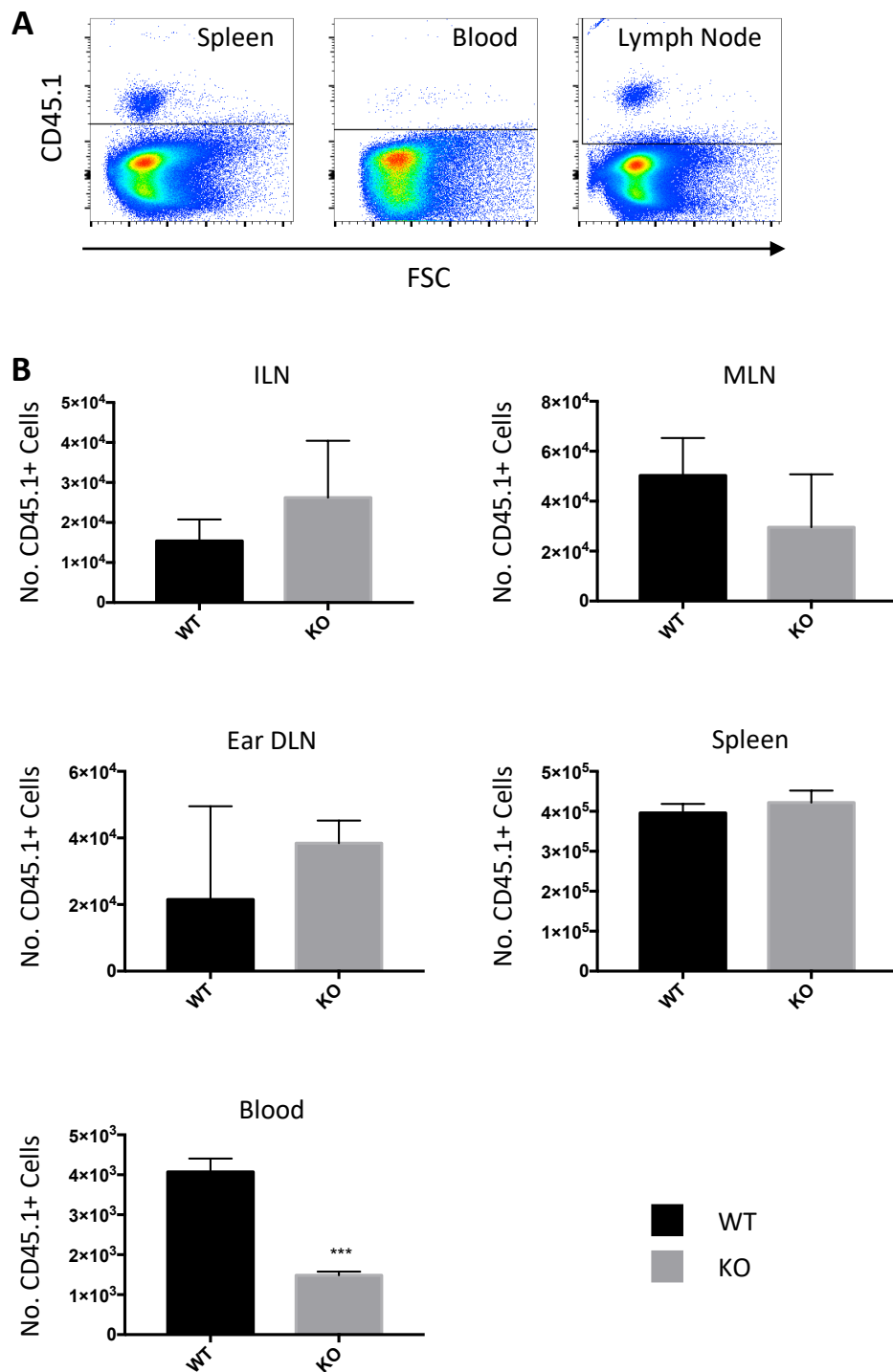


Figure 5-14: After adoptive transfer of CD45.1+ splenocytes, *Ackr4*-null mice have reduced numbers of donor cells in the blood, compared to WT, following Aldara treatment.

WT (■) and KO (■) mice were treated once per day for five days with Aldara on both ears. 16 hours before culling, mice were injected with 2×10^6 splenocytes freshly isolated from Ly5.1 mice into the tail vein. ILN, MLN, ear DLN and spleen were excised and processed to obtain single cell suspensions for flow cytometry, as were cells isolated from blood. All lymph nodes were pooled within each animal and analysed to obtain the absolute numbers of each cell population outlined in Figure 5-6. (n=4). Statistical significance was determined using unpaired t-tests. (* $P \leq 0.05$, ** $P \leq 0.01$, *** $P \leq 0.001$). Error bars represent SD of the mean. **A**) Representative scatter plots show CD45.1+ subsets

identified among CD45+ cells in the spleen, blood and MLN. **B)** Absolute numbers of CD45.1+ cells retrieved from ILN, MLN, ear DLN, spleen and blood of WT and KO mice.

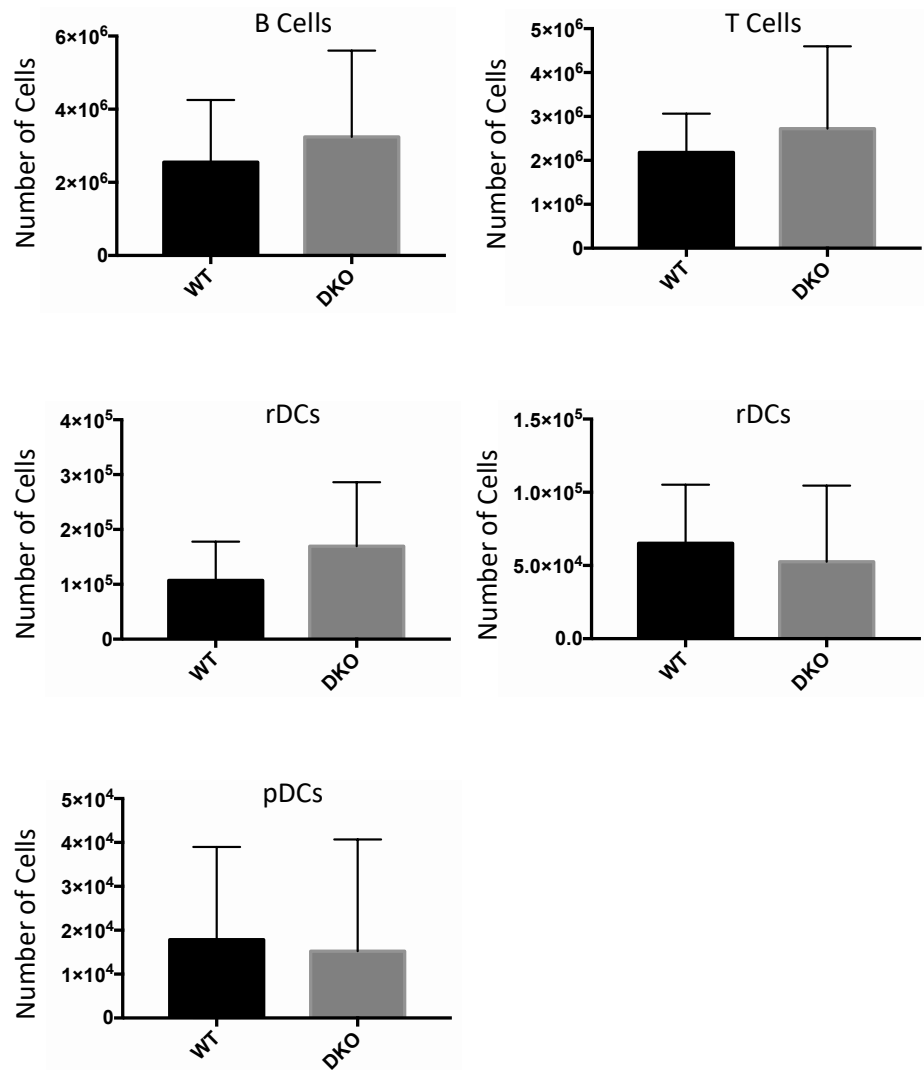


Figure 5-15: Mice lacking both *Ackr4* and *Ccl19* transcripts show no difference in ear DLN cellularity, compared to WT, in response to Aldara treatment.

WT (■) and *Ackr4*^{-/-}, *Ccl19*^{-/-} (DKO, ■) mice were treated once per day for five days with Aldara on both ears. Ear-draining lymph nodes were excised, weighed and processed to obtain single cell suspensions for flow cytometry. All lymph nodes were pooled within each animal and analysed to obtain the absolute numbers of each cell population outlined in Figure 5-6. (n=10 across three experiments). Statistical significance was determined using one-tailed unpaired t-tests. Error bars represent SD of the mean.

Chapter 6: Discussion

6 Discussion

6.1 Function of ACKR3 and ACKR4 on Cultured Human Cells

mRNA and protein expression of ACKRs and their ligands were analysed in cultured human dermal LECs and keratinocytes. The broad findings were that HD-LECs express *ACKR4*, *CCL19*, *CCL21*, *ACKR3* and *CXCL12* by qPCR, and *ACKR4*, *CCL21*, *ACKR3* and *CXCR4* expression were also detected by antibody staining. nHEKs express *ACKR4*, *ACKR3* and *CXCR4* by qPCR, and *ACKR4* expression was also validated by immunofluorescence on these cells.

CXCR4 mRNA expression by LECs appeared highly variable and was not present in all samples, making analysis impossible. It is possible that *CXCR4* is expressed at extremely low levels on resting LECs, which would account for the high variability between samples, and perhaps lead to the transcript being undetectable if cells downregulate *CXCR4*. This could also potentially have been due to RNA degradation during sample handling, although other transcripts were detected successfully in cDNA samples from the same reverse transcription reaction, so this is unlikely, and all -RT controls (no reverse transcriptase enzyme in the reverse transcription reaction) failed to amplify suggesting any *CXCR4* detected was unlikely to be due to DNA contamination.

One of the striking results from the mRNA expression profiling is that both type I and type II interferons appear to be potent inducers of *ACKR4* expression, both in keratinocytes and LECs. IFN- γ showed the strongest effect in both cell types. Unmethylated CpG DNA also induces *ACKR4* expression in LECs but not keratinocytes, while LPS appears to induce *ACKR3* expression strongly in keratinocytes and weakly in LECs, albeit at too low a level to accept confidently without the ability to perform statistical analysis.

Taken together, these results suggest that *ACKR4* can be induced in HD-LECs in response to viral and microbial pathogens, either directly via unmethylated CpG DNA binding to TLR9 or LPS binding to TLR4, and indirectly via type I/II interferons. IFN- α and β are both secreted at high levels by pDCs²¹³, and are normally involved in anti-viral responses, while IFN- γ is mainly produced by activated NK and T cells²¹⁷, and is involved in both anti-viral and anti-microbial responses²¹⁷. Most cell types are capable of producing type I interferons in response to TLR4/9 signalling²¹⁸, so *ACKR4* could potentially be induced

directly by TLR ligand binding, by resulting type I interferon produced by LECs, or by both.

In keratinocytes, *ACKR3* and *CXCR4* appear to be differentially regulated in response to Keratinocyte Growth Factor (KGF), with *ACKR3* showing a trend towards upregulation, while *CXCR4* appears to be downregulated. Although gene expression data originally suggested *ACKR4* was upregulated by KGF (R. Nibbs, personal communication), it had no effect on *ACKR4* expression on cultured human keratinocytes. The result for KGF modulation of *ACKR3/CXCR4* expression is interesting as KGF is a growth factor expressed in the skin that promotes keratinocyte proliferation and differentiation. Given that *ACKR3* is associated with cell survival and proliferation^{155,157,162}, it is interesting that *ACKR3* is potentially upregulated in response to this protein.

The regulation of chemokines secreted by LECs was interesting; as these cells express both *CCL21* and *CXCL12*, yet also express scavenging receptors for these chemokines. In some cases, mRNA for both atypical receptor and chemokine are elevated, for example *ACKR4* and *CCL21* in response to IFN- α , IFN- β and IFN- γ ; and *ACKR3* and *CXCL12* in response to IFN- α . This seems counter-intuitive, as increased chemokine production and increased scavenging receptor expression would appear to be redundant. One consideration is that LECs may be involved in the transport of chemokines via *ACKR4*; in this scenario, *CCL21* upregulation and increased *ACKR4* expression could suggest increased presentation of *CCL21* on the tissue-facing surfaces of LECs.

6.1.1 Cell Culture Issues

Unfortunately, many of the analyses performed on HD-LECs could not be repeated on nHEKs, and several planned experimental enquiries could not be carried out due to continual issues with cell culture contamination and poor proliferative capacity of these cells. Four batches of cells became contaminated. With each batch, all cell culture reagents (media, trypsin and HEPES) were incubated at 37° C to attempt to detect infections. In the first instance, there was a low-level bacterial contamination in the culture medium that went undetected at 4° C. For future batches of cells, all media were filter-sterilised before use to prevent future problems. When a second batch became infected, and the media used appeared free of infection after incubation at 37° C for a week, the water bath was suspected, and care was taken to thoroughly disinfect vials of cells before thawing. In the next batch, the pipette gun used for cell culture was replaced with a communal piece of

equipment as no other lab members appeared to be having infection issues. These steps did not solve the problem of cell culture contamination. Although operator error is, of course, a possibility, every care was taken to practice aseptic technique, and cell culture was carried out successfully for several years using these cell lines before any issues arose. Infection introduced by the supplier could not be ruled out.

One batch of cells also had to be discarded due to poor proliferative capacity, as cells would not adhere to the culture vessel upon thawing. This was most likely due to the cells becoming over-confluent before storing in liquid nitrogen. Due to the significant expense incurred in purchasing human primary cells, these investigations had to be cut short.

Future analyses would have included ACKR3 surface staining on keratinocytes, particularly in tandem with CXCR4 if possible, and investigation of lysosomal/endosomal localisation of these proteins. A scratch assay could also be performed, where a monolayer of serum-starved cells is wounded with a pipette tip, and the clear area is monitored via microscopy to compare the healing of the monolayer. As the cells are incubated without serum during the assay, this should represent cell migration rather than proliferation. This could be carried out in the presence or absence of CCX771, AMD3100 and/or CXCL12 to determine the contribution of ACKR3 and CXCR4 signalling to keratinocyte migration.

6.1.2 Lack of Chemokine Scavenging Activity *in vitro*

Despite clear mRNA expression and modulation of *ACKR3* and *ACKR4* by keratinocytes and LECs, and confirmation of *ACKR4* protein expression by both cell types, no detectable chemokine scavenging occurred in either LECs or keratinocytes. This was studied more extensively in LECs, but none of the experimental conditions tested were successful. This is surprising, as cultured HD-LECs have been shown to scavenge CCL2 *in vitro*¹⁹⁰ and murine dermal LECs to scavenge CCL19 *in vivo*¹⁷⁹. This suggests that the explanation is neither a lack of scavenging activity on LECs, nor an unsuitability of the assay for this cell type. Furthermore, *ACKR4* activity was measured by several mechanisms: uptake of fluorescently-labelled chemokines detected by flow cytometry or fluorescence microscopy, and chemokine depletion from the media.

All of these assays had flaws: in the scavenging assay, the chemokines were removed from the media as quickly in wells containing no cells as in those that did contain cells, suggesting either chemokine sequestration on the culture surface or degradation by

proteases. This does not necessarily suggest chemokine scavenging does not occur but makes it impossible to detect. Uptake of fluorescently-labelled chemokines has been used very successfully in the past, but may be less suitable for cultured cells: although HD-LECs have been successfully used to demonstrate chemokine scavenging via ACKR2, there was very little fluorescent signal in untreated cells, and the only convincing fluorescent chemokine uptake was seen in virally-stimulated cells ¹⁹⁰; however, experiments were attempted with IFN- γ -treated cells, which appear to upregulate *ACKR4* by around 100-fold, with no success.

Positive controls did not always show any uptake signal, which suggests an experimental error was at least partly to blame, but it is uncertain what this could be. In the microscopy experiment, fluorescent CCL19 appeared to associate more readily with the culture surface than with cells, while the streptavidin-fluorophore conjugate used as a control appeared to be highly associated with cells. This, perhaps, suggests that chemokines do rapidly adhere to culture surfaces and that this was a limitation of any assays using chemokines on tissue-culture treated plates.

HD-LECs were used within the 9 passages suggested by the supplier, but evidence has shown that LECs cultured *ex vivo* begin to alter their gene expression profile after 6 passages in culture ²¹⁹; this could be a potential explanation for the lack of scavenging activity detected in these cells. Interestingly, CCL21 expression in LECs also increases after 6 passages *in vitro* ²¹⁹, suggesting this could have played a role in CCL21 expression by these cells.

Another explanation for the lack of ACKR4 scavenging activity detected is the possibility that ACKR4 on LECs does not mainly act as a chemokine scavenging receptor, but instead is involved in transporting chemokines across endothelial surfaces. This is a logical role for ACKR4 on LECs: in order to present CCL21 to CCR7+ DCs and/or T cells migrating into and out of the vessel, CCL21 needs to be bound to the correct surface of the endothelial wall. To support this idea, there is some evidence that ACKR4 is associated with caveolae ¹⁴³, which are vesicles involved in transcytosis.

6.2 ACKR3/CXCR4 Expression *in vivo*

6.2.1 Modulation in the Infundibulum Subset

One striking result from the analysis of ACKR3 and CXCR4 in resting and inflamed skin was the expression and modulation of CXCR4, and of eGFP in *Ackr3^{+gfp}* reporter mice, within the IF subset of keratinocytes. At rest, IF appeared to be the keratinocyte subset with the highest levels of eGFP and second-highest levels of CXCR4 expression, as well as the highest levels of eGFP/CXCR4 coexpression. In inflamed skin, cells in the IF compartment downregulated eGFP expression and upregulated CXCR4 expression, although coexpression data was not available for these cells. Results from cultured human keratinocytes showed similar regulation of these genes in response to TPA, with *ACKR3* downregulated and *CXCR4* upregulated in response to a single treatment. Although cultured basal keratinocytes in low calcium conditions may not be representative of the IF subset, this does suggest reciprocal regulation of the two proteins occurs in response to TPA in both human and mouse cells.

As discussed in the introduction (See section 1.7.1), ACKR3/CXCR4 heterodimers appear to generate differential responses to CXCL12 compared to CXCR4 alone, particularly showing a bias towards β -arrestin signalling as opposed to G-protein signalling¹⁵⁷. Although there is not sufficient data to form any conclusions, the concurrent downregulation of *Ackr3* and upregulation of CXCR4 in the IF could suggest a cellular ‘switch’ from CXCL12 inducing β -arrestin-mediated signalling through ACKR3/CXCR4 heterodimers, towards G-protein-mediated signalling through CXCR4 homodimers. This could potentially represent a functional bias away from cell proliferation and survival and towards cell migration; however, ACKR3 appears to be capable of inducing cell migration itself through Gi-independent mechanisms¹⁶³, so this model (Summarised in Figure 6-1) would likely be an oversimplification. A ‘switch’ away from ACKR3 signalling and towards CXCR4 signalling could alternatively, or concurrently, represent a reduction in CXCL12 scavenging and an increase in CXCL12 responsiveness. As ACKR3 has a higher affinity for CXCL12 than CXCR4¹⁵⁴, cells expressing ACKR3 are likely to be biased towards ACKR3-mediated responses to CXCL12 rather than CXCR4-mediated responses. Lower levels of ACKR3 on IF cells could therefore lead to accumulation of CXCL12 near the hair follicle opening.

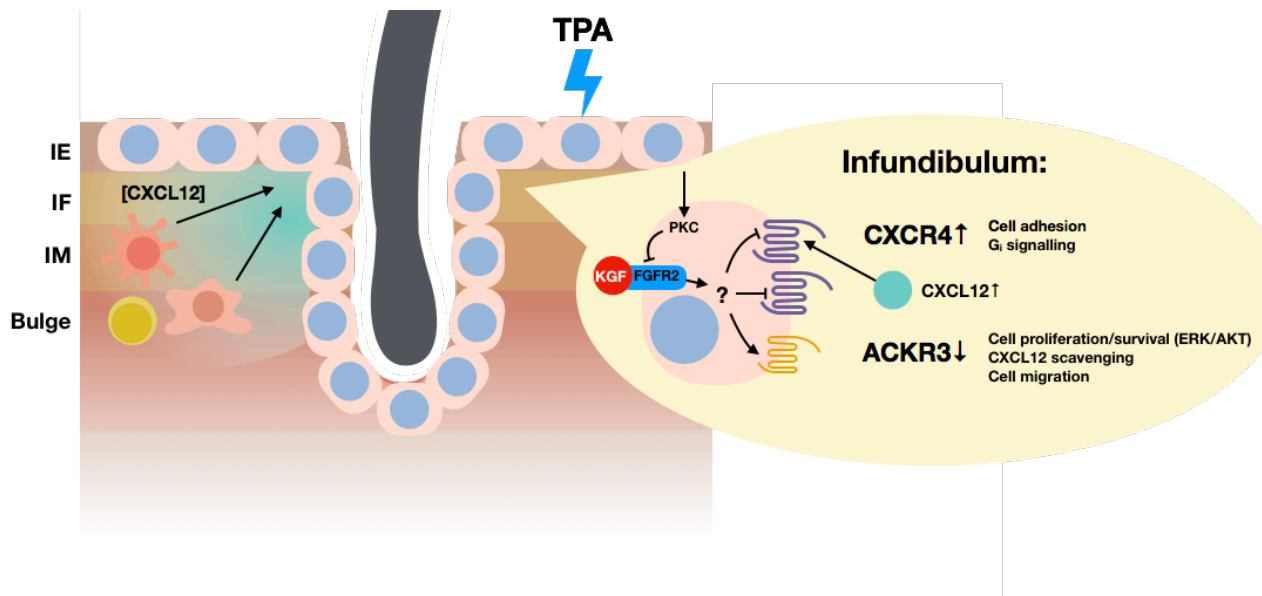


Figure 6-1: Proposed model for ACKR3/CXCR4-mediated TPA responses in keratinocytes.

TPA treatment to the skin leads to increased CXCR4 expression and decreased *Ackr3* expression in keratinocytes, particularly those of the infundibulum. The proposed model shows PKC inhibition of KGF-mediated responses. Keratinocytes respond to KGF by upregulating *Ackr3* and downregulating CXCR4; upon TPA treatment, FGFR2 signalling is interrupted by PKC inactivation and *Ackr3* is instead downregulated while CXCR4 is upregulated. Lack of CXCL12 scavenging by ACKR3 may lead to an increased concentration of CXCL12, which could aid in recruiting CXCR4+ cells including monocytes, macrophages, T cells and Langerhans cells.

The IF subset is of interest as it lies near the opening to the sebaceous glands as well as forming the opening to the hair follicle; this means IF cells come into contact with unique microflora and form a crucial part of the body's barrier against microorganisms²²⁰. IF cells have been shown to be a site of chemokine secretion in response to inflammation, including CCL2, CCL20, CXCL4, CXCL9, CXCL10 and CXCL11⁷⁹. Hair follicles have also been shown to be important structures for LC precursor migration into the skin, as this is impaired in hairless mice⁷⁹, perhaps particularly the infundibulum, as it expresses CCL20 which is one of the chemokines required for this process^{79,221}. Although CXCL12 is not required for the migration of LCs or their precursors to the skin⁷⁹, CXCL12 is involved in LC migration from the epidermis to the dermis^{97,222}. The CXCL12 required for egress from the skin is produced by fibroblasts in the dermis, and it is feasible that CXCL12 scavenging by keratinocytes maintains functional gradients of this chemokine, allowing directional migration of cells towards the dermis and CXCL12+ LECs⁹⁷. Therefore, chemokine scavenging, as well as production, could be another facet to the role hair follicle cells play in modulating cell migration to and from the epidermis.

Infundibulum cells have also been shown to contain the highest proportion of eGFP⁺ cells of all the keratinocyte subsets in resting *Ackr4^{+gfp}* reporter mice (R. Wilson, personal communication). This could suggest that these cells are particularly involved in chemokine scavenging activity at rest; cells of the interfollicular epidermis also expressed high levels of eGFP in both *Ackr3^{+gfp}* and *Ackr4^{+gfp}* reporter mice at rest, but did not appear to extensively modulate eGFP expression in response to TPA treatment; while *Ackr4* expression is reduced in the skin as a whole after TPA treatment (S. Bryce, personal communication), these data are not available for specific keratinocyte subsets. Intriguingly, inverse regulation of *ACKR3* and *CXCR4* also appears to occur in cultured human keratinocytes, where *ACKR3* mRNA is upregulated in response to KGF and LPS and unaffected by IFN- α or IFN- β , while *CXCR4* mRNA is upregulated by IFN- α and IFN- β but unaffected by KGF or LPS. Although the signalling pathways involved in these molecules often overlap (e.g. LPS binding to TLR4 can lead to production of type I interferon), this result was striking and once again suggested that keratinocytes could potentially switch between states of preferential *ACKR3* or *CXCR4* responses.

As outlined in Figure 6.1, this could feasibly occur directly through Protein Kinase C activation, which prevents keratinocyte migration, including via KGF/FGFR2 signalling²²³. Given the inverse response to KGF shown by cultured human keratinocytes, PKC-mediated inhibition of KGF responses could feasibly lead to the observed ‘switch’ in phenotype from *ACKR3* to *CXCR4*-mediated signalling. Interestingly, this includes a lack of cell migration²²³, which is surprising for a pathway that appears to lead to enhanced *CXCR4* expression. *ACKR3*-mediated cell migration has been reported in some cases¹⁶³, and the precise function of *CXCR4* on keratinocytes has not yet been determined, so this would warrant further study.

To further investigate these results, it could be valuable to isolate cells from the IF subset by fluorescence assisted cell sorting (FACS) and analyse them *ex vivo*. qPCR could be used to quantify mRNA expression, giving a more practical approach for generating thorough timecourses to analyse the expression of *Ackr3* and *Cxcr4* expression after TPA treatment. RNA-Seq could also be performed on the different keratinocyte subsets at various timepoints after TPA treatment to help identify key pathways involved in these cells’ differential responses to this inflammatory signal.

Isolated infundibulum cells could also be used for functional assays, for example in Transwell migration assays to analyse LC migration across the cell layer, or *in vitro*

scratch assays to measure cell migration in response to wounding; receptor agonists/antagonists such as AMD3100 (CXCR4 antagonist, ACKR3 agonist) or CCX771 (ACKR3 antagonist) could also be used during treatment with TPA to attempt to elucidate the roles of both these receptors. These approaches could also be carried out *in vivo* using subcutaneously-injected CXCR4 or CCX771 and comparing skin and draining lymph node cellularity in treated and untreated mice after TPA treatment. This approach would have the limitation that any antagonist applied could potentially affect the migration of CXCR4+ infiltrating cells, so the timing of receptor blockade and inflammatory stimulus would need to be balanced carefully. Further immune stimuli could be tested, for example, LPS, to validate qPCR results obtained from cultured human keratinocytes.

6.2.2 Challenges with *Ackr3^{+gfp}* Mice

Ackr3^{+gfp} mice proved challenging to use, because of the need to avoid breeding *Ackr3^{gfp/gfp}* homozygotes, which die as neonates. As only males were used in these studies, and age-matching was attempted, this left only a small pool of suitable animals compared with the number of mice bred. Finding a reliable method for ACKR3 immunostaining would certainly be preferable, but studies on keratinocytes and mouse spleen in the previous chapter did not suggest that uptake of fluorescent CXCL12 would be a reliable method. Although immunostaining using the 11G8 antibody clone has been reported in mouse tissues¹⁵⁰, this was using NOD-SCID mice in order to overcome the problem of non-specific staining that would be expected when using a mouse antibody on mouse tissue. This would not be appropriate for studies involving the immune response.

6.3 Increased Lymph Node Cellularity in Aldara-Treated *Ackr4*-Deficient Mice

Results obtained using the Aldara model of chronic skin inflammation suggested a role for ACKR4 in this pathology. Although *Ackr4* mRNA was strongly downregulated in the skin of Aldara-treated mice, there was apparent enlargement of the lymph nodes draining the treatment site in *Ackr4*-deficient mice compared to wild-types, and increased numbers of B cells, T cells and resident DCs. The initial hypothesis was dysregulation of CCL19 and/or CCL21 due to lack of ACKR4-mediated chemokine scavenging by endothelial cells and keratinocytes. This was largely supported by the evidence obtained: there were elevated levels of CCL19 protein in the plasma of *Ackr4*-deficient mice compared to wild-type

mice, and the observed lymph node enlargement in *Ackr4*-deficient mice was not present in mice also lacking functional *Ccl19*.

6.3.1 Roles for ACKR4 in Chronic Inflammation

Figure 6.2 illustrates and summarises the key results obtained in Chapter 5. Unfortunately, this work was not concluded to the point of obtaining a satisfactory explanation for the differential phenotype seen in *Ackr4*^{-/-} mice compared to WT after five daily Aldara treatments. Some differential observations appear to be widespread (CCL19 overabundance and increased B cell numbers), while others are limited to the LNs draining the treatment site (increased mDC and T cell numbers).

There are several possibilities for the precise nature of the defect caused by lack of *Ackr4* in these mice: leukocytes are unable to exit lymph nodes, cell proliferation has increased, or leukocyte recruitment to the lymph nodes is increased. The third hypothesis appears to be unlikely based on evidence in the literature. The dysregulation of CCR7 ligands is generally reported to impair rather than enhance leukocyte recruitment to the lymph nodes^{101,177,179}. There is some evidence that either supports or fails to refute this hypothesis: migration of adoptively-transferred splenocytes to the SLOs of *Ackr4*^{-/-} Aldara-treated mice was unimpaired compared to wild-type, and there were fewer donor B cells isolated from the blood of these mice. This could indicate enhanced migration of these cells; however, there was no evidence that a greater number of B cells had entered the SLOs. This result could, perhaps, represent decreased survival of B cells that did not migrate to an SLO, but these findings would require further study. Another intriguing observation was the decreased numbers of migratory DCs in the inguinal lymph nodes of *Ackr4*-deficient mice, when these cells were unaffected in the lymph nodes draining the site of Aldara treatment. This could suggest a delayed migration of DCs, which is not detectable in the site-draining lymph nodes by five days after the first wave of DC migration but may become pronounced in more distant skin-draining lymph nodes. This observation could be clarified by studying the lymph node phenotype at multiple timepoints during Aldara treatment. Skin could also be studied at multiple timepoints to measure DC egress in *Ackr4*^{-/-} and wild-type mice. Due to the difficulties encountered in analysing this tissue using flow cytometry, immunohistochemistry could be utilised instead.

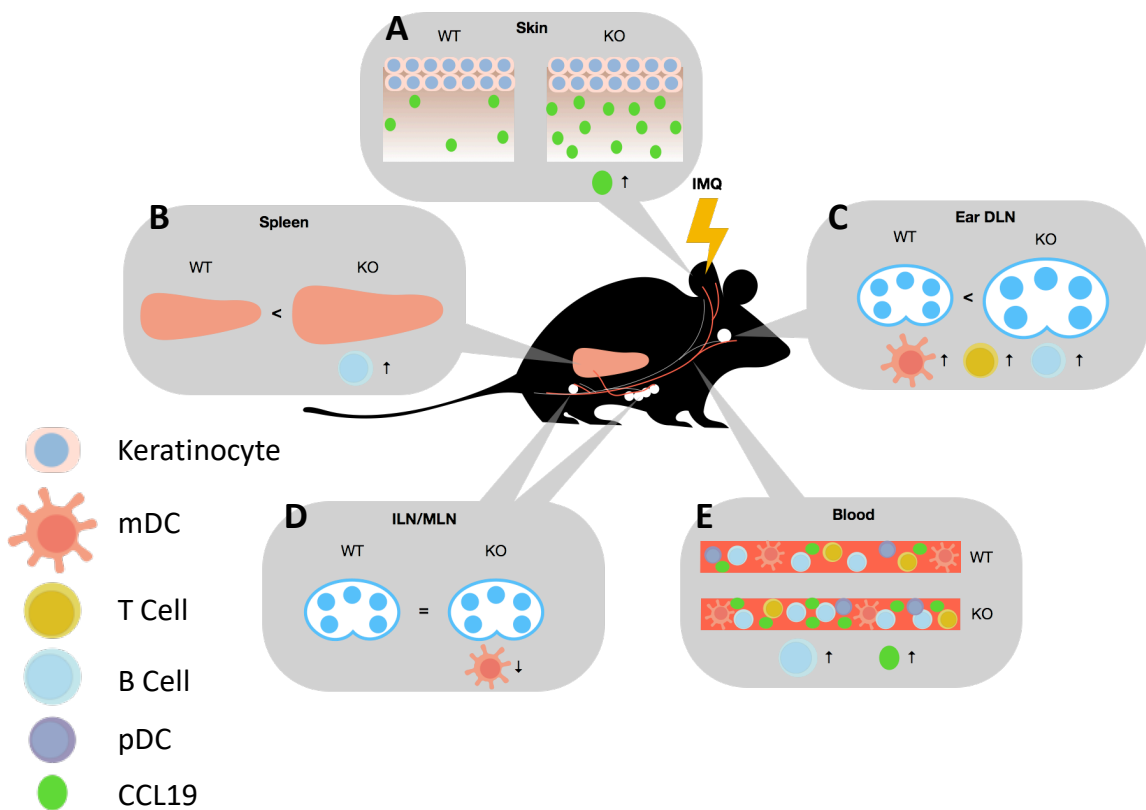


Figure 6-2: Summary of differential responses to five daily Aldara treatments between wild-type and *Ackr4*^{-/-} mice.

The main results from chapter 5, section 2 are summarised here, shown with an illustrative diagram of the locations of sites analysed. **A)** In the skin of *Ackr4*^{-/-} (KO) mice, CCL19 is strongly elevated compared to WT, while keratinocyte proliferation is equal between the two strains. **B)** KO spleens have a higher cellularity compared to WT, and almost double the number of B cells. **C)** The ear DLN of KO mice are significantly larger than WT, and contain greater numbers of mDCs, T cells and B cells (but not rDCs or pDCs). **D)** in the ILN and MLN, the only difference in cellularity detected between WT and KO mice was a decrease in mDCs in the ILN of KO mice. **E)** An increased number of circulating B cells was noticed in KO compared to WT mice, as well as an elevated CCL19 concentration.

Interestingly, previous research has suggested that Imiquimod treatment to the skin leads to increased Langerhans cell migration to the skin-draining lymph nodes²²⁴; this is in contrast with the TPA model of contact hypersensitivity, where LC migration to skin-draining lymph nodes is inhibited due to CCL19 dysregulation¹⁷⁹. As LC migration was not affected in *Ackr4*^{-/-} mice compared to WT in this study, this suggests that LCs are able to overcome the barrier to their exit from the skin caused by CCL19 dysregulation, and perhaps even enhance their migration to the skin-draining lymph nodes, given the increased abundance of migratory DCs detected there.

6.3.2 Limitations of the Aldara Model

The Aldara model presents several serious issues that make interpretation of these results difficult. One problem is that mice topically treated with Aldara will tend to ingest the cream during grooming. It was recently shown that this accounts for not only the systemic effects of Aldara treatment, which include splenomegaly, but also increases the severity of the skin phenotype²²⁵. The authors of this study used collars to prevent mice licking their backs and consequently found a significant reduction in inflammation in response to Aldara. I reasoned that this was not crucial to the described experiments: ACKR4 is found in the skin, throughout the lymphatic system and on endothelial cells of multiple tissues, and therefore the systemic effect is of interest. This does have the limitation that the precise role of ACKR4 in the skin cannot yet be determined, but this could be studied in more detail in the future by comparing the phenotype in mice with and without collars. Ideally, conditional or tissue-specific knock-out mice could be developed to determine the role of *Ackr4* in different tissues, although the cost involved in this would likely be prohibitive.

Another potential issue is that Aldara cream contains isostearic acid as a carrier, which has been shown to have its own inflammatory effects independent of imiquimod²²⁶. Unfortunately, the correct cream could not be sourced for use as a control, so this limits the conclusions that can be drawn from the study. I believe that these observations are valuable as an exploration of the role of ACKR4 in prolonged inflammatory conditions, but it is not possible to conclude whether any differences in mRNA or eGFP expression between treatment and control groups was in response to imiquimod, isostearic acid, or both.

More generally, the Aldara model is an imperfect model of psoriasis. Some of the classic hallmarks of the disease are present, particularly IL-17A and IL-23 upregulation²¹². Some features of Aldara-mediated inflammation do not fit with human psoriasis, however, particularly the fact that it is not genuinely a chronic phenotype as it can be induced in a matter of days. Again, this has limited the conclusions that can be drawn from the study, and without investigating clinical samples it is not possible to determine whether these findings accurately reflect the regulation of *Ackr4* during psoriasis.

6.3.3 Future Investigations

The next steps in this investigation would be to further characterise the cells of the inflamed lymph nodes to determine whether and how *Ackr4* expression is affected in the lymph node stroma. Immunostaining using cell proliferation markers or BrdU labelling could potentially reveal any differences in the levels of proliferation in the lymph nodes between wild-type and *Ackr4*-deficient mice.

One possible next step for investigating the cause of increased lymph node cellularity in *Ackr4*-deficient mice would be to use FTY720, the S1P₁ antagonist, to block leukocyte egress from the lymph nodes. This could indicate whether or not the phenotype observed was related to defects in leukocyte migration from the lymph nodes: if FTY720 treatment created the same phenotype in wild-type and *Ackr4*-deficient mice, this would suggest that leukocytes were becoming trapped in the lymph nodes, while if FTY720 treatment led to a more severe phenotype in *Ackr4*-deficient mice, this would suggest that enhanced proliferation played a role.

Determining the precise role, if any, of ACKR4 expressed by keratinocytes on Aldara-mediated inflammation would be challenging due to the systemic nature of this phenotype discussed above. The simplest method would be to prevent mice from licking the treated areas by either covering them or using collars to restrain their movement. If a differential phenotype between wild-type and *Ackr4*-deficient mice was still observed, this would suggest ACKR4 in the skin played a role in modulating the response to chronic inflammation; however, this would not determine which cell types were crucial for this to occur. It is likely that ACKR4 expressed by a variety of endothelial cells throughout the body is responsible for scavenging CCL19, leading to the build-up of chemokine observed in *Ackr4*-deficient mice. Any effects of ACKR4 on keratinocytes would most likely be detected by closer study of the skin.

The inability to analyse the Aldara-treated skin by flow cytometry was a serious limitation to further exploration of the skin phenotype. Cells were extremely difficult to locate via their forward and side-scatter properties, and when comparing treated to untreated cells, it appeared that samples contained very few cells. This is unlikely to be the case, particularly when visible inflammation suggests a large population of infiltrating leukocytes should be present.

One possibility is that the properties of the cells in the skin are altered by Aldara treatment, or that cells are indeed dying: it has been reported that keratinocytes induce cell death in response to Aldara²²⁶. The failure to isolate leukocytes is not explained by this hypothesis; although these cells are not very numerous in normal epidermis, they can still be isolated reliably, so this should be easier in inflamed skin where the population has increased. Epidermis from Aldara-treated mice appeared to be highly disrupted and seemed to slough off easily before enzymatic digestion. Ear halves are normally floated on top of trypsin to disaggregate the tissue gently, but the permeability barrier of the tissue seemed to be impaired, meaning the tissue would sink. This could have contributed to low cell yields, and perhaps in the future, a shorter and gentler enzymatic digestion approach could be attempted. Immunohistochemistry could also be used to determine the spatial positioning of different cell types, which could reveal defects in migration of cells to or from the skin, or their positioning.

If investigations using cultured human cells are continued, it would be valuable to repeat these experiments using cells obtained from multiple donors. This would give biological replicates which would allow qPCR results to be interpreted with confidence using statistical analysis. This was not carried out in this instance due to the prohibitive costs of obtaining cells commercially.

6.4 Conclusions

The results presented here have shown the expression and modulation of ACKR3 and ACKR4 by keratinocytes in the skin, both *in vitro* in human cells and *in vivo* in mouse tissue, in response to inflammatory stimuli.

Ackr3 expression was shown to be modulated in response to repeated exposure to the phorbol ester TPA, modelling a contact hypersensitivity response. This type of inflammatory stimulus would normally initiate an innate, rather than adaptive, immune response. As ACKR3 and CXCR4 are proposed to heterodimerise on cells that coexpress them, both receptors were investigated. The results showed differential regulation of *Ackr3* and CXCR4 which is intriguing, particularly the finding that the infundibulum subset of the hair follicle in particular downregulates *Ackr3* while upregulating CXCR4 during the inflammatory response. This heterogeneity suggests differential roles for cells of the hair follicle, which could conceivably support directed migration of leukocytes to and from

specific areas of the skin during inflammation, as well as supporting the growth and/or differentiation of particular subsets of keratinocytes.

ACKR4 also appeared to play a role in mediating the response to Aldara-induced inflammation, as the site-draining lymph nodes of *Ackr4*^{-/-} mice contained significantly more cells compared to WT. This phenotype was noted to coincide with accumulation of the chemokine CCL19 in both skin and blood. The phenotype of increased lymph node size was resolved in *Ackr4*^{-/-} *Ccl19*^{-/-} mice, suggesting scavenging of CCL19 by ACKR4 plays a role in the accumulation of lymphocytes in the site-draining lymph nodes.

Although it is not known whether the results obtained in this work impact directly on the organism's ability to resolve any specific disease state, or indeed whether the phenotype seen in *Ackr4*^{-/-} mice would be beneficial or detrimental, the finding that epithelial cells alter their atypical chemokine receptor expression in response to inflammatory stimuli suggests that these receptors do play a role in the inflammatory response, which could have potential relevance in a wide range of diseases. The distinction between a normal and abnormal immune response will include many different factors and the ability of the body to regulate local chemokine concentrations may be one. ACKR-expressing cells could have the ability to modify their chemokine-scavenging activities in response to inflammatory stimuli in order to support the correct migration of leukocytes to and from the site of immune challenge. There is some evidence for the necessity of functioning ACKRs in the immune response to maintain cell responsiveness to chemokines

101,150,179,190 .

ACKR3 and ACKR4 are both found on endothelial cells in a variety of tissues, and while it suited the scope of this study to focus mainly on one easily-manipulated experimental site, the skin, it is feasible that ACKR3 and/or ACKR4 signalling could play a supporting role in resolving a wide range of inflammatory events. Additionally, ACKR3 appears to affect cellular processes distinct from chemokine scavenging. This suggests that ACKR3 may directly affect how stromal cells contribute to processes including immunity and tissue repair, as well as indirectly affecting these processes by modifying availability of chemokines to attract and retain infiltrating leukocytes.

In conclusion, this study has revealed that ACKRs scavenging homeostatic chemokines are expressed on epithelial cells in a number of tissues throughout the body, including SLOs,

and can be modulated at the mRNA and protein level during inflammation suggesting their involvement in a wide range of inflammatory events.

7 Additional Outputs

This PhD studentship has supported the following outputs:

1. Journal article: Bryce, S. A, Wilson, R. A. M, **Tiplady, E. M**, Asquith, D. L, Bromley, S. K, Luster, A. D, Graham, G. J and Nibbs, R. J. B. ACKR4 on Stromal Cells Scavenges CCL19 To Enable CCR7-Dependent Trafficking of APCs from Inflamed Skin to Lymph Nodes. *The Journal of Immunology* **196**, 3341–3353 (2016).
2. Panel Event: ‘Zika Virus: Present, Past and Future’ Glasgow Science Festival, 15 June 2016.
3. Magazine Article: Zika Virus, Biological Sciences Review, *Hodder Education* Vol 30 Issue 1 September 2017.

8 References

1. Brinkmann, V. Neutrophil Extracellular Traps Kill Bacteria. *Science* **303**, 1532–1535 (2004).
2. Bennouna, S., Bliss, S. K., Curiel, T. J. & Denkers, E. Y. Cross-talk in the innate immune system: neutrophils instruct recruitment and activation of dendritic cells during microbial infection. *J. Immunol.* **171**, 6052–6058 (2003).
3. Kalupahana, R. S., Mastroeni, P., Maskell, D. & Blacklaws, B. A. Activation of murine dendritic cells and macrophages induced by *Salmonella enterica* serovar Typhimurium. *Immunology* **115**, 462–472 (2005).
4. Bendelac, A., Bonneville, M. & Kearney, J. F. Autoreactivity by design: innate B and T lymphocytes. *Nat. Rev. Immunol.* **1**, 177–186 (2001).
5. Ohtani, O. & Ohtani, Y. Structure and function of rat lymph nodes. *Arch. Histol. Cytol.* **71**, 69–76 (2008).
6. Kuka, M. & Iannacone, M. The role of lymph node sinus macrophages in host defense. *Ann. N. Y. Acad. Sci.* **1319**, 38–46 (2014).
7. Roozendaal, R. *et al.* Conduits mediate transport of low-molecular-weight antigen to lymph node follicles. *Immunity* **30**, 264–276 (2009).
8. Sixt, M. *et al.* The conduit system transports soluble antigens from the afferent lymph to resident dendritic cells in the T cell area of the lymph node. *Immunity* **22**, 19–29 (2005).
9. Gray, E. E. & Cyster, J. G. Lymph node macrophages. *J Innate Immun* **4**, 424–436 (2012).
10. Albacker, L. A. *et al.* TIM-4, expressed by medullary macrophages, regulates respiratory tolerance by mediating phagocytosis of antigen-specific T cells. *Mucosal Immunol* **6**, 580–590 (2013).
11. Bajénoff, M. *et al.* Stromal cell networks regulate lymphocyte entry, migration, and territoriality in lymph nodes. *Immunity* **25**, 989–1001 (2006).

12. Link, A. *et al.* Fibroblastic reticular cells in lymph nodes regulate the homeostasis of naive T cells. *Nat. Immunol.* **8**, 1255–1265 (2007).
13. Mori, S. *et al.* Mice lacking expression of the chemokines CCL21-ser and CCL19 (plt mice) demonstrate delayed but enhanced T cell immune responses. *J. Exp. Med.* **193**, 207–218 (2001).
14. Bachmann, M. F. *et al.* Distinct roles for LFA-1 and CD28 during activation of naive T cells: adhesion versus costimulation. *Immunity* **7**, 549–557 (1997).
15. Parameswaran, N., Suresh, R., Bal, V., Rath, S. & George, A. Lack of ICAM-1 on APCs during T cell priming leads to poor generation of central memory cells. *J. Immunol.* **175**, 2201–2211 (2005).
16. Ansel, K. M., McHeyzer-Williams, L. J., Ngo, V. N., McHeyzer-Williams, M. G. & Cyster, J. G. In vivo-activated CD4 T cells upregulate CXC chemokine receptor 5 and reprogram their response to lymphoid chemokines. *J. Exp. Med.* **190**, 1123–1134 (1999).
17. Forster, R. *et al.* CCR7 coordinates the primary immune response by establishing functional microenvironments in secondary lymphoid organs. *Cell* **99**, 23–33 (1999).
18. Cyster, J. G. *et al.* Follicular stromal cells and lymphocyte homing to follicles. *Immunological Reviews* **176**, 181–193 (2000).
19. Farrand, K. J. *et al.* Langerin⁺ CD8 α ⁺ dendritic cells are critical for cross-priming and IL-12 production in response to systemic antigens. *The Journal of Immunology* **183**, 7732–7742 (2009).
20. Mahnke, K., Schmitt, E., Bonifaz, L., Enk, A. H. & Jonuleit, H. Immature, but not inactive: the tolerogenic function of immature dendritic cells. *Immunol. Cell Biol.* **80**, 477–483 (2002).
21. Steinman, R. M., Hawiger, D. & Nussenzweig, M. C. Tolerogenic dendritic cells. *Annu. Rev. Immunol.* **21**, 685–711 (2003).
22. Jordan, M. S. *et al.* Thymic selection of CD4⁺CD25⁺ regulatory T cells induced by an agonist self-peptide. *Nat. Immunol.* **2**, 301–306 (2001).

23. Wang, X. *et al.* Follicular dendritic cells help establish follicle identity and promote B cell retention in germinal centers. *J. Exp. Med.* **208**, 2497–2510 (2011).
24. Ansel, K. M. *et al.* A chemokine-driven positive feedback loop organizes lymphoid follicles. *Nature* **406**, 309–314 (2000).
25. Carrasco, Y. R. & Batista, F. D. B cells acquire particulate antigen in a macrophage-rich area at the boundary between the follicle and the subcapsular sinus of the lymph node. *Immunity* **27**, 160–171 (2007).
26. Phan, T. G., Grigorova, I., Okada, T. & Cyster, J. G. Subcapsular encounter and complement-dependent transport of immune complexes by lymph node B cells. *Nat. Immunol.* **8**, 992–1000 (2007).
27. Gatto, D., Paus, D., Basten, A., Mackay, C. R. & Brink, R. Guidance of B cells by the orphan G protein-coupled receptor EBI2 shapes humoral immune responses. *Immunity* **31**, 259–269 (2009).
28. Gatto, D., Wood, K. & Brink, R. EBI2 operates independently of but in cooperation with CXCR5 and CCR7 to direct B cell migration and organization in follicles and the germinal center. *The Journal of Immunology* **187**, 4621–4628 (2011).
29. Reif, K. *et al.* Balanced responsiveness to chemoattractants from adjacent zones determines B-cell position. *Nature* **416**, 94–99 (2002).
30. Garside, P. *et al.* Visualization of specific B and T lymphocyte interactions in the lymph node. *Science* **281**, 96–99 (1998).
31. Crotty, S. A brief history of T cell help to B cells. *Nat. Rev. Immunol.* **15**, 185–189 (2015).
32. Pereira, J. P., Kelly, L. M., Xu, Y. & Cyster, J. G. EBI2 mediates B cell segregation between the outer and centre follicle. *Nature* **462**, 117–126 (2009).
33. Allen, C. D. C. *et al.* Germinal center dark and light zone organization is mediated by CXCR4 and CXCR5. *Nat. Immunol.* **5**, 943–952 (2004).

34. Ley, K., Laudanna, C., Cybulsky, M. I. & Nourshargh, S. Getting to the site of inflammation: the leukocyte adhesion cascade updated. *Nat. Rev. Immunol.* **7**, 678–689 (2007).
35. Matloubian, M. *et al.* Lymphocyte egress from thymus and peripheral lymphoid organs is dependent on S1P receptor 1. *Nature* **427**, 355–360 (2004).
36. Schwab, S. R. *et al.* Lymphocyte sequestration through S1P lyase inhibition and disruption of S1P gradients. *Science* **309**, 1735–1739 (2005).
37. Schwab, S. R. & Cyster, J. G. Finding a way out: lymphocyte egress from lymphoid organs. *Nat. Immunol.* **8**, 1295–1301 (2007).
38. Graeler, M., Shankar, G. & Goetzl, E. J. Cutting edge: suppression of T cell chemotaxis by sphingosine 1-phosphate. *J. Immunol.* **169**, 4084–4087 (2002).
39. Shiow, L. R. *et al.* CD69 acts downstream of interferon-alpha/beta to inhibit S1P1 and lymphocyte egress from lymphoid organs. *Nature* **440**, 540–544 (2006).
40. van de Pavert, S. A. *et al.* Chemokine CXCL13 is essential for lymph node initiation and is induced by retinoic acid and neuronal stimulation. *Nat. Immunol.* **10**, 1193–1199 (2009).
41. van de Pavert, S. A. & Mebius, R. E. Development of secondary lymphoid organs in relation to lymphatic vasculature. *Adv Anat Embryol Cell Biol* **214**, 81–91 (2014).
42. Luther, S. A., Ansel, K. M. & Cyster, J. G. Overlapping roles of CXCL13, interleukin 7 receptor alpha, and CCR7 ligands in lymph node development. *J. Exp. Med.* **197**, 1191–1198 (2003).
43. Vondenhoff, M. F. *et al.* LTbetaR signaling induces cytokine expression and up-regulates lymphangiogenic factors in lymph node anlagen. *The Journal of Immunology* **182**, 5439–5445 (2009).
44. Kim, D. *et al.* Regulation of peripheral lymph node genesis by the tumor necrosis factor family member TRANCE. *J. Exp. Med.* **192**, 1467–1478 (2000).
45. Kong, Y. Y. *et al.* OPG is a key regulator of osteoclastogenesis, lymphocyte development and lymph-node organogenesis. *Nature* **397**, 315–323 (1999).

46. Eberl, G. *et al.* An essential function for the nuclear receptor RORgamma(t) in the generation of fetal lymphoid tissue inducer cells. *Nat. Immunol.* **5**, 64–73 (2004).
47. Swirski, F. K. *et al.* Identification of splenic reservoir monocytes and their deployment to inflammatory sites. *Science* **325**, 612–616 (2009).
48. Mebius, R. E. & Kraal, G. Structure and function of the spleen. *Nat. Rev. Immunol.* **5**, 606–616 (2005).
49. Gunn, M. D. *et al.* Mice lacking expression of secondary lymphoid organ chemokine have defects in lymphocyte homing and dendritic cell localization. *J. Exp. Med.* **189**, 451–460 (1999).
50. Eloranta, M. L. & Alm, G. V. Splenic marginal metallophilic macrophages and marginal zone macrophages are the major interferon-alpha/beta producers in mice upon intravenous challenge with herpes simplex virus. *Scand. J. Immunol.* **49**, 391–394 (1999).
51. Balázs, M., Martin, F., Zhou, T. & Kearney, J. F. Blood Dendritic Cells Interact with Splenic Marginal Zone B Cells to Initiate T-Independent Immune Responses. *Immunity* **17**, 341–352 (2002).
52. Attanavanich, K. & Kearney, J. F. Marginal zone, but not follicular B cells, are potent activators of naive CD4 T cells. *J. Immunol.* **172**, 803–811 (2004).
53. Cinamon, G. *et al.* Sphingosine 1-phosphate receptor 1 promotes B cell localization in the splenic marginal zone. *Nat. Immunol.* **5**, 713–720 (2004).
54. Guinamard, R., Okigaki, M., Schlessinger, J. & Ravetch, J. V. Absence of marginal zone B cells in Pyk-2-deficient mice defines their role in the humoral response. *Nat. Immunol.* **1**, 31–36 (2000).
55. Pillai, S. & Cariappa, A. The follicular versus marginal zone B lymphocyte cell fate decision. *Nat. Rev. Immunol.* **9**, 767–777 (2009).
56. Saito, T. *et al.* Notch2 Is Preferentially Expressed in Mature B Cells and Indispensable for Marginal Zone B Lineage Development. *Immunity* **18**, 675–685 (2003).

57. Tanigaki, K. *et al.* Notch-RBP-J signaling is involved in cell fate determination of marginal zone B cells. *Nat. Immunol.* **3**, 443–450 (2002).
58. Kuroda, K. *et al.* Regulation of marginal zone B cell development by MINT, a suppressor of Notch/RBP-J signaling pathway. *Immunity* **18**, 301–312 (2003).
59. Vinuesa, C. G., Toellner, K. M. & Papa, I. in *Encyclopedia of Immunobiology* 208–215 (Elsevier, 2016). doi:10.1016/B978-0-12-374279-7.09009-3
60. Dudziak, D. *et al.* Differential antigen processing by dendritic cell subsets in vivo. *Science* **315**, 107–111 (2007).
61. Jiang, W. *et al.* The receptor DEC-205 expressed by dendritic cells and thymic epithelial cells is involved in antigen processing. *Nature* **375**, 151–155 (1995).
62. Vremec, D., Pooley, J., Hochrein, H., Wu, L. & Shortman, K. CD4 and CD8 expression by dendritic cell subtypes in mouse thymus and spleen. *J. Immunol.* **164**, 2978–2986 (2000).
63. Shortman, K. & Caux, C. Dendritic Cell Development: Multiple Pathways to Nature's Adjuvants. *Stem Cells* **15**, 409–419 (1997).
64. Steinman, R. M., Pack, M. & Inaba, K. Dendritic cells in the T-cell areas of lymphoid organs. *Immunological Reviews* **156**, 25–37 (1997).
65. Wu, L. & Dakic, A. Development of dendritic cell system. *Cell. Mol. Immunol.* **1**, 112–118 (2004).
66. Haan, den, J. M., Lehar, S. M. & Bevan, M. J. CD8(+) but not CD8(-) dendritic cells cross-prime cytotoxic T cells in vivo. *J. Exp. Med.* **192**, 1685–1696 (2000).
67. Belz, G. T. *et al.* The CD8alpha(+) dendritic cell is responsible for inducing peripheral self-tolerance to tissue-associated antigens. *J. Exp. Med.* **196**, 1099–1104 (2002).
68. Iyoda, T. *et al.* The CD8+ dendritic cell subset selectively endocytoses dying cells in culture and in vivo. *J. Exp. Med.* **195**, 1289–1302 (2002).
69. Iwasaki, A. The importance of CD11b+ dendritic cells in CD4+ T cell activation in vivo: with help from interleukin 1. *J. Exp. Med.* **198**, 185–190 (2003).

70. Pooley, J. L., Heath, W. R. & Shortman, K. Cutting edge: intravenous soluble antigen is presented to CD4 T cells by CD8- dendritic cells, but cross-presented to CD8 T cells by CD8+ dendritic cells. *J. Immunol.* **166**, 5327–5330 (2001).
71. Price, J. D., Hotta-Iwamura, C., Zhao, Y., Beauchamp, N. M. & Tarbell, K. V. DCIR2+ cDC2 DCs and Zbtb32 Restore CD4+ T-Cell Tolerance and Inhibit Diabetes. *Diabetes* **64**, 3521–3531 (2015).
72. Ono, S. & Kabashima, K. Proposal of inducible skin-associated lymphoid tissue (iSALT). *Exp Dermatol* **24**, 630–631 (2015).
73. Kubo, A., Nagao, K., Yokouchi, M., Sasaki, H. & Amagai, M. External antigen uptake by Langerhans cells with reorganization of epidermal tight junction barriers. *J. Exp. Med.* **206**, 2937–2946 (2009).
74. Turunen, A. & Syrjänen, S. Extracellular calcium regulates keratinocyte proliferation and HPV 16 E6 RNA expression in vitro. *APMIS* **122**, 781–789 (2014).
75. Elias, P. M., Ahn, S. K., Brown, B. E., Crumrine, D. & Feingold, K. R. Origin of the epidermal calcium gradient: regulation by barrier status and role of active vs passive mechanisms. *J. Invest. Dermatol.* **119**, 1269–1274 (2002).
76. Schneider, M. R., Schmidt-Ullrich, R. & Paus, R. The hair follicle as a dynamic miniorgan. *Curr. Biol.* **19**, R132–42 (2009).
77. Purba, T. S. *et al.* Human epithelial hair follicle stem cells and their progeny: Current state of knowledge, the widening gap in translational research and future challenges. *BioEssays* **36**, 513–525 (2014).
78. Taylor, G., Lehrer, M. S., Jensen, P. J., Sun, T. T. & Lavker, R. M. Involvement of follicular stem cells in forming not only the follicle but also the epidermis. *Cell* **102**, 451–461 (2000).
79. Nagao, K. *et al.* Stress-induced production of chemokines by hair follicles regulates the trafficking of dendritic cells in skin. *Nat. Immunol.* **13**, 744–752 (2012).
80. Clark, R. A. *et al.* The vast majority of CLA+ T cells are resident in normal skin. *J. Immunol.* **176**, 4431–4439 (2006).

81. Foster, C. A. *et al.* Human epidermal T cells predominantly belong to the lineage expressing alpha/beta T cell receptor. *J. Exp. Med.* **171**, 997–1013 (1990).
82. Tsai, M., Grimbaldston, M. & Galli, S. J. in *Mast Cell Biology* **716**, 186–211 (Springer US, 2011).
83. Henri, S. *et al.* CD207+ CD103+ dermal dendritic cells cross-present keratinocyte-derived antigens irrespective of the presence of Langerhans cells. *J. Exp. Med.* **207**, 189–206 (2010).
84. Idoyaga, J. *et al.* Cutting edge: langerin/CD207 receptor on dendritic cells mediates efficient antigen presentation on MHC I and II products in vivo. *J. Immunol.* **180**, 3647–3650 (2008).
85. Merad, M. *et al.* Langerhans cells renew in the skin throughout life under steady-state conditions. *Nat. Immunol.* **3**, 1135–1141 (2002).
86. Ginhoux, F. *et al.* Langerhans cells arise from monocytes in vivo. *Nat. Immunol.* **7**, 265–273 (2006).
87. Strobl, H. *et al.* TGF-beta 1 promotes in vitro development of dendritic cells from CD34+ hemopoietic progenitors. *J. Immunol.* **157**, 1499–1507 (1996).
88. Kel, J. M., Girard-Madoux, M. J. H., Reizis, B. & Clausen, B. E. TGF-beta is required to maintain the pool of immature Langerhans cells in the epidermis. *The Journal of Immunology* **185**, 3248–3255 (2010).
89. Havran, W. L., Chien, Y. H. & Allison, J. P. Recognition of self antigens by skin-derived T cells with invariant gamma delta antigen receptors. *Science* **252**, 1430–1432 (1991).
90. Jameson, J. M., Cauvi, G., Witherden, D. A. & Havran, W. L. A keratinocyte-responsive gamma delta TCR is necessary for dendritic epidermal T cell activation by damaged keratinocytes and maintenance in the epidermis. *J. Immunol.* **172**, 3573–3579 (2004).
91. Matsue, H., Cruz, P. D., Jr., Bergstresser, P. R. & Takashima, A. Profiles of Cytokine mRNA Expressed by Dendritic Epidermal T Cells in Mice. *Journal of Investigative Dermatology* **101**, 537–542 (1993).

92. Witherden, D. A., Verdino, P., Rieder, S. E. & Garijo, O. The junctional adhesion molecule JAML is a costimulatory receptor for epithelial T cell activation. *Interacting with Computers* (2010).
93. MacLeod, A. S. *et al.* Dendritic epidermal T cells regulate skin antimicrobial barrier function. *J. Clin. Invest.* **123**, 4364–4374 (2013).
94. Jin, C. & Morita, C. T. in *Chemokine Biology — Basic Research and Clinical Application* 59–78 (Birkhäuser-Verlag, 2006). doi:10.1007/3-7643-7423-3_4
95. Jameson, J. A Role for Skin gamma delta T Cells in Wound Repair. *Science* **296**, 747–749 (2002).
96. Ohl, L. *et al.* CCR7 governs skin dendritic cell migration under inflammatory and steady-state conditions. *Immunity* **21**, 279–288 (2004).
97. Ouwehand, K. *et al.* CXCL12 is essential for migration of activated Langerhans cells from epidermis to dermis. *Eur. J. Immunol.* **38**, 3050–3059 (2008).
98. Britschgi, M. R., Favre, S. & Luther, S. A. CCL21 is sufficient to mediate DC migration, maturation and function in the absence of CCL19. *Eur. J. Immunol.* **40**, 1266–1271 (2010).
99. Weber, M. *et al.* Interstitial dendritic cell guidance by haptotactic chemokine gradients. *Science* **339**, 328–332 (2013).
100. Braun, A. *et al.* Afferent lymph-derived T cells and DCs use different chemokine receptor CCR7-dependent routes for entry into the lymph node and intranodal migration. *Nat. Immunol.* **12**, 879–887 (2011).
101. Ulvmar, M. H. *et al.* The atypical chemokine receptor CCRL1 shapes functional CCL21 gradients in lymph nodes. *Nat. Immunol.* **15**, 623–630 (2014).
102. Allen, S. J., Crown, S. E. & Handel, T. M. Chemokine: receptor structure, interactions, and antagonism. *Annu. Rev. Immunol.* **25**, 787–820 (2007).
103. Clark-Lewis, I. *et al.* Structure-activity relationships of chemokines. *Journal of Leukocyte Biology* **57**, 703–711 (1995).

104. Gong, J. H. & Clark-Lewis, I. Antagonists of monocyte chemoattractant protein 1 identified by modification of functionally critical NH₂-terminal residues. *J. Exp. Med.* **181**, 631–640 (1995).
105. McQuibban, G. A. *et al.* Matrix metalloproteinase activity inactivates the CXC chemokine stromal cell-derived factor-1. *J. Biol. Chem.* **276**, 43503–43508 (2001).
106. Guan, E., Wang, J. & Norcross, M. A. Amino-terminal processing of MIP-1 β /CCL4 by CD26/dipeptidyl-peptidase IV. *Journal of Cellular Biochemistry* **92**, 53–64 (2004).
107. McQuibban, G. A. *et al.* Matrix metalloproteinase processing of monocyte chemoattractant proteins generates CC chemokine receptor antagonists with anti-inflammatory properties in vivo. *Blood* **100**, 1160–1167 (2002).
108. McQuibban, G. A. *et al.* Inflammation dampened by gelatinase A cleavage of monocyte chemoattractant protein-3. *Science* **289**, 1202–1206 (2000).
109. Ravindran, A., Sawant, K. V., Sarmiento, J., Navarro, J. & Rajarathnam, K. Chemokine CXCL1 dimer is a potent agonist for the CXCR2 receptor. *J. Biol. Chem.* **288**, 12244–12252 (2013).
110. Nasser, M. W. *et al.* Differential Activation and Regulation of CXCR1 and CXCR2 by CXCL8 Monomer and Dimer. *J. Immunol.* **183**, 3425–3432 (2009).
111. Crown, S. E., Yu, Y., Sweeney, M. D., Leary, J. A. & Handel, T. M. Heterodimerization of CCR2 chemokines and regulation by glycosaminoglycan binding. *J. Biol. Chem.* **281**, 25438–25446 (2006).
112. Guan, E., Wang, J. & Norcross, M. A. Identification of Human Macrophage Inflammatory Proteins 1 α and 1 β as a Native Secreted Heterodimer. *J. Biol. Chem.* **276**, 12404–12409 (2001).
113. Dudek, A. Z. *et al.* Platelet factor 4 promotes adhesion of hematopoietic progenitor cells and binds IL-8: novel mechanisms for modulation of hematopoiesis. *Blood* **101**, 4687–4694 (2003).
114. Proudfoot, A. E. I. *et al.* Glycosaminoglycan binding and oligomerization are essential for the in vivo activity of certain chemokines. *Proc. Natl. Acad. Sci. U.S.A.* **100**, 1885–1890 (2003).

115. Friedl, P., Borgmann, S. & Bröcker, E. B. Amoeboid leukocyte crawling through extracellular matrix: lessons from the Dictyostelium paradigm of cell movement. *Journal of Leukocyte Biology* **70**, 491–509 (2001).
116. Lämmermann, T. *et al.* Rapid leukocyte migration by integrin-independent flowing and squeezing. *Nature* **453**, 51–55 (2008).
117. Lämmermann, T. *et al.* Cdc42-dependent leading edge coordination is essential for interstitial dendritic cell migration. *Blood* **113**, 5703–5710 (2009).
118. Thompson, S. *et al.* Regulation of Chemokine Function: The Roles of GAG-Binding and Post-Translational Nitration. *Int J Mol Sci* **18**, 1692 (2017).
119. Schumann, K. *et al.* Immobilized chemokine fields and soluble chemokine gradients cooperatively shape migration patterns of dendritic cells. *Immunity* **32**, 703–713 (2010).
120. Comerford, I. & Nibbs, R. J. B. Post-translational control of chemokines: a role for decoy receptors? *Immunol. Lett.* **96**, 163–174 (2005).
121. Luther, S. A., Tang, H. L., Hyman, P. L., Farr, A. G. & Cyster, J. G. Coexpression of the chemokines ELC and SLC by T zone stromal cells and deletion of the ELC gene in the plt/plt mouse. *Proc. Natl. Acad. Sci. U.S.A.* **97**, 12694–12699 (2000).
122. Nagasawa, T. *et al.* Defects of B-cell lymphopoiesis and bone-marrow myelopoiesis in mice lacking the CXC chemokine PBSF/SDF-1. *Nature* **382**, 635–638 (1996).
123. David, N. B. *et al.* Molecular basis of cell migration in the fish lateral line: role of the chemokine receptor CXCR4 and of its ligand, SDF1. *Proc. Natl. Acad. Sci. U.S.A.* **99**, 16297–16302 (2002).
124. Mantovani, A. The chemokine system: redundancy for robust outputs. *Immunol. Today* **20**, 254–257 (1999).
125. Graham, G. J., Locati, M., Mantovani, A., Rot, A. & Thelen, M. The biochemistry and biology of the atypical chemokine receptors. *Immunol. Lett.* **145**, 30–38 (2012).
126. Thelen, M. Dancing to the tune of chemokines. *Nat. Immunol.* **2**, 129–134 (2001).

127. Reiter, E. & Lefkowitz, R. J. GRKs and β -arrestins: roles in receptor silencing, trafficking and signaling. *Trends in Endocrinology & Metabolism* **17**, 159–165 (2006).
128. Godfrey, D. I., Kennedy, J., Suda, T. & Zlotnik, A. A developmental pathway involving four phenotypically and functionally distinct subsets of CD3-CD4-CD8-triple-negative adult mouse thymocytes defined by CD44 and CD25 expression. *J. Immunol.* **150**, 4244–4252 (1993).
129. Germain, R. N. T-cell development and the CD4-CD8 lineage decision. *Nat. Rev. Immunol.* **2**, 309–322 (2002).
130. Förster, R., Davalos-Missslitz, A. C. & Rot, A. CCR7 and its ligands: balancing immunity and tolerance. *Nat. Rev. Immunol.* **8**, 362–371 (2008).
131. Wurbel, M.-A., Malissen, B. & Campbell, J. J. Complex regulation of CCR9 at multiple discrete stages of T cell development. *Eur. J. Immunol.* **36**, 73–81 (2006).
132. Zabel, B. A. *et al.* Human G protein-coupled receptor GPR-9/6/CC chemokine receptor 9 is selectively expressed on intestinal homing T lymphocytes, mucosal lymphocytes, and thymocytes and is required for thymus-expressed chemokine-mediated chemotaxis. *J. Exp. Med.* **190**, 1241–1256 (1999).
133. Xu, X. *et al.* Stromal cell-derived factor-1 enhances wound healing through recruiting bone marrow-derived mesenchymal stem cells to the wound area and promoting neovascularization. *Cells Tissues Organs* **197**, 103–113 (2013).
134. Henderson, P. W. *et al.* Stromal-derived factor-1 delivered via hydrogel drug-delivery vehicle accelerates wound healing in vivo. *Wound Repair Regen* **19**, 420–425 (2011).
135. Nishimura, Y. *et al.* CXCR4 antagonist AMD3100 accelerates impaired wound healing in diabetic mice. *Journal of Investigative Dermatology* **132**, 711–720 (2012).
136. Avniel, S. *et al.* Involvement of the CXCL12/CXCR4 pathway in the recovery of skin following burns. *J. Invest. Dermatol.* **126**, 468–476 (2006).

137. Detmar, M. *et al.* Increased microvascular density and enhanced leukocyte rolling and adhesion in the skin of VEGF transgenic mice. *J. Invest. Dermatol.* **111**, 1–6 (1998).
138. Zraggen, S., Huggenberger, R., Kerl, K. & Detmar, M. An important role of the SDF-1/CXCR4 axis in chronic skin inflammation. *PLoS ONE* **9**, e93665 (2014).
139. Takekoshi, T. *et al.* CXCR4 Negatively Regulates Keratinocyte Proliferation in IL-23-Mediated Psoriasiform Dermatitis. *Journal of Investigative Dermatology* **133**, 2530–2537 (2013).
140. Brantley, E. C. & Benveniste, E. N. Signal transducer and activator of transcription-3: a molecular hub for signaling pathways in gliomas. *Mol. Cancer Res.* **6**, 675–684 (2008).
141. Nibbs, R. J. B. & Graham, G. J. Immune regulation by atypical chemokine receptors. *Nat. Rev. Immunol.* **13**, 815–829 (2013).
142. Levoye, A., Balabanian, K., Baleux, F., Bachelier, F. & Lagane, B. CXCR7 heterodimerizes with CXCR4 and regulates CXCL12-mediated G protein signaling. *Blood* **113**, 6085–6093 (2009).
143. Comerford, I., Litchfield, W., Harata-Lee, Y., Nibbs, R. J. B. & McColl, S. R. Regulation of chemotactic networks by ‘atypical’ receptors. *BioEssays* **29**, 237–247 (2007).
144. Girard, J. P. *et al.* Heterogeneity of endothelial cells: the specialized phenotype of human high endothelial venules characterized by suppression subtractive hybridization. *Am. J. Pathol.* **155**, 2043–2055 (1999).
145. Hansell, C. A. H. *et al.* Universal expression and dual function of the atypical chemokine receptor D6 on innate-like B cells in mice. *Blood* **117**, 5413–5424 (2011).
146. Weber, M. *et al.* The chemokine receptor D6 constitutively traffics to and from the cell surface to internalize and degrade chemokines. *Mol. Biol. Cell* **15**, 2492–2508 (2004).

147. Fra, A. M. *et al.* Cutting edge: scavenging of inflammatory CC chemokines by the promiscuous putatively silent chemokine receptor D6. *J. Immunol.* **170**, 2279–2282 (2003).
148. Jamieson, T. *et al.* The chemokine receptor D6 limits the inflammatory response in vivo. *Nat. Immunol.* **6**, 403–411 (2005).
149. Singh, M. D. *et al.* Elevated expression of the chemokine-scavenging receptor D6 is associated with impaired lesion development in psoriasis. *Am. J. Pathol.* **181**, 1158–1164 (2012).
150. Berahovich, R. *et al.* Endothelial expression of CXCR7 and the regulation of systemic CXCL12 levels. *Immunology* **141**, 111–122 (2014).
151. Berahovich, R. *et al.* CXCR7 Protein Is Not Expressed on Human or Mouse Leukocytes. *The Journal of Immunology* **185**, 5130–5139 (2010).
152. Wang, H. *et al.* The CXCR7 chemokine receptor promotes B-cell retention in the splenic marginal zone and serves as a sink for CXCL12. *Blood* **119**, 465–468 (2012).
153. Sierro, F. *et al.* Disrupted cardiac development but normal hematopoiesis in mice deficient in the second CXCL12/SDF-1 receptor, CXCR7. *Proc. Natl. Acad. Sci. U.S.A.* **104**, 14759–14764 (2007).
154. Naumann, U. *et al.* CXCR7 functions as a scavenger for CXCL12 and CXCL11. *PLoS ONE* **5**, e9175 (2010).
155. Burns, J. M. *et al.* A novel chemokine receptor for SDF-1 and I-TAC involved in cell survival, cell adhesion, and tumor development. *J. Exp. Med.* **203**, 2201–2213 (2006).
156. Luker, K. E., Gupta, M. & Luker, G. D. Imaging chemokine receptor dimerization with firefly luciferase complementation. *FASEB J.* **23**, 823–834 (2009).
157. Décaillot, F. M. *et al.* CXCR7/CXCR4 heterodimer constitutively recruits beta-arrestin to enhance cell migration. *J. Biol. Chem.* **286**, 32188–32197 (2011).
158. Tachibana, K. *et al.* The chemokine receptor CXCR4 is essential for vascularization of the gastrointestinal tract. *Nature* **393**, 591–594 (1998).

159. Dambly-Chaudière, C., Cubedo, N. & Ghysen, A. Control of cell migration in the development of the posterior lateral line: antagonistic interactions between the chemokine receptors CXCR4 and CXCR7/RDC1. *BMC Dev. Biol.* **7**, 23 (2007).
160. Balabanian, K. *et al.* The chemokine SDF-1/CXCL12 binds to and signals through the orphan receptor RDC1 in T lymphocytes. *J. Biol. Chem.* **280**, 35760–35766 (2005).
161. Rajagopal, S. *et al.* Beta-arrestin- but not G protein-mediated signaling by the ‘decoy’ receptor CXCR7. *Proc. Natl. Acad. Sci. U.S.A.* **107**, 628–632 (2010).
162. Kumar, R. *et al.* CXCR7 mediated G α independent activation of ERK and Akt promotes cell survival and chemotaxis in T cells. *Cell. Immunol.* **272**, 230–241 (2012).
163. Lee, E. *et al.* CXCR7 mediates SDF1-induced melanocyte migration. *Pigment Cell Melanoma Res* **26**, 58–66 (2013).
164. Ding, B.-S. *et al.* Divergent angiocrine signals from vascular niche balance liver regeneration and fibrosis. *Nature* **505**, 97–102 (2014).
165. Stacer, A. C. *et al.* Endothelial CXCR7 regulates breast cancer metastasis. *Oncogene* **35**, 1716–1724 (2015).
166. Liedtke, D. *et al.* Xmrk-induced melanoma progression is affected by Sdf1 signals through Cxcr7. *Pigment Cell Melanoma Res* **27**, 221–233 (2014).
167. Monnier, J. *et al.* CXCR7 is up-regulated in human and murine hepatocellular carcinoma and is specifically expressed by endothelial cells. *Eur. J. Cancer* **48**, 138–148 (2012).
168. Maishi, N. *et al.* CXCR7: a novel tumor endothelial marker in renal cell carcinoma. *Pathol. Int.* **62**, 309–317 (2012).
169. Schweickart, V. L., Epp, A., Raport, C. J. & Gray, P. W. CCR11 is a functional receptor for the monocyte chemoattractant protein family of chemokines. *J. Biol. Chem.* **275**, 9550–9556 (2000).

170. Comerford, I., Milasta, S., Morrow, V., Milligan, G. & Nibbs, R. J. B. The chemokine receptor CCX-CKR mediates effective scavenging of CCL19 in vitro. *Eur. J. Immunol.* **36**, 1904–1916 (2006).
171. Watts, A. O. *et al.* β -Arrestin recruitment and G protein signaling by the atypical human chemokine decoy receptor CCX-CKR. *J. Biol. Chem.* **288**, 7169–7181 (2013).
172. Leick, M. *et al.* CCL19 is a specific ligand of the constitutively recycling atypical human chemokine receptor CRAM-B. *Immunology* **129**, 536–546 (2009).
173. Townson, J. R. & Nibbs, R. J. B. Characterization of mouse CCX-CKR, a receptor for the lymphocyte-attracting chemokines TECK/mCCL25, SLC/mCCL21 and MIP-3beta/mCCL19: comparison to human CCX-CKR. *Eur. J. Immunol.* **32**, 1230–1241 (2002).
174. Mizuno, S. *et al.* CCR9+ plasmacytoid dendritic cells in the small intestine suppress development of intestinal inflammation in mice. *Immunol. Lett.* **146**, 64–69 (2012).
175. Kunkel, E. J. *et al.* Lymphocyte CC chemokine receptor 9 and epithelial thymus-expressed chemokine (TECK) expression distinguish the small intestinal immune compartment: Epithelial expression of tissue-specific chemokines as an organizing principle in regional immunity. *J. Exp. Med.* **192**, 761–768 (2000).
176. Comerford, I. *et al.* A myriad of functions and complex regulation of the CCR7/CCL19/CCL21 chemokine axis in the adaptive immune system. *Cytokine Growth Factor Rev.* **24**, 269–283 (2013).
177. Heinzl, K., Benz, C. & Bleul, C. C. A silent chemokine receptor regulates steady-state leukocyte homing in vivo. *Proc. Natl. Acad. Sci. U.S.A.* **104**, 8421–8426 (2007).
178. Comerford, I. *et al.* The atypical chemokine receptor CCX-CKR scavenges homeostatic chemokines in circulation and tissues and suppresses Th17 responses. *Blood* **116**, 4130–4140 (2010).

179. Bryce, S. A. *et al.* ACKR4 on Stromal Cells Scavenges CCL19 To Enable CCR7-Dependent Trafficking of APCs from Inflamed Skin to Lymph Nodes. *The Journal of Immunology* **196**, 3341–3353 (2016).
180. Pelkmans, L. & Helenius, A. Endocytosis Via Caveolae. *Traffic* **3**, 311–320 (2002).
181. Shams, K. *et al.* Spread of Psoriasiform Inflammation to Remote Tissues Is Restricted by the Atypical Chemokine Receptor ACKR2. *Journal of Investigative Dermatology* **137**, 85–94 (2017).
182. Nibbs, R. J. B. *et al.* The beta-chemokine receptor D6 is expressed by lymphatic endothelium and a subset of vascular tumors. *Am. J. Pathol.* **158**, 867–877 (2001).
183. Martinez de la Torre, Y. *et al.* Protection against inflammation- and autoantibody-caused fetal loss by the chemokine decoy receptor D6. *Proc. Natl. Acad. Sci. U.S.A.* **104**, 2319–2324 (2007).
184. Whitehead, G. S. *et al.* The chemokine receptor D6 has opposing effects on allergic inflammation and airway reactivity. *Am. J. Respir. Crit. Care Med.* **175**, 243–249 (2007).
185. Littman, D. R. Generation of a Cxcr7 reporter allele. *Jackson Laboratories* (2010). Available at: <http://www.informatics.jax.org/reference/J:156990>. (Accessed: 2nd October 2017)
186. Bollag, W. B. & Hill, W. D. CXCR4 in epidermal keratinocytes: crosstalk within the skin. *Journal of Investigative Dermatology* **133**, 2505–2508 (2013).
187. Kalatskaya, I. *et al.* AMD3100 is a CXCR7 ligand with allosteric agonist properties. *Mol. Pharmacol.* **75**, 1240–1247 (2009).
188. Neusser, M. A. *et al.* The chemokine receptor CXCR7 is expressed on lymphatic endothelial cells during renal allograft rejection. *Kidney Int.* **77**, 801–808 (2010).
189. Takatsuka, S., Sekiguchi, A., Tokunaga, M., Fujimoto, A. & Chiba, J. Generation of a panel of monoclonal antibodies against atypical chemokine receptor CCX-CKR by DNA immunization. *Journal of Pharmacological and Toxicological Methods* **63**, 250–257 (2011).

190. McKimmie, C. S. *et al.* An analysis of the function and expression of D6 on lymphatic endothelial cells. *Blood* **121**, 3768–3777 (2013).
191. Berahovich, R., Penfold, M. E. T. & Schall, T. J. Nonspecific CXCR7 antibodies. *Immunol. Lett.* **133**, 112–114 (2010).
192. Torres, R. & Ramirez, J. C. A chemokine targets the nucleus: Cxcl12-gamma isoform localizes to the nucleolus in adult mouse heart. *PLoS ONE* **4**, e7570 (2009).
193. Na, I.-K. *et al.* Nuclear expression of CXCR4 in tumor cells of non-small cell lung cancer is correlated with lymph node metastasis. *Hum. Pathol.* **39**, 1751–1755 (2008).
194. Rost, B., Yachdav, G. & Liu, J. The PredictProtein server. *Nucleic Acids Res.* **32**, W321–W326 (2004).
195. Brameier, M., Krings, A. & MacCallum, R. M. NucPred--predicting nuclear localization of proteins. *Bioinformatics* **23**, 1159–1160 (2007).
196. Blackburn, P. E. *et al.* Purification and biochemical characterization of the D6 chemokine receptor. *Biochem. J.* **379**, 263–272 (2004).
197. Hulspas, R., O'Gorman, M. R. G., Wood, B. L., Gratama, J. W. & Sutherland, D. R. Considerations for the control of background fluorescence in clinical flow cytometry. *Cytometry B Clin Cytom* **76**, 355–364 (2009).
198. Maecker, H. T. & Trotter, J. Flow cytometry controls, instrument setup, and the determination of positivity. *Cytometry A* **69**, 1037–1042 (2006).
199. Salanga, C. L., O'Hayre, M. & Handel, T. Modulation of chemokine receptor activity through dimerization and crosstalk. *Cell. Mol. Life Sci.* **66**, 1370–1386 (2009).
200. Torzicky, M. *et al.* Platelet endothelial cell adhesion molecule-1 (PECAM-1/CD31) and CD99 are critical in lymphatic transmigration of human dendritic cells. *Journal of Investigative Dermatology* **132**, 1149–1157 (2012).

201. Kriehuber, E. *et al.* Isolation and Characterization of Dermal Lymphatic and Blood Endothelial Cells Reveal Stable and Functionally Specialized Cell Lineages. *J. Exp. Med.* **194**, 797–808 (2001).
202. Pegu, A. *et al.* Human Lymphatic Endothelial Cells Express Multiple Functional TLRs. *The Journal of Immunology* **180**, 3399–3405 (2008).
203. Ford, L. B., Hansell, C. A. H. & Nibbs, R. J. B. Using fluorescent chemokine uptake to detect chemokine receptors by fluorescent activated cell sorting. *Methods Mol. Biol.* **1013**, 203–214 (2013).
204. Hansell, C. A. H., Simpson, C. V. & Nibbs, R. J. B. Chemokine sequestration by atypical chemokine receptors. *Biochem. Soc. Trans.* **34**, 1009–1013 (2006).
205. Ford, L. B. *et al.* Characterization of conventional and atypical receptors for the chemokine CCL2 on mouse leukocytes. *The Journal of Immunology* **193**, 400–411 (2014).
206. Pivarcsi, A., Kemény, L. & Dobozy, A. Innate Immune Functions of the Keratinocytes. *Acta Microbiologica et Immunologica Hungarica* **51**, 303–310 (2004).
207. Stenvik, J. *et al.* Alginates induce differentiation and expression of CXCR7 and CXCL12/SDF-1 in human keratinocytes--the role of calcium. *J Biomed Mater Res A* **100**, 2803–2812 (2012).
208. Chow, K. Y. C. *et al.* A pivotal role for CXCL12 signaling in HPV-mediated transformation of keratinocytes: clues to understanding HPV-pathogenesis in WHIM syndrome. *Cell Host Microbe* **8**, 523–533 (2010).
209. Heng, T. S. P., Painter, M. W. Immunological Genome Project Consortium. The Immunological Genome Project: networks of gene expression in immune cells. *Nat. Immunol.* **9**, 1091–1094 (2008).
210. Berahovich, R. *et al.* Differences in CXCR7 protein expression on rat versus mouse and human splenic marginal zone B cells. *Immunol. Lett.* **154**, 77–79 (2013).
211. van der Fits, L. *et al.* Imiquimod-Induced Psoriasis-Like Skin Inflammation in Mice Is Mediated via the IL-23/IL-17 Axis. *J. Immunol.* **182**, 5836–5845 (2009).

212. Flutter, B. & Nestle, F. O. TLRs to cytokines: mechanistic insights from the imiquimod mouse model of psoriasis. *Eur. J. Immunol.* **43**, 3138–3146 (2013).
213. Gibson, S. J. *et al.* Plasmacytoid dendritic cells produce cytokines and mature in response to the TLR7 agonists, imiquimod and resiquimod. *Cell. Immunol.* **218**, 74–86 (2002).
214. Gerdes, J., Schwab, U., Lemke, H. & Stein, H. Production of a mouse monoclonal antibody reactive with a human nuclear antigen associated with cell proliferation. *Int. J. Cancer* **31**, 13–20 (1983).
215. Okada, T. *et al.* Chemokine requirements for B cell entry to lymph nodes and Peyer's patches. *J. Exp. Med.* **196**, 65–75 (2002).
216. Seth, S. *et al.* CCR7 essentially contributes to the homing of plasmacytoid dendritic cells to lymph nodes under steady-state as well as inflammatory conditions. *The Journal of Immunology* **186**, 3364–3372 (2011).
217. Schoenborn, J. R. & Wilson, C. B. in **96**, 41–101 (Elsevier, 2007).
218. Kawai, T. & Akira, S. The role of pattern-recognition receptors in innate immunity: update on Toll-like receptors. *Nat. Immunol.* **11**, 373–384 (2010).
219. Johnson, L. A. & Jackson, D. G. Inflammation-induced secretion of CCL21 in lymphatic endothelium is a key regulator of integrin-mediated dendritic cell transmigration. *Int. Immunol.* **22**, 839–849 (2010).
220. Schneider, M. R. & Paus, R. Deciphering the functions of the hair follicle infundibulum in skin physiology and disease. *Cell Tissue Res.* **358**, 697–704 (2014).
221. Ouwehand, K. *et al.* CCL5 and CCL20 mediate immigration of Langerhans cells into the epidermis of full thickness human skin equivalents. *Eur. J. Cell Biol.* **91**, 765–773 (2012).
222. Kabashima, K. *et al.* CXCL12-CXCR4 engagement is required for migration of cutaneous dendritic cells. *Am. J. Pathol.* **171**, 1249–1257 (2007).
223. Ando, Y., Lazarus, G. S. & Jensen, P. J. Activation of protein kinase C inhibits human keratinocyte migration. *J. Cell. Physiol.* **156**, 487–496 (1993).

224. Suzuki, H. *et al.* Imiquimod, a topical immune response modifier, induces migration of Langerhans cells. *J. Invest. Dermatol.* **114**, 135–141 (2000).
225. Grine, L. *et al.* Topical imiquimod yields systemic effects due to unintended oral uptake. *Sci Rep* **6**, 20134 (2016).
226. Walter, A. *et al.* Aldara activates TLR7-independent immune defence. *Nature Communications* **4**, 1560 (2013).